FACULTY OF HEALTH SCIENCE

Multiscale characterisation of Achilles tendons during mechanical loading

Anas Khalaf Al Makhzoomi

This thesis is presented for the Degree of

Doctor of Philosophy

of

Curtin University

September 2020

DECLARATION

To the best of my knowledge and belief this thesis contains no material previously published by any other person except where due acknowledgment has been made.

This thesis contains no material which has been accepted for the award of any other degree or diploma in any university.

The research presented and reported in this thesis was conducted in compliance with the National Health and Medical Research Council Australian code for the care and use of animals for scientific purposes 8th edition (2013). The proposed research study received animal ethics approval from the University of Western Australia Animal Ethics Committee, approval number RA/3/200/547.

Signature

Date 06/07/2020

ABSTRACT

The tendon's composition and microstructure are correspondingly related to its function which includes load bearing and transmission of the mechanical force generated by muscles to the skeletal structure which enables joint movement. The performance of these tasks rely on a distinctive set of mechanical characteristics controlled by the extracellular matrix (ECM) and the ability to respond to a broad range of stresses and strains. Muscles influence the torques acting across a joint through the generation of tensile force transmitted through the tendon. Therefore there is a morphological association between the muscle and tendon defined by both form (morphology) and function (mechanical characteristics) at various macro and micro scales. This is specifically important for studies of the Achilles tendon that are related to the significant functional stretch-shortening activities of gait and ambulation.

The Achilles tendon is known as one of the most commonly injured tendons. It is suggested that the incidence of injured Achilles tendon causing pain and dysfunction, is associated with physical activities common in both occupational and sports settings. Tendinopathy and ultimately rupture comprise a large range of disorders reflecting various mechanical damage and degenerative diseases. However, scientific and clinical knowledge of the transition from healthy tendon to pathological tendinopathy and tendon rupture is unclear. Therefore, there is a necessity to understand the mechanisms and source of tendon's pathology to enrich the preventive and rehabilitative strategies.

Repeated loading studies have assessed structural properties at different scales. But, few have concurrently assessed multiple scales. Similarly, mechanical profiling of repeated loading studies for tendons have been undertaken as different scales (Nano - Macro). To date, few if any studies have assessed the structural and mechanical properties concurrently at different scale levels. To achieve this, this project employed a mix methods approach of both observational qualitative and quantitative assessments.

This thesis utilises a mechanical loading device (Instron) to apply controlled cyclic mechanical stimuli to assess the change in mechanical properties of whole tendon. Visual determination of macro-structural changes (Tenocyte morphology, fibre

Anisotropy and waviness) during loading were recorded using digital photography of the confocal microscope (CA). All other sequential structural assessments were undertaken on section preparations that destroyed the tendon so slices were placed on slides after each 1-hour block of mechanical loading. This allowed for visual determination of structural changes at the fibre and fibril level (D-Periodicity) assessed by the traditional histology and the Atomic Force Microscopy (AFM) respectively.

The main study took New Zealand white rabbits (n = 45) and divided them into four groups. A native (control) group and other three groups tested at three strain levels (3, 6 & 9%) after preconditioning. Tendons were subject to 240 cycles per minute for a period of 4 hours (9600 cycles in total) with Mechanical assessment (derived variables - Stiffness, hysteresis, maximum load) and Confocal imaging every 4 minutes.

After each hour three tendons were removed from the testing group and submitted to histological testing. This resulted in a reduction in sample size from 12 to 3 in the fourth hour. The data for the third to fourth hour was only observational. Continuous derived variables (DV) were normalised to a % change from pre-conditioned baseline. The effect size (Pooled data with a Hege's G correction) of repeated measures or paired comparison was determined for the end of the hour results. Statistical significance was set at the 95% level of confidence and no alpha level corrections. Correlations between the mechanical and observational assessments were undertaken using Pearson's correlation.

A secondary study was undertaken to replicate 6% strain loading for 2 hrs for 10 tendons (GAG-depleted) and 10 tendons (controls). Repeatability and reliability of subjective classifications were documented using a double blinded inter and intra testing comparison (Weighted Kappa) and the replication of DV for the matched main study (2 hrs and 6% strain).

The results of the study demonstrated high concordance for the observational assessments within and between sessions and high concordance (Kappa > 0.8 intra and > 0.93 Inter) and replication of derived variables for match controlled groups.

The overall study shows that strain mediated repeated loading induces a significant decline in mechanical function ($p<.01$, Stiffness, hysteresis, maximum load) with increase strain and cycles. The dynamic mechanical DVs correlated strongly ($R^2>$ 0.90) with the Maximum load value (Static DV). The morphology changes (continuous variables such as waviness and tenocyte roundness) were highly linearly correlated ($R^2>$ 0.90) to most mechanical DVs. The changes in Hysteresis were most sensitive to the observed morphological changes, concurrently, tenocyte loss of spindle shape was the most sensitive changes morphologically.

The multiscale assessments show that mechanical and structural elasticity is lost with repeated loading ($P<0.05$) and these happen at all scales. The D-Periodicity of the collagen formation correlated strongly with the overall tendon mechanical changes and macro observations of the tenocyte spindle decline. Tendons that had GAG depletion had a significantly greater decline in mechanical capacity and a clearly greater level of concomitant morphological damage. Of note, however, these associations between the mechanical and structural domains remained consistent with the associations observed (and replicated) in the control tendons.

This is the first study to provide a clear concurrent assessment of form (morphology) and function (mechanics) of tendon undergoing strain mediated repeated loading at multiple scale assessments. A matched and parallel study of the GAG depletions provided an added understanding of the association between these variables. The study design had sufficient statistical power for the first three hours of assessment and the final 4^{th} hour contributed well to the overall observation of the trends in the data into the failure state.

This study makes a significant and original contribution to the multiscale assessments of tendon mechanics and morphology showing the strength of concurrent assessments and observed changes. These were also reported for GAG-depleted (validated depletion amounts) tendons. Since the association between the mechanical and structural changes remain consistent in both control and GAG-depleted tendons then the findings would suggest that both of these domains may be used in tendons of heterogenic GAG-depleted status. This may have implications for clinical assessments where GAG depletion may be a biological variable of interest.

ACKNOWLEDGEMENTS

First of all, I would like to express my deepest appreciation and gratitude to my dear beloved late father Prof. Khalaf Al Makhzoomi and my dear beloved mother Mrs.Mona Mrayyan, who both set a great example for me to appreciate the value of higher education; I'm extremely grateful for their continuous, love, sacrifice and support.

I would like to acknowledge the financial support of the Australian Government Research Training Program Scholarship and Australian Research Council (ARC) Linkage program (LP110100581) I would also like to acknowledge the Curtin University of Technology (CUT), University of Western Australia (UWA) and Royal Perth Hospital (RPH) for the opportunity and support afforded to me. This PhD has been a big life-changing experience and it would not have been possible to undertake without the guidance and support that I received from many other people.

I would also like to extend my sincere and deepest gratitude to my supervisors Prof. Garry Allison and Prof. Brett Kirk for the opportunity to undertake this study, for all the support and encouragement they gave me and their guidance throughout the project. I am extremely grateful to Prof. Garry Allison for his expertise throughout this project. Without his inspiration, assistance and constant feedback, this PhD would not have been achievable. Special thanks to the national ARC Linkage team working on Tendinopathy and, the team in the Large Animal Facility at UWA for their assistance in tissue collection.

Also, I am deeply indebted to the following people for their technical support, assistance and guidance, who devoted many hours helping me with all lab and technical work for my project that has helped to gain my practical experience: Dr. Paul Davey from the school of Physiotherapy and Exercise science, Dr. Danielle Dye from the school of biomedical science, Senior visualisation specialist Dr. Andrew Squelch from the Pawsey Supercomputing Centre, Mrs. Mary Lee from the CELLCentral facility at the School of Anatomy Physiology & Human Biology University of Western Australia, Bioengineer Dr. Alex Hayes from the Medical Engineering and

Physics at RPH and Dr. Thomas Becker from the Scanning Probe Microscopy Facility at the School of Molecular Life Sciences.

I extend my appreciation and thanks to all the wonderful doctoral students, members of the faculties of health science, science and engineering, and other staff at Curtin University. I wish to thank many members for their care and support over the years of my journey, and I hope any of those great people who are not mentioned here know how much they influenced my life. I am honoured knowing you all!

DEDICATION

This dissertation is lovingly dedicated to the soul of my beloved sweetheart father, who I will always be deeply indebted to, Prof. Khalaf Al Makhzoomi, to whom I promised to dedicate this dissertation before he left this world.

His unconditional love, encouragement and support have meant the world to me and have greatly helped me throughout this great experience. He went beyond and above as a father and mentor throughout all stages of my life. Even during his most severe and critical stages of illness, his encouragement and support at the hospital, will always be my inspiration for the success in this life and the hereafter. Although he is my inspiration to pursue my doctoral degree, it is, unfortunately, and I feel deeply sad no to see him in my graduation! I am deeply indebted to him for the rest of my life with deepest everlasting gratitude and love. I ask the satisfaction of Allah Al-Mighty upon him and grant him mercy and paradise! Ameen!

To my beloved sweetheart mother, who I will always be deeply indebted to, Mrs Muna Suleiman, her encouragement, support and constant love have meant the world to me and have greatly helped me throughout my PhD journey. She went beyond and above as a mother and mentor throughout all stages of my life. I am deeply indebted to you mom with my sincere and deepest everlasting gratitude and love. Thank you for your continuous love, sacrifice and support. I hope this achievement makes you proud! I ask the satisfaction of Allah Al-Mighty upon you and to grant you the true happiness and prosperity in this life and hereafter. Ameen!

To my beloved sweetheart wife, Prof. Amal AlNatour, I greatly appreciate your understanding and patience when my PhD project and thesis took my highest priority. I ask the satisfaction of Allah Al-Mighty upon you and ask him to grant you the true happiness and prosperity in this life and hereafter. Ameen!

To my beloved sweetheart children, Master Ahmad and Miss Tala Al Makhzoomi, you have been and will always be the light of my life; and although it is still early for you both to appreciate this achievement, I want you to know my sacrifice was only for a great reason. I deeply thank you for your genuine love, for giving this experience even greater value. I hope by achieving this great dream that I could set an example

and inspiration for you both. I beseech to Allah to provide you with the strength and guidance to pursue your dreams of the highest level of academic achievement, Amen!

To my beloved sweetheart brothers, Dr.Alaa and Mr. Mohammad-Falah Al Makhzoomy and to my beloved sweetheart sisters, Mrs Batool, Prof. Ibtihal and Mrs Afyaa Al Makhzoomy. I beseech to Allah to provide you the prosperity and success in this life and in the hereafter. Ameen!

And to my supervisor, who I will always be deeply indebted to, Prof. Garry Allison, who helped me to reach this great stage in my life. I ask Al-Mighty to grant you the true happiness and prosperity in this life and hereafter. Ameen!

Without your support, this thesis would not be achievable. My deepest thanks to you all!

TABLE OF CONTENTS

LIST OF FIGURES

LIST OF TABLES

TABLE OF ACRONYMS

Acronym	Meaning
2D FFT	two-dimensional fast Fourier transform
3D	three dimensional
AB/PAS	Alcian blue/periodic acid-Schiff base
AFM	atomic force microscopy
ANOVA	analysis of variance
AO	acridine orange
BFB	between fibril bundle
BSA	bovine serum albumin
CA	confocal arthroscopy
Ch-ABC	chondroitinase ABC
Ch-SO_4	chondroitin sulfate
CI	confidence interval
CLSM	confocal laser scanning microscopy
CM	confocal microscopy
D0%	D-periodicity of control
D3%,D6%, D9%	D-periodicity of 3%, 6% and 9% strain groups
D_D%	D-periodicity GAG-depleted tendons
DMMB	dimethylmethylene blue
DS	dermatan sulfate
ECM	extracellular matrix
EM	electron microscopy
FaS	fragmentation of fascicles
FD	fibre dissociation
FDL	flexor digitorum longus
FiS	separation of fibrils
FK	fibril kink
FS	interfibre space
GAG	glycosaminoglycan
GPa	giga pascal
h	hysteresis
H&E	Haematoxylin and Eosin
k	stiffness
k1	ramping stiffness
k2	loading stiffness
LF	Fibre Length
L0	Length between two end points
LM	Light Microscopy
MCL	medial collateral ligaments
MEMS	micro-electro-mechanical systems

ML	Maximum load
MPa	mega pascal
MRI	magnetic resonance imaging
MTC	muscle-tendon complex
OCT	Optimal cutting temperature compound
PBS	phosphate-buffered saline
PFA	paraformaldehyde
PG	proteoglycan
R^2	coefficient of variation
ROI	region of interest
RPMI	Roswell Park Memorial Institute
RUP	fibre rupture patterns
SEM	scanning electron microscopy
SHG	second-harmonic generation
SL	Straight Length
SLRP	small leucine-rich proteoglycan
SP	Straightness Parameter
SR	stress relaxation
Strain Max	Maximum Strain
Strain Zero	Strain at Rest
Tc	tropocollagen
TEC	thermoelectrically cooled
TEM	transmission electron microscopy
WFB	within fibril bundle
SP	Straightness Parameter
XRD	X-Ray Diffraction

CHAPTER ONE:
INTRODUCTION

The composition and microstructure of a tendon corresponds to its function. Tendons that demonstrate properties such as resilience, strength and stiffness have a uniaxial tensile function along the fibre longitudinal axis that enables energy transfer and transmission of generated muscle force to bone (Kannus, 2000; Doral et al., 2010). The wide range of functions that tendons can perform are attributed to the broad range of structural and mechanical properties they exhibit (Benjamin et al., 2008; Kjaer et al., 2009; Abramowitch et al., 2010; Thorpe et al., 2012; Thorpe et al., 2013; Shepherd et al., 2014).

The literature often demonstrates a tendon's nonlinear biomechanical behaviour by a typical stress-strain curve. The stress-strain curve usually displays a non-linear toe-region first that is succeeded by a linear region (Connizzo et al., 2013). Various variables derived from the stress-strain curve are suggested to result from a set of rearrangements of dynamic macrostructural responses (Diamant et al., 1972; Atkinson et al., 1999; Woo, 2000; Lake et al., 2009; Wallace et al., 2010; Rigozzi et al., 2011; Miller et al., 2012; Connizzo et al., 2013; Thorpe et al., 2013). Specifically, the nonlinear behaviour seen in the toe-region has been associated with the disappearing or flattening of fibre crimps and kinks (Atkinson et al., 1999). Fibre alignment, reorientation and anisotropy towards the mechanical load axis also takes place concurrently (Diamant et al., 1972; Atkinson et al., 1999; Lake et al., 2009; Wallace et al., 2010; Miller et al., 2012).

Tendons demonstrate viscoelastic properties, such as hysteresis (h), creep and stress relaxation (SR) (Woo, 2000; Elliott et al., 2003; Gimbel et al., 2004; Screen, 2008; Gautieri et al., 2012). The viscoelasticity of tendons consists of both dynamic and static processes, as exhibited by a decline in maximum stress over time under repeated cyclic loadings (Freedman et al., 2014). These viscoelastic properties highlight the adaptive capability of a tendon's hierarchical structures to cyclic or constant loads, allowing it to reach a biomechanical balance (Einhorn et al., 2007).

The Achilles tendon is known as one of the most susceptible tendons to injury, which consists of pain and dysfunction, and ultimately rupture. It is suggested that the incidence of injury of Achilles tendons is associated with physical activities common in both occupational and sports settings (Wren et al., 2001; Sharma & Maffulli, 2005). Tendinopathy comprises a large range of disorders, reflecting both mechanical damage and degenerative diseases. However, scientific and clinical knowledge of the pathological degeneration from healthy tendon to tendinopathy and tendon rupture is yet not fully understood. Therefore, it is necessary to understand the mechanisms and sources of tendon pathology to enrich preventive and rehabilitative strategies (Sharma & Maffulli, 2005).

It has been suggested that the Achilles tendon may repetitively function close to or at failure (Wren et al., 2001; Freedman et al., 2014). Tendinopathy is thought to be a precursor to lower limb tendon rupture. Cyclic loading and/or overuse has been widely accepted to be a major cause of tendon failure of the Achilles, patella and quadriceps tendons (Järvinen et al., 1997; Paavola et al., 2002).

1.1 Mechanically Induced Macrostructural Changes

Various studies have associated tendon pathology with alterations and damage in the microstructure of tendons, which are induced by mechanical loading (Arner, 1959; Backman et al., 1990; Kannus & Jozsa, 1991; Archambault et al., 2001; Tallon et al., 2001; Nakama et al., 2005; Abate et al., 2009; Fung et al., 2009; Fung et al., 2010; Andarawis-Puri & Flatow, 2011; Maquirriain, 2011; Neviaser et al., 2012), indicating that the aetiology of tendon damage warrants further investigation. Although there is an ongoing biological response to repeated micro-loading during functional tasks, there is a growing body of research that examines the relationship between the observed changes in the microstructure and changes in the mechanical profiles of tendons (Freedman et al., 2014; Freedman et al., 2015; Fung et al., 2010; Ros et al., 2019).

Structural changes following fatigue loading have been assessed using histology (Fung et al., 2009), second harmonic generation (SHG) (Fung et al., 2010; Veres & Lee,

2012; Ros et al., 2013), polarized light imaging (Freedman et al., 2014), scanning electron microscopy (SEM) (Veres et al., 2013), and confocal imaging using photo-bleaching (Thorpe et al., 2014). Only a few mechanical measures of tendon fatigue have been reported (Thorpe et al., 2014), and limited studies have reported correlations between quantified macrostructural changes in tendons, and fatigue loading (Freedman et al., 2014; Freedman et al., 2015). Despite various studies having investigated tendon damage, the quantification of damage in tendons is still a challenging issue, perhaps, in part, because an accurate definition with an appropriate engineering framework, has largely not been applied in tendon assessments.

Studies in the literature have employed different imaging protocols to investigate the cumulative and progressive structural changes induced by fatigue. While changes in mechanical properties appear to be in response to damage of the tissue's microstructure, the link between these mechanical properties and changes in the tissue's microstructure has not been fully explained. To date, limited experiments have incorporated multi-scale assessments of both mechanical and structural observations, and have they correlated concurrent structural image-based quantified measures with the mechanical characteristics of tendons subjected to repeated sub-rupture loading (Freedman et al., 2015; Ros et al., 2019).

Generally, previous imaging experiments have focused only on the macrostructural level, i.e. on the relationship between the applied stress and either the number of loading cycles or strain extensions. Interestingly, none of these studies have included experimental protocols using both strain extensions and the number of cycles. Furthermore, changes to mechanical properties, such as reduced failure stress and strain and decreased stiffness, have been observed when loaded tendons were experiencing repetitive cycles and/or higher stresses (Wren et al., 2003; Sharma & Maffulli, 2005; Veres et al., 2013). To date, there is no single study that has investigated multiscale structural changes within the same non-viable intact/bulk tendon in response to prolonged cyclic and static loading protocols.

Testing of non-viable bulk tendons is relatively straightforward and offers the clearest fatigue-damage mechanical data. It is important to determine the response of collagen to mechanical load across multiple hierarchical levels (fascicle, fibre and fibril) by

correlating concurrent structural image-based and quantified measures (by the use of nondestructive multiscale advanced imaging techniques such as Atomic Force Microscopy (AFM) and Confocal Arthroscopy (CA)) with the mechanical characteristics of the loaded non-viable bulk tendons, using both strain extensions and the number of cycles.

1.2 Mechanically Induced Nanostructural Changes

Since the ultrastructure of collagen is closely related with function (Ottani et al., 2001), various attempts to correlate collagen nanostructure with mechanical characteristics have employed different experimental methods including scanning-electron and optical microscopy of sectioned tissues (Kukreti & Belkoff, 2000; Okuda et al., 2009; Franchi et al., 2010), scattered X-ray spectroscopy of tissue fibres (Misof et al., 1997; Fratzl et al., 1998; Puxkandl et al., 2002; Gupta et al., 2010) or AFM of isolated fibrils (Habelitz et al., 2002; Graham et al., 2004).

However, morphometric analysis of fibril strain by transmission electron microscopy (TEM) and X-ray spectroscopy can be limited by technical difficulties that prevent direct assessments of quantitative measures of fibril length changes (changes in D-periodicities) and ultimately the mechanical strain. AFM can offer very accurate morphometric analysis by measuring the fibril topology (Habelitz et al., 2002; Fang et al., 2012; Su et al., 2014); however, the application of AFM in assessing the strain of fibrils in tendons exposed to mechanical loadings has been limited to one study (Rigozzi et al., 2011). Therefore, the implementation of AFM to quantify precisely the nanostructural mechanical response of individual fibrils of tendons exposed to repeated cyclic loading warrants further investigation.

The mechanism of elongation in tendons at the macroscale level appears to be enhanced by deformation and sliding mechanisms that concurrently occur at multiscale levels (Rigozzi et al., 2011). At the macro- and nanoscale levels, the elongation mechanism is reported to be facilitated by the deformation of fibres, and also by sliding between fibres and between fibrils, with the between-fibril mechanism partly controlled by proteoglycans (PGs) (Rigozzi et al., 2009; Rigozzi et al., 2011).

During the initial response of a tendon to a load, fibril sliding is suggested to contribute to the viscoelastic dynamic behaviour of tendons (Puxkandl et al., 2002; Silver et al., 2002; Connizzo et al., 2014). The change in fibril D-periodicity has been supported by various proposed theoretical models on two mechanisms of fibril deformation. At low strains, the deformation of collagen fibrils appears to start with the elongation of the twisted triple α-helical polypeptidic helical chains, succeeded by an axial lengthening, and eventually an uncoiling at the molecular-scale level (Sasaki & Odajima, 1996; Tang et al., 2010; Gautieri et al., 2011). Consecutive stretching caused by increased forces appears to initiate the sliding of the aligned collagen molecules past each other, and elongation (Mosler et al., 1985; Folkhard et al., 1987; Sasaki & Odajima, 1996). Under strain, Mosler et al. (1985) have suggested an increased molecular D-periodicity, attributing this increase to molecular sliding, resulting in the observable additional elongation of fibrils (Mosler et al., 1985). The relative deformation associated with the straining of collagen molecules can be assessed by measuring the changes of D-periodicity lengths of fibrils (Gupta et al., 2010).

Although changes in D-periodicity induced by different strain levels have provided evidence that D-periodicity of an individual fibril increases with increased applied load (Rigozzi et al., 2011; Connizzo et al., 2014; Connizzo et al., 2015), relative D-periodicity changes appear to represent only 40% of the full macroscopic elongation of the tendon fibres, with the D-periodicity increase caused by fibril elongation and additional lengthening of the fibril believed to be concomitant with sliding between collagen fibrils and fibril bundles (Diamant et al., 1972; Misof et al., 1997; Fratzl et al., 1998; Birch, 2007).

There is no clear consensus between studies investigating the variability of D-periodicity between fibril bundles. For instance, a recent AFM-based study on ovine skin, bone and tendon tissues monitored the relationship between the distribution of fibril D-periodicity in a single fibril bundle and the organization of fibrils across various bundles (Fang et al., 2012). Within a single fibril bundle, the change between the repetitive D-periodical sequence was minimal (±1 nm), indicating a uniform axial arrangement of monomers in the fibril bundle, but the differences across various fibril bundles of the same biological tissue was markedly greater, representing the whole scale of distribution (± 1nm vs. ± 10nm).

Another study has also shown that D-periodicity measures were similar within a single fibril bundle and dissimilar across fibril bundles (Su et al., 2014); however, in this study fibril D-periodicity measures represented only a small distribution (67 ± 2.5 nm). It is unclear if these results would be replicated under sequential loading profiles as no studies have undertaken such an experimental paradigm.

The D-periodicity distribution has not been widely reported and these results may suggest that the between-fibril variation is a normal feature of fibrils, or perhaps the variation can be attributed to fibrilogenesis, or a pathology of the fibrils. This raises the importance of understanding fibril changes under mechanical intervention. The significance of the D-periodicity physical distribution is yet to be investigated.

To date, there is no single study that has explored the existence or range of D-periodicity variation within the same, or different, fibril bundles experiencing different strain levels. Also, no study has yet correlated these variations with other nano- and macrostructural dynamic responses to mechanical load. While tendon structural and functional relationships have been investigated, the hierarchical structure of the tendon, the understanding of the tendon damage mechanisms and the accumulation of damage at the nano- and microstructural levels merits further investigation. Therefore, the precise approach of AFM observation is needed to assess the mechanical strain response of the same fibril, and of fibrils from other fibre bundles that undergo repetitive cyclic loading.

1.3 PGs and their Glycosaminoglycan (GAG) Chains

The organisation and composition and of the PG-rich matrix has been suggested to contribute to collagen fibril sliding (Merrilees & Flint, 1980) and to be directly related to tendon viscoelastic behaviour (Paavola et al., 2002). Previous reports have shown that small-sized PGs rich in leucine (small leucine-rich PGs or SLRPs) such as decorin, biglycan, fibromodulin and lumican are important for the function of a tendon (Iozzo, 1998; Derwin et al., 2001; Yoon & Halper, 2005) and play a role in controlling fibrillogenesis (Vogel et al., 1984; Vogel & Trotter, 1987; Scott, 1995; Scott et al., 1997; Ezura et al., 2000; Corsi et al., 2002; Wenstrup et al., 2004; Raspanti et al., 2007; Kadler et al., 2008; Shi et al., 2010; Orgel et al., 2011; Wenstrup et al., 2011).

The core protein in the decorin molecule appears to be attached to D-periodicity and to exist between collagen fibrils as seen by the electron microscope (EM) (Scott, 1988). Each decorin molecule has a single glycosaminoglycan (GAG) chain, which is mainly dermatan sulfate in tendons (Koob & Vogel, 1987) and is attached covalently to the core decorin protein, demonstrating an orthogonal structure that aligns relatively to the fibril (Weber et al., 1996) and consequently may contribute in the elongation of the fibril as well as the sliding mechanism of macroscale elongation (Minns et al., 1973; Ruggeri & Benazzo, 1984; Birk et al., 1989; Cribb & Scott, 1995; Sasaki & Odajima, 1996; Fratzl et al., 1998; Puxkandl et al., 2002; Raspanti et al., 2002; Redaelli et al., 2003; Scott, 2003; Screen et al., 2005; Vesentini et al., 2005; Screen et al., 2006; Liao & Vesely, 2007; Fratzl, 2008; Rigozzi et al., 2009; Legerlotz et al., 2013).

Regardless of these many studies supporting the role of PGs and GAGs in assisting the elongation of the fibril, as well as contributing to the sliding mechanism in macroscale elongation, there is a growing lack of consensus regarding this role. It was proposed more recently that decorin molecules and associated GAGs d not facilitate the mechanical characteristics of tendon *via* load transfer, debating the notion that decorin PGs may facilitate the elastic behaviour of collagen (Screen et al., 2005; Lujan et al., 2007; Fessel & Snedeker, 2009; Franchi et al., 2010; Lewis et al., 2010; Svensson et al., 2011).

For instance, Rigozzi et al. (2009) have removed 50% of the total GAGs from whole Achilles tendons resulting in a significant loss (46%) in stiffness. Whereas, Svensson et al. (2012) and Screen et al. (2005) have reported that removal of about 90% of GAGs from tested fascicles did not result in a significant loss in fascicle stiffness. The GAG content of the tendons in the cited studies was measured using a spectrophotometric GAG assay (Farndale et al., 1986).

The main source of the inconsistency between reports on the role of PGs and GAGs, is perhaps, due to the heterogeneity of the mechanical response at different hierarchies (tendon *vs* fascicle). For instance, it has been reported that tensile stiffness of a whole tendon is less than that of a small tendon specimen (Stouffer et al., 1985; Butler et al.,

1987). The increased fascicle stiffness in smaller tendons could also be attributed to a lower amount of areolar connective tissue (Danylchuk et al., 1978; Yahia & Drouin, 1988). Danylchuk et al. (1978) have previously proposed that the relative contributions of connective sheaths and collagen fasciculi should be considered for an accurate definition of tensile stiffness (Danylchuk et al., 1978). However, consistent with the finding by Rigozzi et al. (2009), a study by Legerlotz et al. (2013) reported a significant increase in SR of fascicles that had 77% of their GAG removed, contradicting the findings by Svensson et al. (2012).

This finding by Legerlotz et al. (2013) is supported by several studies on hierarchy in ligaments and tendons suggesting that the insertion zone can contain a 20-fold higher concentration of GAG than the mid-zone (Merrilees & Flint, 1980; Koob & Vogel, 1987; Vogel & Koob, 1989; Kannus et al., 1992). However, one study has shown an increased GAG concentration in cultured tendon fascicles subjected to static loading, which was also related to an elevated stiffness (Abreu et al., 2008). This implies that GAG concentration and distribution may cause changes in the mechanical characteristics of the tendon. Consequently, it seems that the role of hierarchical heterogeneity between the depleted tendon and fascicle does not seem to contribute in the mechanical response of the tested tissue.

Investigation of the role of side-chain GAGs in fibril load-sharing has been limited to one study using AFM (Rigozzi et al., 2013). Rigozzi et al. reported a role for GAGs in facilitating the fibril sliding mechanism by linking the absence of GAGs and altered D-periodicities of fibrils in treated tendons with changed mechanical properties. However, there are no studies that investigate the role of GAGs in mediating fibril sliding mechanisms by exploring the existence or range of D-periodicity variation within the same and different fibril bundles of GAG-depleted groups. Also, it appears that no studies have correlated these variations with other quantified macrostructural dynamic responses (e.g., fibre crimp changes) to mechanical load.

Fibril D-periodicity can be used as a metric for fibril elongation, which represents a proxy measure for fibril load sliding (Misof et al., 1997; Fratzl et al., 1998; Rigozzi et al., 2011; Rigozzi et al., 2013). Therefore, it is important to investigate the role of PG side-chain GAG in mediating fibril sliding mechanics by combining nondestructive

multiscale advanced imaging techniques with observations of mechanical characteristics (Screen et al., 2003, 2004; Gautieri et al., 2011; Rigozzi et al., 2011; Miller et al., 2012). CA can be integrated with a mechanical loading device during the mechanical loading experiment to concurrently take images at the fascicle- and fibre-level scales, which in turn can be compared with AFM images that investigate the fibril-level changes. In particular, the mechanical and structural characteristics of collagen fascicles relevant to fibril-level structural deformations (measured by changes in D-periodicity) must be quantified from the same bulk tissue sample. This would identify potential mechanisms of load transfer between different hierarchical levels and additionally explain mechanisms of structural response to load at each level of the hierarchies.

Within the techniques that have provided opportunities to examine tendon mechanics and structural behaviour during loading at nanoscale, AFM has emerged as a powerful imaging technique for biological research, not only allowing the construction of images of surfaces with ultra-high resolution, but also the measurement of molecular interactions and modifications and their mechanical forces at the single-molecule level (Carvalho et al., 2013). AFM has become an important technique for visualising extracellular collagen in tendon tissue without tissue staining or destruction (Bannerman et al., 2014) or the effects of elements such as cryo-protectants, stains, embedments or coatings (Baselt et al., 1993).

To date, studies have mainly focused on the macroscale characteristics of collagen fibres, and there are many earlier works that elucidate the mechanical characteristics of collagen structural hierarchies (Weiner & Wagner, 1998; Fratzl et al., 2004; Screen et al., 2005; Gupta et al., 2006; Carpinteri & Pugno, 2008; Fratzl, 2008; Fung et al., 2009; Fung et al., 2010; Neviaser et al., 2012; Shepherd & Screen, 2013). However, other studies have focused particularly on the characteristics of collagen molecules without linking them to a larger hierarchical collagen response (Cusack & Miller, 1979; Sun et al., 2002; Bozec et al., 2005; Wallace et al., 2010; Wallace et al., 2011; Wallace, 2012; Su et al., 2014).

Only the pioneering works of Sasaki and Odajima (1996) and Fratzl et al. (1998) have included molecular details and suggested an elongation and rearrangement mechanism of collagen fibrils and of their molecules when they were subjected to mechanical load.

Although experimental work has focused on the mechanical characteristics of individual collagen fibrils and provided new insights on fibre stiffness and its nonlinear deformation behaviour (Eppell et al., 2006; Shen et al., 2008), it is important to determine if structural changes at the fibril level can affect the macroscopic structural and mechanical properties or *vice versa*. Therefore, a broader range of mechanical and macro/nanostructural measures need to be incorporated into an animal model to assess different tissue responses across different hierarchies and to understand how the load is transferred across hierarchical scales within the intact bulk of the same tendon with the same boundary conditions.

1.4 Significance of the Project

The characterisation of structure-function relationships in tendons has been mostly limited to comparisons between macroscopic (full tendon) structural and mechanical characteristics. Until now, collagenous tissues have mainly been described at macro-hierarchical levels without a clear understanding of the nano-mechanical contributions at the fibrillar levels that underlie function and pathogenesis. Furthermore, the role of the mechanical stimuli in the structural adaptation and pathology of a tendon, and how the organisation of the tendon's nanostructure leads to the tendon's mechanical characteristics, is unclear. It is therefore important to study these mechanisms to provide a better understanding and clarification of the nanostructural response to mechanical load.

To the best of the author's knowledge, this project is the first to run mechanical assessments across such a broad range of quantitative macroscopic structural characteristics (*fibre crimp, fibre anisotropy, tenocyte morphology)* and quantitative nanoscale composition and structural variables *(fibril crimp and fibril deformation as quantified by changes in D-periodicity*) of the same bulk tendon samples subjected to a mechanical loading protocol, and this is the key innovative contribution of this thesis.

Furthermore, the current study assesses the real-time macrostructural and mechanical characteristics of a tendon during its fatigue life over four hours at three different strain

levels (3%, 6% and 9%) using a CA, and compares these results to a set of GAG-depleted tendons at the 6% strain level over two hours.

Such work is novel as it concurrently assesses the consequences of mechanical intervention on tendon structure across various regions and a large range of strains and doses (cycles). This methodology potentially will assist the interpretation of other assays that monitor real-time structural changes in the mechanical profiles of tendons, such as ultrasound (Riggin et al., 2013) into *in vivo* systems.

The strategy and approach of this study was to investigate how tendons structurally respond to mechanical load through various key structural components of collagen across different hierarchical levels. The study examines the stress-strain parameters of the whole tendon, along with the fibre and fibril changes, using integrated confocal imaging within a mechanical testing environment. These tendons are then sectioned and intensive analysis of the fibril changes assessed using AFM. Finally, a mechanical model of tendinopathy is combined with a depletion model to examine nanoscale changes with a depletion of GAG. This would identify potential mechanisms of load transfer between different hierarchical levels and additionally explain mechanisms of structural response to load at each level of the examined hierarchy.

By investigating the changes in tendon structure and function using the method of this study, it is anticipated that this project will provide an innovative understanding (at multiscale levels) regarding the role of the mechanical environment of a tendon in its structural development and synthesis of cells, along with tendon damage and repair processes.

At the macroscale level, the assessment of the morphological response of tenocytes to micro-damage is crucial for a better understanding of the tenocyte mechano-transduction role, as this may contribute to a better understanding of cell-matrix interactions under different loading protocols. Furthermore, this study will highlight the significance of tenocyte morphological characteristics by contributing to knowledge related to the initiation mechanisms of tendinopathy, proposing that fatigue micro-damage may play a vital role in the initial tenocyte response to damage, corresponding to tenocyte morphological changes. Furthermore, assessment using CA

may reveal non-destructively, and in real time, changes in a tendon's crimp/kink pattern during fatigue loading, and may provide more advanced diagnostic imaging methods to investigate injured and healing tendons, which may eventually improve the monitoring of patients.

At the nanoscale level, measuring the D-periodicity values of fibrils may provide vital structural data for various research areas, for example, the structure of a collagenous molecular model, and collagen fibrillogenesis.

This project may also provide future insight for researchers in the pathological assessment of Type I collagen. This type of nanostructural assessment may allow promising vital structural data regarding Type I collagen in a broad range of collagenous diseases and processes in the extracellular matrix (ECM), such as Ehlers-Danlos Syndrome, Osteoporosis, Osteogenesis Imperfecta, knockout gene models, tissue engineering and wound healing.

To evaluate a tendon's nano- and microstructural changes, conventional histological analysis (such as conventional light or fluorescent or confocal microscopy, SEM and TEM) is often used, which involves collection of biopsies and chemical preparation before assessment. The process of biopsy is fundamentally destructive to the tendon sample. The various limitations of these advanced imaging techniques can lead to inconsistencies in the literature about the structure-function relationship, particularly when investigating this relationship across different hierarchical levels of the tendon. Consequently, this can lead to a poor or erroneous understanding of the pathogenesis of Achilles tendon tendinopathy. The CA and AFM methods used in this project are considered very practicable for nondestructive imaging of the macro- and nanostructure of tendons. CA and AFM have the potential to clarify the precise morphology of micro- and nano-damage in the tissue without any risk of destruction of the sample or artefact-based understanding of the mechanisms of Achilles tendinopathy. Furthermore, the application of CA and AFM avoids the disadvantages brought by the biopsy process and provides an efficient, easy and less laborious method to evaluate the changes in tendons, as compared with conventional histological methods.

1.5 Specific Aims

1) To achieve the stated goals of the study, fresh-frozen rabbit Achilles tendons, with mechanical damage induced by a Micro-mechanical tester (Instron) over 4 hours of repeated cyclic loading under 3 strains, were analysed for macroscale structural and mechanical changes that were observed using CA and conventional histology with repeated measures and comparison between groups across time .

The hypotheses for Aim 1 are:

A) That there are a sequential dose and strain change effects on the tested variables of the examined macrostructural and mechanical domains (fibre crimp frequency, anisotropy, GAG content, tenocyte morphology, hysteresis, maximum load and stiffness) in fatigue loaded tendons.
B) That there are significant differences between the stiffness, hysteresis, and maximum load capacity of the depleted and undepleted tendons.

2) The variable of the examined nanoscopic domain (change in D-periodicity) was examined to detect the nanostructural changes and to determine correlations with the endpoint-of-dose assessments of each tendon from Experiment 1.

The hypotheses for Aim 2 are:

A) That there is a sequential dose and strain change effect on the D-periodicity values of the examined low (3%), moderate (6%) and high (9%) level strain groups that were subject to repetitive static and cyclic fatigue loading.

B) That there are no significant differences between the strained tendon groups in the D-periodicity distribution within and between fibril bundles (WFB and BFB) over different doses (The D-periodicity.

C) That changes in nano-structural derived variables are homogeneous along the fibril length significantly related to changes at the macroscopic level.

D) That there are no significant differences in the characteristic D-Periodicity within the same fibril bundle and between different fibril bundles.

Finally, the mechanical model of tendinopathy was combined with the depletion model to examine the nanoscale changes with a depletion of GAGs.

3) We aim to explain the reported gap in knowledge between collagen fibril strain and applied tendon load by offering a more accurate and direct quantitative approach examining fibril load distribution WFB and BFB as a mechanical strain response of nanostructure to applied tendon load (Aim 3).

To examine this, collagen fibril strain WFB and BFB of the loaded GAG-depleted tendon was measured, presuming that WFB and BFB D-periodicity change is a proxy measure of collagen fibril strain. This group was compared with the strained undepleted control groups from Experiment 1.

Our hypotheses for Aim 3 are:

A) That GAG depletion increases the rate of failure at both the nano and macro scales.

B) That there are significant differences between the mechanical domains of the depleted and un-depleted tendons.

C) That the changes in the nanostructural domain (D-periodicity) are strongly correlated with the changes at the macroscopic structural and mechanical domains.

CHAPTER TWO:
LITERATURE REVIEW

2.1 Introduction

Tendons are anatomically distinctive connective tissues that contribute to the balance of three-dimensional affiliations among muscles, joints and bones (Lanir, 1978). The composition and microstructure of tendons is related to their function, which includes load bearing and transmission of the mechanical force generated by muscles to the skeletal structure, and enables joint movement. To perform these tasks, the tendon relies on distinctive mechanical characteristics controlled by the extracellular matrix (ECM) and the ability to respond to a broad range of stresses and strains. Muscles influence the torque acting across a joint through the generation of tensile force transmitted through the tendon. Therefore, there is a morphological association between the muscle and tendon defined by both form and function at various macro- and microscales. The association between form and function is specifically important for studies of the Achilles tendon that are related to the significant functional stretch and shortening activities of gait and ambulation.

2.2 Background

2.2.1 The Function and Anatomy of the Achilles Tendon

Tendons are surrounded by loose connective tissue and enveloped by the paratenon. The paratenon is a two-layered membrane with a fine layer of connective tissue known as the epitenon located adjacent to the tendon (Kannus & Jozsa, 1991). The fascicles are gathered together, surrounded by epitenon, forming the tissue's gross structure, which is then surrounded by the paratenon. The epitenon joins several fascicles and assists in the development of the tissue's supramolecular configuration. The internal surface of the epitenon is continuous with the endotenon, which surrounds and connects the primary, secondary and tertiary fibre bundles (see below) and binds them together (Paavola et al., 2002) forming large hierarchical structural groups of collagen fibres and fascicles (Figure 2.1). The fascicles are composed of fibre bundles, each is

composed of a fibril bundle. Each fibril bundle is composed of fibrils that each made of a triple helix of peptide strands known as a collagen molecule (Figure 2.1).

Fluids between the epitenon and endotenon provide lubrication and protection of the tendon tissue from friction (Järvinen et al., 1997; Paavola et al., 2002). The fluids facilitate the sliding of the fibre bundles past each other and the free movement of the tendon, and support the vasculature that supplies deeper portions of the tendon, including the endotenon and epitenon (Paavola et al., 2002). Healthy tendons are resilient to mechanical loads, especially tensile forces. The transmitted force at the myotendinous junction relies on both the structural configuration between different muscle fibres and the extracellular matrix (ECM) (Paavola et al., 2002) and on the fibrillar organisation that makes the tendon more resistant to load and able to absorb more energy (Kastelic et al., 1978; Magnusson et al., 2010).

Tendons are made of groups of fascicles that are connected to the muscles. A primary fibre bundle is comprised of a set of collagen fibres. These are grouped together to form secondary fibre bundles. A set of secondary fibre bundles forms the tertiary fascicle (Figure 2.1). Along the endotenon, all nerves, vessels, arterioles and capillaries enter the tendon and do not penetrate the collagen bundles.

The literature does not always describe the scale of the anatomical description of the Achilles tendon. The first level of the hierarchical structure of the Achilles tendon is a cylindrical strand known as a fascicle (Figure 2.1). Zooming further in, the fascicles appear to consist of fibres on the ~10 μm scale and this is the minimal visible unit using light microscopy (Paavola et al., 2002) (Figure 2.1). Bundles of fibres (mostly Type I collagen) form the main body of a tendon, lying parallel to its long axis, which gives the tendon its inherent tensile strength. At higher magnification, the fibres can be seen as bundles of small threads known as fibrils that are the main building blocks of the tendon ECM (Järvinen et al., 1997; Paavola et al., 2002). Fibrils play a fundamental role in force transmission (Magnusson et al., 2003), structural intactness of the ECM and cell homeostasis (Dallas et al., 2006; Sivakumar et al., 2006). The collagen molecules in fibrils can be observed with similar conformations, showing overlapping stripes on the surface of the collagen fibril. These are aligned along the

longitudinal axis and are considered the most important morphological characteristic of the tendon, the so-called D-periodicity (Fratzl, 2008; Fang et al., 2012) (Figure 1).

The D-periodicity is a critical feature of the ultrastructure in the collagen fibril and has been linked to the underlying collagen fibrillogenesis (Fang et al., 2012). At further magnification, the fibrils can be seen as bundles of smaller threads which are called subfibrils. Zooming further in, the subfibrils are seen to be bundles of five smaller tropocollagen units (Marchini et al., 1986) (Figure 1), which are the basic units of the collagenous structure (Järvinen et al., 1997; Paavola et al., 2002). The main characteristic of a fibrillar collagen molecule is the triple-helical polypeptidic chain, and in the collagen molecule these chains are twisted together, forming a super-strong and stable coiled cord. These large multi-level hierarchical groups of tendon fascicles, fibre bundles, fibrils, subfibrils and collagen molecules running parallel to the tendon's long axis, maintain the fibroblasts of the tendon. Fibroblasts have a role in the synthesis of macromolecules for the ECM (Movin et al., 1997). Despite the various ECM hierarchical structures (see Figure 2.1), the aggregation of fibrils forming microscale bundles is abundant among collagenous tissues (Birk et al., 1989).

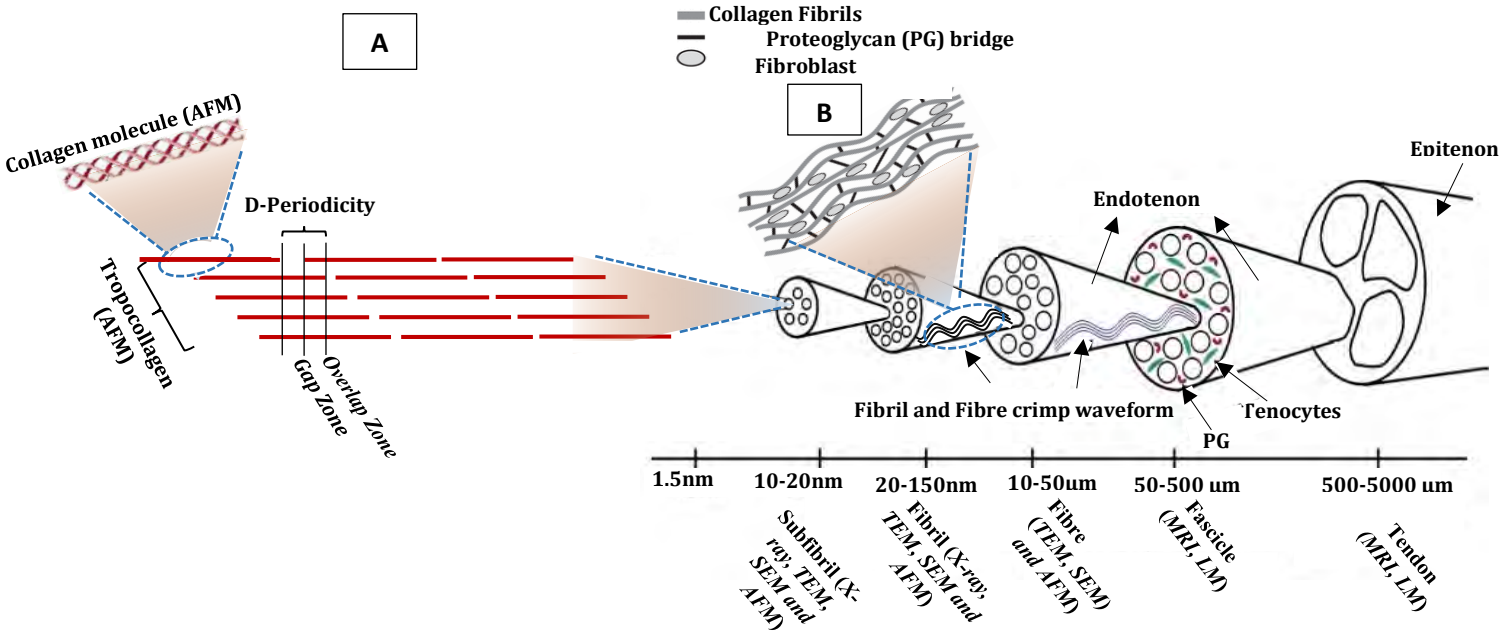

Figure 2.1. A schematic diagram of a tendon showing its organisation as identified from nanoscale to macroscale imaging techniques (Kastelic et al., 1978; Magnusson et al., 2010; Martufi & Gasser, 2012). On the right-hand side, the fascicles are gathered together, surrounded by epitenon, forming the tendon's gross structure. On the left-hand side, the inset image (A) shows the D-Periodicity as a regular stripe that is visible on the surface of the collagen fibril along the longitudinal axis. An overlap of the molecules results from the spontaneous lateral arrangement of the collagen molecules. In each molecule of tropocollagen, the gap zone is seen to lead to the D-periodicity. The inset image (B) describes the structure of fibril-associated proteoglycans (PGs), the collagen fibrils are interlinked by PG bridges and populated by fibroblast cells.

2.2.2 Achilles Tendinopathy Models

A complete subcutaneous tear is one of the distinctive injures that the Achilles tendon most commonly undergoes (Maffulli et al., 2017). The rupture of the Achilles tendon is particularly common in athletes who infrequently take part in sport (Maffulli et al., 2017). Achilles tendinopathy and rupture result from a large range of disorders involving mechanical damage as well as degenerative diseases and symptoms. These affect a wide range of people, from young athletes to aged individuals. However, scientific and clinical knowledge of the pathological development from healthy tendon to tendinopathy and, ultimately, tendon rupture is yet not clear. Tendinopathy is suggested to be the cause of the majority of Achilles, patella and quadriceps tendon ruptures. Indeed, cyclic loading and/or overuse has been widely accepted to be a major cause of tendon failure (Kelly et al., 1984; Järvinen et al., 1997; Paavola et al., 2002). Therefore, tendinopathy is often considered as an overuse pathological condition and, in some particular cases, thought to be related to the fatigue failure of tissues during cyclic loading.

There are two dominant animal models established to model tendinopathy. Firstly, the mechanical model of tendinopathy, where repeated application of a sub-traumatic level stimulus induces tendinopathic changes. This overload model provokes injury through repeated mechanical loading that is, in some models, considered to be a major contributing factor to how tendinopathy develops or is maintained in some human cases. However, Achilles tendinopathy does not always exist in persons who take part in vigorous sports and about one-third of people with Achilles tendinopathy are not involved in high physical activity (Movin et al., 1997). A second, chemical model induces tendinopathy through injecting cytokines to cause inflammation (Stone et al. 1999), collagenase to cause collagen breakdown (Soslowsky et al., 1996), or antibiotics (Kato et al., 1995; Simonin et al., 2000) or prostaglandins (Sullo et al., 2001) where both are thought to have a relationship with tendinopathy. These models permit an interaction between mechanical loading, inflammatory cells and healing of the tendon tissue (Lake et al., 2008) and are usually immediate protocols and generally cause more consistent damage to the tendon's tissue compared to mechanical loading (Dirks & Warden, 2011).

The chemical model of investigation is often used to determine immediate changes in the cellular response. This model differs in many aspects from the fatigue/mechanical loading model of tendinopathy. The mechanical model is beneficial since it is designed to cause tissue damage through cyclic loading, analogous to tendinopathy development in humans.

2.2.3 Tendon Mechanics

The functionality of the tendon is related to its mechanical properties; therefore, it is important to define the mechanical properties of the tendon in order to comprehend the normal and abnormal states of the tendon (Duenwald-Kuehl et al., 2011; Duenwald-Kuehl et al., 2012). Various studies have investigated the stress-strain behaviour of tendons and collagen fibres (Puxkandl et al., 2002; Magnusson et al., 2003; Silver et al., 2003; Dowling & Dart, 2005; Wang, 2006). When the tendon is loaded and stretched, the resulting elongation is depicted as stress-strain relationship (Figure 2.2). In the hydrated state, the typical stress-strain relationship of the tendon demonstrates three distinctive regions (Fratzl et al., 1998). It begins with an initial low-stiffness so-called non-linear toe and heel region, followed by a high-stiffness linear region and consequent failure (Connizzo et al., 2013).

Beyond 4–5% of tendon strain, all of the matrix structure is believed to be mechanically engaged and to cumulatively contribute to resist the load. Therefore, the stress-strain curve beyond this point changes to linear (Wang, 2006) (Figure 2). The fibrils are believed to bear the increased load by straightening and eliminating the microscopic kinks located in the gap region of the molecular quarter, the staggering of collagen and the lateral molecular increased order that exists within these fibrils (Misof et al., 1997). Further, beyond 5% strain, the elongation of D-periodicity is suggested to explain nearly half of the elongation of the fibre (Puxkandl et al., 2002).

The toe region of the stress-strain graph depicts an increasing slope with a strain up to 2%. This strain can be seen by an optical microscope, and is characterised by the elimination of the macroscopic crimp in the collagen fibres and the gradual recruitment of crimped collagen fibres (Abrahams, 1967; Diamant et al., 1972; Cribb

& Scott, 1995; Hansen et al., 2002; Screen et al., 2004; Franchi et al., 2007) (Figure 2.2). The usual linear stress-strain behaviour of the tendon is considered to occur from approximately 3% strain and extends to approximately 4–5% of tendon strain (Wang, 2006) (Figure 2.2). Although the gradient of the overall stress-strain curve of a tendon varies according to the load, the slope of the linear region is commonly defined as stiffness (*k*) (Heinemeier & Kjaer, 2011). While the load remains within the elastic range of elongation (i.e. within the linear range) tendon strain is fully reversible and the tendon returns to resting length as the load is removed (Järvinen et al., 1997). Loading conditions that cause plastic changes in the tendon are often investigated to determine the contribution of sub-elements within the tendon structure to tendon behaviour. For example, repeated stretching with increasing force causes the aligned collagen molecules within the fibre to start to slide along each other and extend (Folkhard et al., 1987; Sasaki & Odajima, 1996). Although this understanding of fibre behaviour has been proposed, it has not been thoroughly studied nor quantified during load testing.

Standard material testing or mechanical assessment of the linear region of the stress-strain relationship is often used to determine the stiffness of the tendon (Arampatzis et al., 2009; Heinemeier et al., 2011). At the end part of the linear region, the collagen fibers begin to slide past one another as the cross-links start to fail which results in microscopic failure, representing the yield or plastic region as the third portion of the stress-strain relationship. This region deviates from the previous linearity and is characterised by lower stresses with substantial variations in elongation (Nigg & Herzog, 1999). Beyond 8% strain, macroscopic failure exists and the capacity of the tendon to support load almost completely vanishes (O'brien, 1992). Further stretching leads to rupture of the tendon (Wang, 2006) (Figure 2.2) with tensile strength in the range of 30–160 MPa (Weiss & Gardiner, 2001; Wren et al., 2001).

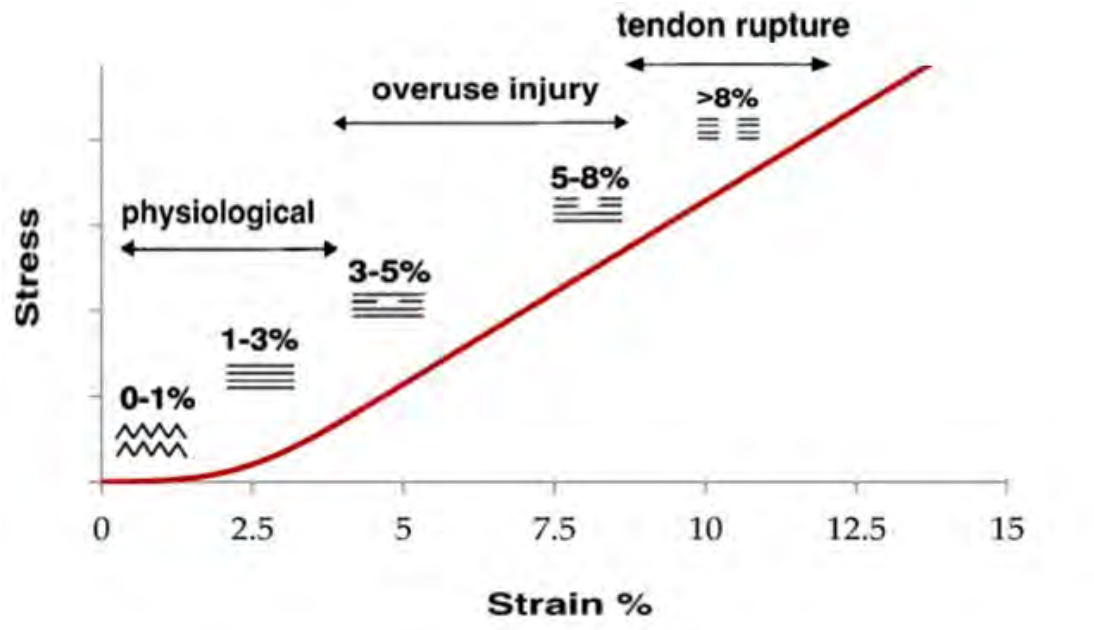

Figure 2.2. A tendon stress-strain curve representing the fibre crimp response to load. Wave-like lines represent the fibre crimp of the tendon at the resting stage. Unbroken straight lines indicate the effect of tensile stresses (at strain levels < 4 %); when the load is removed within the range of this region of the curve, the tendon strain is fully reversible and resumes its original state. One or two broken lines represents the region where the collagen fibrils start to slide along one another due to the failure of intermolecular cross-links. As intermolecular sliding occurs, the D-periodicity elongates because it is reflective of the relative axial positioning of neighboring molecules. The complete set of broken lines represents the macroscopic rupture caused by the interfibrillar shear failure and tensile failure of the fibres. Modified and adapted from (Järvinen et al., 1997; Maffulli, 1999; Young et al., 2016).

It is important to note that although the percent strain characteristics have been described consistently in the literature, there is a lack of consensus about the points at which the three phases occur. One major factor in this is that there are large variations in testing protocols, and more importantly, the strain is often defined after a preliminary “preconditioning” of the samples. Furthermore, repeated testing protocols may maintain either a constant stress (force) or strain (elongation) and therefore the progression to failure is likely to be a product of the repetitions and the degree of strain (or stress).

A. Stress relaxation (SR), creep and hysteresis (*h*)

Tendons exhibit viscoelastic characteristics known as creep, *h* and SR (Woo et al., 2005; Finni et al., 2013). These velocity- and time-dependent characteristics are considered to be vital for the optimal function of the macroscopic tendon tissue (Purslow et al., 1998) and have been widely investigated in tendons (Butler et al., 1978; Järvinen et al., 1997; Puxkandl et al., 2002; Robinson et al., 2004; Screen et al., 2004; Provenzano & Vanderby, 2006; Wu, 2006; Wu et al., 2006).

As a useful technique, SR tests have been frequently employed in rheology to explain the viscoelastic behaviour of tendons, giving insight into the function of the tendon sub-components (Wu, 2006; Wu et al., 2006). Due to the broad diverse range of materials, a variety of linear and non-linear viscoelasticity equations have been suggested to demonstrate the relationship between time and stiffness (or stress, or force) of tendons (Hernández-Jiménez et al., 2002; Abu-Abdeen, 2010). SR denotes a non-linear decline in stress over a period of time under a constant tension (strain) where the decline in associated load is measured (Atkinson et al., 1999). Basically, this explains the situation when the tendon is under loading – the fibrils, fibres and fascicles gradually relax/elongate over time until reaching a stable state.

Alongside some curve-fitted mathematical expressions, the experimental data are usually demonstrated according to mechanical models, and consist of different linkages of ideal dashpot (according to Newton's law) and spring (according to Hooke's law) elements. Among these, the Maxwell model is the most common model in the literature employed to study the SR behaviour of various materials.

Applications of the Maxwell model used to describe the normalised force as a function of time have shown two relaxation functions with variable half-relaxation times (Usha et al., 2001; Gupta et al., 2010). These two SR modes are classified as slow and fast relaxation times (Usha et al., 2001; Gupta et al., 2010). Usha and colleagues suggest that the fast-relaxation mode was concomitant with the sliding of collagen molecules that are held by hydrogen bonds. Their results indicate that fibres with more crosslinks relax faster.

The slow-relaxation mode was associated with the engorgement and dissociation of the fibre bundles, which is mediated by different pH levels. Two important conclusions about the SR of human patellar tendons were first reported by Atkinson et al. (1999). First, the SR is larger when bigger tendon portions are loaded. This is crucial since it points to the fact that during SR, the intrinsic strength differences of different fascicle or fibre locations are being exposed. This may suggest that during SR there is a differential loading and elongation of the fibres within the tendon, and that as some fibres elongate, the internal stressors are transferred to other fibres over time. There are relatively new clinical hypotheses that stress shielding may be a mechanism of sustained tendinopathy in humans after repeated cyclic loading (Orchard et al., 2004).

In comparison to SR (where strain is kept constant), creep is observed when a tendon is held under a constant load and the increase in extension (length) is measured. In this situation, creep is defined as the proportional increase in length during the load-bearing time (Butler et al., 1978; Järvinen et al., 1997). Therefore, both SR and creep describe a common domain of the tendon's response to sustained mechanical load. However, these responses also take place during cyclic loading, (Ker, 2002; Legerlotz et al., 2013) where the cyclic testing maintains displacement (strain) or load (stress) control respectively (Thornton et al., 2002; Legerlotz et al., 2013). Under different conditions, the two testing methods would be anticipated to stimulate different responses of the loaded tendon. The testing of SR of tendon fascicles is usually more straightforward to accomplish, while creep testing is more relevant to physiology. The time-dependent characteristics of tendon will certainly influence the conversion of contraction of muscles into skeletal movement, and so, both SR and creep behaviours should be clearly defined to predict tendon behaviour accurately (Duenwald et al., 2009).

Hysteresis (*h*) refers to the amount of energy lost within the tendon during dynamic loading and unloading testing and accounts for a gradual change in the stress-strain curve with tendon loading and unloading. This energy dissipation is calculated as the area between the loading and unloading stress-strain curves in cyclic tensile testing (Freedman et al., 2014; Freedman et al., 2015; Connizzo et al., 2016). The stretching

and recoiling of the tendon during a loading cycle is indicated as a loop in the stress-strain curve (see Figure 2.3).

The amount of *h* is crucial for efficient locomotion. High *h* is related to high energy dissipation, and therefore less energy can be recoiled to drive movement activities. The literature reports *h* < 10% in sheep plantaris tendons (Ker, 1981) and about 10% in tendons from other mammals (Bennett et al., 1986; Pollock & Shadwick, 1994).

Although high *h* values have been reported particularly in *in-vivo* human-based studies, other authors have reported that lower *h* values seem to be more realistic since they ensure higher elastic recoiling and can reduce heat damage (Bennett et al., 1986; Alexander, 2002; Ker, 2002). Furthermore, these authors attribute the differences observed in the human studies to inconsistencies and difficulties of *in-vivo* tendon stretching measurements (Finni et al., 2013).

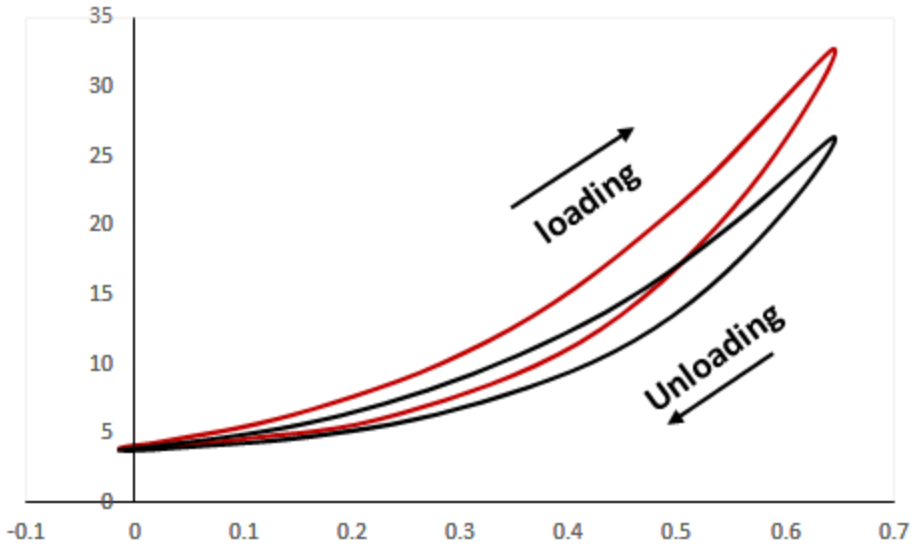

Figure 2.3. The stress-strain curve during the repeated cyclic loading of a tendon. The stress-strain curve progressively shifts to the right as a reduced amount of *h* under cyclic loading and ultimately a reproducible stress-strain curve is observed.

The elongation of the tendon is higher during lower strain rates. Therefore, the tendon is less effective in transferring loads since it absorbs more strain energy. With higher strain rates, tendon elongation is smaller (higher stiffness) and more efficient load transfer takes place (Järvinen et al., 1997; Wren et al., 2001; Alexander, 2002).

However, an examination of the viscoelastic behaviour of rat-tail tendons has shown that the overall strain of the tendon is always larger than the strain in individual fibrils (Puxkandl et al., 2002). Therefore, the behaviour of the whole tendon is more than the cumulative capacity of the collagen fibres. It has been argued that there is some elongation in the matrix between fibrils where both the interfibrillar matrix and collagen fibrils interact as a coupled viscoelastic structure (Puxkandl et al., 2002).

Provenzano and Vanderby (2006) came to a similar conclusion:; the attachment (specifically decorin) to collagen fibrils that occurs during tensile elongation was shown to improve the transfer of energy among fibrils (Provenzano & Vanderby, 2006). Nevertheless, it was also proposed that the interfibrillar PG bridge did not transfer the force in the tendon but directly transferred force through the fibrils, and the underlying mechanism of the viscoelastic behaviour was attributed to the sliding of the collagen fibres (Screen et al., 2004; Bruehlmann et al., 2005; Provenzano & Vanderby, 2006; Cheng & Screen, 2007). While the viscoelastic behaviour of tendons and collagen fibres has been extensively studied, the underlying mechanism for this behaviour is yet not fully determined.

B. Tendon fatigue in response to mechanical loading

Cyclic loading of Achilles tendons during walking or running induces micro-damage of the tendon and provokes repair processes to retain tendon homeostasis. Tendon damage can reduce the mechanical strength and change the biomechanical behaviour of tendons, and consequently can impair normal functions, for example, joint movement and stabilization (Duenwald-Kuehl et al., 2012). Tendon damage can exist even if the tendon is loaded within physiological limits since repetitive accumulation of microtrauma may lead to an imbalance in the equilibrium between the cellular-driven rate of repair and the rate of damage (Archambault, 2003; Archambault & Banes, 2005; Maffulli, 2011). Microtrauma can be induced by nonuniform stresses within the tendon tissue producing frictional forces between fibrils, abnormal load concentrations and localised fibre damage (Maffulli, 2011). It is reported that cyclic loading in tendons causes ‘sub-failure injuries’ or ‘micro-damage’ ‘gradually at the collagen nanoscale level’, and the injuries and damage are collectively known as

‘mechanical fatigue damage’(Wren et al., 2003; Kongsgaard et al., 2005; Fung et al., 2010). Fatigue testing can be conducted by repeated elongation from repeated cyclic loading, either under displacement (strain) or load (stress) control (Shepherd & Screen , 2013). Although Achilles tendon rupture may appear to be a sudden event, degenerative changes are commonly observed in ruptured tendons (Bell et al., 2015), supporting a proposed aetiology associated with a gradual accumulation of micro-damage (Wren et al., 2003; Wang, 2006). Tendon damage increases when the number of loadings and the maximum strain increases, indicating that the Achilles tendon is susceptible to an over-use injury and potentially can rupture.

C. Mechanical changes

The progression mechanisms of tendinopathy remain poorly understood and are yet to be elucidated. Understanding these mechanisms related to early tendinopathies and further damage accumulation is fundamental to develop effective therapeutic interventions. Investigating the structure-function relationships during high dynamic loadings is crucial for understanding the potential mechanical mechanisms that govern fatigue-induced damage and injury. Tendon fatigue is characterised as a three-phase pattern of damage (see below). This damage is suggested to accumulate and may be reflected in an experimental protocol that utilises creep-based loading experiments (Wang & Ker, 1995). In the experiment of Wang & Ker (1995) it was reported that stiffness decreased throughout the experiment, slowly at first, before increasing immediately prior to failure.

The majority of previous studies focus on the relationship between the applied stress and time, or number of cycles, to failure. However, only limited *in-vivo* and *ex-vivo* animal model studies have been conducted using structural image-based measures to correlate the mechanical and structural responses to fatigue loading (Fung et al., 2010; Andarawis-Puri et al., 2011; Neviaser et al., 2012). Also, there are only limited studies reporting sub-rupture tendon behaviour (Backman et al., 1990; Archambault et al., 2001; Nakama et al., 2005; Fung et al., 2009) and as yet no experimental protocols use both strain extensions and a number of cycles. Increasing cyclic strain can cause a clamp-to-clamp elongation of the tendon indicating that when the fibre length

increases increased levels of fibril damage may exist. This is supported by pioneering *ex-vivo* and *in-vivo* work that has successfully described the structural response of the tendon to fatigue loading using the rat flexor digitorum longus (FDL) (Fung et al., 2009; Fung et al., 2010; Andarawis-Puri et al., 2011).

These studies quantified the changes at controlled fatigue levels in the mechanical characteristics and the associated morphological changes that reflect microstructural changes (Fung et al., 2009; Fung et al., 2010; Andarawis-Puri et al., 2011). The paradigm of the work included repeated cycles of a controlled load (stress) to investigate the early onset of tendinopathy and was therefore important for the assessment of the progressive relationship between damage and load. The mechanical results show that maximum strain has three transitional clear phases during fatigue loading to failure. The first transitional phase at 6–7% applied strain (low level, ~300 cycles) shows an increase in maximum cyclic strain and tendon stiffness but no change in *h*.

After the first phase there is a transition to a second transitional phase. This phase, at 8.5–9.5% strain (moderate level, ~500 cycles), was characterised by no change in either *h* or *k* and a plateau in maximum cyclic strain. The third transitional phase, at 11–12% strain (high level ~700 cycles), showed a significant decrease in both hysteresis and stiffness and a sudden increase in maximum cyclic strain. However, the number of cycles was a significant ($p < 0.001$) factor for tangent stiffness, peak strain and hysteresis, and all mice tendons reached the second phase of fatigue loading (Fung et al., 2009) without rupture even after 1,000 cycles of fatigue loading (Freedman et al., 2015).

There is, however, inconsistency in all levels of fatigue between the mechanical results reported by Fung et al. (2009) and those been reported by Fung et al. (2010), Neviaser et al. (2012) and Andarawis-Puri and Flatow (2011). These latter studies defined the three stages of fatigue as low (0.6%, 2,232 cycles), moderate (1.7%, 10,579 cycles) and high (3.5%, 16,997 cycles) (Fung et al., 2010; Andarawis-Puri et al., 2011; Neviaser et al., 2012)). At the low and moderate fatigue levels, *k* increased by about ~18% and *h* decreased by ~30%. Whereas, high-level fatigue loading produced a ~17% decrease in *k* and a ~25% increase in *h*. Significant differences in *k*

and *h* were observed between the high fatigue level and both low and moderate fatigue levels. Evaluation of the three stages of fatigue loading in the above studies support the hypothesis that fatigue loading induces cumulative fatigue damage, demonstrated by morphological changes. To date, few studies have repeated the fatigue levels reported by Fung et al. (2009). Moreover, these studies examined the sustained load (stress) while reporting increased elongation or strain. Therefore, future research may be able to contribute to the understanding of fatigue loading using models controlling strain and examining load.

The main source of inconsistency in the mechanical results between the above studies is perhaps the significant differences in the number of loading cycles and strain levels used in their experimental protocols. This inconsistency is supported by the findings of an *ex-vivo* study by Wren et al. (2003) who have also investigated the fatigue response of human Achilles tendons to cyclic mechanical loading in an *in-vitro* model (Wren et al., 2003). They studied the static creep effects on the mechanical characteristics of human Achilles tendons and reported that the strain (as measured at first loading to a predetermined stress level) was the best predictor of cycles or time to failure (Wren et al., 2003). This supports the suggestion that strain is the primary mechanical factor leading to injury and accumulation of damage in tendons (Wren et al., 2003). During the first transitional phase, the uncrimping of a combination of fibres and the loading of other fibres, happens while water is being extruded. During the second transitional phase, most fibres are responding to the increase in maximum strain.

The sudden increase in maximum strain reported by Fung et al. (2009) is likely due to the recruitment of fibres and redistribution of load from damaged to undamaged fibres (Fung et al., 2010; Andarawis-Puri et al., 2011). During the third transitional phase (high-level loading), more damage may result from nonuniform stress within tendons in such a way that it cannot overcome the fibre recruitment and load redistribution mechanism (Fung et al., 2010); therefore, the tendon's tissue may experience increased force concentrations, fibrillar frictional forces, and local fibre damage (Maffulli, 2011).

This eventually results in fibre rupture, a sudden increase in tendon strain and a reduced stiffness that can eventually cause gross tendon failure under continuous load (Thornton et al., 2003). However, the mechanisms of damage progression and severity in the matrix structure and at multiscale levels, as well as the distinctive contribution of the magnitude, pattern and frequency of loading over a prolonged period time of mechanical intervention has yet to be fully assessed. Therefore, there is a necessity to develop a mechanical-damage tendon model that incorporates broader mechanical static and dynamic measures (for example, SR, *h* and *k*).

D. Mechanically induced macrostructural changes

An important characteristic of tendinopathy is the disruption of the tendon microstructure (Longo et al., 2008; Arya & Kulig, 2010), making the analysis of collagen structure critical in order to comprehend tendon response to cyclic loading. Early studies of tendon fatigue observed that an increased applied stress gave an exponential decline in the number of cycles required for failure in the wallaby hind leg (Ker et al., 2000) and human extensor digitorum longus (Schechtman & Bader, 1997). However, the evaluation of structural changes in these studies was limited to a few derived variables (Wang & Ker, 1995; Schechtman & Bader, 1997; Pike et al., 2000; Wren et al., 2003; Freedman et al., 2014).

Methods for the assessment of structural changes following fatigue loading have ranged from histology, (Fung et al., 2010; Shepherd et al., 2014) to second harmonic generation (Fung et al., 2010; Ros et al., 2013), polarized light imaging (Freedman et al., 2014), scanning electron microscopy (SEM) (Veres et al., 2013), and confocal imaging using photo-bleaching (Thorpe et al., 2014). However, although there are a number of reported tendon fatigue mechanics (Veres et al., 2013; Thorpe et al., 2014) limited studies have reported relationships between structural changes during fatigue loading (Fung et al., 2009; Fung et al., 2010; Freedman et al., 2014). For example, Fung et al. (2009) found that unloaded control tendons exhibit highly parallel and aligned collagen fibres, characterised by crimp formation and a columnar arrangement of the tenocytes between the fibres. While the study by Fung et al. (2009) validates the loss of stiffness as a damage marker that resulted from cyclic loading, their results

also show that clamp-to-clamp strain is an accurate and useful indicator of cumulative damage in tendon fatigue progression (Fung et al., 2009). Also, in this study the tendons only demonstrated significant changes in hysteresis and stiffness with high levels of fatigue, but microscale structural changes were evident early in the experimental loading protocol. These changes included isolated kinked deformations in the fibres (Fung et al., 2009). These observations are supported by other studies which have reported similar observations (Fung et al., 2010; Neviaser et al., 2012), as well as reports of other damage markers such as a disturbed tenocyte arrangement and organization when tendons are loaded to a low-level fatigue (Fung et al., 2009; Shepherd & Screen, 2013).

Tendons loaded to a moderate-level fatigue have shown analogous changes; however, the changes occur in larger areas, there is a greater density of deformation patterns comprising fibre dissociation (Fung et al., 2010; Neviaser et al., 2012) and few examples of isolated fibre disruption have been noted (Fung et al. 2009 and Shepherd et al. 2012). In high-level fatigue-loaded tendons, severe micro-architecture disruption, discontinuity, thinning and increased anisotropy and dissociation of fibres have been observed (Fung et al., 2009; Fung et al., 2010; Neviaser et al., 2012; Shepherd & Screen, 2013).

A better understanding of tendon damage accumulation can be established by correlating the microstructural damage from controlled *ex-vivo* (Fung et al., 2009; Shepherd & Screen, 2013) and controlled *in-vivo* morphological data (Fung et al., 2010; Andarawis-Puri et al., 2011) together with mechanical results from Fung et al. (2010) and Neviaser et al. (2012) (See Table 2.1). Notably, the development of macrostructural changes seems consistent in all fatigue-damage methods employed by these studies.

Table 2.1. The development of fatigue damage from fatigue controlled *ex-vivo* (Shepherd & Screen, 2013) and controlled *in-vivo* (Fung et al., 2010; Andarawis-Puri et al., 2011; Neviaser et al., 2012) loading studies demonstrating the effect on collagen fibre morphology and mechanics.

Fatigue level with a constant stress	**Collagen fibre morphological changes**	**Mechanical changes**
No fatigue	Highly parallel and aligned fibres, characterised by distinctive crimp formation	
Low fatigue level	Isolated kink fibre formation and disturbed tenocyte arrangement and organisation	Decreased hysteresis and an increased stiffness
Moderate fatigue level	Kink fibre deformation, greater density of deformation patterns comprising of broadening of the inter-fibre space and isolated fibre ruptures	No difference from changes at the low fatigue level
High fatigue level	Severe fibre disruption, discontinuities and fibre angulations, thinning and increased anisotropy of fibres and increased dissociation among the fibres	An increase in hysteresis and a decrease in stiffness, with a sudden increase in tendon strain

Generally, previous imaging experiments focused completely on the macrostructural level of the tissue. However, the nature of multiscale fatigue-induced damage has not been fully explained. To date, there is no study examining the multiscale structural changes within the same nonviable intact/bulk tendon in response to prolonged cyclic and static loading protocols. Testing of nonviable bulk tendons is comparatively straightforward and has been suggested to provide clear data regarding the mechanics of fatigue damage (Shepherd & Screen, 2013).

It is important to determine the response of the tendon to mechanical load across multiple hierarchical levels (fascicle, fibre and fibril levels) and to quantify the structural changes by combining non-invasive and nondestructive multiscale advanced techniques with techniques that measure mechanical characteristics (Screen et al., 2003, 2004; Rigozzi et al., 2011; Miller et al., 2012). The gap in the current literature is, therefore, a single study that utilises an instrument such as the confocal arthroscope that can be integrated with a mechanical loading device during mechanical loading experiments. This will allow concurrent loading and imaging at the multifascicle and fibre-level scales, which in turn can be compared with atomic force microscopy (AFM) images that examine the fibril level. Therefore, multi-scale imaging of the same bulk tendon tissue that includes the use of equipment that does not require sectioning of samples, such as CA, and can conserve tissue's structural details, such as AFM, warrants further investigation.

E. Mechanically induced nanostructural changes

Although many previous studies have examined the tendon structure-function relationship at the nanoscale level, many of these studies are unclear with regards to the exact nanostructural mechanisms that led to the viscoelastic mechanical properties of the tendon (Gupta et al., 2010). Non-collagenous matrix composition and collagenous fibril morphology are broadly suggested to govern the macroscopic behaviour of the tissue (Robinson et al., 2004; Screen et al., 2006; Fessel & Snedeker, 2009; Rigozzi et al., 2009). However, the mechanisms by which these characteristics are translated to the function of the tissue is still poorly understood. This is partially

due to limitations in the methodologies used to quantify strain under mechanical load (Sasaki et al., 1999; Kukreti & Belkoff, 2000; Franchi et al., 2010).

For instance, a study using X-ray diffraction has reported that an application of 20 MPa of stress to tendons has been associated with a 3% D-periodicity change (nearly 2 nm) (Brodsky et al., 1980), while another study using scattering X-ray spectroscopy reported that a macroscopic tendon strain of 3% was associated with a 1 nm change in D-periodicity (Sasaki et al., 1999). Furthermore, another study using transmission electron microscopy (TEM) reported an average 4% increase in D-periodicity with a gross ligament strain of 8% (Kukreti & Belkoff, 2000).

Each of these studies has provided vital but partial insight into tendon nanomechanics; however, none of the methods used in these studies could characterise the heterogeneity in the load distribution of fibrils. From these studies, the size of D-periodicity change as a function of tendon strain is not broad enough to explain the D-periodicity distribution seen across different tissues, which has a characterised range of 10 nm (Wallace et al., 2010; Fang et al., 2012; Erickson et al., 2013).

A comprehensive investigation of the relationship between structure and function of tissues is complex and requires a multiscale approach. Since the ultrastructure of collagen is closely related with function (Ottani et al., 2001), attempts to correlate collagen nanostructure with mechanical characteristics have used different methodological equipment such as optical microscopy and SEM (Okuda et al., 2009; Franchi et al., 2010), X-ray scattered spectroscopy (Misof et al., 1997; Puxkandl et al., 2002; Gupta et al., 2010) or AFM (Habelitz et al., 2002; Graham et al., 2004). However, the morphometric analysis of fibril strain by TEM and X-ray spectroscopy is limited by technical difficulties that prevent direct assessments of quantitative measures of fibril length changes (changes in D-periodicities) and ultimately the mechanical strains.

There have been limited studies focused on correlations between tendon characteristics across hierarchical structures. It has been noted that diurnal changes in tendon stiffness (where there is greater stiffness in the evening than in the morning) relate to the hypothesis of continued fibril damage and repair establishing a

homeostasis of mechanical function (Onambele-Pearson & Pearson, 2007). The findings of such studies are consistent with various other models in animal-based studies that reported an accumulation of fibril damage under load and strain as a result of diurnal activities (Sereysky et al., 2012). Damage in fibrils may be more complicated than damage in tissue at the macroscale level. Initial damage possibly involves denaturing, stretching, fraying, fragmenting and splitting of the collagen fibrils and fibres that then lead to a complete rupture (Kastelic & Baer, 1980; Kannus & Jozsa, 1991; Sonnabend et al., 2001; Jarvinen et al., 2004; Fung et al., 2009; Sereysky et al., 2012). Fung et al. (2009) have suggested a useful animal model of fibril damage (Figure 2.4) based on the histological appearance.

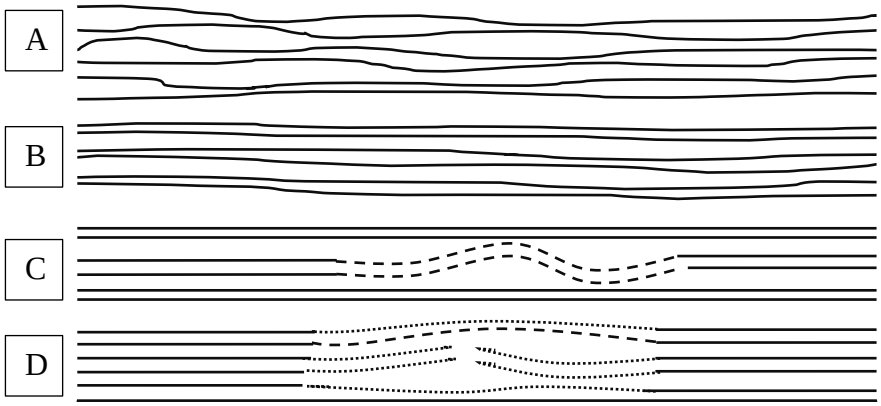

Figure 2.4. A proposed schematic diagram of the fatigue-damage mechanism. Initially, fatigue loading extends the fibrils from the crimping (A) to the uncrimping (B) condition. Increased loading extends the local aggregation of fibrils into their plastic deformity range (C, dashed line), leading to the kinked deformed fibrils. Further, with increased loading, the fibrils with plastic deformation may rupture (D, dotted line). Consequently, loading is assumed by the remaining, intact longer fibrils and/or higher fatigue quality (dashed line). Modified and adapted from Fung et al. (Fung et al., 2009).

Fibril fatigue damage may be seen in focal or generalised modes. Focal damage of collagen fibrils is evident by their breakage (Provenzano et al., 2005). Whereas, generalised damage is evident by the distortions and repetitive forms of kinks on several fibrils that occur at distinct spacing intervals (Veres & Lee, 2012). How focal and generalised damage modes are interrelated remains unclear; however, it is

purported that the association may be dependent on the type and occurrence of fibrillar cross-linkages (Svensson et al., 2013).

Increased crosslinkage between tropocollagen molecules may increase the stiffness of tendons, such as patellar and Achilles tendons, and so would lead to the focal mode of fatigue damage (Svensson et al., 2013). However, generalised damage has been reported to mainly exist early at the nanostructural level during repeated loading (Veres et al., 2013). Furthermore, Freedman et al. (2015) also reported findings similar to those of Veres et al. (2013) while observing changes of fascicle crimp at the macroscale. Therefore, this supports the view that fatigue loading changes the collagen structures at multiscale levels of the tendon.

Additionally, changes in the length of tendon fibres is provoked by the straining mechanisms at different scale levels. At the tissue level, this elongation is enhanced by straining mechanisms at the fibre level similar to mechanisms that exist between fibrils, which are partly controlled by PGs (Screen et al., 2005; Fessel & Snedeker, 2009). The D-periodicity change in fibrils has been strongly supported by different theoretical models that suggest two fibril elongation mechanisms discussed below in more detail under Sections 2.4.1 and 2.4.2.

The changes in D-periodicity induced by different strain levels has provided evidence that D-periodicity of an individual fibril increases with increased applied load (Sasaki & Odajima, 1996; Gupta et al., 2010; Connizzo et al., 2014; Connizzo et al., 2015). However, there is no single study that explores the existence/range of D-periodicity variation within the same and different fibril bundles experiencing different strain levels.

Moreover, no study to date has correlated D-periodicity variations with other nano- and macrostructural changes in responses to mechanical loads. While the tendon's structural and functional relationships have been investigated and the hierarchical structure of the tendon is well characterised, the understanding of tendon damage mechanisms and accumulation at the nano- and microstructural levels is still limited. This raises the potential for understanding fibril changes in pathology and under mechanical loading profiles. Therefore, the physical and biochemical significance of

the variance of D-periodicity is yet to be determined. Increased sample thickness and complexity in these models weakens the quality of cell/tissue imaging and leads to variation between samples.

The number of studies that have used a range of assessment platforms to cover the full range of scales of assessment of the Achilles tendon is limited. The majority of previous studies have focused on a single hierarchical scale level in the assessment, therefore, this may contribute to the complexity and the broad terminology used for the range of hierarchical scales. The hierarchical structures of the tendon have a broad range in size from Angstroms to millimetres. Furthermore, tendons usually function in complex conditions and are exposed to multi-axial loads. The effectiveness of the tendon response under these conditions is directly determined by its unique highly ordered broad multiscale structures. With these broad structural scales from nano- to macro-levels, the structure of entire tendons becomes, unfortunately, much more complex than can often be analysed and addressed with the different approaches or techniques that are typically employed to evaluate the univariate and independent effects of a single structural or biochemical variable on tendon mechanics. Therefore, whole-tendon models must involve substantial processing to assess the cellular and structural changes concomitant with fatigue loading.

The following sections will review the mechanical, biochemical and structural analytical techniques that have been employed, both individually and together, to highlight the nano- and macromechanical characteristics of the tendon and its homeostasis, investigating the structural interactions between components in the tendon matrix. These sections have adopted a specific hierarchy, as shown in Figure 2.1, to permit comparison between various reports, and highlight the current understanding at the nano/micro hierarchical level and explore collagen nano- and micromechanics focusing only on the inter-fibril mechanics.

2.3 Nanomechanical Characterisation Conducted by a Range of Experimental Techniques

2.3.1 Elongation of triple helices

Stereochemical modelling suggests that due to the staggered arrangement of the triple helix, collagen comprises two domains – a flexible and a rigid domain. The critical domain that influences the mechanical response is the flexible domain, which experiences an initial elongation within its elastic limit, thereby storing elastic energy (Silver et al., 2002). The molecular spatial arrangement of the collagen triple helix includes a high content of the repeating amino acid sequence $(Gly\text{-}X\text{-}Y)_n$. This conformation is the rigid region of the triple helix and is believed to stabilise and prevent stress-denaturation of the protein (Shoulders & Raines, 2009). The molecular packing of the triple α-helical polypeptidic chains causes the formation of quasi-hexagonal aggregates of collagen molecules that intertwine with adjacent molecules and super twist, forming microfibrils and the distinctive D-periodicity that is observed in collagen fibrils under AFM (Shoulders & Raines, 2009; Stylianou, 2017).

Various models have been suggested to elucidate the pathogenesis of mechanical injury of the tendon. The choice of the model is often defined by the hierarchical scale of the experimental investigation. For example, a recent molecular-based model (Gautieri et al., 2011) using collagen fibril mechanics combines the mechanical and biochemical assessments from collagen fibrils with biochemical information and molecular structure. The results from these studies provide crucial information on structural alterations at the molecular collagen level as well as an important description about the translation of molecular structural alterations to collagen fibril dynamics.

An atomistic modelling of collagen microfibril mechanics has shown that when the mechanical loading is increased, the behaviour of the microfibril demonstrates a significant elongation, occurring from the straightening of the triple α-helical polypeptidic chains. Then, an axial lengthening, and eventually an uncoiling at the molecular level takes place (Sasaki & Odajima, 1996; Tang et al., 2010; Gautieri et al., 2011). Moreover, using SEM and enzyme probes for denatured collagen on overloaded bovine tail tendons, the existence of the molecular uncoiling at distinct,

repetitive locations forming kink regions along the length of the previously straight fibrils was demonstrated (Veres & Lee, 2012). This study proposed that tissue failure occurred along the full fibril length (Veres & Lee, 2012).

Consecutive stretching resulting from cyclic loading with increased force has been shown to cause aligned collagen molecules to start to slide along each other and extend (Folkhard et al., 1987; Sasaki & Odajima, 1996). For example, Folkhard et al. (1987) monitored changes in the D-periodicity of stretched native fibres from rat tail tendon. Furthermore, Sasaki & Odajima (1996) have also reported strain-induced increased D-periodicity, which they purported to be evidence of relative sliding between the molecules, contributing to the additional elongation of fibrils (Sasaki & Odajima, 1996).

In a comparison study between molecular and fibril elongation using mechanical and X-ray diffraction measurements, Mosler et al. reported that molecular elongation only represented a small fraction of the total fibril elongation (Mosler et al., 1985). It has also been reported that continued sliding of collagen molecules can be explained by the SR behaviour of fibrils while the tendon is under constant strain (Mosler et al., 1985). Folkhard et al. (1987) reported that elongation of the collagen triple helices does not occur concurrently with sliding. They suggested that elongation can be limited when the maximum amount of sliding, enabled by the fibril crosslinks, has been reached.

Both mechanisms are recoverable to a limit, and Folkhard et al. (1987) demonstrated a recoverable D-periodicity increase of nearly 2%, suggesting that tendon damage can be irrecoverable if further stretching is applied.

The non-concurrent events of elongation and sliding of collagen triple helices may impact on SR (and possibly creep or *h*). The whole-tendon mechanical profile smooths out granular (fine or small scale) mechanical changes.

If there are two phases (elongation and sliding) then it follows that there may be a phase change in the mechanical variables that could be determined if repeated

temporal assessments were measured serially. It is likely that if there were a non-linear step-change in the mechanical or morphological changes then maintaining the same strain and allowing the number of cycles to create a fatigue response may allow a more sensitive observation of such changes.

2.3.2 Fibril elongation and sliding

Although mechanical characteristics of single fibrils have been measured by nano-tensile testing approaches using nanoscale manipulation techniques such as AFM or optical tweezers (Thompson et al., 2001; Sun et al., 2002; Gutsmann et al., 2004; Bozec & Horton, 2005), the mechanical behaviour of collagen fibrils has not been able to explain the (macro) complete tendon mechanical behaviour. Fibril elongation and sliding has been considered as one factor contributing to tendon viscoelastic behaviour (Silver et al., 2002), and is thought to happen during the toe region of mechanical loading tests.

Stress-strain curves for molecules and fibrils have been derived using an AFM tip although this method has introduced some artefacts from the chemical extraction of intact collagen fibrils to attach and pull these fibrils for mechanical testing (Eaton & West, 2010). Due to the structural complexity present in Achilles tendon hierarchies, the AFM tip method is incapable of providing a clear and complete explanation of the fibril mechanics of the same fibril bundle (fibre) compared to fibrils of different fibril bundles.

Various studies have demonstrated that relative changes in fibril elongation, expressed as changes in the D-periodicity values, represent less than half of the full macroscopic elongation (40%) recorded from tendon fibres (Diamant et al., 1972; Misof et al., 1997; Fratzl et al., 1998; Puxkandl et al., 2002; Birch, 2007; Rigozzi et al., 2011). This suggests that other mechanisms impact the load-transmission response of tendons. Some factors that are suggested to play roles are discussed in more detail later. With the aid of EM images of tendons, a model of fibril sliding under load has been developed by Puxkandl et al. (2002) to demonstrate the variations in stiffness that are visualised in hierarchical scales of the tendon tissue (Puxkandl et al., 2002). This

model suggests that fibril shearing is controlled by PGs when the tendon is under load (Puxkandl et al., 2002). A detailed diagram of the molecular and fibrillar hierarchies is depicted in Figure 2.5, demonstrating the elongation mechanisms suggested in the studies reviewed under the Sections 2.3.1 and 2.3.2.

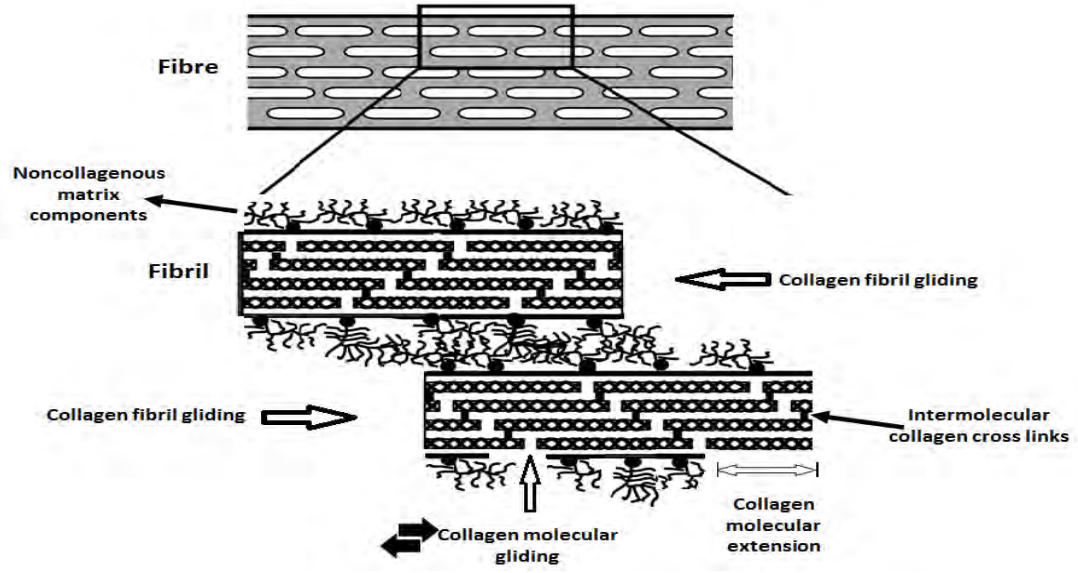

Figure 2.5. A diagram representing a mechanical model showing the elongation mechanisms of the molecular and fibrillar hierarchies suggested for tendons. Arrows demonstrate collagen molecular elongation and sliding between molecules and fibrils. Covalent cross-linkages between the collagen molecules are depicted within the fibrils. The figure is modified from (Puxkandl et al., 2002).

2.3.3 The D-periodicity of collagen fibrils

A. The D-periodicity distribution in Type I collagen tissues

The ultrastructure and function of collagen are closely associated (Ottani et al., 2001). Molecular elongation of fibrils observed as an increase in the gap regions in the fibril D-periodicity (Folkard et al., 1987; Sasaki et al., 1999) has supported the proposition that the D-periodicity is the most important ultrastructure feature of collagen fibrils in various collagenous tissues. Qualitative assessment of the ultrastructure of collagen from biological samples such as fibril bundles from skin, tendons and lamellae from bone have been quantified using instruments such as SEM or TEM (Franchi et al.,

2007; Starborg et al., 2013) and polarised light microscopy (Lavker et al., 1987; Bromage et al., 2003).

The earliest ultrastructural assessment of the human skin D-periodicity by electron microscopy measured D-periodicity values of 64.6 ± 5.3 nm (Schmitt et al., 1942; Gross & Schmitt, 1948). Recently, AFM imaging and two-dimensional fast Fourier transform (2D FFT) analysis have been developed to quantify the D-periodicity at the microscale and nanoscale levels (Wallace et al., 2010; Erickson et al., 2013). Variations of D-periodicity in Type I collagen of tooth, dermis, tendon and bone in human, murine and ovine samples have been assessed using these techniques (Wallace et al., 2010). The distribution of lengths of collagen D-periodicity has been quantitatively characterised (Schmitt et al., 1942; Gross & Schmitt, 1948; Habelitz et al., 2002; Wallace et al., 2010; Fang et al., 2012). Other studies have reported the mean D-periodicity in normal tissue such as dermis and cornea as 64 nm, and slightly longer in bone and tendon (67 nm). These values have been derived from X-ray diffraction (XRD) studies (Bear, 1944; Brodsky et al., 1980), which have become popular for the study of microfibrillar aggregation within collagen fibrils.

Although techniques based on measuring the D-periodicity of individual fibrils continuously reported a distribution of D-periodicity values (Figure 2.6), the biological and significance of D-periodicity variation was brought to light when significant changes in bone collagen D-periodicity distribution were reported in long-term oestrogen depletion and Osteogenesis Imperfecta (Wallace et al., 2011). This formed the argument that the D-periodicity could be a very good marker of micro-damage to collagen substrates. The D-periodicity distributions of individual fibrils are measured by different instruments (given in Figure 2.6). The significance of this literature suggests that there is a very narrow range of D-periodicity that exists across the range of specimens and methods

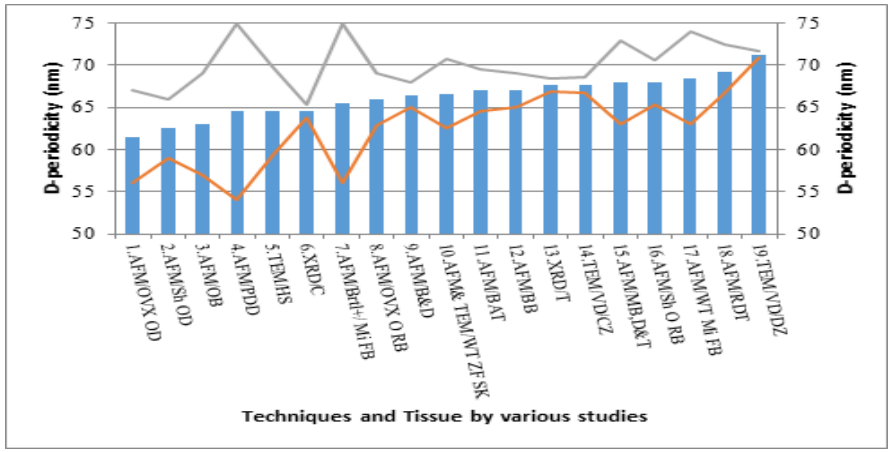

Figure 2.6. The D-periodicity variations reported in the literature. Abbreviations: XRD: X-ray diffractometry, TEM: transmission electron microscopy, AFM: atomic force microscopy, OVX: ovariectomized, WT: wild type, a: Predictable from the distribution histogram from Gross and Schmitt (Gross & Schmitt, 1948), HS: Human skin, C: Cornea, T: tendon, VD DZ: Vitrified predentin distal zone, PDD: Partially demineralized dentin, RDT: Rat digital tendon, MB, D&T: Mice bone, dentin and tendon, Sh O RB: Sham ovine radius bone, OVX O RB: ovariectomized ovine radius bone, Brtl/+ Mi FB: Heterozygous col1a1 allele of mice femur bone, WT Mi FB: Wild Type mice femur bone, Sh OD: Sham ovine dermis, OVX OD: ovariectomized ovine dermis, OB: Ovine bone, BAT: Bovine Achilles tendon, BB: Bovine bone, B&D: bone and dentine, WT ZF SK: Wild type Zebrafish skeleton,1: (Gross & Schmitt, 1948); 2, 3: (Marchini et al., 1986); 4, 5: (Beniash et al., 2000); 6: (Habelitz et al., 2002); 7: (Bozec et al., 2007); 8: (Wallace et al., 2010); 9: (Wallace et al., 2011); 10, 11: (Wallace et al., 2010), (Wallace et al., 2011); 12: (Wallace et al., 2011); 13,14: (Fang et al., 2012); 15: (Fang et al., 2012); 16: (Su et al., 2014); 17: (Sasaki et al., 2002); 18: (Bozec et al., 2005); 19: (Ge et al., 2007). The grey and orange lines represent the maximum and minimum values of the D-periodicity variation measured by these studies.

B. The origin of D-periodicity variability

The existing literature is focused on normal tissue and reports that the collagen sequences (D-periodicity) within and between fibrils are relatively stable. This reflects the consistent mechanism of collagen fibril assembly with the majority of D-periodicity measurements reading between 64 nm and 67 nm. In other contexts, observed variability is linked to a response to environmental and/or pathological factors. However, the factors that induce variations both within and between fibrils are still poorly understood. The following factors that influence the variability of D-periodicity are reviewed in detail in Appendix 1.

- **Non-mechanical factors**

  - Intracellular determinants
  - Environmental determinants
  - Biological determinants
  - Intrafibrillar determinants

- **Mechanical stress determinants**

The underlying mechanisms of collagen load distribution have been extensively explored at different multiscale levels (Sasaki & Odajima., 1996; Screen et al., 2004; Gupta et al., 2010). The most attention has been paid to the collagen fibril and fibre responses to applied forces (Puxkandl et al., 2002). At the tissue level, elongation is enhanced by mechanisms at the fibre level, which are similar to mechanisms that exist between fibrils and are partly controlled by PGs (Fessel & Snedeker, 2009; Rigozzi et al., 2009).

An increase in the D-periodicity seems to be a function of gross strain, as the D-periodicity values increase with the increased strain at the ultrastructural level in murine Achilles tendons (Rigozzi et al., 2011), the medial collateral ligaments (MCL) of New Zealand white rabbits (Kukreti & Belkoff, 2000), bovine Achilles tendons (Gutsmann et al., 2004), rat-tail tendons (Puxkandl et al., 2002; Van Der Rijt et al., 2006), femoral bovine bone (Gupta et al., 2005) and the bovine Achilles tendon (Sasaki et al., 1999).

Only a limited number of studies have focused on the behaviour of single collagen fibrils in their native bundles under macroscopic mechanical loads. These studies have provided evidence that with increased applied load, D-periodicity increases; therefore supporting the hypothesis that this involves the stretching of individual collagen fibrils (Rigozzi et al., 2011; Connizzo et al., 2014; Connizzo et al., 2015). The increase in the D-periodicity is stated to be caused by the stretching of the fibril (Diamant et al., 1972; Misof et al., 1997; Fratzl et al., 1998; Birch, 2007) and additional lengthening of fibrils is associated with sliding between collagen fibrils or bundles (Puxkandl et al., 2002; Silver et al., 2002; Connizzo et al., 2014).

There is a non-consensus between studies that have investigated the variability of D-periodicity between fibril bundles. For instance, a recent AFM-based study on ovine skin, bone and tendon tissues has explored the association between the collagen fibril D-periodicity distribution of a single bundle and fibril bundle organisation across different bundles (Fang et al., 2012). Within a single collagen fibril bundle (WFB), variation between the repeated D-periodicity sequence was very small (±1 nm), suggesting uniform axial packing of collagen monomers within a fibril bundle, but the between-fibril bundle (BFB) variability (across different bundles and within the same biological tissue) was substantially greater (± 1 nm *vs* ± 10 nm) and gives rise to the full-scale distribution.

A nested analysis of variance (ANOVA) study divided the variance constituents at the fibril, bundle and animal levels and reported that the variance at the bundle level represented 76% of the total variance (Fang et al., 2012). In other words, the variance in BFB D-periodicities is large compared to the variance between different animals and the WFB D-periodicity variance. However, another recent AFM-based study has questioned the findings of Fang et al. (2012) and reported that the D-periodicity values of Type I collagen fibrils present only a narrow distribution (67 ± 2.5 nm) (Su et al., 2014). The WFB D-periodicity values of the collagen fibrils in this study were similar and the BFB values were dissimilar (Su et al., 2014). It should be noted that the D-periodicity of the fibril bundles reported by these studies was in tissues that did not experience any mechanical load.

D-periodicity variation has not been widely reported in the literature. BFB variance may be a marker of normal fibril variation, or possibly the differences in D-periodicity are due to the status of the fibrils, indicating fibrilogenesis, disease or pathology. This shows the importance of understanding fibril changes in pathology and under mechanical loading profiles. The physical and biochemical significance of the variance of D-periodicity is yet to be determined. The literature suggests that the WFB D-periodicity is highly stable across a wide range of biological tissues (Shoulders & Raines, 2009).

There is growing evidence that there are a variety of factors that influence the BFB and WFB variance of D-periodicity. Nevertheless, the similar BFB D-periodicity values that has been observed in skin tissue that has experienced insignificant mechanical stress contradicts the possibility that mechanical stress is associated with an increase in D-periodicity since the tissues were not experiencing any mechanical load (Fang et al., 2012).

However, this does not exclude the possibility that osteoblasts under different mechanical stresses may cause variations in D-periodicity. Consistent with this, a study using XRD has reported that a 20 MPa stress applied to tendons has been associated with a 3% D-periodicity change (nearly 2 nm) (Brodsky et al., 1980), while another study using scattering X-ray spectroscopy has reported that a macroscopic tendon strain of 3% was associated with a 1 nm change in D-periodicity (Sasaki et al., 1999). Furthermore, another study using TEM reported an average 4% increase in D-periodicity with a gross ligament strain of 8% (Kukreti & Belkoff, 2000). Each of these studies has provided vital but partial insight into tendon nanomechanics, yet, none of the methods used in these studies could characterise the heterogeneity in load distribution of fibrils. Moreover, these studies have only shown the changes to D-periodicity following a single strain level and therefore there is limited current knowledge of the impact of cyclic loading at different strain levels on the D-periodicity of fibrils and bundles.

From these studies, the magnitude of D-periodicity change as a function of tendon strain is not broad enough to explain the D-periodicity distribution seen across different tissues (Wallace et al., 2010; Fang et al., 2012; Erickson et al., 2013).

Therefore, mechanical strain is still considered at least one of the factors causing the 10 nm variation in D-periodicity. However, the WFB and BFB variability in the same structure that has experienced mechanical load has not yet been investigated.

These studies on the D-periodicity distribution at the fibril and bundle levels do not show any systematic trends that may explain the deviation in variability across different biological tissues. Therefore, the factors that induce variations both within and between fibrils are still poorly understood. This opens a potential area of future research to investigate the relationship between D-periodicity distribution and early nanomechanical changes due to different pathologies and loadings in tendons.

To the best of the author's knowledge, no study has investigated the WFB and BFB D-periodicity distribution of tissues that are exposed to a repeated cyclic loadings of different strains. Conducting such studies could assist in determining if the WFB and BFB variability in D-periodicity is a likely marker of disease or pathology. Such studies are crucial for our understanding of the possible mechanisms and factors affecting fibril D-periodicity distribution and may lead to vital constructional information in various research areas such as collagen fibrogenesis, related diseases and collagen molecular models.

2.4 Macromechanical Characterisation Conducted by a Range of Experimental Techniques

In the previous section, a general overview of the literature was provided on the nano-hierarchical scale and described the fibril strain facilitated by the molecular elongation and sliding mechanisms. As stated previously, relative changes in fibril elongation, expressed as changes in the D-periodicity values represents less than half of the full macroscopic elongation recorded from the tendon fibres (Diamant et al., 1972; Fratzl et al., 1998; Birch, 2007).

Therefore, other mechanisms at different hierarchical scales contribute to the total tendon elongation (Diamant et al., 1972; Fratzl et al., 1998; Birch, 2007). There is no consensus in the literature about the continuity of collagen fibrils along the full length

of the tendon and the assessment of fibril and fibre length remains questionable. An EM-based study speculated that inter-fibrillar linkages are unimportant, arguing that fibrils are continuous and extend the whole length of the tendon as very few fibril ends were seen in the EM images. Therefore, fibrils were thought to directly transfer the applied load (Provenzano & Vanderby, 2006). Other studies have indicated the discontinuity of fibrils and fibres (Craig et al., 1989; Raspanti et al., 2008), stating that the additional tendon elongation exists only between the fibrils themselves, and suggesting that there are discontinuous units of molecules, fibrils and fibres (Craig et al., 1989; Raspanti et al., 2008) as proposed from nanomechanical studies (Knorzer et al., 1986). Therefore, these hierarchical units are considered to mechanically combine to transfer load when the tendon is under an applied load (Mosler et al., 1985; Fratzl et al., 1998).

The various contradicting reports in the literature suggest that the mechanical behaviour of the tendon is not able to be solely explained by the structure and composition. This indicates that possibly there are other mechanisms of load transmission such as:

- tenocyte morphology (Matyas et al., 1994; Screen et al., 2003)
- collagen crosslinks (Gautieri et al., 2011)
- fibre realignment (Masic et al., 2011)
- fibre crimping (Hurschler et al., 2003; Franchi et al., 2008) and uncrimping (Rigby et al., 1959; Viidik, 1969; Hansen et al., 2002; Miller et al., 2012)
- fibril elongation and sliding (Silver et al., 2002; Connizzo et al., 2014)
- stress transfer through the non-collagenous matrix (e.g. PGs) (Merrilees & Flint, 1980; Puxkandl et al., 2002; Smith et al., 2002; Scott, 2003; Robinson et al., 2005; Raspanti et al., 2008)

2.4.1 Tenocyte morphology

Confocal microscopy (CM) has provided the ability to monitor mechanical characteristics in viable unprocessed tendons (Wright et al., 1993). Various studies

have focused specifically on the cell shape deformation when tissue is under load and have suffered difficulties in quantifying these deformations especially in explants, due to challenges in imaging dense tissues such as tendons.

Fung et al. (2010) (using multiphoton microscopy) and Shepherd & Screen (2013) (using CM) have reported that when tendons are loaded to a low-level fatigue, they have shown isolated kinked deformations in the fibres and a disturbed tenocyte arrangement and organization (Fung et al., 2010; Shepherd & Screen, 2013), suggesting that the mechano-perception of tenocytes is influenced by fibre crimp or kink (Szczesny et al., 2018). This suggestion seems to refute the findings by Lavagnino et al. (2018) and (Mehdizadeh et al., 2017) who found that waviness in tendons is a response of cellular tension and is governed, in part, by mechanisms of cell contraction. Although these experimental studies have provided insight into the structural changes of tendons during mechanical intervention, it is important to determine which structural changes at the macroscopic level are occurring first and how they are regulated and provoked. Therefore, a broader range of macro and nanostructural measures need to be incorporated in an animal model to assess different tissue responses across different hierarchies within the intact bulk of the same tendon under the same boundary conditions.

Microscopic studies using CM on ligament tissues have demonstrated nucleus and cell deformations when tissues are subjected to strain (Matyas et al., 1994; Tallon et al., 2001; Sharma & Maffulli, 2005; Scott et al., 2007; Hamilton et al., 2008; Magra & Maffulli, 2008; Riley, 2008; Shepherd et al., 2013). It has been reported that for equine tendon fibres subjected to cyclic loading *in vitro,* changes in cell morphology from spindle to round shapes were accompanied by matrix damage (Thorpe et al., 2015). These alterations were more distinct in regions where damage to the fibres was obvious (Ros et al., 2019). This is consistent with previous studies, which have observed round tenocytes in overloaded and tendinopathic tendons (Scott et al., 2007; Riley, 2008). It is likely that cyclic loading causes focal damage, changes the cell strain environment and disturbs cell-matrix interactions, which may change tenocyte morphology to the round shape. In contrast, Maytas et al. (1994), Arnoczky et al. (2002) and Screen et al. (2003) found a limited correlation between strain and the nucleus deformation of tenocytes, in which the nuclei became thinner and longer in

the viable tendon fascicles (Arnoczky et al.,2002; Matyas et al., 1994; Screen et al., 2003) .

Since tenocytes are organised in long rows between fibres (Figure 2.7), the load environment of these cells can be significantly affected by the inter-fibre mechanics, with changes impacting the ability of resident tenocytes to interact with, and respond to their native tissue environment *via* mechano-transduction pathways (Screen et al., 2003), therefore impacting the ability of these tenocytes to trigger reactive tendinopathy (Cook & Purdam, 2009) and tissue remodelling activities (Riley, 2008; Spiesz et al., 2015).

Although tenocytes are known for their sensitivity to the surrounding mechanical environment (Lavagnino et al., 2015; Wang et al., 2018), it is still unclear what governing mechanisms mediate change within the cell and subsequently the cell environment, including cell-matrix interactions. The cascade of events that triggers structural changes in tenocyte morphology from spindle to round shape as a response to cyclic loading warrants further investigation. Moreover, future studies are required to investigate the tenocyte morphological response to micro-damage and to determine if the morphology itself mediates the regulative pathways for mechano-transduction of tenocytes.

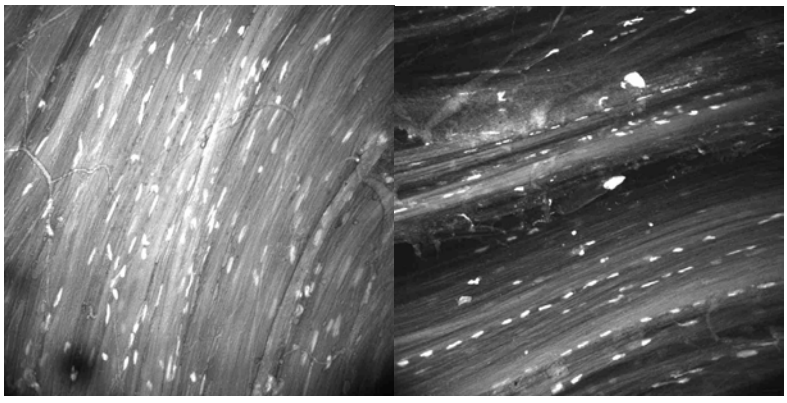

Figure 2.7.Two CA images depicting the morphology and distribution of tenocytes between collagen fibres. Acridine orange was used to stain the nuclei of the tenocytes.

2.4.2 Collagen fibre anisotropy

Collagen fibres are directionally dependent and show anisotropy, which means there is homogeneity of the fibres in all directions. The nonlinear biomechanical behaviour of tendons demonstrated by a typical SR curve starts with a non-linear toe region and then a subsequent linear region (Connizzo et al., 2013). The non-linearity, particularly the low-stiffness toe region, is suggested to result from a set of rearrangements of dynamic macrostructural tendon responses (Woo, 2000; Rigozzi et al., 2011; Miller et al., 2012; Connizzo et al., 2013; Thorpe et al., 2013; Connizzo et al., 2014).

In particular, the nonlinearity of the toe region of the SR curve is thought to occur due to collagen uncrimping and realignment and the reorientation of fibres to the load axis (Diamant et al., 1972; Atkinson et al., 1999; Lake et al., 2009; Wallace et al., 2010; Miller et al., 2012). This reduces the variation of fibre angulation when the tendon is subjected to load. This observation is supported by the decline in crimp waveform crimp amplitude and frequency reported in loaded Achilles tendons of rats (Franchi et al., 2007).

The collagen fibre, the primary structural constituent that confers mechanical strength under load, exhibits anisotropic behaviour (Voleti et al., 2012). Excessive loading disrupts collagen fibres and their anisotropy, which can affect the biomechanical behaviour of the whole tendon adversely (Wren et al., 2003; Screen et al., 2004; Williams et al., 2008; Lake et al., 2009; Wallace et al., 2010; Sereysky et al., 2012; Szczesny & Elliott, 2014). A nanoindentation-based study on fibrils from rat-tail tendons demonstrated fibril and microfibril anisotropy. Wenger et al (2007) reported a decreased stiffness (Young's modulus) within the range of 5–11.5 GPa of the indented fibrils and observed that the fibrils comprise microfibrils that are arranged axially to the fibril. Also, the indentation on the fibril surface produced small marks which indicated the anisotropy of the collagen fibril (Wenger et al., 2007).

Although direction-dependent experimental studies are essential to investigate the anisotropic characteristics of collagen fibres (Sacks, 2000; Holzapfel & Ogden, 2009) there are several studies that report long-term changes of tendon anisotropy (Screen et al., 2004; Williams et al., 2008; Wallace et al., 2010; Szczesny & Elliot, 2014). Novel

experimental systems were designed to allow for real-time measurement of tendons, to determine the level of fibre anisotropy when tendons were subjected to mechanical loading (Screen et al., 2004; Wallace et al., 2010; Miller et al., 2012). These approaches have shown different realignments when measured at different locations throughout mechanical testing, suggesting that these differences are location dependent.

Realignment is considered as one suggested mechanism of preconditioning of collagen fibres (Miller et al., 2012). When a tendon is subjected to load, collagen fibres change their anisotropy axially to the loading direction and reduce the fibre angles (Figure. 2.8). Miller and co-workers have used a cross-polariser technique and measured the fibre architecture in small sections of the human supraspinatus tendon to determine the role of preconditioning in explaining the realignment of the mid-substance portion of the fibres. This device comprised a mechanical loading system (Instron, Norwood, MA) combined with a polarised light imaging setup that simultaneously obtained a series of images. They demonstrated that most of the collagen realignment was caused by preconditioning and a lesser quantity of collagen realignment was depicted in the toe and linear regions (Miller et al., 2012). This may explain the increased strength of tissues visualised in preconditioned tendons that are highly aligned, indicating a tissue structural response to loading occurring after applying a small load (stress or strain).

The fibre alignment and mechanical characteristics have been shown to have significant correlations in the supraspinatus tendon (Lake et al., 2009). It has been suggested that the greater stiffness and alignment of disorganised fibres at the supraspinatus insertion may be elucidated by an *in-vivo* complex multiaxial loading environment of the supraspinatus muscle morphology (Lake et al., 2009). Furthermore, it was suggested that strain no longer increases at the fibre level after the fibres have realigned in the direction of loading within the excised fascicle (Screen et al., 2004).

However, a recent *in-vivo* work using the Instron by Fung et al. (2010) on rat patellar tendons that were fatigued to three different damage levels, found less fibre alignment and organization (or anisotropy) in tendons with each increased level of fatigue (Fung et al., 2010). Fibre organization was found to be poor (more anisotropy) in tendons

loaded to a high damage level showing a statistically significant correlation within the high-damage group (Fung et al., 2010).

The normalisation of fibre anisotropy is expected with preconditioning; however, it is unclear whether the anisotropy changes under sustained repeated cycling when there is a specific level of mechanical damage. To date, few studies have repeated the multiple fatigue levels as reported by Fung et al. (2010). Moreover, these studies examined fibre organisation and alignment (anisotropy) under sustained load (stress) while reporting increased elongation or strain. Additionally, collagen fibre realignment during a tensile ramp-to-failure or SR of preconditioned tendons has not yet been examined. Therefore, future research may be able to contribute to the understanding of the poor fibre alignment and organisation (anisotropy) in tendons that have experienced different fatigue-damage levels, if the developed fatigue loading models control strain and examine load.

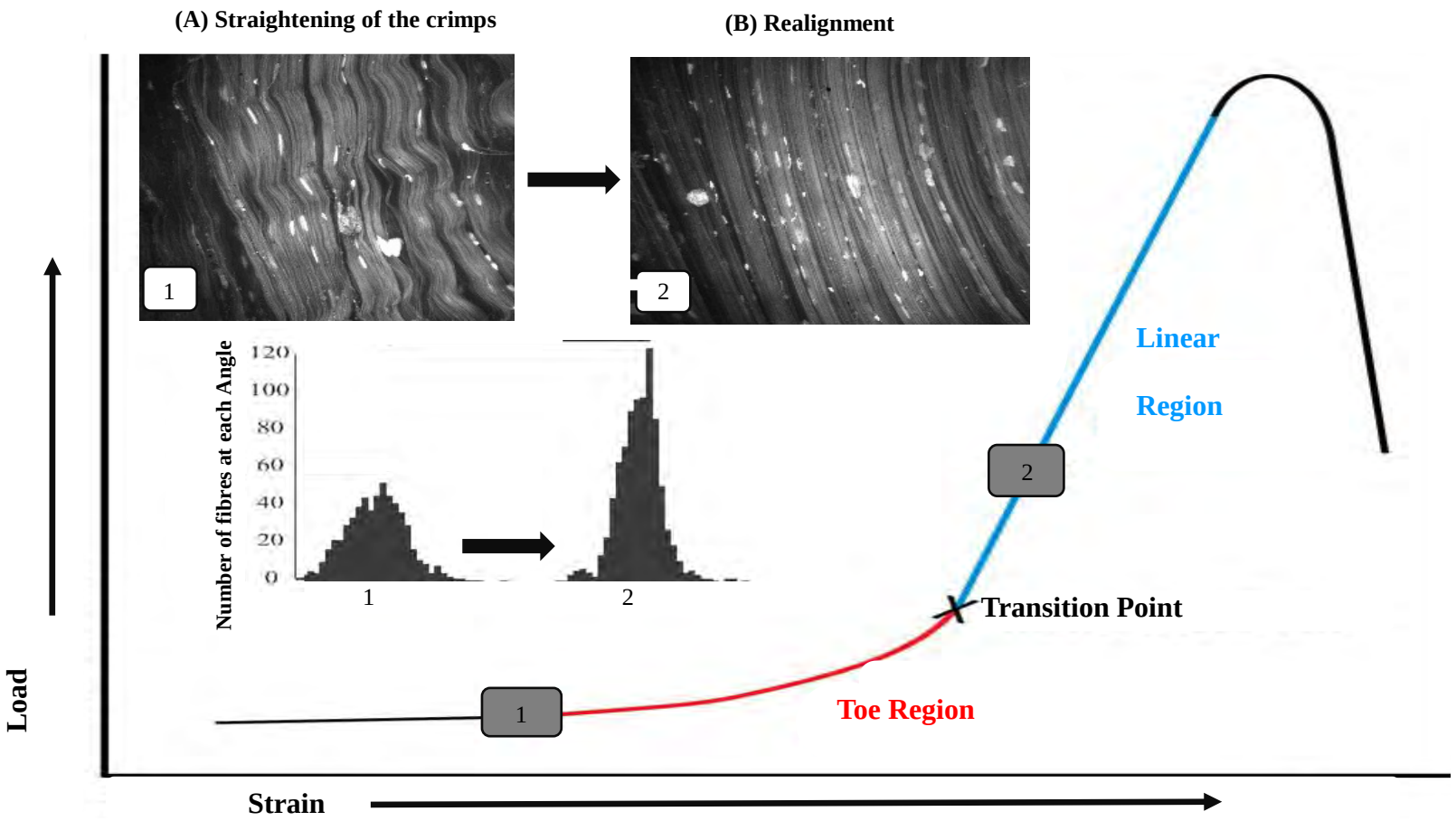

Figure 2.8. A stress-strain curve of a tendon demonstrating an extended low-stiffness area in the toe that transitions to high stiffness in the linear region. (A) and (B) represent two response mechanisms to load (the straightening of the crimps and realignment of collagen fibres) within the toe region, demonstrated by a declined variation of fibre angle distribution from the toe to linear region. Modified and adapted from Connizzo et al. (2013)

2.4.3 Collagen fibre waviness

Waviness is a periodic formation of buckled collagen on both the fibril and fibre level and is concomitant with the mechanical behaviour of collagen (Järvinen et al., 1997; Waterston et al., 1997; Woo et al., 2000; Hamilton et al., 2008; Mehdizadeh et al., 2017). It is a marker of lateral tension or tertiary structure loss (Sivaguru et al., 2014). Previous reports have suggested that the mechanism of fibre kink formation (Fung et al., 2009; Andarawis-Puri et al., 2011) was the heterogeneous elongation of a small group of fibres into the range of plastic deformity (Pingel et al., 2014). Upon unloading, they are then compressed and kinked due to the shortening of parallel elongated elastic fibres (Herod et al., 2018). The formation of such micro-damage may allow a further elongation with consequent load.

During a mechanical loading profile, the non-linear toe region shows a non-uniform straightening of collagen crimp fibres along the lengthwise axis of the tendon (Abrahams, 1967; Diamant et al., 1972; Cribb et al., 1995; Atkinson et al., 1999; Hansen et al., 2002; Screen et al., 2004; Franchi et al., 2007) and this is a proposed mechanism of tendon response to mechanical load (Diamant et al., 1972).

Histologically, the fibre crimp waveform shows birefringence, patterns of bright and dark bands under polarised light (Rigby et al., 1959; Rigby, 1964; Viidik, 1969; Miller et al., 2012). While this birefringence of light and dark patterns has been extensively explored at the fibre, fascicle and gross tissue levels (Screen et al., 2004; Franchi et al., 2007; Franchi et al., 2008; Franchi et al., 2010), limited studies have investigated crimp at the nano-hierarchical level (Raspanti et al., 2005).

Uncrimping of collagen fibres occurs during an increase of strain between 1% and 5% (Rigby et al., 1959; Rigby, 1964; Viidik, 1969; Miller et al., 2012). This reflects a very wide range of strain, and uncrimping is not well controlled by standardised preconditioning. Screen et al. (2004) demonstrated that rat-tail tendon fascicles show collagen fibres straightened at between 1% and 2% strain. At these strain levels, it was reported that all fascicles had uncrimped and realigned to the axis of load by the end of the toe-region (Screen et al., 2004). While results from rat-tail tendon fascicle

studies find no evidence of fibre realignment or uncrimping following the toe-region, tendon level studies in rotator cuff tendons have demonstrated that fibre alignment continues throughout the tendon's fibre bundles until tissue failure (Thomas et al., 2012). This may be associated with the sequential loading and rupture of fibrils that support internal axial loading and by the nature of the supraspinatus tendon, which means that the loading axis changes during the sequential loading.

Structural change seems to start first at the tendon gross level, then transfers through the multi-scale hierarchies from the fascicle level, down to fibre, fibril and finally to the molecular hierarchical level. For instance, an elegant analysis of fibril crimps using SEM and TEM has provided images of crimp that were visualised as knots within the fibre bundles, as irregular collagen fragments, which were seen to be bent, squeezed or twisted, and corresponded to the crimps seen at the fibre scale (Franchi et al., 2007). These findings are also supported by Raspanti et al (2005) who observed the crimps at the top of the collagen fibrils to be bent with different sharp angles, while their D-periodicities were not distinguished (Raspanti et al., 2005). Furthermore, the molecular crimps did not disappear although the crimps in the fibre bundles disappeared (Franchi et al., 2007). Interestingly, after the crimps on the fascicle or multi-fascicle level were straightened, the crimps in the fibre level could still be seen (Franchi et al., 2007).

The observations of these studies are supported by a study that reported a 5% gap in the fibril strain level compared to the applied tendon strain (Rigozzi et al., 2011). The collagen fibrils may not bear load until the hierarchical structure of fascicle and fibre have reorganised in response to load. In other words, fibrils may not be strained until fibre crimp disappears or is straightened at the fibre hierarchical level and the fibres are aligned to the loading axis. This is supported by Puxkandl et al. (2002) who suggested that beyond 5% strain, the elongation of D-periodicity is suggested to account for nearly half of the measured elongation in fibre (Puxkandl et al., 2002).

Furthermore, the fibrils are believed to bear increased load as straightening and elimination of the microscopic kinks located in the gap region of the molecular quarter-staggered array of collagen occurs and a lateral molecular increased order then exists within these fibrils (Misof et al., 1997).

Fibril kinks with disruptions are seen as localised points scattered at kinked regions (Herod & Veres, 2018), mostly having discrete plasticity patterns caused by molecular denaturation seen all over the fibril length, representing a generalised mode of fibril damage (Veres & Lee, 2012; Veres et al., 2013; Veres et al., 2014). This mode of damage is characterised by an increased serial density of kinks seen as severe kink patterns on locally damaged fibrils, with disruption of the collagen repeated within the D-periodic sequence that became undistinguished (Veres & Lee, 2012; Veres et al., 2013; Veres et al., 2014), likely corresponding to a loss of load-bearing capacity among various portions of fibril bundles (Ros et al., 2019), with the load bearing to be redistributed to other intact fibre portions in the tendon.

It is possible that each level of hierarchy has a specific mechanism to handle mechanical load and that such mechanisms may rely on the type of strain or load experienced at each scale. For example, uncrimping and realignment are characterised as potential mechanisms at the fascicle hierarchical level (Miller et al., 2012) while fibre sliding may be the predominant mechanism at the fibre hierarchical level (Screen et al., 2004).

Although fibre crimp has been widely investigated at unknown load conditions or when tendons are slack (Hurschler et al., 2003; Franchi et al., 2007; Franchi et al., 2008; Franchi et al., 2010), limited studies have been able to evaluate crimp morphology during mechanical load (Lujan et al., 2009; Miller et al., 2012). Overall, these studies have characterised collagen fibre crimp when subjected to load, but have not yet quantified the crimp behaviour in particular throughout a cyclic loading testing protocol. Only two reports have shown correlations between fatigue loading and fibre crimps in tendons (Freedman et al., 2014; Freedman et al., 2015). Therefore, further studies are required on the morphological features of tendon crimps and their quantitative and qualitative alterations during repeated cyclic loading.

It is important to determine if structural changes at the fibril level affect macroscopic mechanical characteristics or *vice versa*. In particular, the characteristics of collagen fascicles with fibril-level structural changes must be quantified in an intact tendon, in addition to examining strain at the fibril scale. Such studies have not been widely

reported. No previous study has investigated the crimp integrity at the nano and macroscales as a response to mechanical load. It is unclear what happens to crimp morphology with repeated cyclic loading at the macroscopic scale and if this correlates with changes over time at the nanoscale level. Further studies are required to investigate the ability of the fibre and fibril crimp to serve as a structural metric of fatigue-induced multiscale structural changes.

Most imaging technique capabilities are limited to within a specific hierarchical level and are not applicable to assessing other hierarchies for the same intact bulk of the tendon tissues. For instance, the second-harmonic generation (SHG) image analysis is limited to approximately 30 µm depth. However, confocal arthroscopy (CA) has an imaging depth of up to 250 µm. Also, many other imaging techniques used may be expensive, time-consuming, or damaging to the tissue sample (Fung et al., 2010; Thorpe et al., 2014) and so unsuitable to investigate the hierarchical changes of tendons subjected to mechanical load. Increased sample thickness and complexity as found in whole or bulk tendons may reduce the imaging quality of tissue (and cells) and may cause variability between tissue samples (Bojsen-Møller & Magnusson, 2019). Therefore, an innovative and non-invasive multiscale approach (e.g., usage of CA and AFM) is required to allow the same bulk tissue and load-dependent multiscale characteristics to be investigated in tissue that has undergone repeated cyclic loading, without destructively altering the tendon.

2.4.4 Knockdown and knockout models

While it is well established that collagen fibres are the primary load-bearing structures that drive macroscopic mechanical behaviour characteristics, there is a lack of understanding of the contribution of the nano and microstructure of the tendon to the macroscopic mechanical behaviour and response to load. One method used to study the mechanisms of this contribution is to alter the ECM to regulate the effects of these mechanisms on the multiscale mechanics of the tissue. Use of genetic knockdown and knockout experimental animals has provided the ability to examine separately the effects of various ECM proteins on tissue mechanics at different scales.

Knockdown and knockout studies offer vital mechanisms for assessing the role of key PGs in the function and development of the structural constituents of tendons. Knockout experiments on small leucine-rich proteoglycans (SLRPs) or Type V collagen have demonstrated early embryonic death and irregular fibril formation (Reed & Iozzo, 2002; Zhang et al., 2006) showing the vital roles PGs play in organising the formation of collagen fibrils. Moreover, changes in PG binding and crosslinks can also cause changeable packing fractions leading to D-periodicity variation (Fang & Holl, 2013).

Nevertheless, knockdown models do have limitations that should be taken into account. The complete effects of gene knockdowns are unidentified, and the mutation may affect other characteristics of the tissue beyond the protein under investigation. For instance, in a study on ageing male and female mice, Kilts et al. reported that loss of fibromodulin, biglycan, or both led to ectopic ossification in tendons (Kilts et al., 2009).

Although knockdown mice have shown the ability to compensate for the knockdown and the interaction between PGs (Hjelle et al., 2002), it has been reported that the lack of specific genes that cause a lower PG concentration do not confirm compensation to reinstate the same function in the body (Robinson et al., 2005; Wang, 2006). A study by Raspanti et al. (2008), has shown that it is very difficult to remove or isolate one part of the data involved in the various interactions between different fibrils and glycosaminoglycans (GAGs) (Raspanti et al., 2008). Consequently, there is uncertainty in the findings of these studies.

2.4.5 The removal of non-collagenous components – PGs and GAGs

The study of the effects of structural components on mechanical characteristics in tendons can also be carried out by enzymatic digestion through manipulating the non-collagenous components in the ECM (for example, GAG removal). This can provide the ability to examine the effects of various ECM proteins separately.

At the nanoscale level, the elongation of the tendon is triggered by the mechanisms of collagen fibril sliding and fibril elongation that exist concurrently in a balance-critical manner. These mechanisms at the nanoscale level trigger the elongation of the fibres and fascicles at the micro and macroscale level.

PGs are well-known to govern this balance (Henninger et al., 2009; Rigozzi et al., 2010) and the small leucine PG decorin is also known for its role in transferring the load between the fibrils through their GAG sidechains (Minns et al., 1973; Ruggeri et al., 1984; Cribb et al., 1995; Sasaki & Odajima, 1996; Fratzl et al., 1998; Redaelli et al., 2003; Screen et al., 2005; Liao & Vesely, 2007; Legerlotz et al., 2013). Therefore, it appears that collagen load-bearing is the ultimate factor regulating the mechanical properties in the tendon (Copeland et al., 1993; Soslowsky et al., 2000; Rigozzi et al., 2010).

The composition and organisation of the PG-rich matrix is suggested to affect the sliding of the collagen fibrils (Merrilees & Flint, 1980) and is directly associated with the viscoelastic behaviour of the tendon (Paavola et al., 2002). Previous reports have shown that small sized Proteoglycans rich in leucine (SLRPs) such as decorin, biglycan, fibromodulin, and lumican are important for the function of a tendon (Iozzo, 1998; Derwin et al., 2001; Yoon & Halper, 2005) and play a role in controlling fibrillogenesis (Vogel et al., 1984; Koob & Vogel, 1987; Scott, 1995; Scott et al., 1997; Ezura et al., 2000; Corsi et al., 2002; Wenstrup et al., 2004; Raspanti et al., 2007; Kadler et al., 2008; Shi et al., 2010; Orgel et al., 2011; Wenstrup et al., 2011)

Decorin is linked to a molecule's D-periodicity by its protein core and exists between collagen fibrils as seen by EM (Scott, 1980, 1988). Decorin comprises a single GAG chain, that is mainly dermatan sulfate (DS) in tendons (Minns et al., 1973; Ruggeri et al., 1984; Koob & Vogel, 1987; Cribb et al., 1995; Sasaki et al., 1996; Fratzl et al., 1998; Redaelli et al., 2003; Screen et al., 2005; Liao & Vesely, 2007; Legerlotz et al., 2013) and is also attached covalently to the core protein as the exclusive sulfated GAG chain of the interfibrillar PG.

The GAG is aligned orthogonally to the fibril's lengthwise axis (Weber et al., 1996). PGs and their GAG chains contribute to the structural integrity of fibrils and fibres by

forming interfibrillar linkages (Minns et al., 1973; Ruggeri et al., 1984; Cribb et al., 1995; Sasaki & Odajima, 1996; Fratzl et al., 1998; Redaelli et al., 2003; Screen et al., 2005; Liao & Vesely, 2007; Legerlotz et al., 2013). Naturally, they are highly hydrophilic, therefore retaining water within the tendon's tissue (~70% water), and assisting in the elongation of the fibril as well as contributing to the sliding mechanism for macroscale elongation (Koob, 1989; Paavola et al., 2002; Screen et al., 2006). Therefore, GAGs are considered a key factor for regulating the viscoelastic characteristics of tendons and ligaments (Minns et al., 1973; Ruggeri et al., 1984; Cribb et al., 1995; Sasaki & Odajima, 1996; Fratzl et al., 1998; Puxkandl et al., 2002; Raspanti et al., 2002; Redaelli et al., 2003; Scott, 2003; Screen et al., 2005; Vesentini et al., 2005; Liao & Vesely, 2007; Fratzl, 2008; Rigozzi et al., 2009; Svensson et al., 2011; Shepherd et al., 2013).

Despite the many studies supporting the role of PGs and their GAGs in assisting the elongation of the fibril as well as contributing to the sliding mechanism at macroscale elongation, there a growing lack of consensus on this role. It was proposed more recently that decorin does not facilitate the mechanical characteristics of tendons *via* load transfer, debating the notion that decorin PGs may promote the elastic behaviour of collagen (Lujan et al., 2007; Fessel & Snedeker, 2009; Franchi et al., 2010; Lewis et al., 2010; Svensson et al., 2011). The main source of inconsistency between those reports rejecting the role of PGs and their GAGs and those reports supporting this role, is the hierarchical level of the experiments conducted, the heterogeneity of the mechanical response at different hierarchies (tendon *vs* fascicle), and the heterogeneity of the mechanical testing machines, experimental setups and the treated samples.

For example, Rigozzi et al. (2009) (who support the role of PGs and have used whole tendon tissue) report a lower stiffness, whereas studies by Svensson et al. (2012) and Screen et al. (2005) (who reject the role and have used fascicles in their GAG assays), have reported higher stiffness. The studies by Svensson et al. (2012) used fascicles from human patellar tendon, and experiments were carried out in phosphate-buffered saline (PBS) solution at 37°C by a mechanical micro-tensile tester while the studies by Screen et al. (2005) on rat tail fascicles were carried out at room temperature and sprayed lightly with PBS using a custom-designed rig. However, in the study by Rigozzi et al. (2009) whole Achilles tendons tested using universal testing machines

were moistened with PBS throughout the entire experiment. The findings reported by Rigozzi et al. (2009) indicate 50% total removal of GAG from whole Achilles tendons with a significant loss (46%) in stiffness. Whereas, Svensson et al. (2012) and Screen et al. (2005) report about 90% removal of GAG from the tested fascicles and show a nonsignificant loss in fascicle stiffness. The GAG content of the tendons in the mentioned studies was measured by a spectrophotometric GAG assay (Farndale et al., 1986). These are conflicting findings and thus warrant further investigation.

The absolute assessment of the change in mechanical behaviour of the tested tissue upon GAG removal from a whole tendon or a small tendon specimen appears to be muddied by the incomplete removal of GAGs from their tissues (from 50% to 90% in the aforementioned studies). Consequently, an argument could be made that depleted tissue samples with higher percentages of remaining GAG would be sufficient to sustain the tissue mechanics to a larger degree.

However, the inconsistencies in the mechanical outcomes between Rigozzi et al. (2009), which used the whole tendon and those studies that used fascicles in their GAG assays are perhaps due to the heterogeneity of the mechanical response at different hierarchies (tendon *vs* fascicle). This is supported by a previous study that reported that tensile stiffness of a whole tendon is less than that of smaller specimens of a tendon (Butler et al., 1987). The increased fascicle stiffness could also be attributed to the decreased amount of areolar connective tissue in smaller tendon specimens (Danylchuk et al., 1978; Yahia & Drouin, 1988). The relative contributions of connective sheaths and collagen fasciculi should be considered for an accurate definition of tensile stiffness (Danylchuk et al., 1978).

Further conflicting literature exists with the assessment of SR and the interaction of multiscale assessments. Similar to the finding by Regozzi et al. (2009), a study by Legerlotz et al. (2013) reports a significant increase in SR of fascicles that had 77% of their GAG removed, contradicting the findings by Svensson et al. (2012). Taking together those similar and dissimilar findings from the above-cited studies, the depleted whole tendons and the depleted small tendon specimens have demonstrated marked differences in stiffness and SR between control and depleted groups.

Consequently, it seems that the understanding of the role of hierarchical heterogeneity on the mechanical response of the tested tissue has been weak.

Other studies have reported that decorin may contribute to tissue hydration (Koob, 1989; Paavola et al., 2002). For instance, increased stiffness has been visualized in fascicles after the removal of GAG from rat-tail tendons (Screen et al., 2006), indicating that GAG may have a lubricating effect. The buffer used likely has reduced the swelling of the fascicles, leading to an increase in stiffness to the level seen under ambient conditions. This may possibly explain why the effect of buffer on stiffness was not visualised in other studies in which the swelling effect by the buffer was controlled by polyethylene glycol (Fessel & Snedeker, 2009). Reconciling the results found in another study where swelling was not successfully controlled or fixed (Lujan et al., 2009) with these controlled studies is difficult. The buffer choice likely indicates that it does not affect the mechanical response. Therefore, it is important to determine the role of the PG-rich matrix across multiple hierarchical levels (fascicle, fibre and fibril levels) in facilitating the sliding of the collagen by quantifying structural changes through combining non-destructive multiscale advanced techniques with mechanical characteristics (Screen et al., 2003, 2004; Rigozzi et al., 2011; Miller et al., 2012).

Although the literature includes numerous studies that examine a single scale within the well-known hierarchical tendon morphology, only limited studies have investigated the role of the PG-rich matrix in the interfibrillar linkages at both macro and nano levels (Screen et al., 2005; Franchi et al., 2010). These studies combine tendon mechanics with macroscale images using CM and SEM and nanoscale images using TEM (Screen et al., 2005; Franchi et al., 2010). It is noted that there is not a consensus on the role of PGs and their GAGs between these two studies (Screen et al., 2005; Franchi et al., 2010). Additionally to findings by Franchi et al. (2010) that refute the facilitation role of PGs and their GAGs, they also report that TEM and SEM images demonstrate that PGs and their GAGs do not influence fibre and fibrillar crimp morphology, and possibly do not play a key role (such as collagen fibre and fibril recoiling and shock absorption) in the function of fibrillar crimp (Franchi et al., 2010). These inconsistent data on the role of PGs and their GAGs in facilitating viscoelastic tensile behaviour merits further investigation of the role of GAG and its relationship with the 3D microstructural integrity of tendon fibrillar and fibre crimps.

Since the elongation mechanisms of strain and the sliding of the collagen triple helices do not occur concurrently (Folkhard et al., 1987), it seems that the nanostructural response to load is a sequential process including uncrimping within the toe region of the stress-strain curve then elongation (observed as an increase in fibrillar D-periodicities) then sliding of fibrils. For instance, in both controls and GAG-depleted tendons, no D-periodicity elongation was detected until 5% strain was applied (Rigozzi et al., 2013), which corresponded to the loss of collagen fibre crimping at the macroscale (Misof et al., 1997). Nevertheless, at 15% applied strain, higher levels of fibril strain (measured as increased D-periodicities) in the GAG-depleted tendons were observed compared to control groups.

To date, there is still a poor understanding of the role of PGs and their GAGs in the distribution of collagen fibril D-periodicity within and between collagen fibril bundles. The association between the PG network and D-periodicity within and between collagen fibril bundles of tissues induced with a cyclic mechanical loading protocol warrants further investigation. This could be performed by conducting a quantitative nanoscale investigation of collagen fibril load-sharing as a function of fibril elongation. In particular, the mechanical and structural characteristics of the GAG-depleted tendon with fibril-level structural elongations (measured by changes in D-periodicity) must be quantified from the same tendon tissue bulk sample that is subjected to a mechanical cyclic loading protocol.

Furthermore, for a better understanding of the structure-function relationship at different hierarchies, more dynamic measures from the nano and macroscales must be incorporated in a cyclic loading protocol to investigate the structural responses of these hierarchies to mechanical load.

2.5 Scale-Dependent Mechanical Characteristics of Collagen Type I

Although the mechanical characteristics of whole tissues have been well investigated, the link from the mechanical characteristics of collagen at a specific hierarchical level to the characteristics of whole tissue is not well established. The stress-strain curve proposed by Sasaki and Odjimma (Sasaki & Odajima, 1996) demonstrates the relationship of whole tissue with the collagen fibril and the tropocollagen (Tc) molecule. The curve is obtained from simultaneous mechanical testing and X-ray diffractometry experiments to measure the mechanical response of Tc molecules and collagen fibrils in bovine Achilles tendons from the initial loading until the whole tendon reached a strain equal to 6% (Sasaki & Odajima, 1996). The strain for the Tc molecule was calculated by measuring the strain corresponding to changes in the range of distance between neighbouring amino acids. The strain of the collagen fibril was calculated by measuring the changes in the D-periodicity. The strain of the tendon was determined by tensile loading test.

The toe to heel region of the curve reflects the continuous straightening of the microscopic crimps. These crimps are considered to absorb any excessive load to prevent damage to the collagen fibre bundle. With increased load, the crimps are straightened, elongation continues elastically, and this seems to exist at a strain of 2%. At any given strain level up to 6%, the stiffness of the structural unit becomes larger as the hierarchical level lowers (the Tc molecule exhibited the largest stiffness and the stiffness of collagen fibril falls in between the stiffness of the Tc molecule and the whole tendon). With regards to strain for a particular stress, the strain value increases with a higher hierarchical level. Therefore, this suggests that the Tc molecule exhibited the lowest elongation compared to the collagen fibril and whole tendon. It is noted that the elongation of the collagen fibril under load falls somewhere between that of the whole tissue and the Tc molecule.

Findings derived from small-strain mechanisms employing different techniques such as AFM (Aladin et al., 2010) X-ray diffraction (Sasaki & Odajima, 1996) and the use of micro-electro-mechanical systems (MEMS) (Eppell et al., 2006; Espinosa et al., 2007; Shen et al., 2008) are consistent with the findings of nanomechanical testing of

hydrated collagen microfibrils (Gautieri et al., 2011). Two distinctive elongations were featured by the hydrated collagen microfibrils when subjected to mechanical load (Gautieri et al., 2011). For the larger-strain elongation (> 10%), the microfibril exhibited a Young's modulus of about 1.2 GPa with a dramatic increase in tangent stiffness. In the small-strain elongation (< 10%), the microfibril exhibits a dramatic increase in stiffness and a Young modulus of around 300 MPa (Vesentini et al., 2013).

Nevertheless, a comparison of the mechanical characteristics between single collagen molecules and microfibrils indicates that mechanical characteristics are highly scale-dependent (Figure 2.9). Particularly, a strong change of the modulus was found when a single collagen molecule was compared with a collagen microfibril, as presented in Figure 2.9. A direct numerical calculation yielded a small-strain microfibril Young's modulus with few hundred MPa compared to a greater strain for a single molecule with several GPa, demonstrating a dramatic variation in mechanical characteristics between the hierarchical scales. This finding is strongly in line with experimental data on small-strain mechanisms derived from studies that employed various experimental techniques and theoretical analyses (Sasaki & Odajima, 1996; Van Der Rijt et al., 2006; Shen et al., 2008; Aladin et al., 2010).

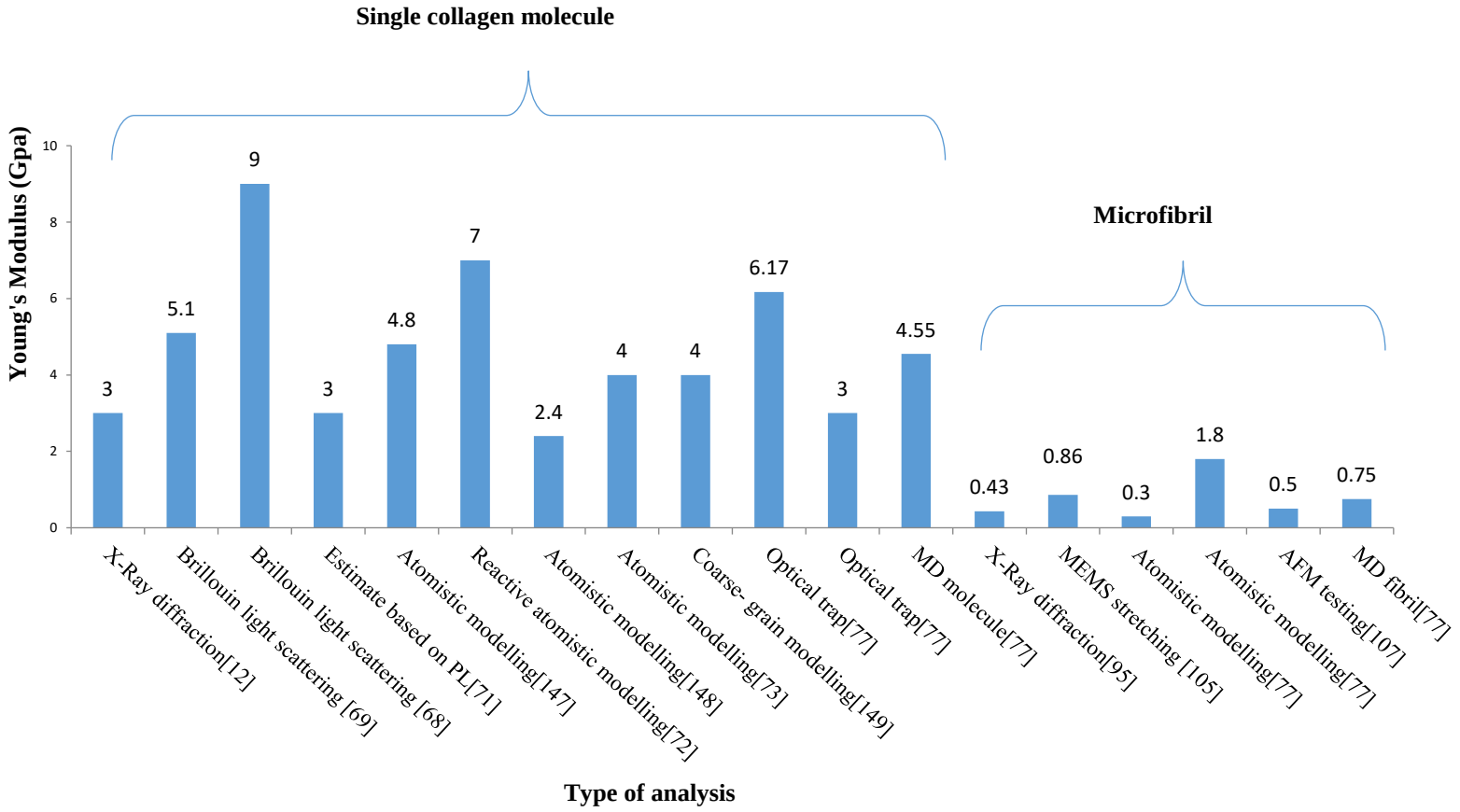

Figure 2.9. A direct comparison of the mechanical characteristics (Young's modulus) between single collagen molecules and microfibrils. Adapted and modified from (Gautieri et al., 2011; Vesentini et al., 2013)

2.6 Advantages of AFM and CA Over Other Imaging Techniques

AFM has various advantages compared to other high-resolution imaging tools such as SEM. Electron microscopy can only offer a two-dimensional image of the specimen unless complex stereo techniques are used. However, AFM can routinely offer three-dimensional images. One key feature is the exceptionally accurate capability of AFM in the vertical and lateral displacement of the sharp probe tip relative to the specimen surface by a computerised piezo scanner that permits precise dimensions of heights and distances. Moreover, AFM specimens do not need any specific preparation, such as carbon or metal coatings that might change or damage the specimen permanently. SEM can also be very expensive since it needs a costly vacuum environment to operate and requires significant setup time before the operation. Moreover, AFM is more suitable for biological macromolecules since all of its modes can operate routinely in an ambient air or liquid environment.

Furthermore, AFM can offer superior image resolution to SEM as it can provide true atomic resolution in ultra-high vacuum (Sylvain Ferrero, 2001) and liquid environments (Tolksdorf & Revenko, 2005). After staining the prepared tendon tissue with a heavy metal compound such as osmium tetroxide or uranyl acetate, most electron microscopes can then investigate the ultrastructure of tendon specimens. Controlling the ability of staining reagents to stain the tendon specimen is difficult. Therefore, electron microscopy studies compromise mainly with handling and specimen preparation to obtain artefact-free images. The preparation of the sample for SEM imaging requires fixation, coating, and dehydration for electron conduction. However, this preparation is very expensive and laborious.

These processes are unavoidable and unfortunately are concomitant with changes in tissue characteristics, resulting in undesirable changes in the morphological microstructure of the tendon. Special experimental protocols required for some procedures can deform tissue structure permanently. Furthermore, the preparation nature and environment of imaging can be damaging and can limit the use of electron

microscopy on *ex-vivo* and fixed samples. Electron microscopy suffers difficulties in the identification of specific matrix compositions (Bannerman et al., 2014). In contrast, AFM does not require quick-freezing, fixation, embedment, and staining of the sample for reliable conservation of the details of its morphology.

Ultrasound images can reveal the dimensions and the water content of the examined tendon tissue, and gives information on peritendon and collagen integrity. Different studies have identified an increase in Achilles vascularity and tendinopathy, which appears to correlate well with pain (Alfredson et al., 2003; Zanetti et al., 2003; Richards et al., 2005). Asymptomatic tendon damage demonstrates a tendon sheath swelling, an increase in the tendon dimensions, and a collagen discontinuity (Cook & Purdam, 2002). Ultrasound has a poor ability to distinguish between partial ruptures and tendon degeneration (Paavola et al., 1998) and is limited to superficial tendon tissue (Harvey et al., 2010).

Magnetic resonance imaging (MRI) has been employed with high tissue contrast to monitor pathological conditions of tendons. MRI can acquire images from transverse, longitudinal and oblique planes. The full potential of MRI has been poorly realised in providing a functional understanding into the microstructure of the tendon. This is possibly because of the low MRI signal intensity acquired from tendons, which appear as dark bands. These dark bands cause difficulties in extracting any physiological and structural meaningful information (Harvey et al., 2010). Furthermore, MRI suffers from difficulties in identifying specific matrix compositions. Although ultrasound and MRI (Chen et al., 2003; Nissi et al., 2004), were developed for the direct imaging of tendon microstructure composition and studying the Achilles tendon tendinopathy without the need for tissue processing, images revealed from these technologies often suffer from low spatial resolution, low chemical specificity and a difficulty in identification of the specific matrix composition.

Consequently, such images are incapable of providing a detailed picture of the Achilles tendon microstructure and the relationship of its molecular, cellular and extracellular components. This can lead to a poor or disturbed understanding of the pathogenesis of Achilles tendon tendinopathy. The micro/nanostructure of the tendon’s biomolecules and cells, the microsecond processes, complexity and diversity

of the molecular, cellular and extracellular interactions, the components of the tendon's microstructure and the pico-Newton level of these interactions, suggest that the aforementioned conventional bio-techniques are inadequate. Therefore, it is very important to explore new microscopic bio-techniques to study the microstructure and composition of Achilles tendons. This may assist in a better understanding of the clinical scenarios and an understanding of how the pathoanatomy correlates to the signs and symptoms of tendinopathy.

AFM has emerged as a powerful technique for biological research, not only offering an accurate investigation of collagen fibril nano-morphology (Graham et al., 2004) due to its unique accessibility to the ultra-high resolution of the three-dimensional nano/microstructural measurements of tissues, but also the study of molecular interactions and their mechanical forces such as friction and adhesion force, viscoelastic characteristics and stiffness (Carvalho et al., 2013; Vahabi et al., 2013). For a better understanding of tendon structure it is necessary to investigate the underlying morphological characteristics of the tissue and determine its relevant functional parameters.

Another advantage of AFM is its capacity to incorporate with other microscopy techniques such as fluorescence, optical, CA, SEM, Raman spectroscopy and other complementary microscopical techniques.

Fluorescence microscopy is illuminated usually by a high-energy ultraviolet light with a short wavelength, which results in a reduced depth of light penetration and the possibility of severe imaging damage to living tissues (Konig, 2000) Furthermore, the background noise caused by secondary fluorescence throughout the areas located up and down the focal plane can limit the sensitivity and spatial resolution. Confocal microscopy (CM) is one of the imaging techniques most commonly used in medical and biological science. This microscope is different from the fluorescence microscope in two main elements: a pinhole and the light source. CM has an aperture that can increase the sensitivity, spatial and image resolution to a large degree. If this aperture is opened, the resolution of the image can be disturbed and decreased. Also, because of the aperture, the absolute number of photons collected can be limited, affecting the resolution capacity (Zipfel et al., 2003). Compared to the fluorescence microscopes,

the excitation wavelengths of CM are very limited. However, CM high-intensity laser irradiation can be harmful to living tissues. The various disadvantages of the aforementioned imaging technologies can lead to different information about the hierarchical microstructure of a tendon in the literature.

In comparison with wide-field microscopy, the high-resolution image from confocal laser scanning microscopy (CLSM) has a lower speed. It is much faster to scan an image using an optical microscopic approach than using CLSM, and the image size is generally much smaller. Additionally, the excitation of the high-intensity laser in CLSM system can cause photodamage in some cases, and therefore it is important to have an optimal setting of laser power for imaging.

Recent technological developments have also provided great imaging techniques that have continuously approached the limitations in resolution and handling, with these developed CLSM operating systems. For example, the developments achieved with CA (described previously) (Jones et al., 2004; Smolinski et al., 2008; Wu et al., 2015) have brought a new concept of "sending the microscope to the tissue sample" with the *in situ* histological evaluation of ligaments, muscles, cartilage and tendons by CM using a small and light probe that is easy to operate and can be managed with one hand at the surface of the tissue.

CA includes high-resolution and high-magnification confocal capabilities within the boundaries of an arthroscopic probe to offer the imaging needed to accomplish a detailed evaluation of the examined tendon. It has a similar imaging technique to that of CLSM but still differs with a distinctive reduced laser scanning mechanism. CA is considered a high-resolution fluorescence microscopy that enhances the capabilities of conventional microscopy and assists in obtaining three-dimensional high-resolution images of thick tissues. The use of contrast agents with CA produces images with resolutions analogous to traditional histological evaluations (Kiesslich & Neurath, 2006; Aisenberg, 2008). It is also a well-established device that uses a minimally invasive approach to provide a video arthroscope in a probed tissue. CA imaging is non-destructive to the microstructure of tendons and can offer the benefits of clarifying the precise morphology of micro-damage in the tissue. To evaluate the tendon's microstructural changes, conventional histological analysis is generally used, which

involves collecting biopsies. The biopsy process itself is fundamentally destructive to the tendon sample. Therefore, a non-destructive evaluation technique is essential. The development of CA has avoided the disadvantages brought by biopsy and provided an efficient, easy and less laborious method to evaluate the changes in tendons as compared with histological methods.

A recent study attempted to assess the micromorphology of tissues without the need for mechanical biopsy. Wu et al (2016) developed a technique using CA to produce high- resolution images of the tendon's structure (Wu et al., 2015). They examine the potential of CA as a real-time optical histology for assessing the structural and pathological condition of rotator cuff tendons. They compare the confocal arthroscopic assessment for human rotator cuff tendinopathy with the traditional histological assessment demonstrating a 60% association between the two assessments. They suggested that CA can potentially be developed as a real-time optical histology for examining the collagen microstructure of tendons.

Although intensive experimental work has been carried out on the mechanical characteristics of individual collagen fibrils and provided new insights on stiffness and nonlinear deformation behaviour (Van Der Rijt et al., 2006; Shen et al., 2008), the mechanism by which the nanostructural changes at the fibril level cause macroscopic structural, biochemical and mechanical changes within the same intact bulk tissue has not yet been investigated. It is important to determine whether structural changes at the fibril level affect the macroscopic structural and mechanical properties or *vice versa*.

Therefore, a broader range of mechanical and macro/nanostructural measures needs to be incorporated in an animal model to assess different tissue responses across different hierarchies and to understand how load is transferred across hierarchical scales within the intact bulk of the same tendon with the same boundary conditions.

This can be achieved by utilising AFM to evaluate the nanoscale quantified changes and by integrating CA with a mechanical testing device to evaluate the macroscale changes that can be compared with the AFM images. Since CA has been regarded as the gold standard for assessing articular cartilage (Hjelle et al., 2002) and degenerative

and non-degenerative aspects of articular cartilage that has been implemented by CA (Jones et al., 2004), the CA assessment of articular cartilage or other tissue such as tendons seem like a promising next step in orthopaedic and biomechanics research. Therefore, it seems that a device incorporating both CA and mechanical testing could successfully play an important role in the assessment of micro and macroscale structural changes in such small tissues subjected to different mechanical interventions (Figure 2.10).

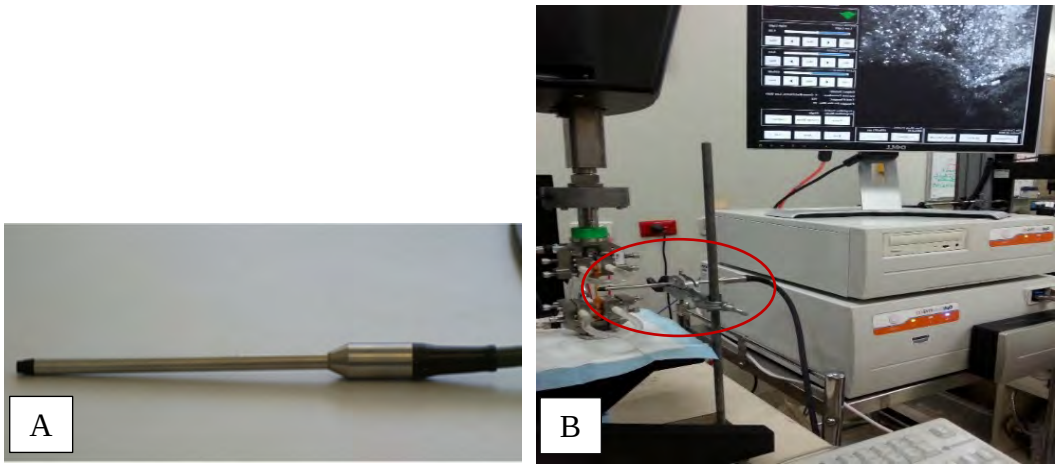

Figure 2.10. The combination of CA with the tensile mechanical device (Instron). This integration of the Instron with CA can precisely probe the macro-morphological and mechanical changes of a rabbit tendon that is embedded within a repeated cyclic loading of different strains throughout a complete mechanical testing protocol of the same intact tendon with the same boundary conditions. Then these macrostructural changes can be linked to the same tendon with the nano-morphological changes that can be probed by the powerful AFM.

CHAPTER THREE:
MATERIALS AND METHODS

3.1 Introduction

The hierarchical structures of tendons range in size from Angstroms to millimetres and all contribute to the overall mechanical characteristics of the tendons. The role of the tendon is complex, and controlled loading during functional tasks, often induced by multi-axial loads, is important for tendon health. Investigations of tendon function and pathology are often restricted to a limited range or scale of assessment. This results in the employment of a wide range of different approaches or techniques to evaluate changes in the structures within the tendon during repetitive loading. Very few studies have attempted to correlate parallel changes at different scales of the tendon.

This study made multiscale assessments of the characteristics of tendons exposed to different levels of strains using a repeated cyclic loading protocol. Tendons were conditioned using three strain levels (3%, 6% and 9%) with four different blocks of cyclic loading (for durations of one to four hours). Also, tendons exposed to chemical GAG depletion were studied to examine the effect of depletion on the mechanical and structural properties of the tendon.

The study utilised different imaging and assessment techniques to determine characteristics at multiple scales. A mechanical loading device was utilised to apply controlled cyclic mechanical stimuli to assess the change in mechanical properties of the whole tendon. A visual determination of structural changes at the fascicle and fibre level during loading was recorded using confocal microscope (CM) digital photography. All other sequential structural assessments were undertaken on section preparations that destroyed the tendon, so slices were placed on slides after each one-hour block of mechanical loading. This allowed for a visual determination of structural changes at the fibre and fibril level assessed by traditional histology and atomic force microscopy (AFM).

The significance of this study is that it is the first to examine a mechanical fatigue 'tendonopathy' model across a large range of strain and dose. It is also the first study to run mechanical assessments across such a large scale of investigation. Finally, the mechanical model of tendinopathy is combined with the depletion model to examine the molecular interactions and changes that occur with a depletion of GAG. This work has the potential to contribute to a better understanding of the inconsistencies in the literature about the hierarchical structure of a tendon.

3.2 Ethics

Animal samples were collected from the large animal facility, the Animal Care Services, at The University of Western Australia, Perth. White rabbits were euthanised and used for a separate medical school teaching course (Physiology of Cardiovascular and Respiratory Systems PHYL3002) approved by The University of Western Australia's animal experimentation ethics committee. Tendons harvested from those rabbits were used in this study, with approval for post-mortem studies at Curtin University granted by the university's laboratory officer. Secondary approval for post-mortem collection was granted by the Human Ethics Committee UWA (HREC) No. RA/3/200/547. (Animal ethics approval is shown in Appendix 2.) Ethics approval was sought by Curtin University through reciprocal approval from The University of Western Australia. The teaching activity did not systematically impact the lower limb, nor the tendons used for investigation. The tendons were made available after sacrificing the rabbits.

3.3 Experimental Design

The experimental work reported in this thesis was undertaken on white New Zealand rabbit Achilles tendons using varying doses of repeated cyclic mechanical loading. The mechanical profiles during these repeated loadings were recorded and the mechanical characteristics were correlated with the observed changes in structure from multiscale assessments of the tendons. The thesis is categorised into two studies:

Study 1A – Visual Assessments

Study 1A was the repeated assessment of the changes to confocal visual assessments under the different mechanical loading profiles (three strain levels and four dose periods).

This study specifically focused on the mechanical and macrostructural changes of Achilles tendons following repeated cyclic loading. After harvesting, the tendons were separated into two experimental groups. Nine tendons were placed into the control group as intact normal healthy tendons,) and 36 were used in the strained group. The allocation of the left and right side tendons was randomised.

Study 1B – Mechanical Assessments

Study 1B was the same as Study 1A in the aspect of the mechanical intervention; however, the structural analysis was undertaken at the nanoscale level using AFM. This study reported an experimental approach combined the macroscopic mechanical loading of tendons from Study 1A with a morphometric nanoscale assessment of longitudinal and cross-sectional collagen fibril responses to load. The AFM analysis of the cryosections assessed the nanostructural variables and compared them with the tendon's mechanical and macrostructural changes in the strained group. The sections from the control group were also compared with sections from the strained group.

Study 2 – Depletion study

Study 2 was a repetition of Study 1; however, it used only one strain level (6%) and dose period (two hours). New tendons were allocated randomly to either a control or a GAG-depletion preconditioning group. Extensive laboratory protocols were used to document the level of GAG depletion achieved by the preconditioning to ensure the validity of the depletion model. The specific assay used to measure GAG content is reported in Appendix 3.

Study 2 incorporated a multiscale assessment of a separate set of tendons (both controls and GAG-depleted) that received the same mechanical cyclic loading interventions and structural assessments as those in Study 1. This study was undertaken to examine the chemical depletion model following mechanical loading.

This study used the experimental approach of Study 1A and B, and combined macroscopic structural and mechanical characteristics with a morphometric nanoscale assessment of the longitudinal and cross-sectional collagen fibril responses to load of GAG-depleted fibrils. The AFM analysis assessed changes in the nanostructural variables in cryosections and then compared these with tendon mechanical changes and GAG content in the GAG-depleted groups. The sections from the control group were compared with sections from the strained group where GAG had been enzymatically depleted using chondroitinase ABC (Ch-ABC) prior to mechanical testing. Overall, the experimental design of Studies 1 and 2 incorporated a repeated assessment with load (strain) and dose (cycles/time) as the independent control variables.

First Intervention Control Parameter (control parameters

First intervention control parameter was the Load): The load. Load was defined by three levels of strain. As described by Wang et al. (2013) (our collaborators from the University of Western Australia on the ARC (Australian Research Council) Linkage project) 3%, 6%, and 9% strain were used as the different loads, these were established following a standardised preconditioning protocol described in detail under section (3.8).

Second Intervention Control Parameter (the intervention control parameter was Dose): The dose of the mechanical stimulus was defined by duration (number of cycles). Tendons were randomly assigned to five equal groups (n = 9) namely: control (preconditioning only), one, two, three, and four hours duration. The control group was preconditioned with 3%, 6%, and 9% strain (for each strain level n = 3). The loaded tendons (n = 36) received 3%, 6%, or 9% strain loading for one, two, three, or four hours (see Figure 3.1). All tendons were subjected to cyclic repeated loading at a frequency of 1 Hz.

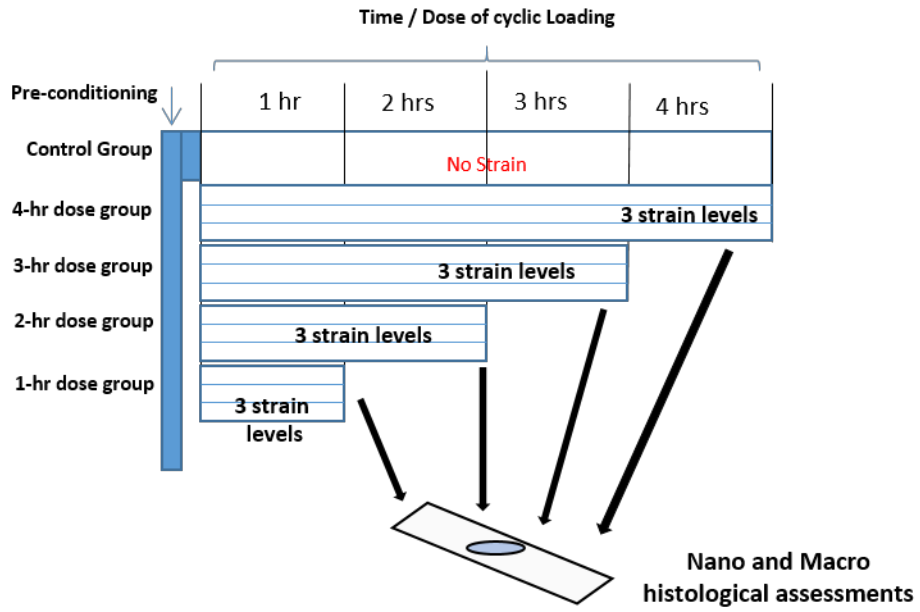

Figure 3.1. Schematic representation depicting the experimental design for the fatigue testing of tendons over one, two, three, or four hours of repeated cyclic loading under three strain levels (3%, 6%, or 9%).

The load and the dose (hours of duration of cycles) are the independent variables. The load was defined by the three levels of strain. Note that the mechanical loading data was recorded continually and therefore data for a one-hour duration was recorded for all tendons, three groups had two hours of data, two groups had three hours, and only one group had four hours of data.

The study utilised different imaging and assessment techniques to determine characteristics at multiple scales. To determine the effects of fatigue loading on the macroscale mechanical and structural characteristics of the tendons, all of the prepared tendon samples were assessed by subjecting them to confocal imaging and quasi-static tensile testing using a confocal arthroscopy (CA) conjugated with an Instron tensile testing machine (Figure 2.10).

Several post-processing macro-mechanical variables were calculated from the loading data to examine both load and time-dependent properties. After preconditioning, the Instron's preloading feature (preload limit ~5 N) was used to remove slack, similarly

to the methods described by (Thorpe et al., 2014), and then to start the mechanical testing.

To ensure that each tendon started from the same strain and load point, all the strain sourced either from the extensometer or the crosshead extension was auto-balanced after the time of preloading. Therefore, the gauge length was adjusted by the preloading state. Data were sampled at 50 Hz and time-stamped data were saved to a CSV file. The data in the CSV files were read into a custom-built (Curtin University School of Physiotherapy and Exercise Science) LabVIEW program that derived the raw data and further statistical analysis of the data was undertaken.

There were two main phases of assessment in each loading block. The first phase in each block was a sustained hold period and the second phase was the repeated cyclic loading (240 cycles in each block). The following section outlines the variables in each phase.

3.4 Mechanical Variables

The cyclic loading testing protocol (described in Section 3.7) incorporated a static hold phase and then a dynamic cyclic loading phase. The variables in each phase are described below.

3.4.1 Static loading Variables

A. Stress-Relaxation (SR)

In each loading sequence, a sustained hold for 60 sec at a set strain (length) was performed while the stress (force) was recorded. As defined within the literature, the decline in the stress over the static hold length is known as stress or force relaxation at a set strain value. Stress values were determined at the beginning (SR1 $Strain_{Max}$), middle (SR2) and end (SR3) of the static hold (Figure 3.2).

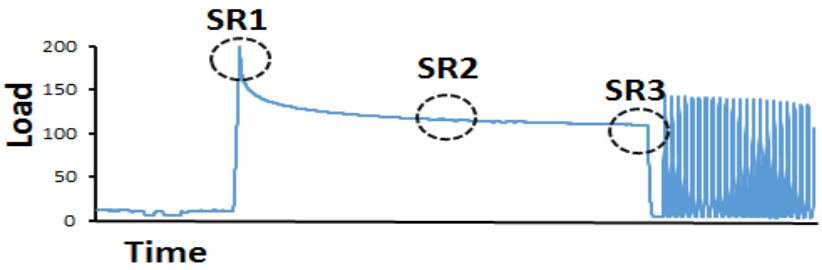

Figure 3.2.The SR at three different points during the 60 sec maximum hold period ($Strain_{Max}$) expressed as the maximum value at the start (SR1) then a decreased amount of relaxation at the middle (SR2) and at the end of the strain dose (SR3).

In order to remove interference (noise) caused by CA being measured during the SR block, the load *vs* time data was fitted to a dual exponential model (eq 3.1):as per the method of Fratzl (2008):

$$FR = k_0 + k_1 e^{-t/\tau_1} + k_2 e^{-t/\tau_2} \quad \text{(eq 3.1)}$$

Where k_0 characterizes the percentage stress at the equilibrium state of the relaxation process and τ_1 and τ_2 are the short and long term time constants, respectively. The variables were determined from the fitted curve.

B. Ramping Stiffness (*k1*)

The ramping stiffness was calculated as the linear slope (*k*) of the high-strain regions of the force-displacement data. The end of the linear region was identified automatically by the algorithm as follows: a linear regression was employed to fit the first strain data subset (that with the highest stress) and the coefficient of variation (R^2) was calculated for a linear fit. If the R^2 values exceeded a cut-off threshold value of 0.99, then the following lower-strain value was added to the subset. This process of adding the following lower-strain data point was repeated until R^2 declined below the cut-off threshold value of 0.99. The final data point that dropped the overall R^2 below the determined threshold was selected as the initial transitional point between the exponential region and the linear region. This method was adopted as it was consistent with (Rainis, 2007; Drury, 2008).

C. Maximum Load (ML)

The ML was defined as the peak load value which corresponded to maximum stress.

3.4.2 Cyclic Loading Variables

A. Loading Stiffness (*k2*)

The loading stiffness was calculated as the slope of the end of the linear portion fit of the load-displacement curve in the cyclic phase of testing. It was calculated according to the piecewise method described above (ramping stiffness). As a result, there were two calculations of stiffness for each of the cycle blocks.

B. Energy Dissipation (Hysteresis, *h*)

Since the tendons were viscoelastic, some of the energy stored during loading of the strained groups was lost during unloading or the recoil from the stretch. The amount of this lost energy is known as hysteresis. This energy dissipation (hysteresis area) was calculated as the area between the loading and unloading force-displacement curves in cyclic tensile testing (Freedman et al., 2014; Freedman et al., 2015; Connizzo et al., 2016) (See Figure 3.3). In each cycle of a dynamic tensile test, area a_1 was found by stretching the tendon and area a_2 was recovered in the subsequent unloading recoil. The percentage energy dissipation is given as (eq 3.2):

$$h = 100(a_1 - a_2)/a_1 \qquad \text{(eq 3.2)}$$

A larger *h* area calculated for a specific tendon sample reflected a lower recoil ability of this tendon sample (Butler et al., 1978; Taylor et al., 1990).

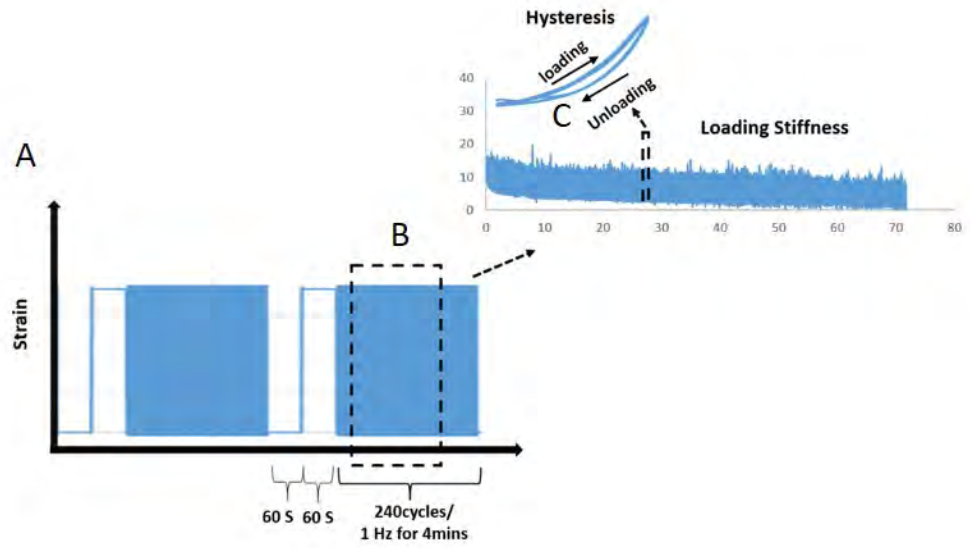

Figure 3.3. A demonstration of the repeated cyclic loading phases and the analysed variables (hysteresis and loading stiffness). The expanded figure B shows the load outputs for 70+ cycles. The expanded figure C shows the representative stress-strain curve for one cycle of loading and unloading. From this the hysteresis was calculated.

3.5 Macroscale Structural Variables

A. Qualitative Macrostructural Variables

i. GAG Content

GAG concentration and distribution have been suggested to contribute to the mechanical behaviour of the tendons (Merrilees & Flint, 1980; Koob & Vogel, 1987; Koob, 1989; Vogel & koob, 1989; Kannus et al., 1992; Paavola et al., 2002; Smith et al., 2002). The GAG content was estimated by assessing Alcian blue-stained slides (obtained from conventional histological images). The slides were stained with Alcian blue (pH 2.5 %)/periodic acid-Schiff (AB/PAS) for detection of GAG-rich areas to assess GAG content (more detail is given in Appendix 4). The degree of staining was assessed using a semi-quantitative score based on a validated four-point scoring system (Maffulli et al., 2000; Svensson et al., 2005; Gagliano et al., 2013) which is a modification of the scoring systems of Movin and Kartus (Movin et al., 1997; Movin, 1999; Kartus et al., 2000), where:

1. *No alcianophilia:* no staining seen between collagen fibres
2. *Slight alcianophilia:* slight staining between the collagen fibres
3. *Moderate increase in alcianophilia*: moderate staining
4. *Markedly increased alcianophilia:* strong staining forming blue lakes

This is a scale of 1–4, where 4 represents very strong staining and 1 represents no staining. Three sections were selected randomly from each tendon specimen and were assessed by two independent examiners and the average scores were used for comparison.

ii. Fibre Structure

The fibre structure was described according to a validated scoring system used by Chen et al. (2011), Svensson et al. (2005), Gagliano et al. (2013) and Maffulli & Kader (2000) who have used a modification of the scoring system of Movin and Kartus (Movin et al., 1997; Movin, 1999; Kartus et al., 2000). (More details on the scoring system are in Appendix 5)

1. *Severely fragmented fibres:* strongly discontinuous and separated fibres showing major gaps along the fibre longitudinal axis
2. *Moderately fragmented fibres:* a mix of continued and discontinued long fibres but with fibres that were moderately separated from each other with larger gaps along their axis
3. *Slightly fragmented fibres:* packed continuous long fibres but with fibres slightly separated from each other with some minor gaps along their longitudinal axis
4. *Non-fragmented fibres:* packed continuous long fibres with no gaps between the fibres along their longitudinal axis

This is a scale of 1–4, where 4 represents a continuous, long fibre, and 1 represents a severely fragmented fibre. (More detail on the scoring system is given in Appendix 5.) These variables were used to assess the histological changes induced by mechanical load on the different loading and unloading groups.

Three sections were selected randomly from each tendon specimen and were assessed by two independent examiners and the average scores were used for comparison.

iii. Fibre Arrangement and Orientation

Fibre orientation and arrangement were described according to a validated scoring system used by Chen et al. (2011) and Maffulli & Kader (2002) who have used a modification of Aström's (1995) system, and according to another system by Movin (Aström et al., 1995; Movin et al., 1997; Movin, 1999).

1. *Severely abnormal appearance*: moderately loose and wavy, fibres crossing each other with an unidentified pattern.
2. *Moderately abnormal appearance*: increasingly loose and wavy, and fibres cross each other
3. *Slightly abnormal appearance*: slightly loose and wavy
4. *Normal appearance*: compacted, parallel, regular and well-ordered

This is a scale of 1–4, where 4 represents a normal appearance and 1 represents a severely abnormal appearance. (More detail on the scoring system is given in Appendix 5.) Multiple sections were randomly selected from each sample.

iv. Tenocyte morphology

Tenocyte morphology was described according to a validated scoring system used by Chen et al. (2011) and Maffulli et al. (2000) who have used a modification of the system by Movin et al. (Movin et al., 1997; Movin, 1999; Kartus et al., 2000).

1. *Normal appearance*: long spindle-shaped cells
2. *Slightly abnormal appearance*: slightly rounding nuclei
3. *Moderately abnormal appearance*: moderately rounding nuclei
4. *Severely abnormal appearance*: severely rounding nuclei

This is a scale of 1–4, where 4 represents a normal appearance and 1 represents a severely abnormal appearance. (More detail on the scoring system is given in Appendix 5.)

Three sections were selected randomly from each tendon specimen and were assessed by two independent examiners and the average scores were used for comparison.

B. Quantitative Macrostructural Variables

i. Tenocyte Morphology

It has been reported that change in cell morphology of equine tendon fibres subjected to cyclic loading *in vitro* from a spindle shape to a round shape is accompanied by matrix damage (Thorpe et al., 2015). Tenocyte morphology was assessed using the tool kit "Circularity" (an ImageJ-plug-in) in the widespread image analysis software ImageJ (NIH, MD) as previously reported (Schochlin et al., 2014). For the analysis of extracted image cell shapes, "analyse particle" was applied and the following three measurements for analysis were used:

- *Circularity:* defined as: $4*\pi*\text{area}/\text{perimeter}^2$
- *Aspect ratio:* defined as major_ axis / minor_ axis
- *Solidity:* defined as area/ convex_ area

Briefly, the greyscale /8-bit or 16-bit CA image was opened (See Figure 3.4A). A copy of the image was made by applying Image>Duplicate.

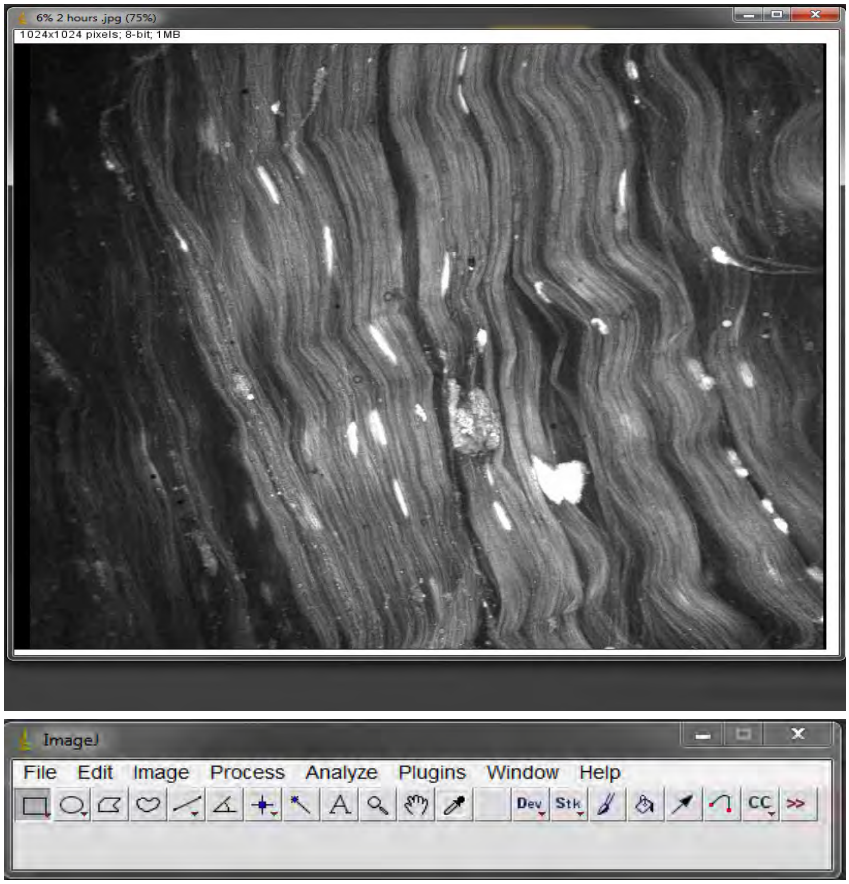

Figure 3.4A. The extracted image of the cell for shape analysis

Figure 3.4B. A binary image created by applying Image>Adjust>Threshold options

This copy was used to create a binary image. A binary image was created by applying the Image>Adjust>Threshold options (See Figure 3.4B) to highlight all of the structures in the image (fibres and cells). The binary image was highlighted either by the sliders, or the “set” button was used to type in a known range of pixel intensities. To subtract the “noise” or background pixels that were highlighted and not wanted, applying Process>Subtract background with rolling helped keeping only the targeted elements highlighted in the image (the cells). This created a binary version of the image with only two-pixel intensities: black = 0 and white = 255 (See Figure 3.4B).

To avoid all the intensity values from the binary image being read as 255, the Analyse>Measurements option was applied and the Redirect to line was set to the name of the copy of the image that was still grayscale. The binary image (See Figure 3.4B) was clicked to select it, then Analyse>Analyse Particles was applied (See Figure 3.4C). As for quantifying the different tenocyte shapes within each image, tendon cells were classified based on factor values, representing the cell shapes, and sorted into four categories:

- *Cat 4: Spindled*, circularity values > 0–0.35
- *Cat 3: Elongated,* circularity values ≥ 0.35–0.6
- *Cat 2: Oval,* circularity values ≥ 0.6–0.8
- *Cat 1: Round*, circularity values ≥ 0.8–1.0

as previously described (Schochlin et al., 2014).

The form factor 1.0 represented a perfect circle and 0 represented a straight line.

Figure 3.4C. The quantification of different tenocyte shapes within each image. Shapes were classified as elongated based on a factor value (circularity values 0.35–0.6).

ii. Fibre Crimp Frequency

The crimp frequency is the number of occurrences of a repeating periodic wave formation. The waviness characteristic of collagen bundles in the tested groups was quantified according to methods used by (Rezakhaniha et al., 2012). Briefly, in three different regions of interest (ROI) of each CA image (See Figure 3.5), the distance between the visible endpoints of a collagen bundle (L0), the length of the fibre bundle (LF) and the thickness were calculated using the tool kit "NeuronJ" (an ImageJ-plug-in) from the widespread image analysis software ImageJ according to methods described previously (Abràmoff et al., 2004; Meijering et al., 2004; Meijering, 2010). This plug-in was designed for neurite tracing and analysis (Meijering et al., 2004). The plug-in traced the fibres on a 2D image and provided the output the fibre length (LF) in addition to the coordinates of the endpoints. Most fibre bundles were larger than the field of view (50 Microns), therefore, these parameters were measured for the portion of the fibre bundle seen in the field of view.

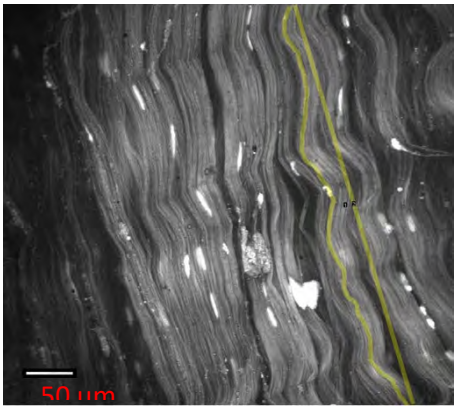

Figure 3.5. A demonstration of the defined parameters and length (LF) and the straight length (SL) connecting the ends of the measured fibre bundle. To quantify the waviness of fibres, the straightness parameter (SP) is defined as, SP = *SL/LF* (1). SP was confined to between 0 and 1. The lower the value of SP, the higher the waviness of the fibre. A bundle with SP = 1 indicates a completely straight fibre. SP approaches zero when the fibres become highly wavy.

iii. Fibre orientation and anisotropy

The fibre anisotropy is the property of the fibre bundles being directionally dependent as seen and well-ordered fibres in the CA images. The orientation and anisotropy of fibres structures

in CA images were analysed using the tool kit “FibrilTool” (an ImageJ-plug-in) in the widespread image analysis software ImageJ (NIH,MD) (See figure 3.6).

This tool was validated to study the collagen orientation and anisotropy previous studies [25, 26]. More specifically, FibrilTool concept is based on the nematic tensor, to quantify the main orientation of fibre structures in CA images and measure their alignment. Briefly, this tensor was calculated by computing the pixel intensity level in a specific region of interest (ROI) in the CA image. The gradient of intensity level permits the characterization of a tangential unit vector to fibres. The smoothing step was unrequired when using this tool since it basically included only a first derivative and it was less sensitive to noise.

To extract quantified information, circular statistics from the FibrilTool software were utilised, which were adapted to directional data, to analyse the properties of the tangent direction over the ROI. The average orientation in this region (fibre orientation) and the score assessing whether the fibres were well ordered (fibre array anisotropy) were both defined by the tangent’s circular average and variance directions respectively. The anisotropy score was defined as the following scoring scale: 0 for no identifiable pattern (purely isotropic fibres) and 1 for parallel, regular and well-ordered fibres (purely anisotropic fibres).

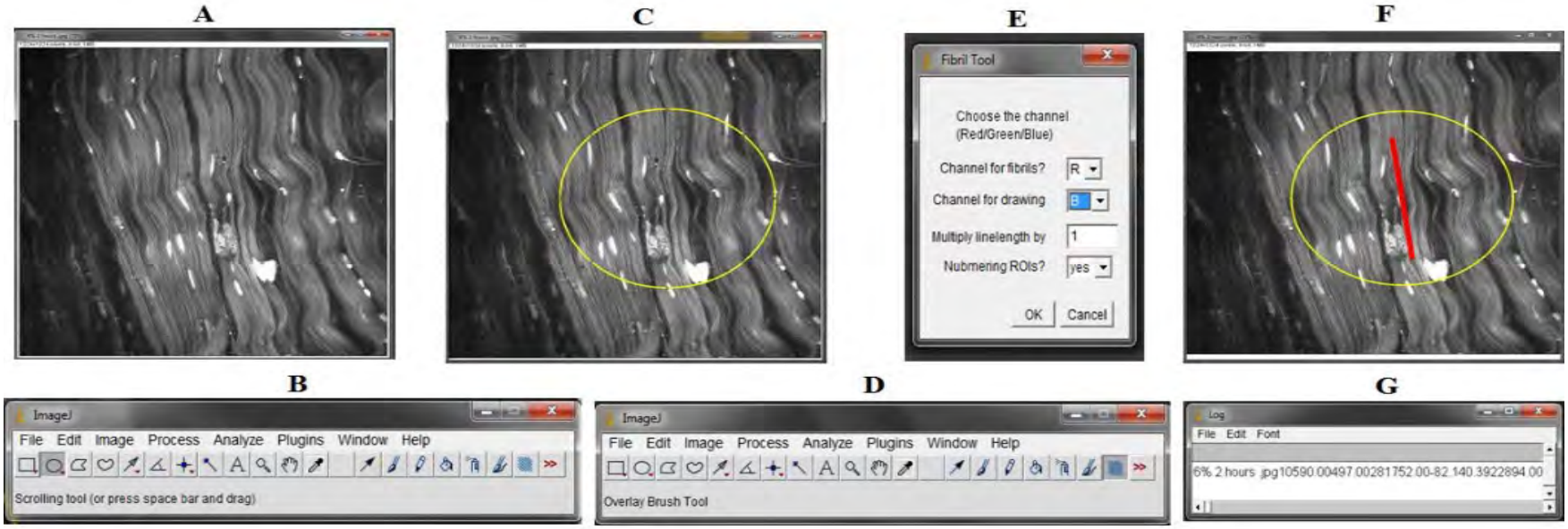

Figure 3.6. A demonstration of the FibrilTool plug-in the image analysis software ImageJ. A) The image is opened in ImageJ. (B) The circle tool is used to mark the ROI. (C) A ROI is selected by a circle tool, avoiding saturating pixels. (D) The FibrilTool plug-in appears as a striped square in the toolset. (E) The FibrilTool dialogue box allows channels to be selected and a multiplying factor for the length of the line segment that was drawn on the image to be chosen (visualising the anisotropy of the array) and a decision as to whether the ROI number is to be shown or not. F) Output from FibrilTool: A red segment appears, its orientation corresponds to the average orientation of fibres in the image, whereas its length is proportional to a number (termed anisotropy) that quantifies how parallel the fibres were in the ROI. (G) A log file collects the quantifications, notably including the average orientation and anisotropy of the fibre.

3.6 NanoStructural Variables

A. Quantitative Nanostructural Variables

i. Fibril D-periodicity

The cryosections parallel and perpendicular to the tendon surface were suitable for AFM imaging. Tendon specimens were sectioned and the cutting plane was set to be parallel with the long axis of the tendon. Random locations on the samples were imaged by AFM in search of fibril bundles. From each section, a minimum of five 3.5 µm by 3.5 µm ROI were analysed. For each ROI, 10–15 individual fibrils were randomly identified for analysis within each fibril bundle and different fibril bundles in each location were analysed. For each analysed fibril, a line of analysis was selected on the long axis of the fibril in the x–y imaging plane, and the two-dimensional profile in the z-axis was plotted (See Figure 3.7). 10 D-Periodicities were averaged to provide the D-Peridoicity length measurement for each fibril. The D-periodicity was calculated from the plot obtained from the Nanoscope software (Wallace et al., 2010; Fang et al., 2012; Erickson et al., 2013) to reveal the periodic banding frequency (See Figure 3.7).

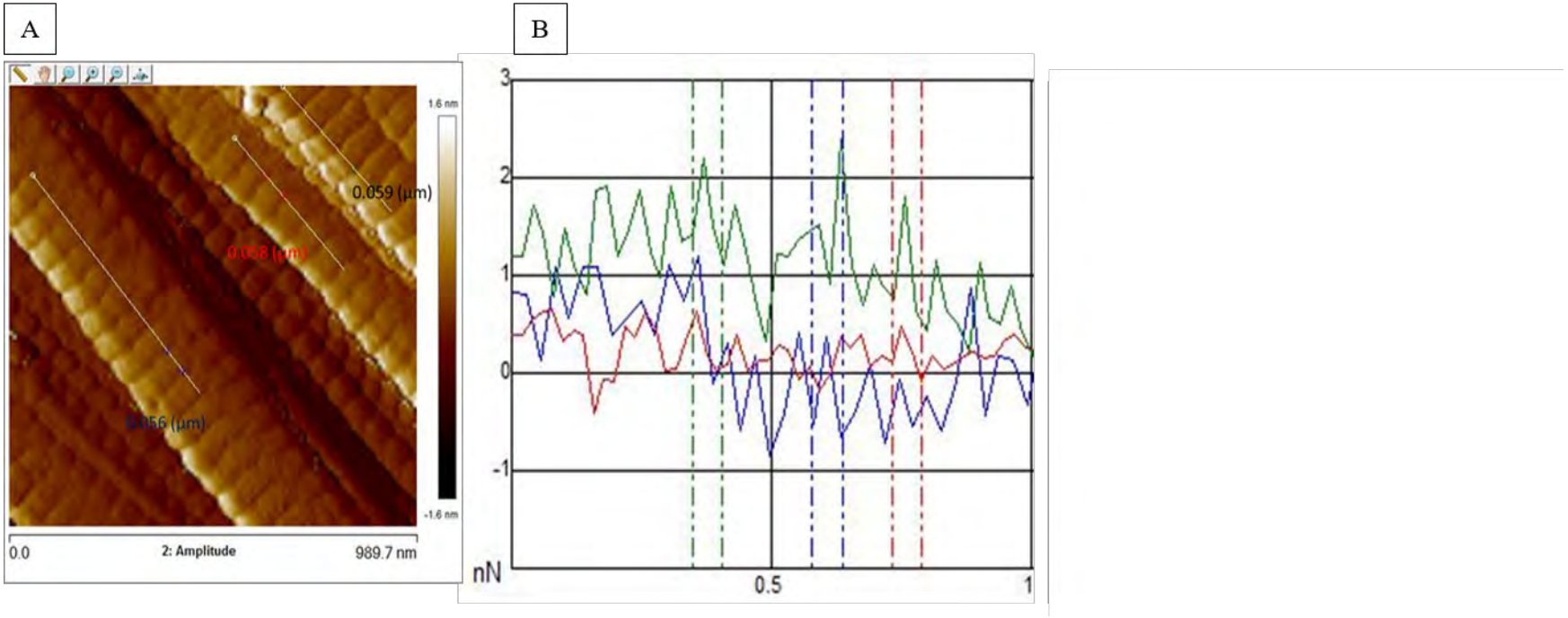

Figure 3.7. A schematic representation of the D-periodicity measurements of Type I collagen from Achilles tendons. (A) AFM amplitude image of tendon fibrils. The D-periodicity is observed as striped patterns perpendicular to the fibril axis. (B) A two-dimensional profile of the three lines. In (B) the 2D profile from inset (A) is presented to show the correspondence of fibril D-periodicities.

To examine the D-periodicity distribution of the mid-substance across tendon strain conditions (3%, 6%, and 9% strain groups), all D-periodicity lengths of measured collagen fibrils within a given tendon were pooled. The reference D-periodicity length in the tendon was determined. The control group (from Study 1A) was used as a reference for statistical comparison for elongation or strain. Therefore, all D-periodicity lengths were accordingly normalised to the control D-periodicity length to calculate the D-periodicity spacing strain. For any within-fibril-bundle (WFB) and between-fibril-bundle (BFB) variations of same and different regions, multiple regions along the axial direction of a fibril bundle (fibre) (20–50 μm distance) were investigated. (See Figure 3.8).

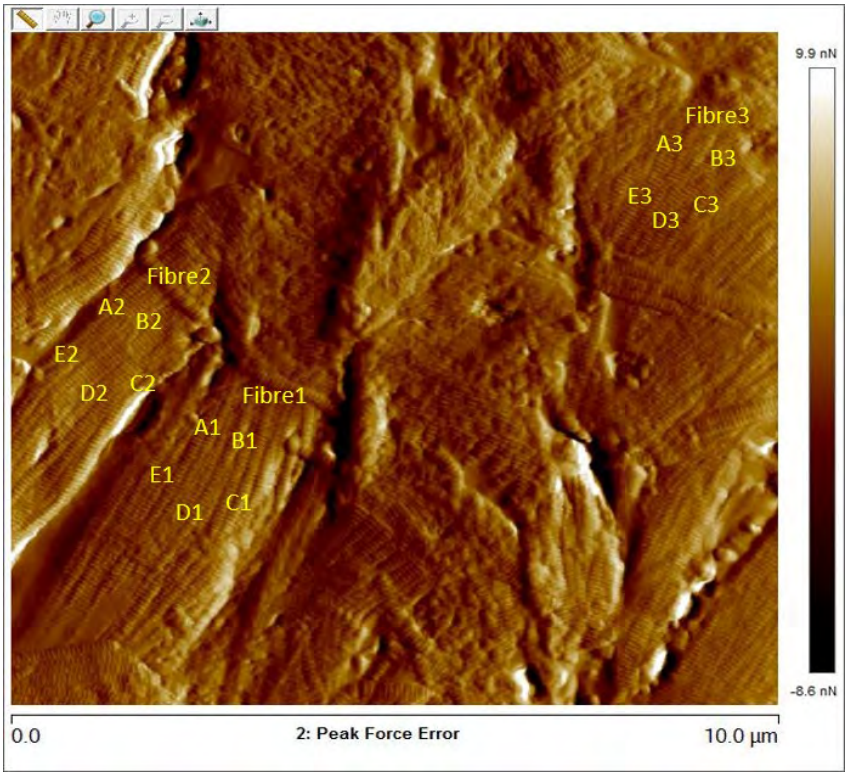

Figure 3.8. An AFM image depicting the height images of collagen fibrils within their bundles. Two fibres within 3.5 μm × 3.5 μm ROI were labelled by sequence (A, B, C, D and E) and covered on the 10 μm scan. The D-periodicity spacing was calculated by examining five regions (A1–E1) at Fibre 1 (noted as Fibre 1) while five other regions (A2–E2) were similarly examined at Fibre 2 and again at Fibre 3 (A3–E3).

Table 3.1. The mechanical and macro- and nanoscale structural variables assessed by different instruments and technical procedures.

Scale	Variables	Instrument/Technique/Software used for Investigation
Macroscale	Stress/strain curves (*h*, ML, *k*)	Mechanical instrument (Instron)
	Fibre structure	Qualitative histological scoring according to modified Movin and Kartus scoring systems
	GAG content	Qualitative histological scoring according to modified Movin and Kartus scoring systems
	Fibre crimp frequency	CA/Image J
	Fascicle orientation and anisotropy	CA/Image J
	Shape of tenocytes	CA/Image J
Nanoscale	WFB and BFB D-periodicity	AFM

3.7 Experimental Protocols

A. Study 1A

i. Tendon Collection and Preparation – Mechanical Loading

In total, 45 full-length Achilles tendons, including the bone-tendon and tendon-muscle junction were dissected from the hind limbs of 10–20 week-old, 2–4 kg, female and male euthanised New Zealand white rabbits (*Oryctolagus cuniculus*). All tendons were obtained approximately 20 minutes after the euthanising of the rabbits and were immediately frozen at –20°C.

ii. Thawing and Anatomical Preparation

Tendons were defrosted overnight in a refrigerator at 4°C and on the day of testing, the tendons were thawed to room temperature. The samples consisted of the Achilles tendon, and part of the gastrocnemius muscle proximally and the calcaneum distally. Preparation of the tendons involved the removal of all accessory tendon insertions and extra muscle tissue by sharp dissection.

iii. Fluorescent Staining

Tendons were stained with fluorescent acridine orange (AO); a cationic selective nucleic acid dye used widely for imaging including cell nuclei tracking during mechanical testing visualised under the confocal microscopy (Screen et al., 2003, 2004). As a permanent fluorophore under the 488 nm excitation wavelength, AO offers high contrast images of the cell nucleus by binding to fragments and nucleic acids. Acridine orange solution (Eugene, Oregon, USA), was used at optimal staining duration and concentration (0.3 g/L for 45 mins) in order to provide maximum contrast and image resolution; this was followed by three repeated washings with phosphate-buffered saline (PBS) to remove the excess stain. At higher concentrations (> 0.3 g/L), the staining became non-specific and stained the matrix and collagen constituents.

iv. Cross-Sectional Area

A digital Vernier caliper (accuracy to ± 0.01 mm) was employed to measure each tendon's diameter twice at its narrowest point. The distance between grips was

measured with the digital caliper and was defined as the initial length. After preconditioning, the distance between the grips was measured again with the digital caliper and was defined as the preload length. The strain was calculated based on the preload lengths or the baseline status after pre-conditioning. Then the tendons were preloaded with ~5 N and underwent the designed interventions (3%, 6%, and 9% strain for one, two, three and four hours).

v. Tendon Fixation for Instron

Both ends of each tendon were placed in the lower and upper freezing micro-grips (See Figure 3.9) with 16 mm to 30 mm gauge lengths. The two freezing grips were serrated and tightened by two screws, securing a connection. In the experimental design, both freezing grips had a thermoelectric cooler to cool the outer gripping surface. The thermoelectric cooler was isolated electrically from the outer gripping surface of the freezing grips. The outer surface of the freezing grips contained an unfixed jaw plate that included an outer unique surface appropriate for the gripping of various sizes of tendon tissues.

Fascicle orientation and alignment were checked under CA to confirm that fibres were aligned with the direction of loading (vertical). The angle of the grips was changed to minimise the degree of twisting of the gross tendon. The gripping surfaces were then cooled and the tissue neighbouring the gripping surface was frozen within the thermoelectrically cooled (TEC) grips as described by (Hayes, 2017). The frozen parts of both of the tendon's ends were clamped by the freezing grips with an applied load sufficient to hold the tissue while tolerating the compression forces of the freezing grips with minimal deformation. The tissue neighbouring the gripping area was also frozen, thus the grip's clamping load was distributed equally among the tendon's gross tissues and potential tissue damage was decreased.

The freezing grips assisted in testing the mechanical properties of the tendon without damaging and breaking its tissue at the gripping site. No slippage was observed, neither during the mechanical testing, nor when inspecting the clamped parts upon test completion. A controller was electrically attached to the Laird thermoelectric liquid

cooler to control the temperature and the cooling rate of the outer gripping surface of the freezing grips.

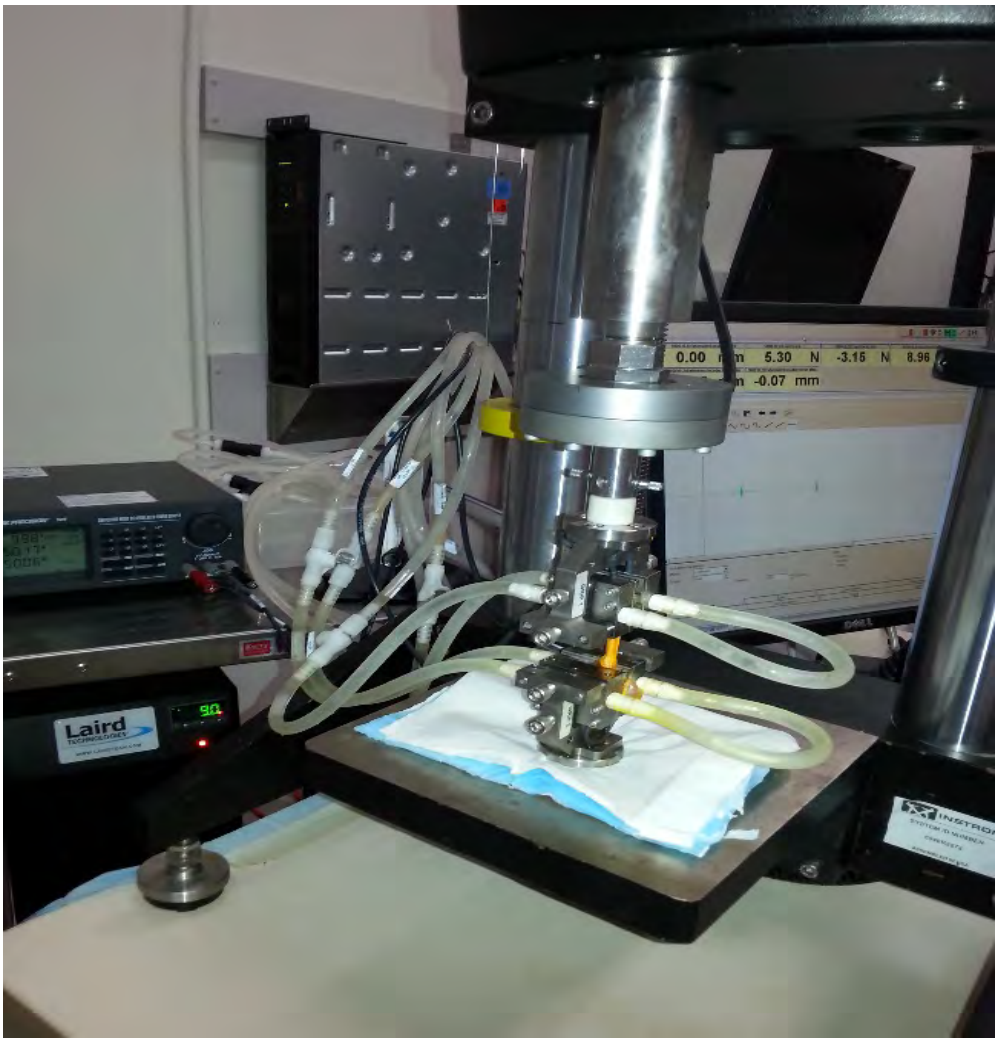

Figure 3.9. An image of the micro freezing grips coupled electrically to a temperature control system and power supply. The upper grip was connected to the actuator of the testing machine via a 2 kN load cell of custom design.

3.8 Macroscale Mechanical Protocol

A. Mechanical Preconditioning

The test protocol consisted of consecutive sets of SR loadings after a consistent preconditioning protocol. Each tendon was preconditioned for 720 cycles at a specific strain (3%, 6% and 9%). Then each strain was used for the subsequent cycles over one mechanical cycle sequence. (See Figure 3.10A).

B. Cyclic Loading

The mechanical loading for each tendon was predominantly a cyclic loading model. After the preconditioning of each tendon, the length of each tendon was remeasured to recalibrate the strain (and hence load). However, to facilitate confocal images to be taken at both zero and maximal strain levels, the cycles were blocked with a static hold for 60-s periods at zero strain ($Strain_{Zero}$) and maximum strain ($Strain_{Max}$) (see Figure 3.10B). These relaxation periods were required to allow for confocal imaging to be conducted in the last ten seconds of this imaging phase and this is consistent with the protocol by Wenger et al. (2007) and Thorpe et al. (2013). This relaxation period has previously been shown to be sufficient time for significant if not complete SR to have occurred (Cheng & Screen, 2007; Thorpe et al., 2013). The first mechanical cycle loading sequence is composed of consecutive blocks as described below. Block 1 of loading includes a 60 s hold at the at zero strain ($Strain_{Zero}$) (see Figure 3.10C) and is followed by Block 2 – a 1 s rise time considered as a ramp, followed by Block 3 where the tendon was strained to maximum strain ($Strain_{Max}$) at a constant displacement rate and held for another 60 s to allow further imaging (see Figure 3.10D).

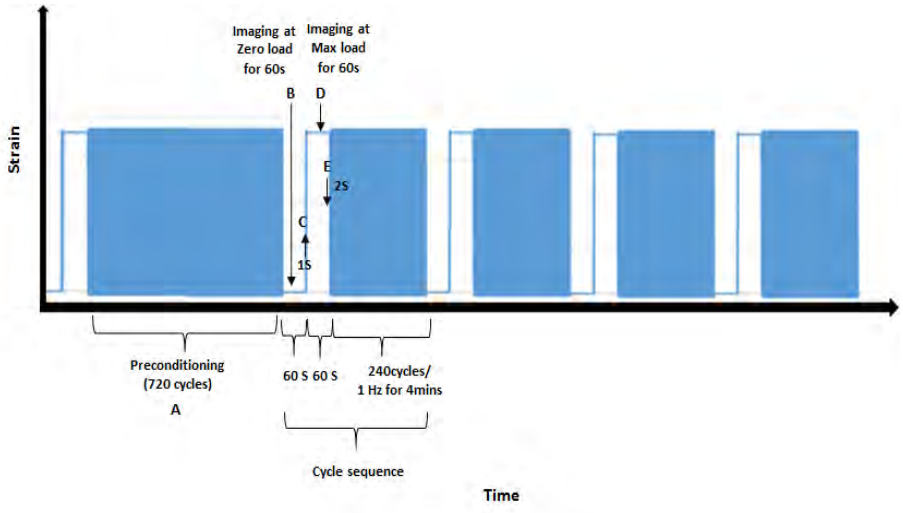

Figure 3.10. Schematic representation depicting the strain and imaging protocol during the cyclic loading of the tendon over one, two, three or four hours of repeated cyclic loading under three strain levels (3%, 6%, or 9 %). The mechanical cyclic loading was 240 cycles at 1 Hz/cycle for four minutes. A) preconditioning; (B) relaxation period ($Strain_{Zero}$) – CA imaging was undertaken at the end of each SR period for one minute at zero load; (C) ramp testing; (D) maximum hold ($Strain_{Max}$) – another 60 s of CA imaging at was then stored to disc with a timestamp; (E) ramp testing; (F) cyclic loading of 240 cycles at 1 Hz/cycle for 4 min. These data provided 240 high-resolution images (60 per hour) of the macroscale damage due to cyclic fatigue loading.

The tendon was then exposed to another 1-s decline time (Block 4), a 1-s hold time (Block 5) considered as a relaxation time (see Figure 3.10 E) and followed finally by a cyclical tensile loading for 240 cycles (Block 6) at a frequency of 1 Hz/cycle with a sine waveform at the set strain for 4 min. Following this, Blocks 1–5 are repeated. This sequence was repeated for periods of one-hour blocks resulting in a total dose for each hour such that the tendon received 2,400 cycles (one hour), 4,800 cycles (two hours), 7,200 cycles, (three hours), or 9,400 cycles (four hours).

Prolonged mechanical interventions in repeated loading protocols (as used in our study) are likely to cause excessive fluid exudation from the tested tendons. Therefore, it was essential to compensate for the excessive fluid exudation by keeping the tendons within physiological ambient conditions by spraying the tested tendons with saline repetitively and intermittently throughout the fatigue loading intervention.

Spraying the tendons with saline occurred throughout the preparation and during the cyclic loading repetitive test (particularly at zero and maximum strain). This, perhaps, has increased the loading stiffness repetitively and intermittently reflected as the rough fluctuating line in the curve (for example, figures for loading stiffness under appendix 10). However, the spraying effect was minimal during the static loading repetitive test since the spraying times during this resting period were minimised.

3.9 Macroscale Structural Protocol

Within each cycle sequence, the static hold block of 60 s at $Strain_{Zero}$ and another 60 s block at $Strain_{Max}$ allowed a static period for confocal imaging. The confocal arthroscope (Optiscan Pty Ltd., Melbourne, Australia) comprised a Φ 6.3 mm × 150 mm imaging probe with 7 μm axial and 0.7 μm lateral image resolution for three-dimensions (See Figure 3.11A). At an axial imaging step of 4 μm, the screening of the macrostructure of the tendons was clear and images were obtained.

The imaging probe lightly contacted the surface of the tendon. Various parts of the mid-substance region were considered and assessed by CA (See Figure 3.11B); imaging was undertaken after every 240 cycles (according to the protocol described in Figure 3.10) and images were stored to disc in a.jpg file with a time stamp. These data provided 240 images (40 per hour) of the macroscale damage due to cyclic fatigue loading. An imaging scanning rate of 0.7 frames per second was employed to obtain a volume of images at 475 μm × 475 μm fields of different parts of the mid-substance region.

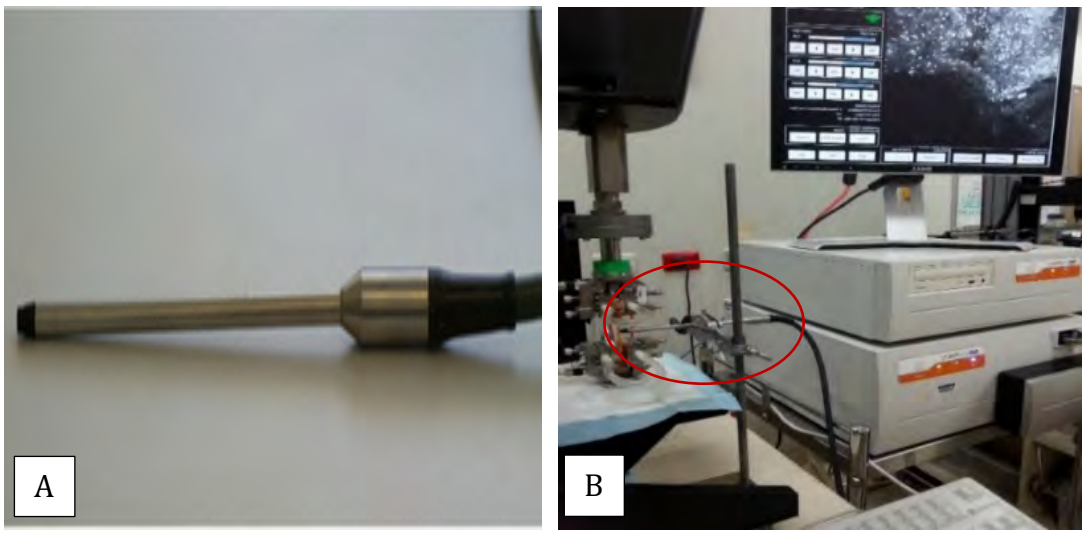

Figure 3.11. The imaging probe of the CA showing its attachment to the tendon's surface. As seen in the circle, the imaging probe (A) of the arthroscope is fixed and pointed to the surface of the mechanically tested tendon (B) to allow imaging during the SR and zero load periods.

An illumination laser with a 488-nm excitation wavelength was used for the confocal arthroscopic imaging in order to provide maximum contrast and image resolution. The microscope has been manufactured to have an imaging depth range from 0 mm to 250 μm but in this study, a depth between 40 μm and 60 μm was used.

- **Data Analysis**

Data analysis allowed definition of the stability of the CA images over time in the control group and also allowed the definition of the susceptibility to rupture of tendons on extreme load and dose. Each tendon was recorded and identified so that the sections were able to be linked back to the macroscale findings. All samples were imaged enabling the accurate visualisation of cell nuclei by a fixed CA. Groups of nuclei within the body of the fascicle were identified for imaging. Structural changes were examined with CA.

- **Histology**

At the end of each mechanical testing dose, the tendons were removed from their grips, post-fixed in 4% paraformaldehyde (PFA) overnight and placed into PBS for rinsing (two rinses of 15 min each). Then, each of the tendons were further grossly cut in half and were separated into two groups. The first group was kept overnight in 70% ethanol for further histological assessments.

All histological preparations of parrafix wax for macrostructural assessments were carried out in the CELLCentral Histology facilities at The University of Western Australia (further detail in Appendix 4). After cutting the tendons from the mid-portion area for both the control and strained groups (3%, 6%, and 9%), the tissue samples were fixed in formalin overnight, washed three times with PBS, dehydrated with graded alcohol, cleaned with xylene and embedded in paraffin blocks. Histological sections were cut on a microtome and stained with Haematoxylin and Eosin (H&E) and Alcian blue. The sections were cut from the mid-tendon of both the control and strained groups (3%, 6%, and 9%). Blind general histological scoring was performed by two individuals. All histological protocols employed including paraffin processing, cutting of wax sections and H&E staining procedures (Drury & Wallington, 1967; Luna, 1968; Bancroft & Gamble, 2008) and Alcian blue (Gagliano et al., 2013), were used at the CELLCentral (more detail in Appendix 4).

The Scanscope H&E and PAS/AB (pH 2.5%) histological images were acquired using the tiling function within the Aperio ImageScope software (Leica Microsystems Pty Ltd). The images were fixed approximately at the field of the view corresponding to the CA images from the Scanscope histological image to score the morphological changes of the three assessed domains in the tendon specimen and to compare CA images with traditional histology.

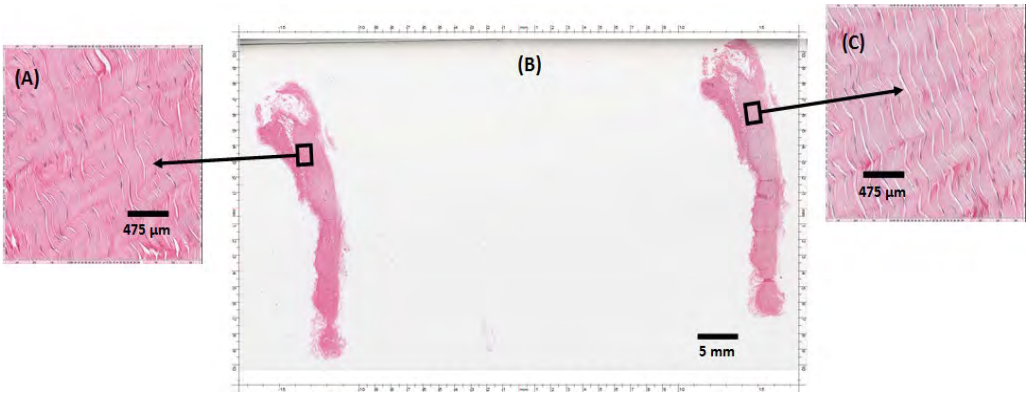

Figure 3.12. Scanscope H&E (A) and Periodic acid-Schiff/Alcian blue (AB/PAS) (pH 2.5%) (C). The Scanscope histological image was acquired by the Aperio Scanscope XT scanner with a 60× objective lens (B). Histological images acquired by using the tiling function within the Aperio ImageScope software.

B. Study 1B

Study 1B was the same as Study 1A in the aspect of the mechanical intervention; however, the structural analysis was undertaken at the nanoscale level using AFM. Study 1B combined the macroscopic mechanical loading of tendons from Study 1A with a morphometric nanoscale assessment of longitudinal and cross-sectional collagen fibril responses to load. The AFM assessed the nanostructural variables (see Section 3.6) in cryosections and then compared them with the tendon's mechanical and macrostructural changes in the strained groups. The sections from the control group were compared with the sections from the strained groups.

i. Sample Preparation – AFM Variables

This study used the endpoint of dose assessments of each tendon from Study 1A. Each tendon was recorded and identified so the sections were able to be linked back to the macroscale findings. The samples were then removed from PBS and placed overnight into 30% sucrose solution made up in PBS. Overnight, samples were placed into pure optimal cutting temperature (OCT) compound to remove any sucrose and stored at –80°C until they were cryosectioned for further nanostructural assessment by AFM.

Cryosections were prepared from all groups using a cryomicrotome (Leica Cryostat CM3050). The tendons initially were cut at the midsection and embedded with OCT fluid and then cut longitudinally into slices of from 5 µm to 50 µm thickness. Finally, the prepared cryosections were numbered and mounted on glass slides, left to dry in the air and frozen at –18°C to be observed and examined later via AFM.

ii. Nanoscale Imaging Protocol – AFM

Under the AFM, a group of cryosections (prepared as described above) from both the control and strained groups (3%, 6%, 9%) were examined to detect the nanostructural properties (the variables as listed in Table 3.1). Tissue specimens were imaged in air using a *Dimension FastScan* AFM in tapping mode as described in Appendix 6 in greater detail.

C. Study 2

This study combined the macroscopic structural and mechanical characteristics with a morphometric nanoscale assessment of the longitudinal and cross-sectional collagen fibril response to load of GAG-depleted fibrils. This study was undertaken to examine the chemical depletion model following mechanical loading.

i. Tendon Collection and Preparation

A separate set of 20 tendons (10 treatment and 10 controls) were collected, frozen, thawed and prepared using the same procedures as applied to the tendons in Study 1A.

The GAG-depletion solution consisted of 50 mM Tris, 60 mM sodium acetate buffer, 0.2% bovine serum albumin (all from Sigma-Aldrich) at pH 8 with 1 unit/ml of Ch-ABC (Sigma-Aldrich, Catalogue number 3667). Ch-ABC enzymatically detaches GAG chains from their proteoglycan (PG) core protein (Koob, 1989) to reduce the number of PG GAG sidechains (Woo et al., 1993; Puxkandl et al., 2002; Screen et al., 2004). Control tendons (n = 10) were incubated in buffer alone (50 mM Tris, 60 mM sodium acetate buffer, 0.2% bovine serum albumin (BSA), pH 8).

a Dimethylmethylene Blue (DMMB) GAG Quantification

- **Assay Optimisation Part 1**

To ascertain if Ch-ABC digestion of tendon pieces would deplete sulfated GAGs, several optimisation experiments were performed. The first experiment was a proof of principle. One tendon was freeze-dried, two portions were divided equally and weighed, and placed in a 1.5 ml microfuge tube. Samples were treated with either 1 ml of buffer only (50 mM Tris, 50 mM sodium acetate buffer, 0.2% BSA) or in 1 ml of buffer containing 1 unit of Ch-ABC. Tendon samples were left overnight at 37°C with agitation. The tendon samples were then removed from the solution, rinsed in distilled water and digested with equal volumes of 0.2% collagenase Type I in RPMI media overnight at 37°C with agitation. Following clarification, treated and control tendon supernatants were tested using the DMMB assay, along with chondroitin sulfate (Ch-SO_4) standards. The amino acid concentration of each sample was also assessed using absorbance at 260 nm.

Initial experiments using isolated tendons revealed that overnight incubation at 37°C using 1 unit/ml of Ch-ABC was sufficient to achieve a 30–40% reduction in GAG content, as measured by the 1,9-dimethylmethylene blue (DMMB) assay (see below) (Figure 3.13).

- **Assay Optimisation Part 2**

The next experiment involved assessing the ability of Ch-ABC to deplete GAGs from a whole tendon, with the muscle attachments still present; as this format was required for the mechanical testing. For this experiment, two tendons (left and right) from a

single rabbit were obtained. One tendon was chosen as the control tendon and was immersed in 10 ml buffer (50 mM Tris, 50 mM sodium acetate buffer, 0.2% BSA) whereas the tested (depleted) tendon was isolated from the muscle attachment using dialysis tubing (see Figure 3.13A). Buffer (1 ml) containing 1 unit of Ch-ABC was placed inside the dialysis tubing, and the entire tendon was then immersed in buffer. In this way, the tendon was in contact with Ch-ABC whereas the rest of the material was not.

Following overnight incubation 37°C, the tendons were rinsed in distilled water and the muscle attachments removed by a surgical blade. The tendons were weighed (wet weight) before being digested overnight at 37°C in 0.2% collagenase Type I, then clarified and the Ch-SO_4 content measured using the DMMB assay. As the wet weight is not as accurate as dry weight, the amino acid concentration of each sample was also assessed using absorbance at 525 nm and these data used to calculate relative GAG concentrations between control and depleted samples. Samples were tested neat and diluted 1:2. The neat and diluted samples fell in the linear range of the assay and gave the same results. Thus, only the values for the neat samples are shown. Following this, the GAG concentration of the depleted sample was adjusted to account for the relative amount of starting material (as indicated by amino acid concentration); and was calculated using the following equation: (2.988/2.028) x 0.009 (see table 4.6). Following this, the GAG concentration of the depleted sample was adjusted to account for the relative amount of starting material (as indicated by amino acid concentration). This is required as the tendon pieces analysed for control *vs* GAG-depletion varied in size due to the amount of sample available for analyses. The whole tendon treated with Ch-ABC was found to have approximately 60% of the GAG content of the control tendon (i.e. a 40% reduction); consistent with the data obtained for the small tendon pieces.

ii. GAG Depletion in Tendons Undergoing Mechanical Testing

Whole tendons for mechanical testing were prepared for GAG depletion as described above. Only one control and one test tendon were prepared each time, and mechanically both were strained at 6% over two hours according to the mechanical protocol. The left tendon was used as the control and the right tendon as the depleted

sample for the optimisation assay (part 2) experiment. This was to streamline sample processing and analysis.

Mechanical testing was undertaken with the tendon fully intact of 10 control and 10 GAG depleted tendons. No systematic allocation of Left or Right tendons was made to either group. Each tendon of the treatment group was carefully encased in SnakeSkin dialysis tubing (35 mm diameter, 10 kDa molecular weight cut-off, Thermo Fisher). A 10 cm length of dialysis tubing was submerged in buffer alone and the tendon threaded into the tubing. One end of the tubing was secured with a string knot around one of the insertion sites of the tendon. A small amount of the buffer solution was added into the tubing to test if there was leakage of the solution from the tied end. The buffer was then removed, and 1 ml of the Ch-ABC solution was added. The open end was then securely tied with a knot around the remaining insertion site of the tendon. In this way, the Ch-ABC solution was in contact only with the tendon of the test sample. Finally, the tendons from the depleted and control groups were placed into a plastic container with buffer only (Figure 3.13A) and incubated overnight for 16 hours at 37°C. In this way, controls and treated tendons received identical treatment apart from the enzyme, and any differences in mechanical testing should be due to GAG depletion.

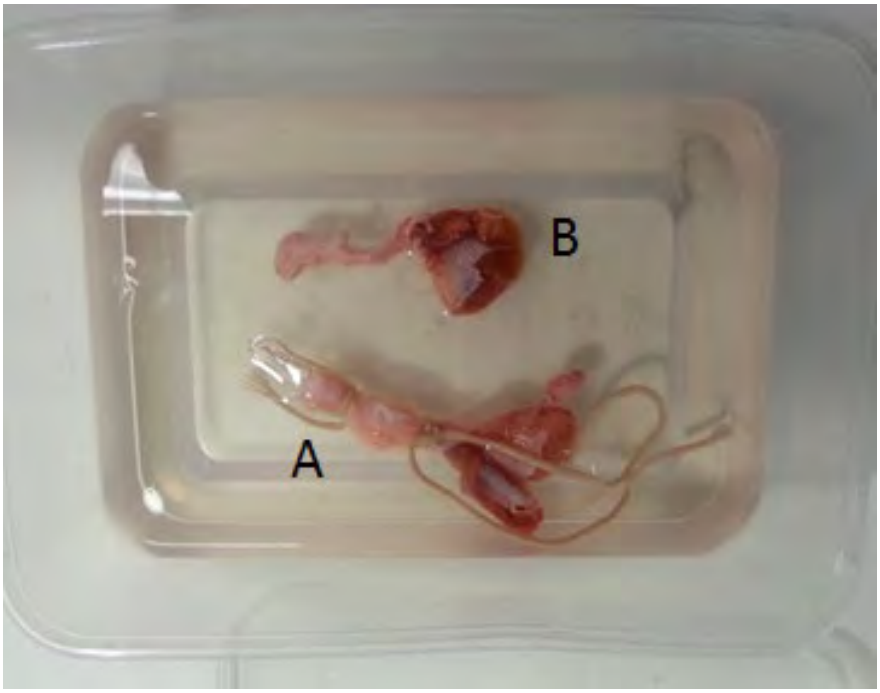

Figure 3.13. An image showing the tendons incubated overnight for 16 hours at 37°C in a plastic container with an adjusted buffer solution at pH 8. The treatment tendon (A) is incubated inside the SnakeSkin dialysis tubing with the Ch-ABC solution. The control tendon (B) is only incubated in the buffer solution.

iii. Fluorescent Staining

Tendons were stained with fluorescent AO using the same procedures as described in Study 1A. It has been demonstrated that AO can stain the highly negatively charged proteoglycans in a more expanded state (Brandes & Reale, 1990). This can impact the measurement of GAG *via* the 1,9-dimethylmethylene blue (DMMB) assay by affecting the absorption spectrum of the DMMB dye (Farndale et al., 1986). Therefore, the superficial parts of the tendons (the medial and lateral heads of the gastrocnemius muscle) were not stained with AO but kept moist throughout the mechanical testing protocol and the deeper-lying part of the tendon composed of the superficial flexor digitorum muscle was stained with AO (Figure 3.14) according to the staining protocols used in Study 1A.

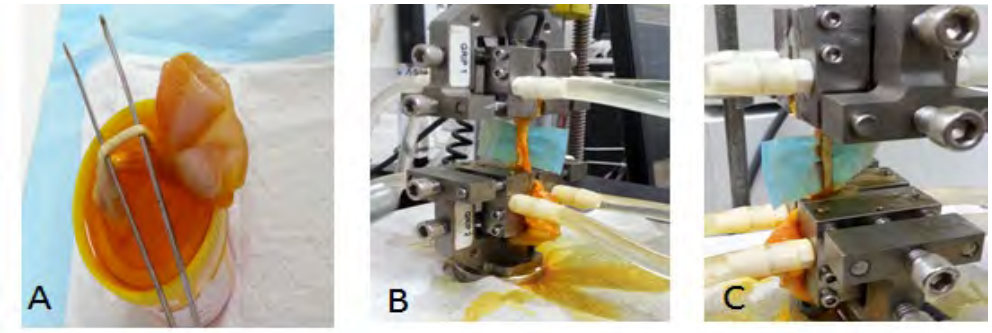

Figure 3.14. A representation of the stained and unstained tendon parts. Image (A) shows the superficial part of the tendon that is composed of the medial and lateral heads of the gastrocnemius muscle and is not stained with AO. The underneath deeper-lying part of the tendon composed of the superficial flexor digitorum muscle was dipped in the AO staining solution according to the staining protocols described in Study 1A. Image (B) shows the deeper-lying part of the tendon after staining with AO and image (C) shows the unstained superficial part separated from the stained part with a waterproof surgical pads.

iv. Tendon Fixation for Instron and Macroscale Mechanical Protocols

The ends of each tendon were placed in the lower and upper freezing micro-grips and fixed according to the procedures described above. The tendons from both groups received the same mechanical cyclic loading interventions and protocols as in Study 1. However, both groups were subjected only to a repeated cyclic loading strain of 6% for two hours (4,800 cycles).

v. Glycosaminoglycan (GAG) Assay

Following the repeated cyclic testing, tendons were collected and the GAG content was measured by a spectrophotometric GAG assay (Farndale et al., 1986; Burkhardt et al., 2001; Screen et al., 2005; Fessel & Snedeker, 2009; Fessel & Snedeker, 2011; Rigozzi et al., 2011; Legerlotz et al., 2013). Briefly, the treated and control tendons (Farndale et al., 1986) were weighed and then fully digested overnight at 37°C in 0.2% collagenase Type I (Sigma-Aldrich, C0130) in Roswell Park Memorial Institute (RPMI) tissue culture media (Life Technologies). The solutions were clarified by centrifugation (1,000 G, 5 min) and the supernatant transferred to a fresh tube. The undigested component was minimal.

The GAG content was measured using a spectrophotometric method based on mixing the clarified supernatants with DMMB solution. The DMMB solution was prepared by dissolving 16 mg DMMB (Sigma-Aldrich, catalogue number 341088) in 1 L water containing 3.04 g glycine, 1.6 g NaCl and 95 ml of 0.1 M Acetic Acid (all from Sigma-Aldrich). The solution was then filtered through Whatman® 3MM paper and stored in the dark at 4°C. DMMB is a thiazine chromotrope agent that depicts a change in the absorption spectrum as a result of the induction of metachromasia when attached to sulfated GAG, facilitating the rapid detection of GAG in solution (Farndale et al., 1986). The sulfated GAG content of each tendon supernatant was determined by adding 5 µl, 10 µl or 20 µl of sample to the well of a 96-well plate. If 5 µl or 10 µl was used, the volume was adjusted to 20 µl using RMPI (to match the base solution of the tendon supernatants). A standard curve was prepared for each assay by serial dilution of bovine chondroitin-4-sulfate (Sigma-Aldrich, catalogue number: C9819) prepared in RPMI. Concentrations tested were from 1 mg/ml to 0.0078 mg/ml, with a final volume of 20 µl per well. Next, 200 µl of DMMB solution was added to each well containing the standard curve, test samples or buffer only and the absorbance of each sample was immediately measured at 525 nm using an EnSpire plate reader

(Perkin Elmer). The background absorbance (0.17) observed in buffer-only wells was subtracted from the absorbance of standards and samples, the standard curve was graphed and the linear range of the curve determined for each assay. For the linear range of the assay, a line of best fit was determined, and this equation was used to calculate the GAG concentration in the control and GAG-depleted samples. The GAG concentration for each sample was normalised relative to the starting weight of each tendon before digestion. (Greater details of the GAG assay (Farndale et al., 1986; Whitley et al., 1989; Coulson-Thomas, 2014) are in Appendix 3).

vi. Nanoscale Imaging Protocol, Nanostructural Variables and Mechanical Variables

Under the AFM, a group of cryosections from the control and GAG-depleted tendon groups were imaged and the above quantitative nanostructural variables were assessed according to the AFM imaging protocols described in Appendix 8. The AFM analysis assessed the changes in the nanostructural variables in cryosections (described above for Study 1B) and then compared them with GAG content and the tendon's mechanical changes in the GAG-depleted groups. The sections from the control group were compared with sections from the strained group of the study where GAG had been enzymatically depleted using Ch-ABC prior to mechanical testing. The mechanical variables (as described above) of the GAG-depleted strained tendons were calculated from the stress-strain curves and compared with the mechanical profiles of the control group. The GAG content in each of the H&E slides prepared from the control and GAG-depleted strained groups, was estimated by assessing the Alcian blue-stained slides according to methods described above (more detail is in Appendix 4).

3.10 Statistical Analysis and Investigation Model

This study design was based on the context of the literature in assessing tendon structure and function. Within the literature, there are a number of observational studies (i.e. morphology, and associations) describing the anatomical structure and there are a number of quantitative studies that address mechanical function. Among all of this literature, concurrent multiscale assessments of tendons are rarely undertaken. Furthermore, the mechanical studies often select a single cycle load to failure or a series of repeated loading cycles. The cyclic research is often controlled by maintaining the amount of force (stress) resulting in increased elongation (strain).

Less commonly, studies maintain the amount of strain resulting in a declining degree of force (stress).

The investigation model chosen for this thesis was one that considered the following design parameters:

- A high number of repetitions of loading will be assessed where concurrent mechanical (stress-strain) assessments are made with observational assessments of morphology.
- Mechanical variables will include the usual dynamic assessments but also an SR (static) assessment.
- The design will be able to demonstrate the internal repeatability of the mechanical variables.
- Observations will be continued well past the number of cycles usually reported in observational studies.
- Observations will continue even as the sample size declines due to destructive sampling of the tendon cohort.
- Three strain levels will be used for cohort comparisons.

The research design selected in this thesis, therefore, utilises a hybrid model of both quantitative and observational analysis examining structure and function at multiple scales.

The main disadvantage of the current design is the sequential destruction of a proportion of the samples as the multiscale assessments are undertaken. As a result, the sample size declines as the loading progresses and consequently the inferential statistical power of the study declines with the loss of sample size. Therefore, data collected at three to four hours were primarily considered observational in the results and discussion.

A. Data Presentation – Inferential *vs* Observational

The trajectories of the changes over four hours for all variables were plotted. Where applicable, data for mechanical testing were normalised after preconditioning. The differences between time points and strain groups were assessed for the first three (hourly) time points. The fourth-hour trajectory was only considered as an observation. Statistical pairwise comparisons were only taken at the end of each hour, not at every data point, to minimise repeated comparisons. The graphs (Chapter 4) show all the data in a trajectory pathway.

i. Timepoint comparisons

The data were considered in pairwise comparisons for effect size at the 95% level of confidence. Unless otherwise stated, each sample point in the data represents the median of adjacent samples (n-1, n, n+1).

ii. Effect-size changes

The effect size (d) was determined by the difference in the mean divided by the pooled standard deviation (SD) (eq 3.3).

$$\text{Hedges' } g = \frac{M_1 - M_2}{SD^*_{pooled}} \qquad \text{(eq 3.3)}$$

www.polyu.edu.hk/mm/effectsizefaqs/effect_size_equations2.html (accessed Jan 2020).

Where the pooled SD is calculated by eq 3.4):

$$SD^*_{pooled} = \sqrt{\frac{(n_1 - 1)SD_1^2 + (n_2 - 1)SD_2^2}{n_1 + n_2 - 2}} \qquad \text{(eq 3.4)}$$

A bias factor (Hedges correction) was undertaken to calculate the standard effect size.

$$g \cong d\left(1 - \frac{3}{4(n_1 + n_2) - 9}\right) \qquad \text{(eq 3.5)}$$

Equation adapted from Hedges and Olkin (2014)(p.81). www.polyu.edu.hk/mm/ (accessed Jan 2020).

The 95% confidence limits were calculated using 1.96 times the standard error. Statistical significance was recorded for effect size 95% confidence intervals that did not include zero.

For normalised data (all values calculated at time zero) the effect size was determined using a 0.1% variance from time zero. This equates to a conservative 95% CI change from the 100% normalised value. Although effect sizes are used, there is no discussion on the clinical significance of these effects size such as is found in Cohen et al. (1988). That stated, the comparisons of the percentage of the non-overlap of the compared cohorts is shown in Table 3.2.

Table 3.2. The interpretation of Cohen's d as the difference between the means, M1 – M2, divided by the standard deviation, s, of either group. Cohen argued that the standard deviation of either group could be used when the variances of the two groups are homogeneous. The effect sizes are "small, d = 0.2," "medium, d = 0.5," and "large, d =0.8", and Cohen states that "there is a certain risk in inherent in offering conventional operational definitions for those terms for use in power analysis." (Cohen; 1988)

Cohen's Standard	*Effect Size*	*Percentile Standing*	*Percent of Non-overlap*
	2.0	97.7	81.1%
	1.8	96.4	77.4%
	1.6	94.5	73.1%
	1.4	91.9	68.1%
	1.2	88	62.2%
	1.0	84	55.4%
Large	0.8	79	47.4%
	0.6	73	38.2%
Medium	0.5	69	33.0%
	0.4	66	27.4%
Small	0.2	58	14.7%
	0.0	50	0%

iii. Alpha Level and Multiple Comparisons

The 95% confidence limits were set for all statistical levels of confidence. Since there were multiple comparisons and a blend of qualitative and quantitative review of the data, only the first full two hours of cyclic loading were considered in the inferential statistics of significance. That said, the calculations were still undertaken for the third hour. No alpha-level adjustments were made for repeated comparisons. Declining numbers in each time period with a generally small sample size did not allow a multivariate analysis to be undertaken.

B. Reliability, Research Design and Assessments

When observations were made on structural classifications, the subjective assessments of these were tested in a double-blind protocol as described below. This is the first study found on the repeatability of the classifications of cell morphology and structural breakdown reported in the literature. The validity of the subjective classifications undertaken in this study is based on the descriptions within the current literature.

The testing protocols were difficult to run concurrently so Study 2 was undertaken that addressed the impact of GAG depletion on tendons. The testing protocol repeated a subset of dose (6% strain for two hours) for a control group and GAG-depleted tendon groups. The outcomes for the control group in the second study can be compared with the main study tendons with the same loading profile. As a result, unlike any other study in the literature, this model was able to compare the reliability of all variables for this loading profile.

C. Tests of Association/Correlation

Pairwise comparisons of the continuous variables were plotted in x–y plots as % change in the normalised variables. In cases where both variables declined, the axes were placed to have the data represented in the 3rd quadrant of the x–y plot (see Figure 3.15).

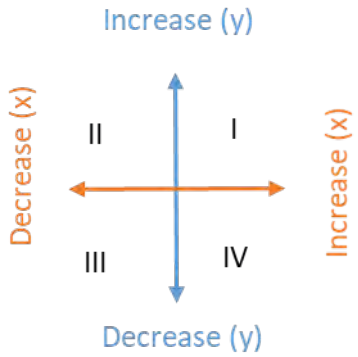

Figure 3.15. A representation of the x–y plots that were presented using quadrant III when both variables declined.

Pearson correlation coefficients were calculated (Excel 2016) and best-fit curves were used to assess the form of the association. In most cases, the primary fit was linear unless a second-order polynomial fit increased the increased the total coefficient of determination (R^2) by more than 10%. This was particularly important when the pattern of the association was observed across multiple strains and conditions. Furthermore, associations were made for the full data set and the endpoint data was representative of a smaller sample size. Therefore, the linear fit was most commonly used to describe the general observation of the pattern of the association. The reporting of the p-value was an inferential comparison with no association (R = 0) being detected, the magnitude of the association was reflected in the coefficient of the determination (R^2).

D. Sample Size and Power – *A priori* Calculations

The number of tendons used in the study is substantial when compared to other studies in the literature using animal models. For each strain level, there were initially 12 samples. Since the expectation was that the level of strain and also the number of cycles would be a strong mediator of change, the *a priori* power estimates were undertaken using a one-sided comparison.

For independent between-group comparisons, the study was 95% (alpha) certain of detecting a change of 1.2 (SD) with a power of 90% (beta) in the first hour. For the second hour (n = 9) to maintain the same statistical power an effect size of 1.4 SD was

necessary. The within-group comparisons had similar power modelling. It was expected that the effect-size changes for these mechanical tests would be substantially larger (> 1.2 SD) than this modelling. Tests at three and four hours had sample sizes too small to validly estimate the power and variance.

At the longer-hour durations, smaller numbers of samples were available due to the destruction of the tendons for histological assessments. All hypotheses were set, but statistical differences for the comparisons after two hours are obviously less powered. The third and fourth hour of the mechanical intervention were modelled to be qualitative or observational.

E. Reliability and Agreement Assessments

Reliability represents the distinguishable extent to which the variables can differ from each other, regardless of measurement errors; it links the measurement error of the derived variable of the domains to the normal variability of the population (De Vet et al., 2006; Kottner et al., 2011). The agreement refers to the extent at which a measurement can measure the same derived variable of the domains on varying occasions.

To date, there are no studies that report the reliability of the many different measures of observational classification of tendon structures. It would seem that the validity of the descriptions in the literature (Svensson et al., 2005; Gagliano et al., 2013) is used to validate the proposed model and therefore infer robustness. This is a major weakness in the literature. Therefore the observed variables used in this study used the same protocols as described in the literature for validity but there is also an independent reliability assessment to establish the full robustness of the following variables.

For classification of data, Kappa and % agreement for test-retest were generated on the following domains: fibre arrangement and orientation, fibre structure and tenocyte roundness. These domains were determined using a semiquantitative scoring system similar to a system based on a validated four-point scoring system of Movin and Kartus (Movin et al., 1997; Kartus et al., 2000) used by Svensson et al. and Gagliano

et al. (Svensson et al., 2005; Gagliano et al., 2013) as described above (see Appendix 5 for representative images and definitions).

Briefly, a sample of images representing the quality of tissue were sent to an independent researcher who randomly selected 58 images. These images were then replicated and renamed using a random code. In the replicated sample the images were manipulated to further reduce the chance of a visual memory of the image. This included at least two of the following three digital image manipulations: rotation ± 90° or 180°, reflection and change to image contrast (± 20%). The tester was not aware of the digital manipulations and thought that 116 images were selected from the originals submitted. The images were then assessed in order of presentation without returning to previously assessed images. This was undertaken on two occasions one week apart. On the second assessment, the names of the images were altered. In 116 cases, to test recall bias of the image names, different images had their names swapped (all 116 images were concordant even with the change of names). The result of the subjective classification was sent to the second researcher and decoded to match the paired results. This provided a within-sessions and between-sessions reliability assessment of the classification undertaken by the assessor. Also, image-name recall was assessed for recall bias.

A second independent assessor (not associated with the research team) also scored the images to generate a between-assessor reliability. Comparisons between percent agreements for test-retest of the first and second assessors was made to detect any differences between the resulting paired contingency tables on the categorical classifications for the variables.

From these paired results of the classification (ordinal data), a contingency table of concordance was used to derive weighted Kappa statistics. The Kappa-value points to the observed agreement as the agreement percentage that is anticipated only by chance. A value of 1 represents a perfect agreement and a value of 0 shows no agreement (Ashby, 1991).

F. Reliability Results and Summary

i. Observational Classification of Tendon Morphology

Tables 3.3 and 3.4 show the test-retest contingency for all the observation paired data between weeks. The within-test blind repetitions were consistent with the between-sessions assessments. The inter-tester reliabilities for within-session and between-sessions were all greater than 0.93. The Kappa statistical result shows an excellent level of inter-rater and a very good intra-rater reliability for the measured domains: fibre arrangement and orientation, fibre structure and tenocyte roundness (the inter-reliability was > 0.93 and the intra-reliability was >0.70). Full results on the inter- and intra-reliability for fibre arrangement and orientation and fibre structure are in Appendix 11.

Table 3.3 shows the contingency for the four categorical assessments (tenocyte morphology) undertaken on two occasions, one week apart by the same rater. The weighted Kappa score was 0.9849 (95% CI = 0.956 to 1.00).

Table 3.3. Cohen's weighted Kappa values for pairwise comparison of the inter-tester for between-sessions for qualitative evaluation of tenocyte morphology.

		Week 2.			
	Category*	I	II	III	IV
Week 1	I	30	0	0	0
	II	1	58	0	0
	III	0	0	17	0
	IV	0	0	0	3

*Weighted Kappa 0.8274, Standard Error 0.0509, 95% CI = 0.9555 to 1.000

Table 3.4. Cohen's weighted Kappa values for pairwise comparison of the intra-tester for qualitative evaluation of tenocyte morphology.

		Week 2.			
	Category*	I	II	III	IV
Week 1	I	2	0	0	0
	II	1	17	0	0
	III	0	1	52	6
	IV	0	0	12	24

*Weighted Kappa 0.8274, Standard Error 0.0509, 95% CI = 0.6579 to 0.8575.

Table 3.5. The mechanical and macro- and nanoscale structural variables assessed by different instruments and technical procedures.

Scale	**Variables**	**Instrument/ Technique/ Software used for Investigation**
Macroscale	Stress/strain curves (*h*, ML, *k*)	Mechanical instrument (Instron)
	Fibre structure	Qualitative histological scoring according to modified Movin and Kartus scoring systems
	GAG content	Qualitative histological scoring according to modified Movin and Kartus scoring systems
	Fibre crimp frequency	CA/Image J
	Fascicle orientation and anisotropy	CA/Image J
	Shape of tenocytes	CA/Image J
Nanoscale	WFB and BFB D-periodicity	AFM
	Fibril structure	AFM
	Fibril arrangment and orientation	AFM

CHAPTER FOUR:

RESULTS

4.1 Mechanical Loading Outcomes (Study 1)

A. Macromechanical Loading Outcomes

i. Preconditioning

The experimental protocol consisted of consecutive sets of repetitive cyclic loadings leading to a repeated stretching of the tendon sample to a sub-failure load (see Chapter 3). Preconditioning is a standard protocol for assessment and comparison of mechanical testing and has been shown to improve the baseline variability of the stress-strain data. Preconditioning can potentially provide tendons with a consistent loading history from a completely unloaded resting state.

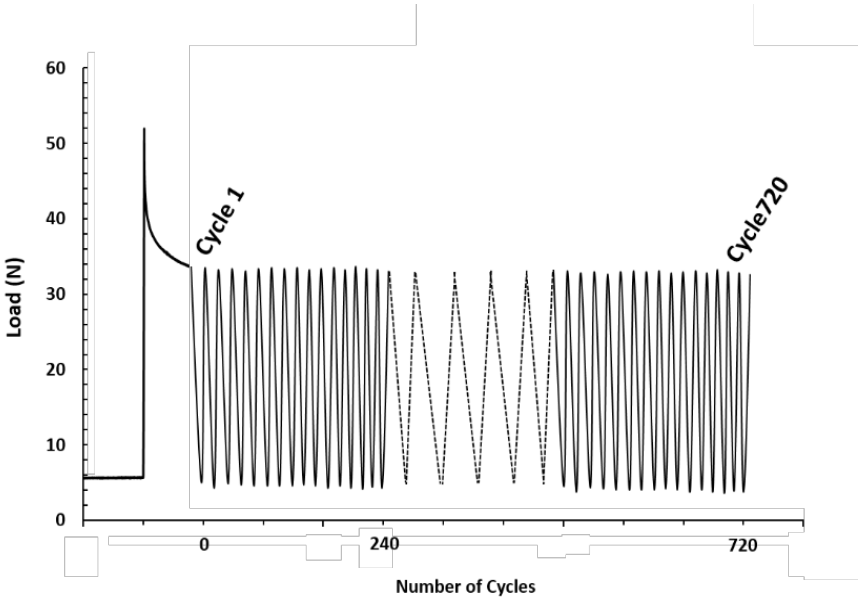

Figure 4.1. The repeatable stress-strain curve of preconditioned tendons demonstrating a consistent loading history.

In this study the preconditioning included 720 cycles; a steady state was reached for all tendons of all three strain groups (3%, 6% and 9%). Each group was preconditioned with a constant number of cycles but at the strain set for each of the groups.

Preliminary studies showed that the preconditioning impacted on the mechanical characteristics of the tendons. This was important as the study protocol was controlled by strain. Figure 4.2 shows the raw data of a tendon conditioned to a 3% strain for 720 cycles from rest (A) and after preconditioning then having the starting length reassessed to re-establish the 3% strain (B). Following the preconditioning, the stress-strain curve is more representative of the literature (Figure 4.2 B). As a result, the starting point of every mechanical testing protocol in this study used the preconditioned status of the tendon.

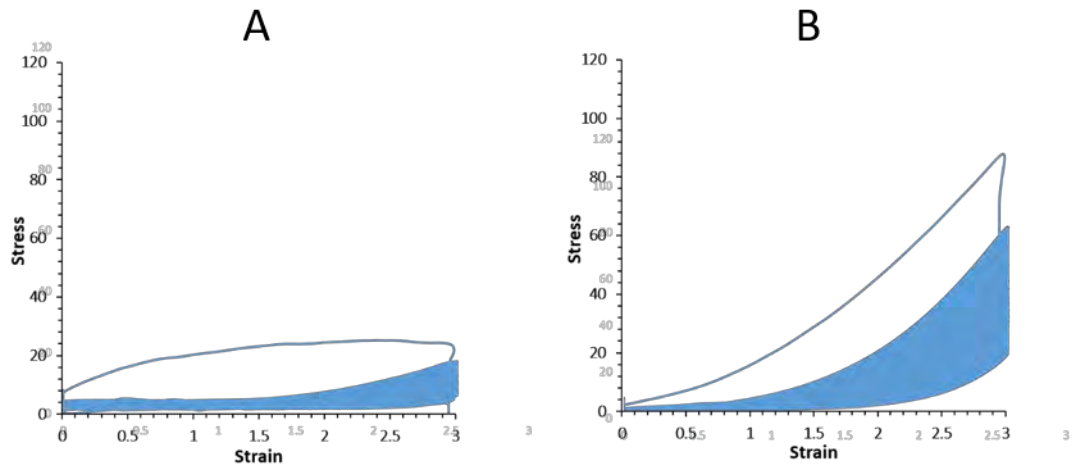

Figure 4.2. Stress-strain curves of the unpreconditioned tendon (A) and the preconditioned tendon (B).

ii. Dynamic Testing

a Loading Stiffness (k2)

There were two stiffness measures (*k1* and *k2*) taken during the experimental protocol that used similar methods to assess stiffness. The assessments occurred at two different windows during the repeated loading (see Chapter 3). The first was known as ramping stiffness (*k1*) and this was a stiffness assessment at the beginning of the sustained or stress relaxation (SR) testing protocol. The loading stiffness (*k2*) was undertaken at the beginning of the cyclic loading profile. All the data for loading stiffness (*k2*) assessments were found to be highly correlated with ramping stiffness (*k1*) (R^2 = 0.86–

0.97, P < 0.0001). The replication of associations for the loading stiffness (*k2*) are placed in Appendix 7. Therefore, all data on stiffness is nominated as *k*.

b Hysteresis (*h*)

- Observational differences

Figure 4.3 illustrates the relative change in *h* for tendons tested over four hours (9,600 cycles) at three different strain levels. The *h* declined over time (cycles) with greater changes associated with the level of strain. At 4,800 cycles (two hours), the *h* decreased by 36%, 45% and 56 % in the low- (3%), moderate- (6%) and high-strain (9%) groups respectively. By the end of an additional 4,800 cycles (at 9,600 cycles – four hours), the decline reached 40%, 60% and 73% respectively, demonstrating the interactive dose effect of repetitions and strain levels.

- Statistical differences

Figure 4.3 shows the points at which the *h* significantly varies between the strain groups (P < 0.05). In all groups, *h* declined over time, this was significant for all time points. The differences were significant (P < 0.05) in the 9% group from the beginning of testing to each time point (hour) and from the first to the second hour. For all groups the differences were nonsignificant from the second to the third hour.

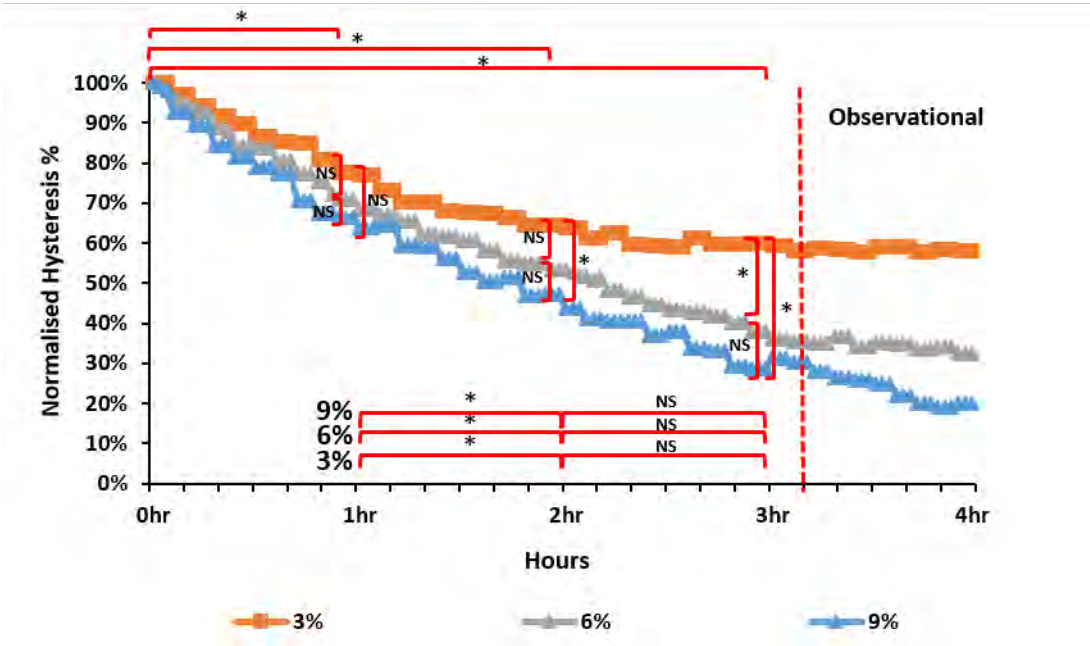

Figure 4.3. The normalised hysteresis (h) of tendons from the 3%, 6%, and 9% strain groups over 1, 2, 3 and 4 hours of repetitive loading. (Asterisks indicate a p-value < 0.05, NS denotes nonsignificant.)

iii. Static testing

a Stiffness (k)

- Observational differences

The *k* of tendons of each strain group (3%, 6%, and 9%) is reported in Figure 4.6A. The data demonstrates a greater decrease in *k* with higher strain levels for all time points. By the end the first hour, a 25% decrease in *k* in the 9% group, and a 15% decrease in the 6% group was observed, while a decrease of only 9% was observed in the 3% group for the same time point. By the end of fourth hour, a 46 % decrease was observed in the 9% group, while only 20% and 29% decreases were observed in the 3% and 6% groups respectively.

- Statistical differences

Figure 4.6 A shows the points at which the *k* significantly varies between the strain groups ($P < 0.05$). In all groups, *k* declined over time, this was only significant for the 6% and 9% groups between the first and second hours. The normalised *k*-value decline from the beginning of testing to each time point (hour), and from the first to the second hour was significantly different for the 6% and 9% groups ($P < 0.05$). This difference was nonsignificant for the 3% group. From the second hour to the third hour for all groups the differences were nonsignificant. Despite the observed decrease in *k* in the 9% group at all time points, there were significant differences between 9% and the 3% groups over the first, second and third hours.

b Maximum Load[1]

- Observational differences

The maximum load (ML) curves from the tendons of each strain level (3%, 6% and 9%) are shown in Figure 4.6 B. There is a greater ML for tendons of higher strain levels over one, two, three and four hours of repetitive loading. By the end of first hour, the average decrease in ML was 29% in the 9% group compared to less than 13% and 19%, in the 3% and 6% groups, respectively.

Despite a considerable decrease in the 9% group compared to the 3% and 6% groups, there was a greater difference in ML between the 9% group and the other two groups by the end of the fourth hour. ML decreased by 62% in the 9% group compared to 25% and 48%, in the 3% and 6% groups, respectively.

- Statistical differences

Figure 4.6 B shows the points at which the ML significantly varies between the strain groups ($P < 0.05$). In all groups, ML declined over time. The normalised ML declines from the beginning of testing to each time point was significantly different for all groups ($P < 0.05$). However, this was nonsignificant from the first to the second hour for the 3% group and from the second to the third hour for all groups. Despite the observed decrease in ML in the 9% group over four hours, there were significant

[1] The stress relaxation (SR) is expressed as the decline in the stress over the static held length. The decline is represented as three different points during the 60 s maximum hold period ($Strain_{Max}$) expressed as the max value at the start (SR1) then a decreased amount of relaxation at the middle (SR2) and at the end of the strain dose as (SR3) (Figure 3.2). For all tendons from Study 1 (Figure 4.5) and Study 2 (Figure 4.8) of static repetitive loading, the three cohorts (SR1, SR2 and SR3) are highly correlated ($R^2 = 0.87–0.99$, $P < 0.0001$) (all correlations are shown in Appendix 7). Therefore, the decline of ML over time represents the SR.

differences between the 9% and the 3% groups and no significant differences between the 9% and the 6% groups by the end of the first, second and third hours.

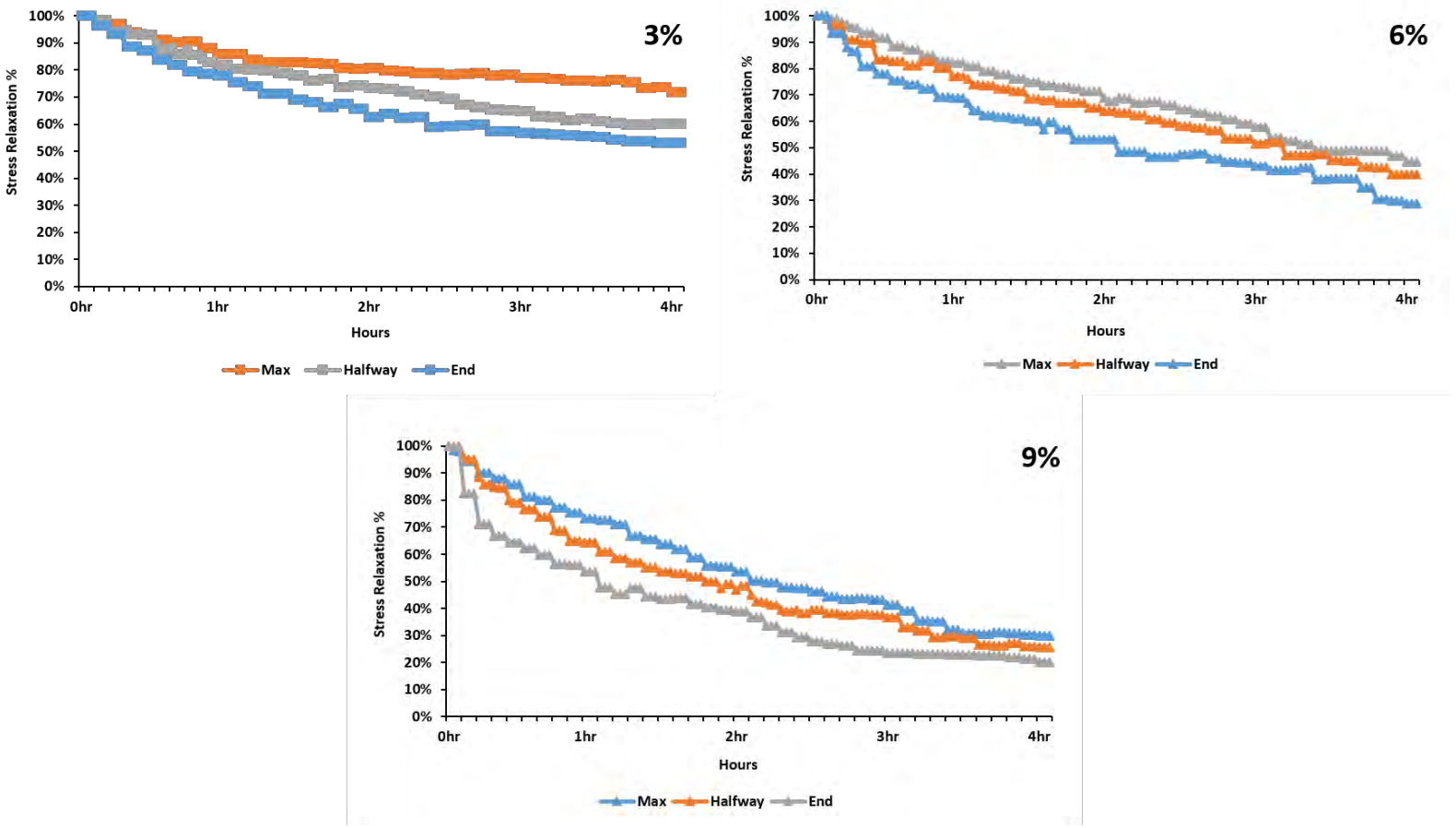

Figure 4.5. The SR of tendons from the 3%, 6%, and 9% strain groups over one, two, three and four hours of static repetitive loading. SR is expressed as the decline in the stress over the static held length. The decline is represented as three different points during the 60 S Max hold period ($Strain_{Max}$) expressed as the max value at the start (SR1) then a decreased amount of relaxation at the middle (SR2) and at the end of the strain dose (SR3).

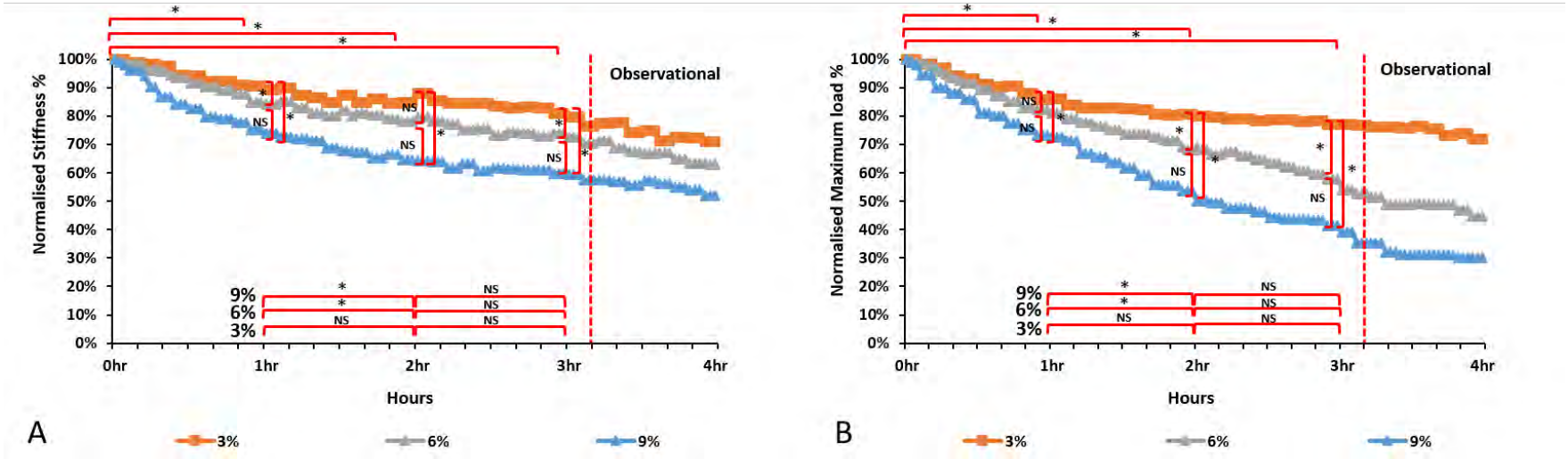

Figure 4.6. The normalised stiffness (k) [A] and normalised maximum load (ML) [B] of tendons from the 3%, 6% and 9% strained groups over one, two, three and four hours of static repetitive loading. (Asterisks indicate a p-value < 0.05, NS denotes nonsignificant.)

4.2 Mechanical Loading Outcomes (Study 2)

Introduction

This section repeats the assessments from Study 1 with the GAG-depleted subgroup of tendons for comparison (Study 2). This pairwise comparison is undertaken only for the 6% strain profile for two hours (4,800 cycles).

A. Macromechanical Loading Outcomes

i. Dynamic testing

a Loading stiffness (k2)

All the data for loading stiffness (*k2*) assessments were found to be highly correlated with ramping stiffness (*k1*) (R^2 = 0.95 – 0.98, P < 0.0001). The replication of associations for the loading stiffness (*k2*) are placed in the Appendix -7.

b Hysteresis (h)

- Observational and statistical differences

Figure 4.7 illustrates the relative change in *h* over two hours (4,800 cycles) in two control[2] groups and a GAG-depleted group and shows the significant differences at the 95% level of confidence. The differences were greater in the GAG-depleted group for all time points. The normalised declines in *h* from the beginning of testing to each time point were significantly different (P < 0.05) and from the first to the second hour were not significantly different for all groups. By the end of the first hour, the *h* decreased by 68% in the depleted group, compared to only 29% and 30% in the two control[3] groups, showing significant differences between the control[4] and the GAG-

[2, 3, 4] The second control group is the data from the Study 1.

depleted groups ($P < 0.05$). By the end of the second hour, the *h* decreased 71% in the depleted group; whereas it only decreased by 48% and 49% in both control groups. There were no significant differences between the controls.

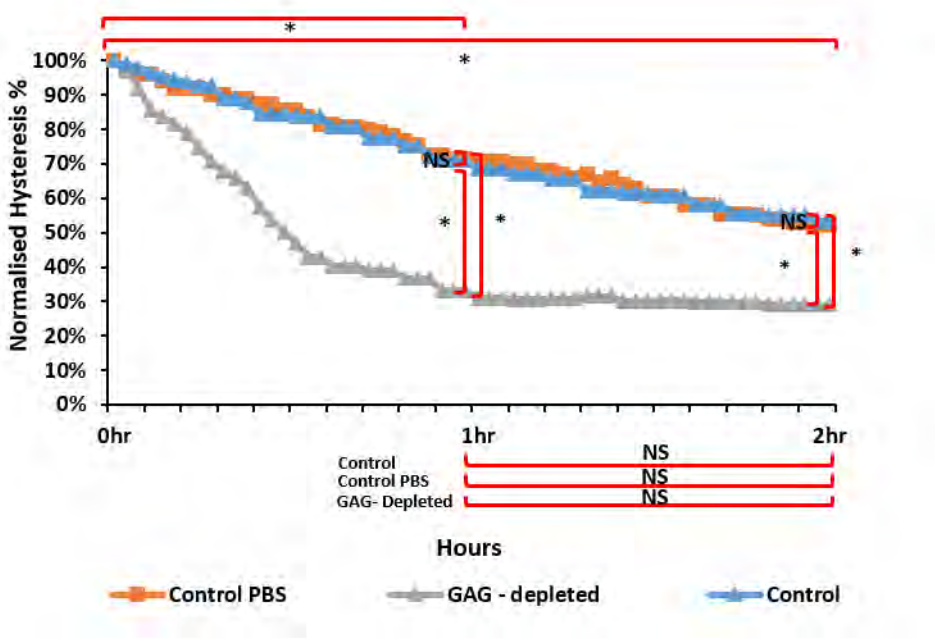

Figure 4.7. The normalised hysteresis (h) in the control and a GAG-depleted groups over two hours of repetitive loading. The GAG-depleted and control samples are also compared with the data from Study 1(blue line) showing high concordance and replication of findings. (Asterisks indicate a p-value < 0.05, NS denotes nonsignificant.)

ii. Static testing

a Stiffness (k)

- Observational and statistical differences

Figure 4.9A illustrates the relative change in *k* over two hours (4,800 cycles) in two control groups and one GAG-depleted group and shows the significant differences at the 95% level of confidence, i.e., the points at which *k* significantly varies between the controls[5] and the GAG-depleted group ($P < 0.05$). The control group data is again consistent with the other control data from Study 1. The differences in *k* were greater in the GAG-depleted group for all time points. The normalised declines in *k* from the beginning of testing to each hour and from the first to the second hour were significantly different ($P < 0.05$) for all groups. By the end of the first hour, the *k* decreased by 40% in the GAG-depleted group compared to only 19% and 16% in the two control[6] groups, showing a significant difference between each of the control[7] groups and the GAG-depleted group ($P < 0.05$). By the end of the second hour, the *k* decreased 58% in the depleted group, whereas, it decreased 31% and 20% in the control[8] groups showing significant differences between the control groups[9] and the GAG-depleted groups ($P < 0.05$).

[5, 6, 7, 8] and [9] The second control group is the data from Study 1.

b Maximum Load (ML)

- Observational and statistical differences

Figure 4.9B illustrates the relative change in ML over two hours (4,800 cycles) in two control groups and one GAG-depleted group and shows the significant differences at the 95% level of confidence, i.e. the points at which ML significantly varies between both control groups and the GAG-depleted group ($P < 0.05$). The control group data is again consistent with the other control data from Study 1. The differences were greater in the GAG-depleted group for all time points. The normalised declines in ML from the beginning of testing to each time point were significantly different ($P < 0.05$) and nonsignificant from the first to the second hour for all groups.

By the end of first hour, the ML decreased by 39% in the GAG-depleted group compared to only 21% and 20% in the two control[10] groups, showing a significant difference between the control[11] and the GAG-depleted group ($P < 0.05$). By the end of the second hour, the ML decreased 48% in the depleted group; whereas it decreased by 32% and 30% in the control[12] groups. However, there was only a significant difference between one control group[13] and the GAG-depleted group ($P < 0.05$).

[10] The first control group is the data from Study 1.
[11] The control group is the data from Study 2.
[12] The second control group is the data from Study 1.
[13] The control group is the data from Study 2.

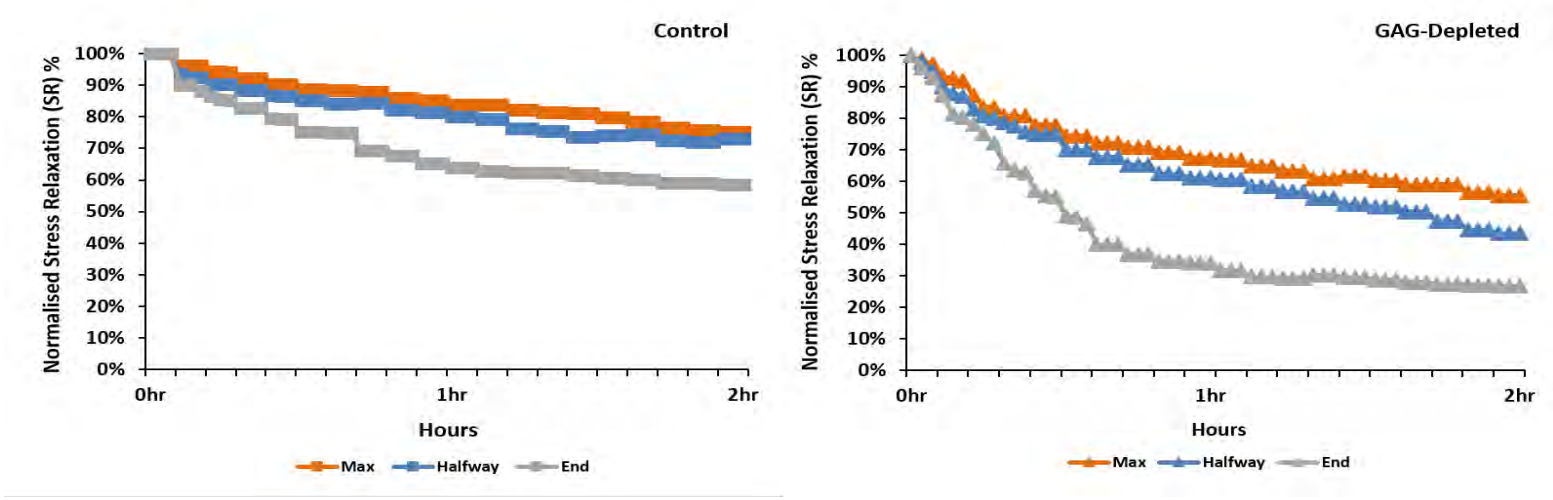

Figure 4.8. The SR of tendons from control and GAG-depleted groups over two hours of static repetitive loading. SR is expressed as the decline in the stress over the static held length. The decline is represented as three different points during the 60 s maximum hold period ($Strain_{Max}$) expressed as the maximum value at the start (SR1) then a decreased amount of relaxation at the middle (SR2) and at the end of the strain dose as (SR3) (See Figure 3.2).

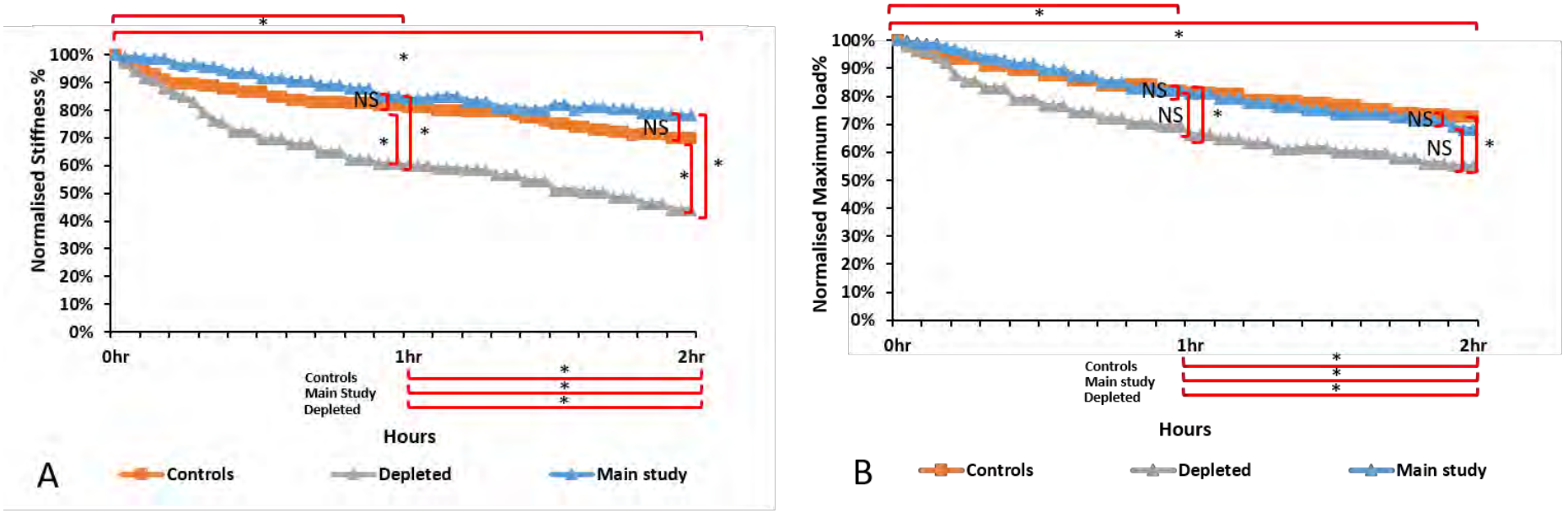

Figure 4.9. The normalised stiffness (k) [A] and maximum load (ML) [B] of control and GAG-depleted groups over two hours of static repetitive loading. The GAG-depleted and control samples are also compared with the 6% data from Study 1 (blue line) showing high concordance and replication of findings. (Asterisks indicate a p-value < 0.05, NS denotes nonsignificant.)

4.3 The Association Between Mechanical Loading Outcomes in Study 1

The following sets of graphs show the association between the changes in the mechanical variables (*k*, *h* and SR).

- Stiffness (***k***) and hysteresis (***h***)

Figure 4.10 shows the concomitant changes in *k* with the corresponding *h* during three prolonged strains of different levels. There is a decrease in *k* and *h* over the repeated testing cycle. The two variables are significantly associated with a linear correlation (R^2 = 0.94, 0.97 and 0.94, P < 0.0001 for the 3%, 6% and 9% strain levels respectively).

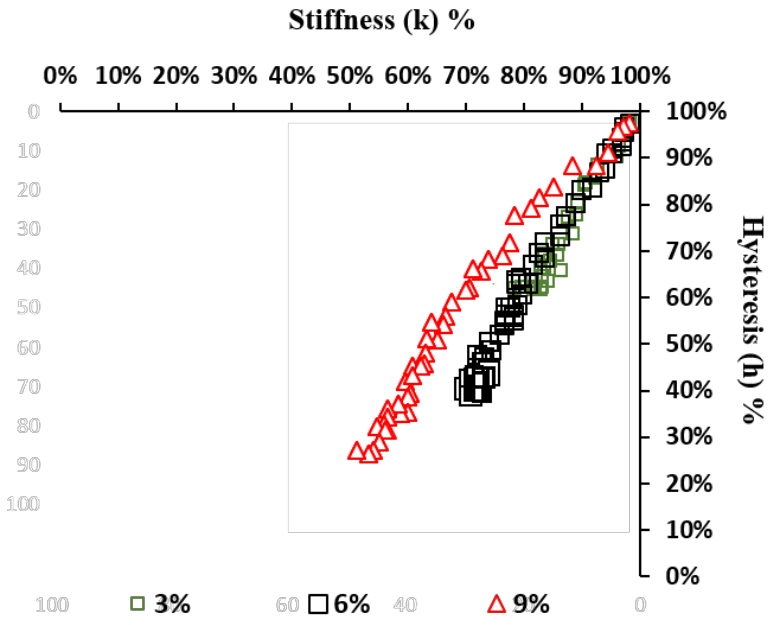

Figure 4.10. The change in the normalised *k vs h*. This graph shows the association for the three strain levels.

- Stiffness (***k***) and maximum load (ML)

Figure 4.11 shows the changes in the normalised tendon *k* with the corresponding ML during prolonged testing of the three different strain levels. There is a decrease in *k* and ML over the repeated testing cycle. The two variables are significantly associated, with a linear correlation (R^2 = 0.94, 0.99 and 0.96, P < 0.0001 for the 3%, 6% and 9% strain levels respectively).

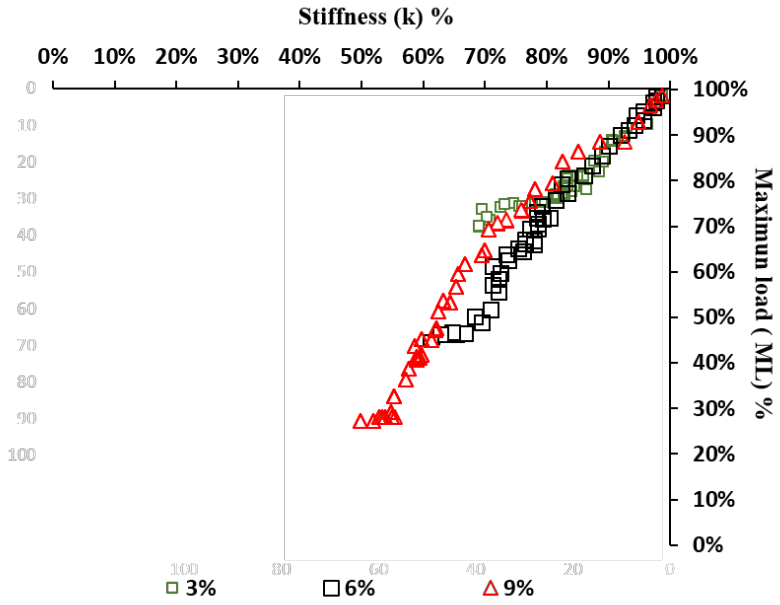

Figure 4.11. The change in *k* vs ML. This graph shows the association for the three strain levels.

- Maximum load (ML) and hysteresis (***h***)

Figure 4.12 shows the changes in the normalised tendon ML with the corresponding *h* during prolonged testing at three different strain levels. There is decrease in ML and *h* over the repeated testing cycle. The two variables are significantly associated with a linear correlation (R^2 = 0.98, 0.99 and 0.99, P < 0.0001 for the 3%, 6% and 9% strain levels respectively).

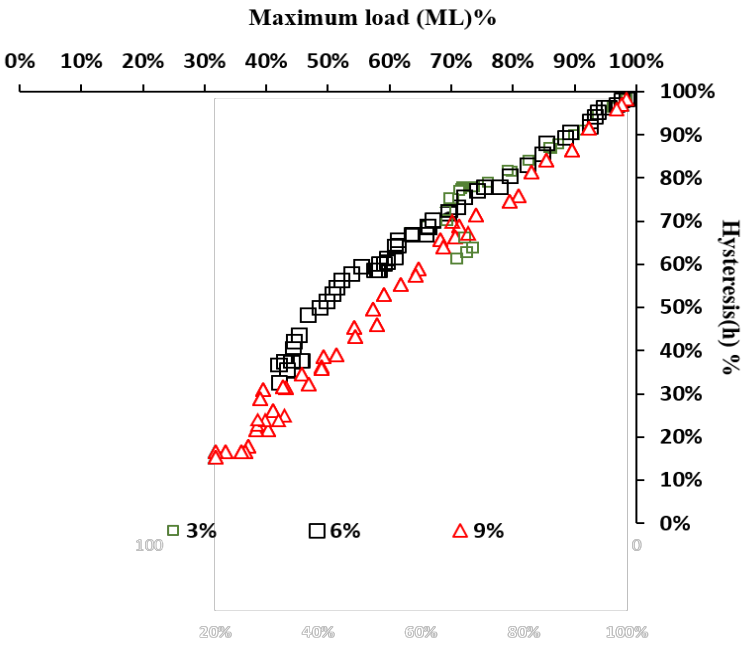

Figure 4.12. The change in the normalised ML vs *h*. This graph shows the association for the three strain levels.

4.4 The Association Between Mechanical Loading Outcomes in GAG-depleted Samples (Study 2)

- Stiffness (***k***) and hysteresis (***h***)

Figure 4.13 shows the changes in *k* with the corresponding *h* during the prolonged testing of three different strain levels. There is a decrease in *k* and a decrease in *h* over the repeated testing cycle. The two variables are significantly associated, with a linear correlation (R^2 = 0.98 for controls and 0.97 for GAG-depleted samples, $P < 0.0001$)

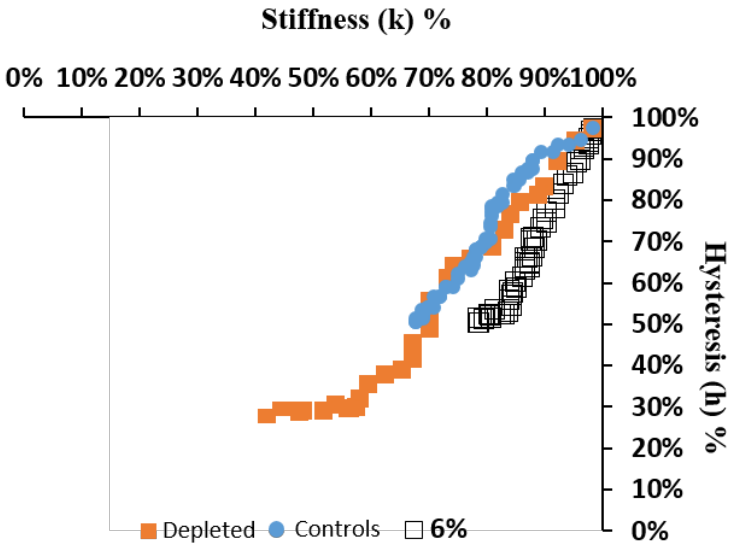

Figure 4.13. The change in *k* vs *h*. This graph shows the association for the three strain levels.

- Stiffness (***k***) and maximum load (ML)

Figure 4.14 shows the changes in *k* with the corresponding ML during prolonged testing at three different strain levels. There is a decrease in *k* and ML over the repeated testing cycle. The two variables are significantly associated with a linear correlation (R^2 = 0.98 for controls and 0.99 for GAG-depleted samples, $P < 0.0001$).

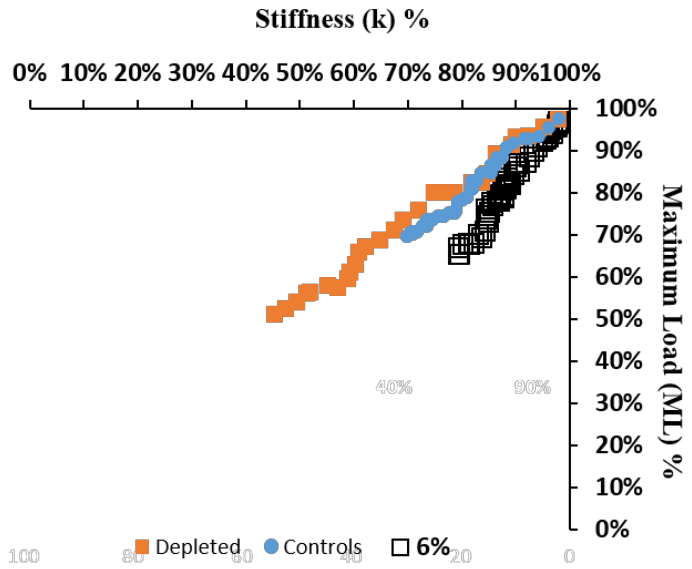

Figure 4.14. The change in *k vs* ML. This graph shows the association for the three strain levels.

- **Maximum load (ML) and hysteresis (*h*)**

Figure 4.15 shows the concomitant changes in the tendon ML with the corresponding *h* during prolonged testing at three different strain levels. There is a decrease in ML and *h* over the repeated testing cycle. The two variables are significantly associated with a linear correlation ($R^2 = 0.97$ for controls and 0.99 for GAG-depleted samples, $P < 0.0001$).

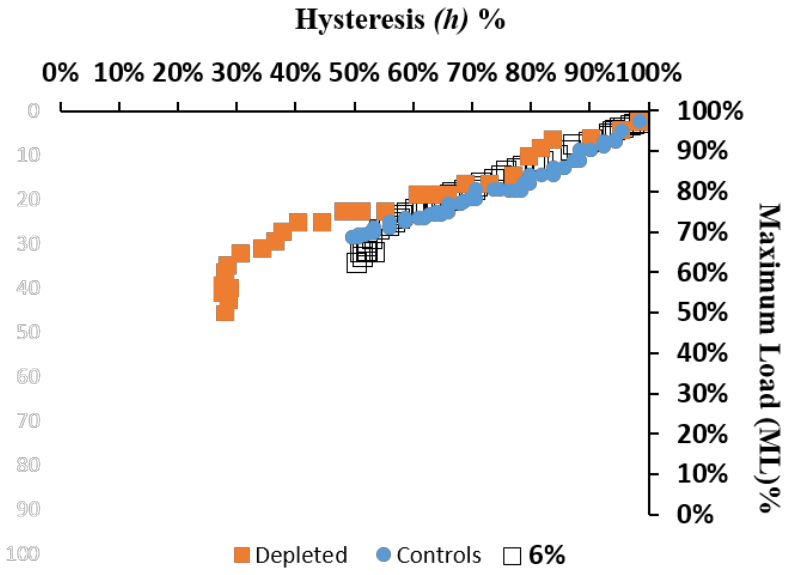

Figure 4.15. The change in ML versus *h*. This graph shows the association for the three strain levels.

4.5 Macro-morphological Outcomes During Mechanical Loading (Study 1)

A. Semi-quantitative assessment - confocal and histological assessments

Under the confocal arthroscope, the preconditioned tendon group demonstrated typical patterns that have been reported in the literature (Diamant et al., 1972; Cribb et al., 1995; Khan et al., 1999; Franchi et al., 2007). These patterns consist of spindle-shaped tenocytes arranged in a columnar fashion between the collagen fibres. The patterns are highly aligned, parallel and bundled tightly with their wavy characteristic configuration (crimps). Therefore, according to the literature, the vast majority of the preconditioned tendons were classified as Grade 1 in fibre structure, arrangement and orientation and in cell roundness (Section 3.5).

The semi-quantitative confocal assessment of tendons undergoing a repetitive cyclic loading of low, moderate- and high- levels of strain (3%, 6% and 9%) over one, two, three and four hours allowed for three-dimensional (3D) imaging of the tendon microstructure. The morphology clearly showed distinct different types of micro-damage which were not observed in the nonloaded (preconditioned) tendons.

Within the first hour of repeated loading, tendons subjected to the low-level loading (3%) demonstrated a slightly increased disruption of fibre arrangement and orientation that changed from parallel to slightly loose and wavy fibres exhibiting fibre kinks (FK) (see Figures 4.16 and 4.17:A1,1'), a slight separation and fragmentation of collagen fascicles without any evidence of fibre rupture (FaS) (see Figures 4.16 and 4.17:A1,1') and slight tenocyte morphological changes from long spindle cells (1A) to oval-shaped cells (2A) (Figures 4.16 and 4.17:A1,1').

During the second and third hour of repetitive loading, the tendons exhibited progression of damage. For example, in the third hour increased separation, fragmentation and dissociation of fascicles and increased roundness of tenocytes were characterised. A significant widening of the interfibre space and dissociation of collagen fibres also became evident during the fourth hour (FS and FD in Figures 4.16 and 4.17:A4, 4').

The tendons were graded 1 for fibre structure, arrangement and orientation and in cell roundness in the first hour, whereas in these areas the tendons graded 2 for the second, third and fourth hours.

The tendons that underwent a moderate level (6%) of repeated loading exhibited similar damage changes to those seen in the low-level group (3%), but the changes had a larger distribution. The changes were characterised by increased loose, irregularly and unequally crimped fibres with increased waviness that became evident from the first hour of repeated loading (Figures 4.16 and 4.17: B1, 1', B2, 2', B3, 3' and B4, 4'). Fibre dissociation (FD) and interfibre space (FS) between fibres was also observed during the first hour (Figures 1 and 2: B1, 1'). For the first hour, fibre structure, arrangement and orientation and in cell roundness graded 2. Whereas, for second, third and fourth hour, the tendons graded 3 for these characteristics.

Changes similar to those in the 6% group were also observed in the 9% group. However, these changes were seen earlier, in larger distribution and with increased severity of damage (Figures 4.16 and 4.17: C1, 1', C2, 2', C3, 3' and C4, 4'). During the third and fourth hour, severe fibre disruption, loss of alignment, significantly increased roundness of tenocytes, fibre thinning and significantly increased fragmentation (FS) and dissociation (FD) and fibre rupture patterns (RUP) between fibres became more evident in the 9% group (FS, FD and RUP in Figures 4.16 and 4.17: C3,3' and C4,4').

Out-of-plane discontinuity was only found in tendons from the 9% group that were subjected to more than three hours of repeated loading (Figures 4.16 and 4.17: C4, 4'). For the 9% group, the distribution of damage areas continued to increase, and were microstructurally comprised of ruptured fibres that subsequently seemed to form a curl or kink pattern at the rupture sites (Figures 4.16 and 4.17: C3, 3' and C4, 4'). For the first, second and third hours, fibre structure, arrangement and orientation and cell roundness graded 3. Whereas, the tendons graded 4 for the fourth hour.

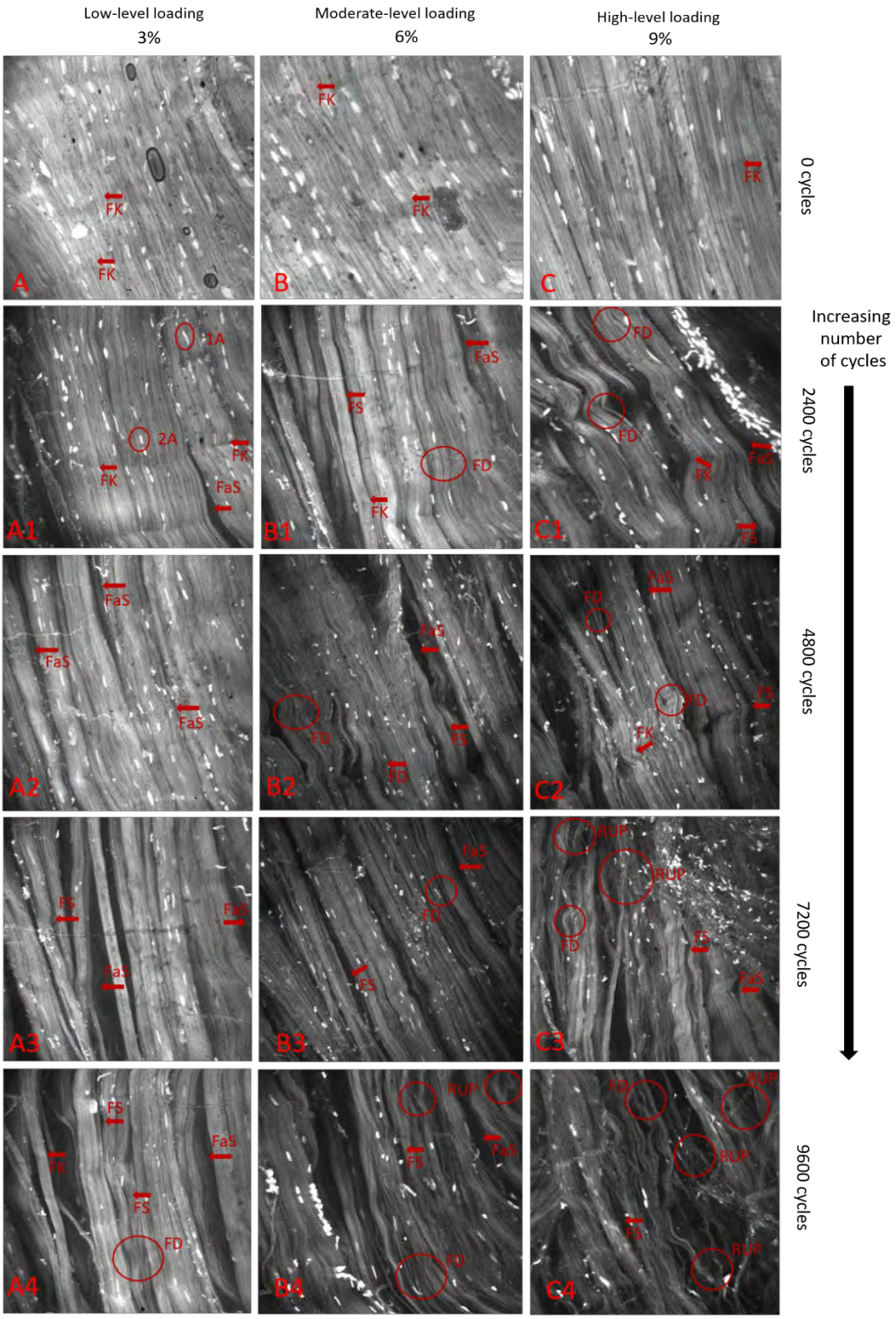

Figure 4.16. CA images demonstrating the progression of morphological changes of the unloaded and fatigued tendons undergoing three strains (3%, 6% and 9%) over one, two, three and four hours. Original magnification 475 μm.

Similar findings in the thick bulk histological sections stained with periodic acid-Schiff/Alcian blue (PAS/AB) and Hematoxylin and Eosin (H&E) (Figures 4.17: C3, C3', C4 and C4') describe a consistent pattern of structural change with increasing cycles and strain load. The Scanscope conventional histological images in Figure 4.17 and 4.18 rule out any ruptured areas of blurry thinned fibre discontinuities seen in the images taken by CA.

All of the assessments conducted for the confocal arthroscope and the Scanscope histological images representative of all group levels throughout the four-hour time frame were consistent at the end-points of each hour after the first hour.

The Scanscope H&E (Figure 4.17) and PAS/AB (Figure 4.18) histological images below correspond with the confocal arthroscopic assessment (Figure 4.16) and were acquired by the Aperio Scanscope XT scanner with a 60× objective lens.

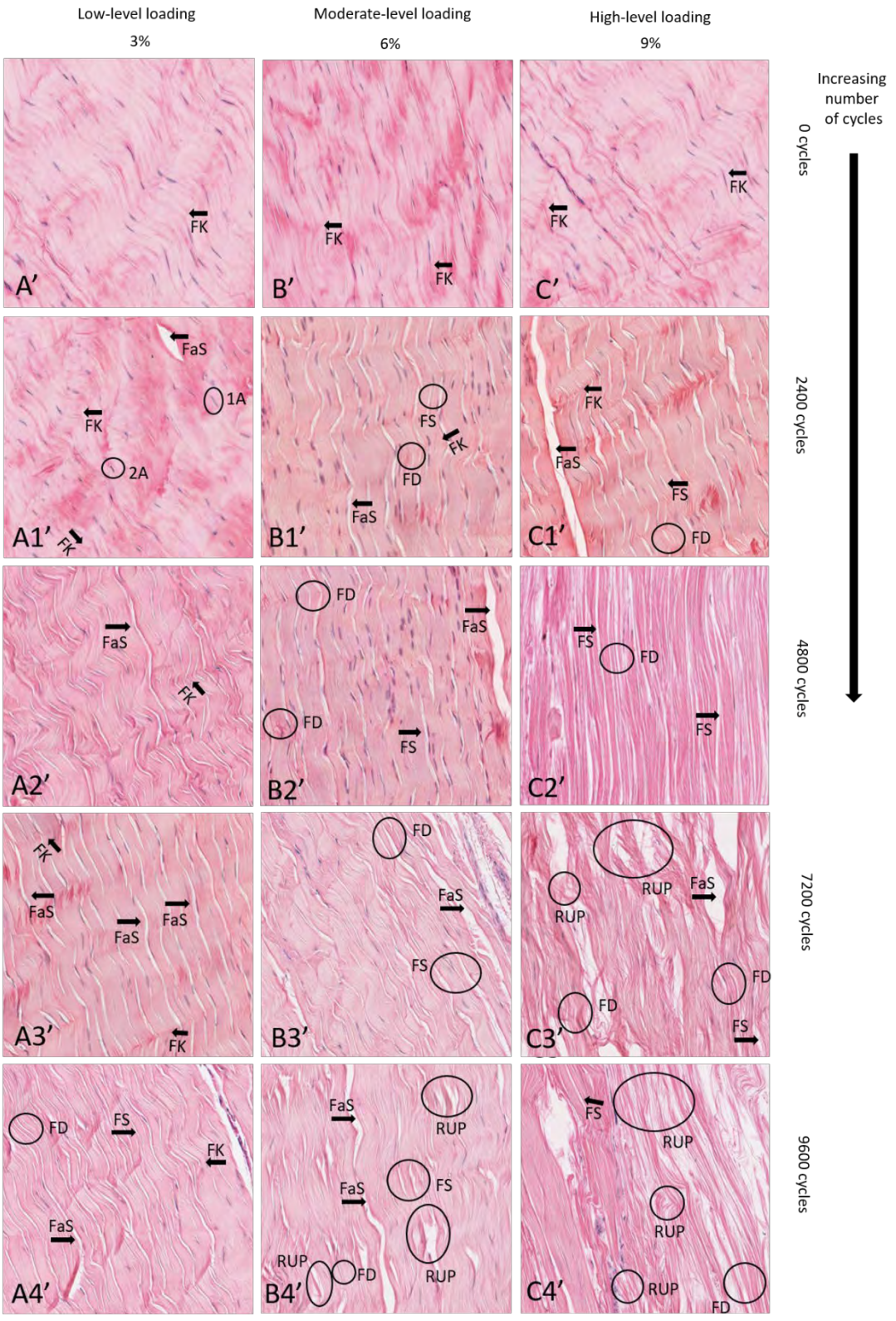

Figure 4.17. Scanscope H&E histological images demonstrating the progression of morphological changes of the unloaded and fatigued tendons undergoing three strains (3%, 6% and 9%) over one, two, three and four hours. Original magnification 475 μm.

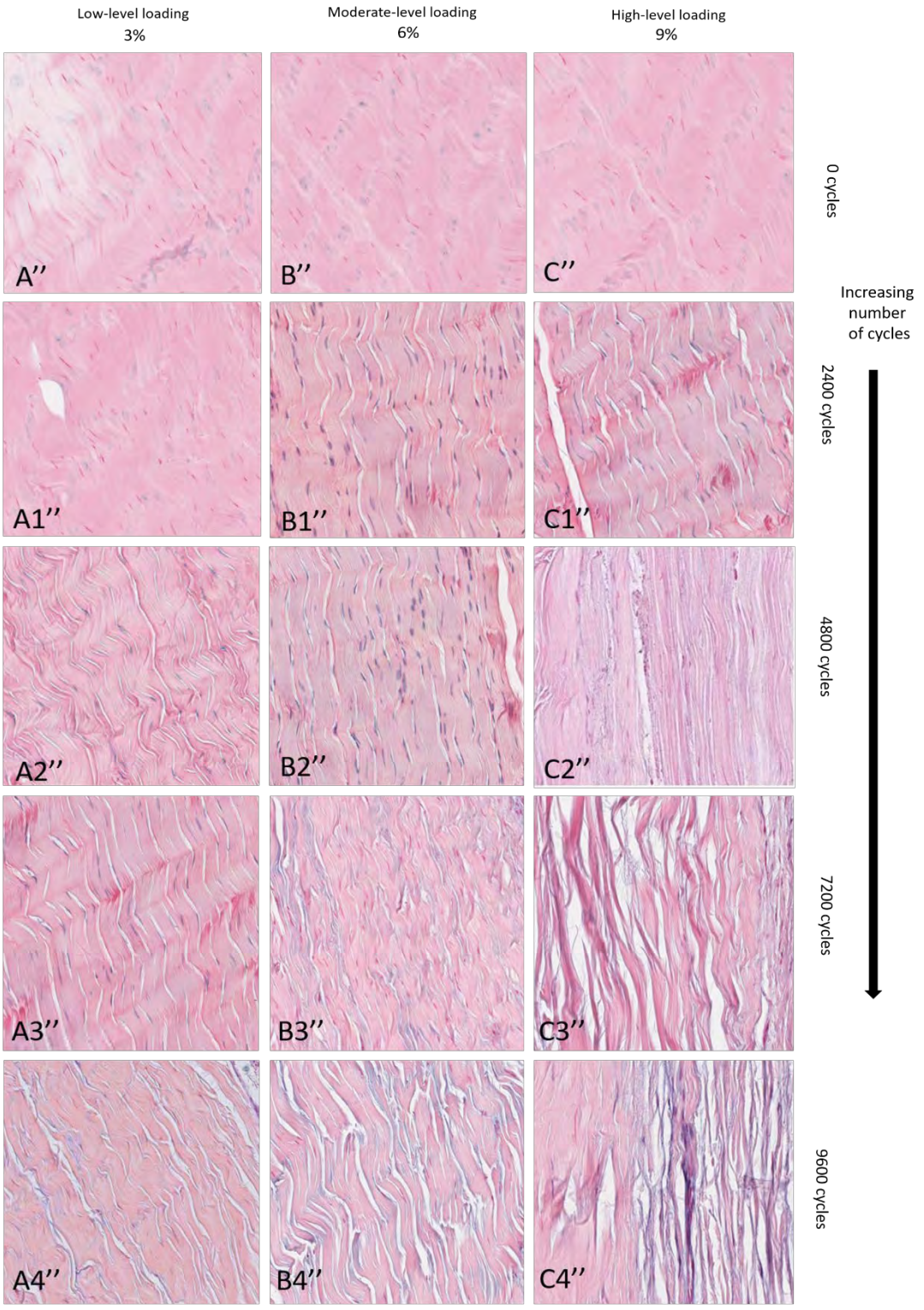

Figure 4.18. Scanscope PAS/AB histological images demonstrating the progression of morphological changes of the unloaded and fatigued tendons undergoing three strains (3%, 6% and 9%) over one, two, three and four hours. Original magnification 475 μm.

The GAG content was estimated by assessing the PAS/AB stained slides (at pH 2.5) that were obtained from the conventional Scanscope histological images (Figure 4.18). A strong increase of total GAG content was observed in tendons subjected to higher strain and number of cycles of repetitive loading.

The 3% group showed a moderate increase of alcianophilia between the collagen fibres only at the end-point of the fourth hour, whereas slight alcianophilia was observed at the first, second and third hours of the cyclic loading. In comparison, the 6% group had a slight increase in alcianophilia in the first hour, and a moderate increased alcianophilia at the end points thereafter. The 9% group revealed a moderate increase in alcianophilia level in the first hour and a marked increase in alcianophilia between the collagen fibres at the end points thereafter.

B. Semi-quantitative assessment - confocal assessments

During loading, the strained groups demonstrated a progression in changes in tenocyte morphology, fibre structure and fibre arrangement and orientation. This section of the results shows the progressive categorical shifts that were affected by the mechanical intervention.

i. Data Interpretation – Variance

The data are reported graphically showing the proportion of cells identified in each category over time for each of the three strain rates. Note the study methodology means that a high level of repeated sampling is undertaken but the samples may be different visual fields of the same sample tendon. Furthermore, the sample size declines with each hour. As a result, there is variability towards the end of the sampling (due to a decrease in n) and cases where there are increases or improvements in the microstructure damage.

Figure 4.19 shows the visual representation of the data sets subsequently presented – the changes in the proportion of cells in different categories over time.

- *Cat 4: Spindled*, circularity values > 0–0.35

- *Cat 3: Elongated*, circularity ≥ 0.35–0.6
- *Cat 2: Oval*, circularity ≥ 0.6–0.8
- *Cat 1: Round*, circularity ≥ 0.8–1.0

(For more information see Section 3.5B.)

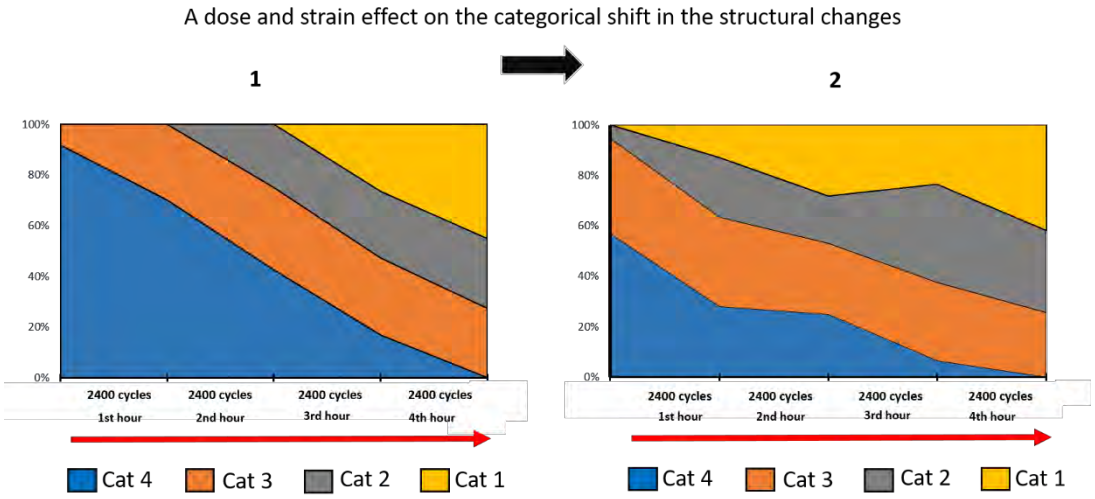

Figure 4.19. The dose and strain effect on the category shift of the morphological changes (from 1 to 2). Cat 4: long, spindle-shaped tenocytes; Cat 3: slightly rounded tenocytes; Cat 2: moderately rounded tenocytes; Cat 1: severely rounded tenocytes.

A marked difference was observed in the progression of change from Cat 4 to Cat 3 between the three strained groups (Figure 4.20). By the end of first hour and by 30 minutes of repetitive loading, about 40% and 60% of the long, spindle-shaped tenocytes (Cat 4) had become slightly rounded (Cat 3) for the 3% and 6% strain groups, respectively. Whereas, as early as the end of the first 10 minutes about 80% of long spindle shape tenocytes (Cat 4) changed to slightly rounded (Cat 3) in the 9% strain group. No marked difference was observed for the progression of change from Cat 3 to Cat 2 and from Cat 2 to Cat 1 between the 3% and 6% groups during the second, third and fourth hour of repetitive loading. The tenocytes belonging to Cat 3 and Cat 2 were predominant for both groups during the second and third hour.

A marked difference in the shift from Cat 2 to Cat 1 was observed in the three strain groups. For the tenocytes that belonged to 3% and 6% groups, a marginal shift (10%) of the moderately rounded tenocytes (Cat 2) became severely rounded (Cat 1).

This marginal shift only started at the end of one hour and 30 minutes and continued until the end of the third hour of repetitive loading. Whereas, the 9% group displayed about a 60% change from moderately to severely rounded tenocytes (from Cat 2 to Cat 1) by the end of fourth hour of repetitive loading. This shift started within the first hour and represented about 30% of tenocytes by the end of the third hour of repetitive loading.

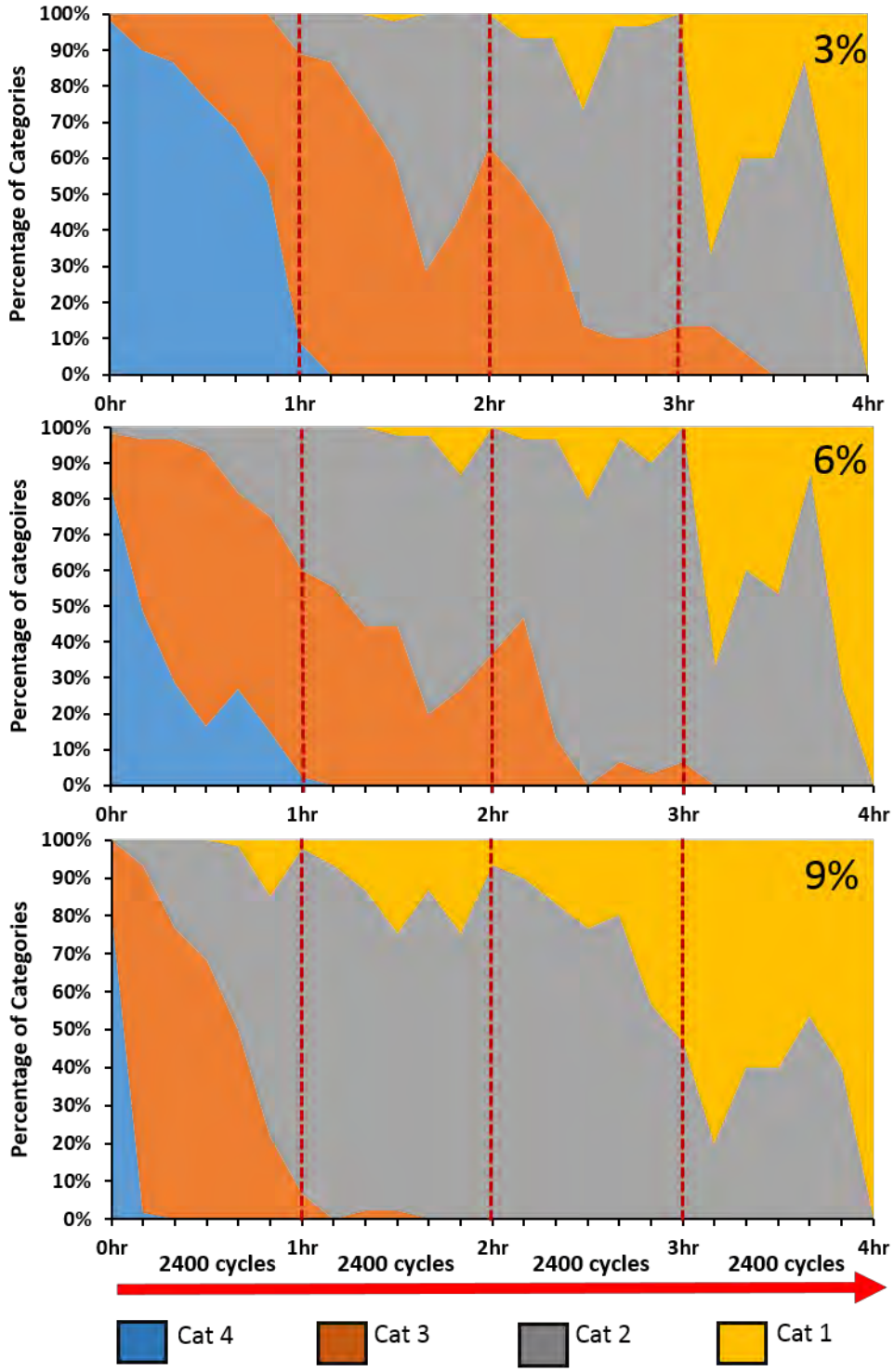

Figure 4.20. The tenocyte morphology category shift of tendons subjected to 3%, 6% and 9% strain over one, two, three and four hours. Cat 4: long, spindle-shaped tenocytes; Cat 3: slightly rounded tenocytes; Cat 2: moderately rounded tenocytes; Cat 1: severely rounded tenocytes.

The change in fibre arrangement and orientation is shown in Figure 4.21. Under the repetitive loadings, the 3%, 6% and 9% strain groups all demonstrated a progression change in fibre arrangement and orientation that moved from Cat 4 to Cat 1 over the one, two, three and four hours of strain (Figure 4.21).

A marked difference was observed in the change from Cat 4 to Cat 3 between the three strain groups (Figure 4.21). By the end of first 20 minutes of repetitive loading, about 20%, 60% and 100% of the collagen fibres have shifted from Cat 4 to Cat 3 for the 3%, 6% and 9% groups, respectively. The compacted, parallel, regular and well-ordered fibres (Cat 4) changed to slightly loose and wavy (Cat 3). By the end of the first two hours, 50%, 70% and more than 95% of fibres shifted from Cat 3 to Cat 2 for the 3%, 6% and 9% groups, respectively. The slightly loose and wavy fibres changed to moderately loose and wavy and the fibres crossed each other (Cat 2).

By the end of the third hour, no marked difference was observed between 3% and 6% groups for the shift from Cat 2 to Cat 1. Only 20% of the moderately loose, wavy fibres became fibres with no identifiable patterns (Cat 1). Whereas, more than 50% of the fibres in 9% group changed to Cat 2 by the end of the third hour. More than 95% of the fibres changed to Cat 1 by the end of the fourth hour for all groups respectively.

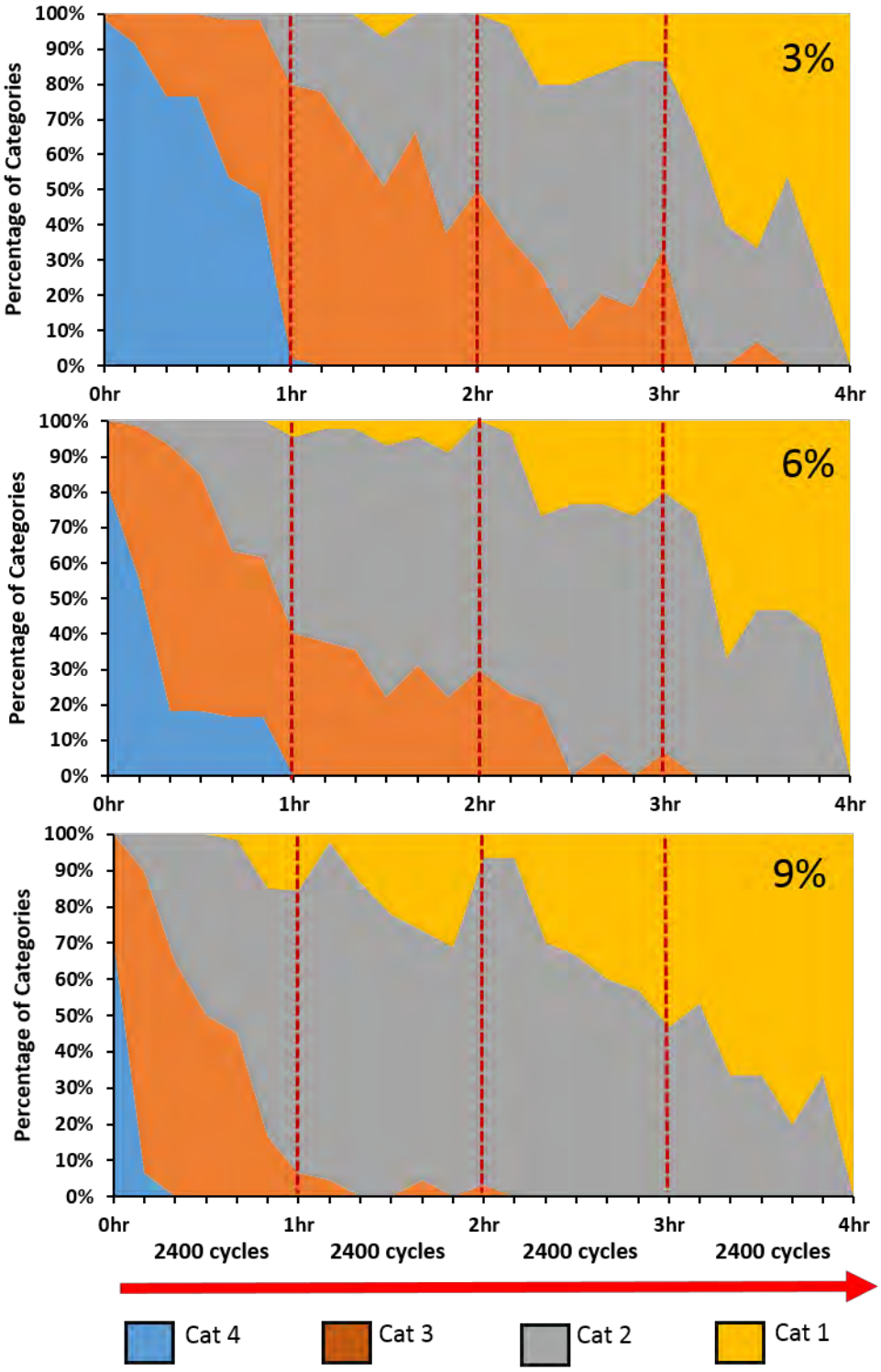

Figure 4.21. The fibre arrangement and orientation category shift of tendons subjected to 3%, 6% and 9% strain over one, two, three and four hours. Cat 4: compacted, parallel, regular and well-ordered fibres; Cat 3: slightly loose and wavy fibres; Cat 2: moderately loose, wavy fibres; Cat 1: fibres with no identifiable patterns.

A marked difference was observed in the progression of change in fibre structure from Cat 4 to Cat 3 between the three strained groups (Figure 4.22). Within the first hour for all groups, about 25%, 90% and 100% of fibres changed from Cat 4 to Cat 3 for the 3%, 6% and 9% strain groups, respectively. The long continuous fibres changed from slightly wavy fragmented and separated (Cat 4) to increasingly wavy, fragmented and separated fibres (Cat 3). In comparison with the 3% and 6% groups, these changes occurred earlier in the 9% group.

By the end of the second hour, a moderate severity of waviness, separation and fragmentation (Cat 2) became evident with a shift from Cat 3 to Cat 2 in about 50% and 60% of the fibres in the 3% and 6% groups respectively. Whereas, more than 90% of these fibres shifted to Cat 2 at the beginning of the second hour of the intervention for the 9% strain group.

Until the end of the third and fourth hours, no marked difference was observed between fibres from the 3% and 6% strain groups in the shift from Cat 2 to Cat 1. About 20% of fibres in the 3% group and 50% in the 6% group shifted from Cat 2 to Cat 1 after the second hour and became severely separated and fragmented. While by the end of the third and fourth hours, 60% and 80% of the fibres, respectively, were severely separated and fragmented in the 9% strain group.

During the second and third hour for the 3% and 6% strain groups, the majority of the fibres ranged between increased and moderate separation and fragmentation, while the majority of fibres in the 9% group ranged between moderate and severe fragmentation and showed a complete loss of structure.

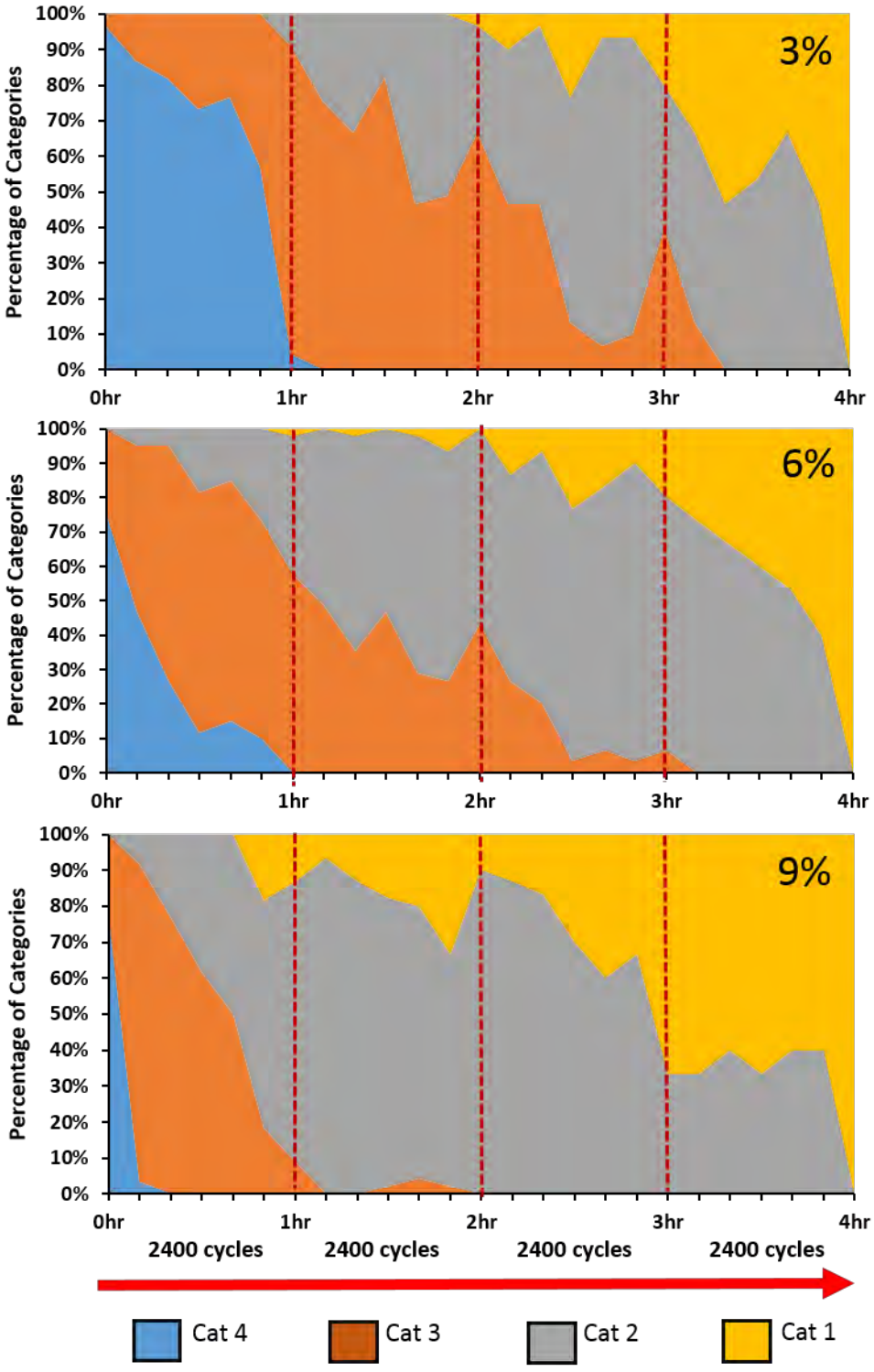

Figure 4.22. The decreasing progression of categorical shift in fibre structure of tendons subjected to 3%, 6% and 9% strain over one, two, three and four hours. Cat 4: slightly wavy fragmented and separated fibres; Cat 3: increasingly wavy, fragmented and separated fibres; Cat 2: moderate waviness, separation and fragmentation; Cat 1: severely separated and fragmented fibres.

C. Quantitative assessment - confocal assessments

i. Tenocyte shape, fibre waviness and anisotropy

The 3%, 6% and 9% strain groups demonstrated a progression change in tenocyte roundness and fibre waviness characterised by marked decreasing categorical shifts (Figures 4.23–4.28). With fatigue loading, a marked decrease was observed in the progression of tenocyte morphology and fibre waviness category shifts in tendons subjected to low, moderate and high levels of strain (3%, 6% and 9% strain) and loading over one, two, three and four hours, whereas the anisotropy of fibres did not demonstrate any marked changes. In the 3%, 6% and 9% strain groups, the changes that were observed in tenocyte roundness can be categorised into Cat 4 (circularity values 0.00–0.35): long spindle-shaped tenocytes; Cat 3 (circularity values 0.35–0.60) slightly rounded tenocytes; Cat 2 (circularity values 0.60–0.80): moderately rounded tenocytes; Cat 1 (circularity values 0.80–1.00): severely rounded tenocytes. (For more information see Section 3.5B.)

There was a linear decrease in the number of tenocytes in Cat 4 through the first two hours for the 3% strain group (changing from 60% to 30% Cat 4 tenocytes). The other three categories (Cat 3, 2, and 1) concomitantly increased during the loading and no change was observed between these categories over the four hours.

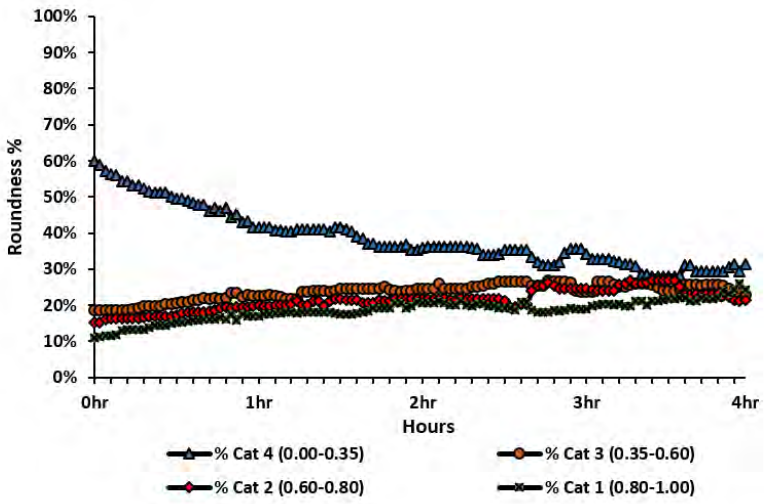

Figure 4.23. The effect of fatigue loading on tendon tenocyte shape in the 3% strain group over the first, second, third and fourth hour of repetitive loading. Cat 4: long spindle-shaped tenocytes; Cat 3: slightly rounded tenocytes; Cat 2: moderately rounded tenocytes; Cat 1: severely rounded tenocytes.

In the 6% strain group by the end of the second hour, a rapid decline in spindle tenocytes (Cat 4) (from 60% to 25%) occurred, with the tenocytes changing to become slightly rounded (Cat 3). No marked changes were observed during the third and fourth hours. The other three categories (Cat 3, 2, and 1) concomitantly increased with a greater increase in Cat 3 after the first hour.

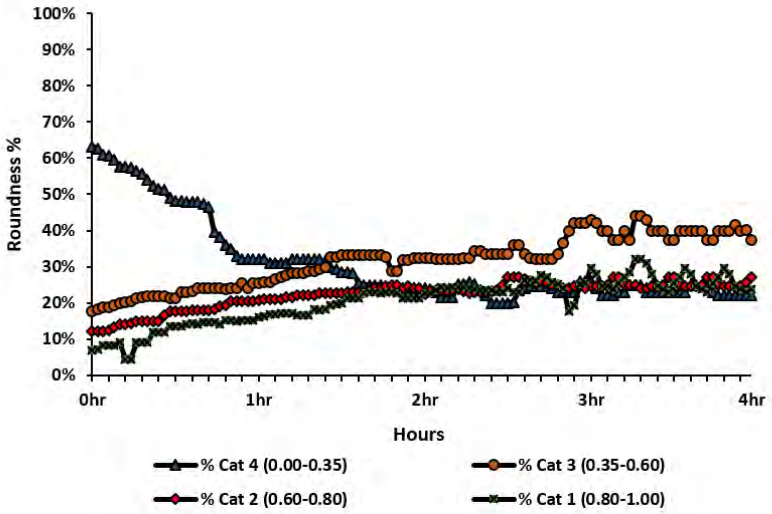

Figure 4.24. The effect of fatigue loading on tendon tenocyte shape in the 6% strain group over the first, second, third and fourth hour of repetitive loading. Cat 4: long spindle-shaped tenocytes; Cat 3: slightly rounded tenocytes; Cat 2: moderately rounded tenocytes; Cat 1: severely rounded tenocytes.

In the 9% strain group, a sharp rapid decline in spindle tenocytes (Cat 4) (from 68% to 10%) occurred by the end of the second hour, the tenocytes changing to Cat 3. No marked changes were observed during the third and fourth hours. The other three categories (Cat 3, 2, and 1) concomitantly increased with a marked increase in Cat 1 after the first hour. There was also greater noise in the image analysis.

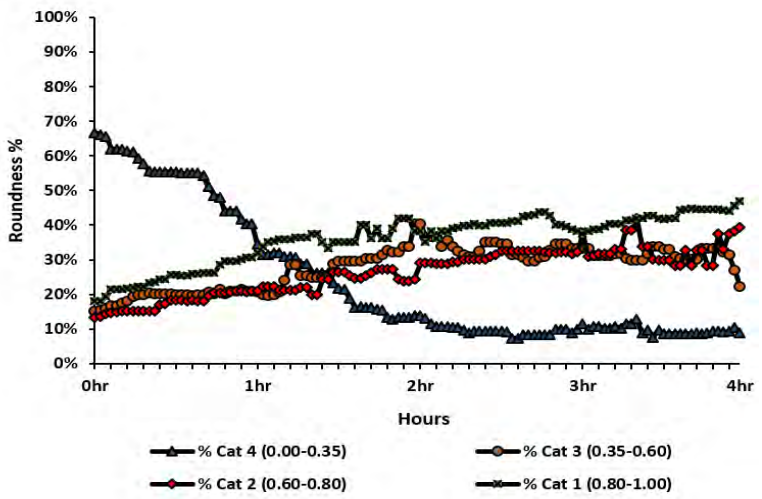

Figure 4.25. The effect of fatigue loading on tendon tenocyte shape in the 9% strain group over the first, second, third and fourth hour of repetitive loading. Cat 4: long spindle-shaped tenocytes; Cat 3: slightly rounded tenocytes; Cat 2: moderately rounded tenocytes; Cat 1: severely rounded tenocytes.

Figure 4.26 shows the points at which the tenocyte morphology significantly varied between the strain groups ($p < 0.05$). The tenocyte morphological change in the three strain groups demonstrated significant differences over the first, second, third and fourth hours. The spindle tenocytes (Cat 4) declined over time (cycles) with greater changes associated with the level of strain. Although the differences between the three prolonged strained groups (for 3%, 6% and 9%) were nonsignificant at the first hour, the normalised changes from start to each hour and from the first to the second hours were significantly different ($p < 0.05$). Further, the change was significant for all groups from the first to the second hours and nonsignificant from the second to the third hours.

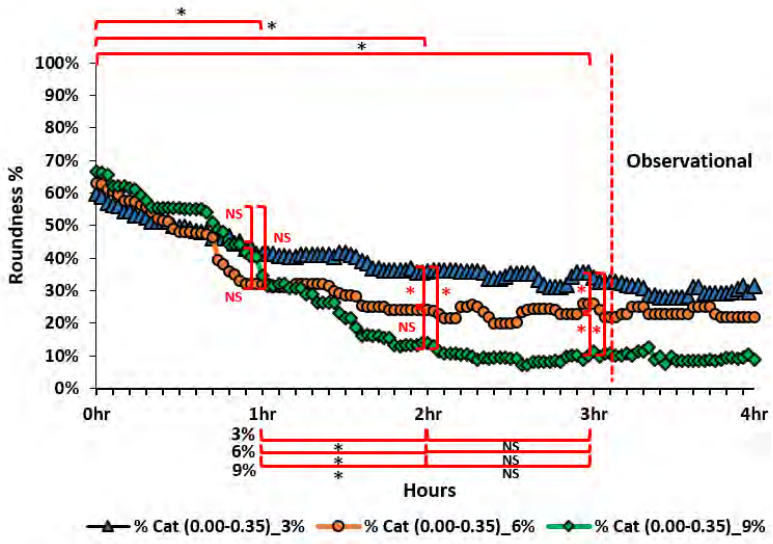

Figure 4.26. The differences in the effect of fatigue loading on tendon tenocyte shape. The percentage of cells in Cat 4 in the 3%, 6% and 9% strain groups over the first, second, third and fourth hour. (Asterisks indicate a p-value < 0.05, NS denotes nonsignificant.)

Figure 4.27 illustrates the relative change in the fibre waviness for tendons over four hours (9,600) cycles at the three different strain levels and the points at which the fibre waviness has significantly varied between the strain groups ($p < 0.05$). The waviness increased over time (cycles) with greater changes associated with the level of strain. This was significant for all groups at all-time points. The differences were significantly ($P < 0.05$) greater in the 9% group at the first, second and third hour of loading. The normalised changes from the beginning to the first hour, from the first to the second hour, and from the second to the third hour were significantly different for the 3%, 6% and 9% strain groups ($p < 0.05$).

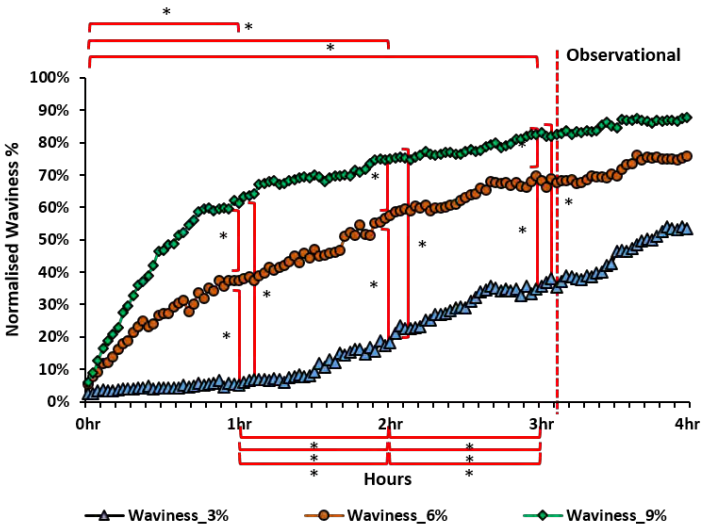

Figure 4.27. The differences in the effect of fatigue loading on fibre waviness between the 3%, 6% and 9% strain groups over the first, second, third and fourth hour. (Asterisks indicate a p-value < 0.05, NS denotes nonsignificant.)

In Figure 4.28, significant differences in fibre anisotropy can be observed between the 3% strain group and the other groups over the first, second, third and fourth hour of the mechanical intervention ($p < 0.05$). No significant differences were observed between the 6% and 9% strain groups for all time points. For all groups, no significant differences were observed from the start to each of the time points. All the differences between the 6% and 9% groups existed during the preconditioning of the samples.

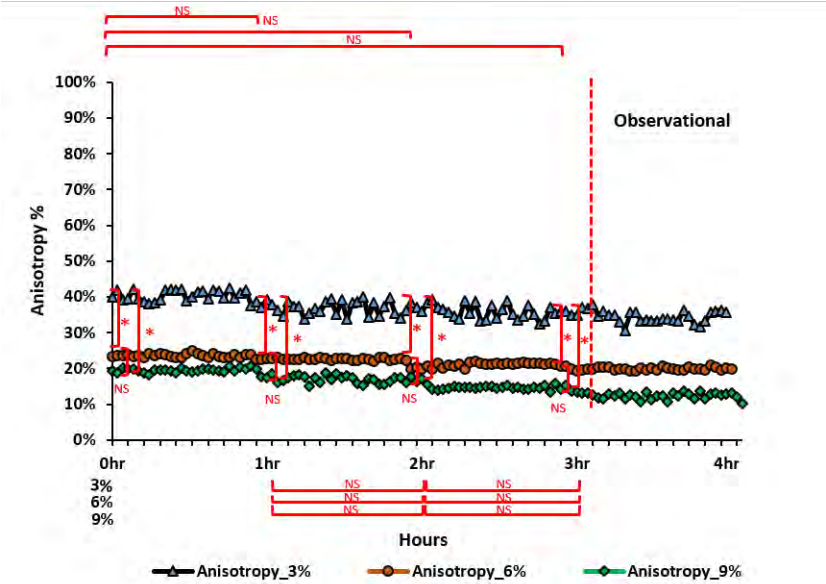

Figure 4.28. The differences in the effect of fatigue loading on fibre anisotropy between the 3%, 6% and 9% strain groups over the first, second, third and fourth hour. (Asterisks indicate a p-value < 0.05, NS denotes nonsignificant.)

4.6 The Association Between Mechanical and Macro-morphological Changes Over Time

The following sets of graphs show the changes in the mechanical profiles[14] (declining) with the corresponding changes in cell morphology for the prolonged strain testing of the tendons under three different strain levels. All the tendons start with almost all of cells identified as spindle-like and over time the proportion of spindles declines with an increase in the proportion of roundness in the remaining cells.

- Tenocyte Roundness (3%)

Figure 4.29A shows the declining proportion of cells in the samples that are spindle-like (Cat 4) as the stiffness declines, demonstrating a significantly linear association between the two variables ($R^2 = 0.97$, $P < 0.0001$). The corresponding proportional increase in the three remaining categories of roundness (Cat 3, Cat 2 and Cat 1) as stiffness declines is shown in Figure 4.29B. Each of these have a linear association $R^2 > 0.88$, $P < 0.0001$.

[14] The loading stiffness (*k2*) was measured at the beginning of the cyclic loading profile. All the data for stiffness assessments were found to be highly correlated ($R^2 = 0.84–0.97$, $P < 0.0001$ for the 3%, 6% and 9% strain groups). The replication of the associations for *k2* are in Appendix 8.

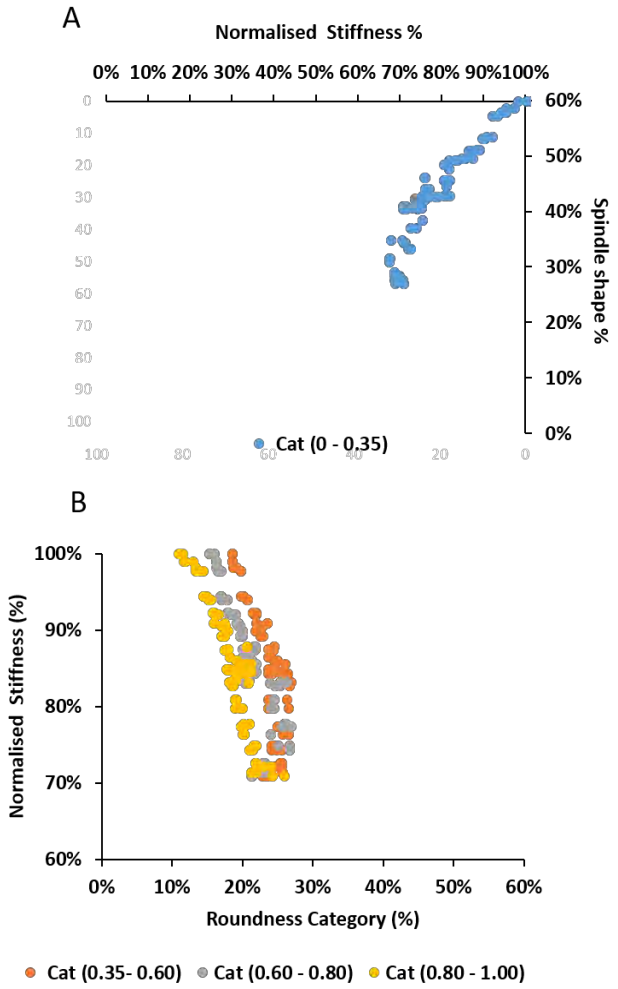

Figure 4.29. Changes in *k* vs tenocyte roundness in the 3% strain group over four hours of cyclic loading. A shows the proportion of cells with a spindle shape (Cat 4) compared with *k* decline. B shows the increase in proportion of cells in the three remaining categories of roundness (Cat 3, Cat 2 and Cat 1) compared with *k* decline.

Figure 4.30A shows the declining proportion of Cat 4 cells as *h* decreases, demonstrating a significantly linear association between the two variables ($R^2 = 0.96$, $P < 0.0001$). The corresponding proportional increase in the three remaining categories of roundness (Cat 3, Cat 2 and Cat 1) is shown in Figure 4.30B. Each of these have a linear association $R^2 > 0.87$, $P < 0.0001$.

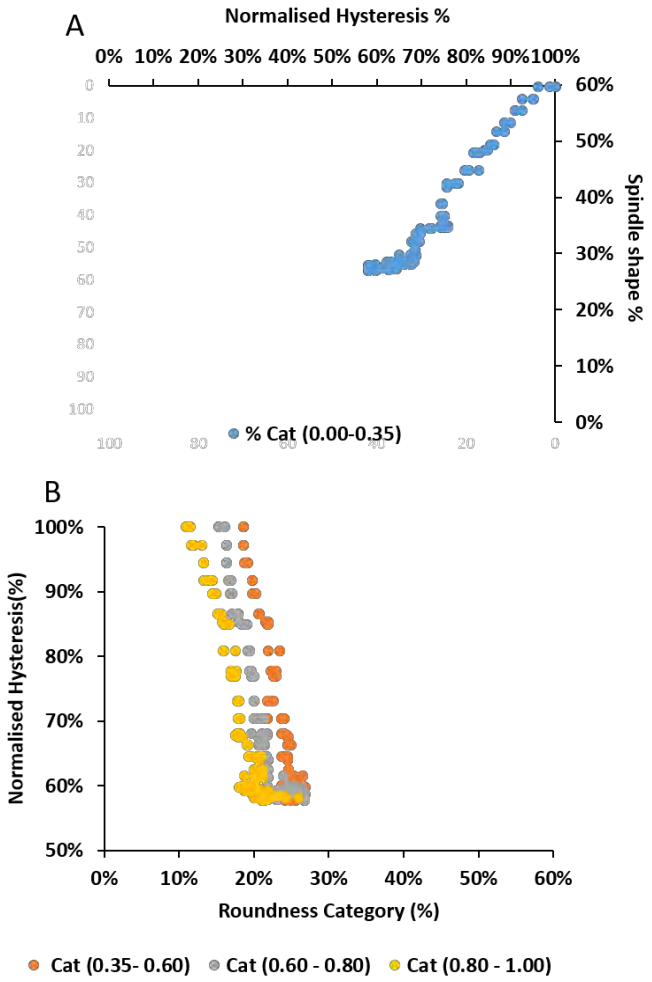

Figure 4.30. Changes in *h* vs tenocyte roundness in the 3% strain group over four hours of cyclic loading. A shows the proportion of cells with a spindle shape (Cat 4) compared with *h*. B shows the increase in proportion of cells in the three remaining categories of roundness (Cat 3, Cat 2 and Cat 1) compared with *h*.

Figure 4.31A shows the declining proportion of Cat 4 cells as ML declines, demonstrating a significantly linear association between the variables (R^2 = 0.97, $P < 0.0001$). The corresponding proportional increase in the three remaining categories of roundness (Cat 3, Cat 2 and Cat 1) is shown in Figure 4.31B. Each of these have linear associations $R^2 > 0.86$, $P < 0.0001$.

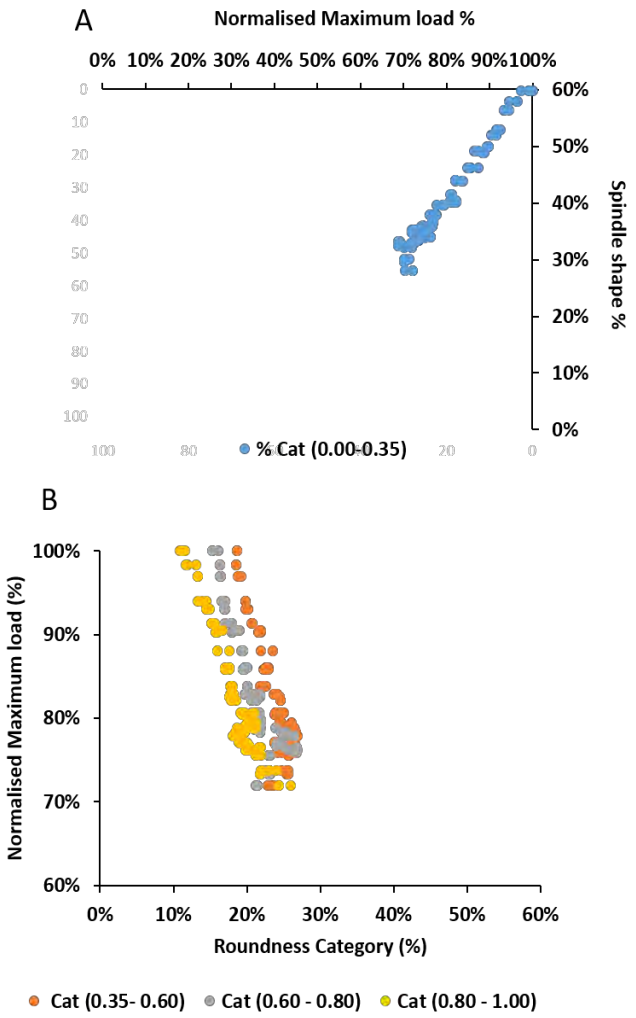

Figure 4.31. Changes in ML vs tenocyte roundness in the 3% strain group over four hours of cyclic loading. A shows the proportion of cells with a spindle shape (Cat 4) compared with ML. B shows the increase in proportion of cells in the three remaining categories of roundness (Cat 3, Cat 2 and Cat 1) compared with ML.

- Tenocyte Roundness (6%)

The following graphs show the concomitant changes in the tendon *k* (declining) with changes in cell morphology. Figure 4.32A shows the declining proportion of Cat 4 cells as the stiffness declines, demonstrating a significantly linear association between the variables ($R^2 = 0.88$, $P < 0.0001$). The corresponding proportional increase in the three remaining categories of roundness (Cat 3, Cat 2 and Cat 1) is shown in Figure 4.32B. Each of these have linear associations $R^2 > 0.90$, $P < 0.0001$.

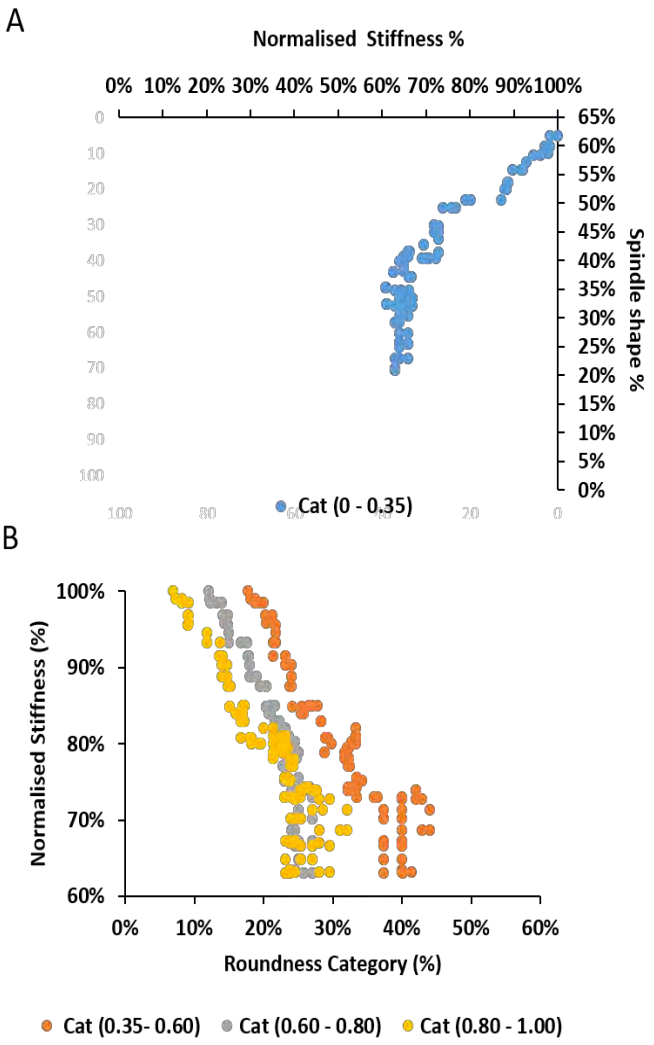

Figure 4.32. Changes in *k* vs tenocyte roundness in the 6% strain group over four hours of cyclic loading. A shows the proportion of cells with a spindle shape (Cat 4) compared with *k* decline. B shows the increase in proportion of cells in the three remaining categories of roundness (Cat 3, Cat 2 and Cat 1) compared with *k* decline.

Figure 4.33A shows the declining proportion of Cat 4 cells as *h* declines, demonstrating a significantly linear association ($R^2 = 0.91$, $P < 0.0001$) between the variables. The corresponding proportional increase in the three remaining categories of roundness (Cat 3, Cat 2 and Cat 1) is shown in Figure 4.33B. Each of these have a linear association $R^2 > 0.93$, $P < 0.0001$.

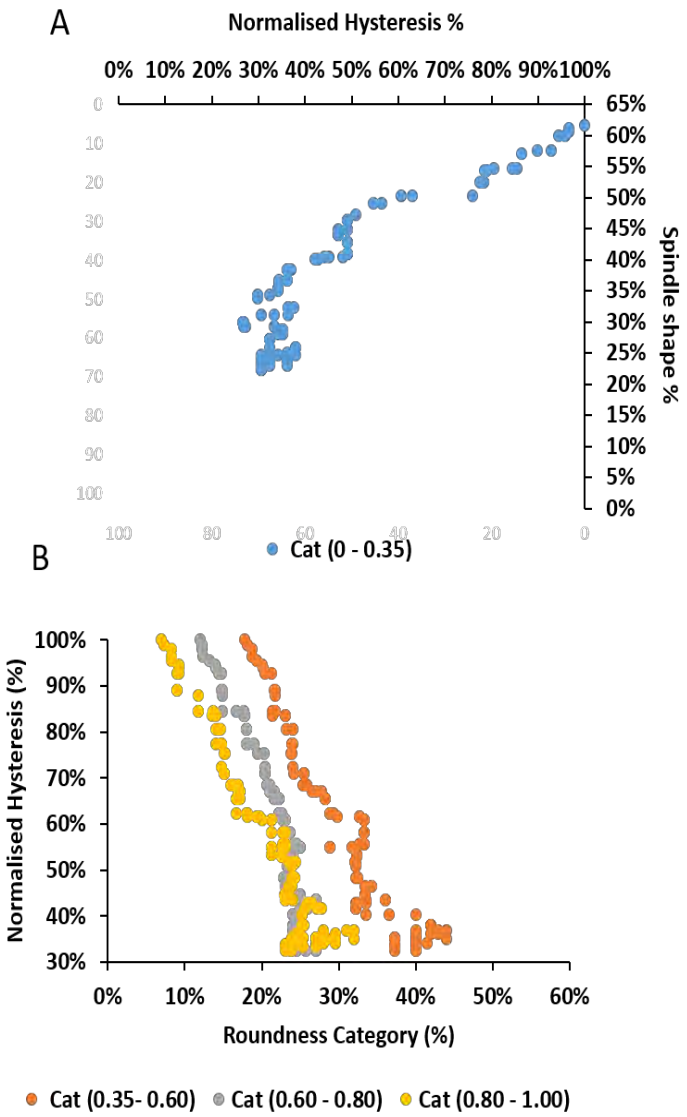

Figure 4.33. Changes (*h* vs tenocyte roundness) in the 6% strain group over four hours of cyclic loading. A shows the proportion of cells with a spindle shape (Cat 4) compared with *h*. B shows the increase in proportion of cells in the three remaining categories of roundness (Cat 3, Cat 2 and Cat 1) compared with *h*.

Figure 4.34A shows the declining proportion of Cat 4 cells as the ML declines, showing a significantly linear association ($R^2 = 0.88$, $P < 0.0001$). The corresponding proportional increase in the three remaining categories of roundness (Cat 3, Cat 2 and Cat 1) is shown in Figure 4.34B. Each of these have a linear associations $R^2 > 0.88$, $P < 0.0001$.

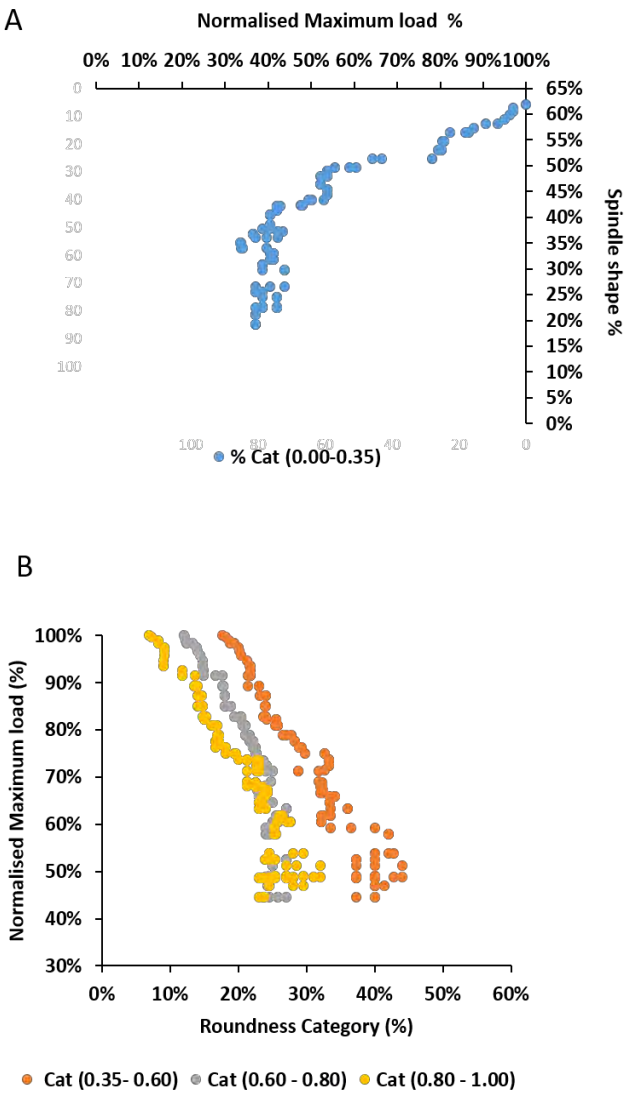

Figure 4.34. Changes in ML vs tenocyte roundness in the 6% strain group over four hours of cyclic loading. A shows the proportion of cells with a spindle shape (Cat 4) compared with ML. B shows the increase in proportion of cells in the three remaining categories of roundness (Cat 3, Cat 2 and Cat 1) compared with ML.

- Tenocyte Roundness (9%)

Figure 4.35A shows the declining proportion of Cat 4 cells as the *k* declines, demonstrating a significantly linear association (R^2 = 0.95, P < 0.0001). The corresponding proportional increase in the three remaining categories of roundness (Cat 3, Cat 2 and Cat 1) is shown in Figure 4.35B. Each of these have a linear association $R^2 > 0.84$, P < 0.0001.

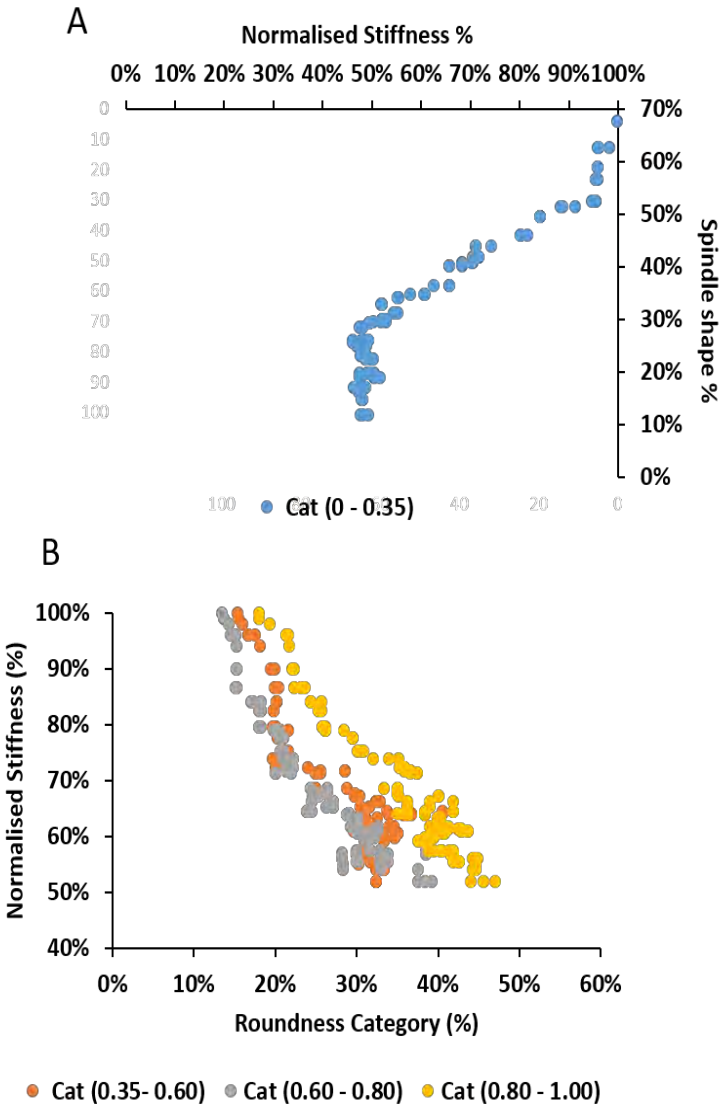

Figure 4.35. Changes in *k vs* tenocyte roundness in the 9% strain group over four hours of cyclic loading. A shows the proportion of cells with a spindle shape (Cat 4) compared with k decline. B shows the increase in proportion of cells in the three remaining categories of roundness (Cat 3, Cat 2 and Cat 1) compared with k decline.

Figure 4.36A shows the declining proportion of Cat 4 cells as the *h* declines, demonstrating significantly linear association (R^2 = 0.91, P < 0.0001). The corresponding proportional increase in the three remaining categories of roundness (Cat 3, Cat 2 and Cat 1) is shown in Figure 4.36B. Each of these have a linear association R^2 < 0.79, P < 0.0001.

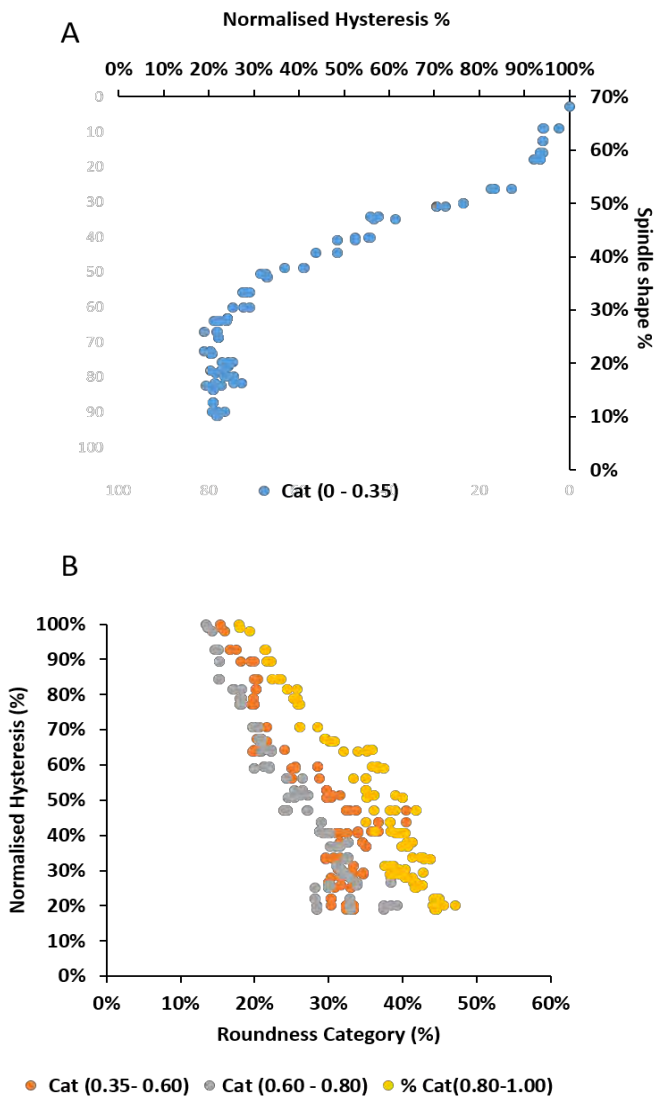

Figure 4.36. Changes in *h vs* tenocyte roundness in the 9% strain group over four hours of cyclic loading. A shows the proportion of cells with a spindle shape (Cat 4) compared with *h*. B shows the increase in proportion of cells in the three remaining categories of roundness (Cat 3, Cat 2 and Cat 1) compared with *h*.

Figure 4.37(A) shows the declining proportion of Cat 4 cells as the ML declines, showing a significantly linear association between the variables (R^2 = 0.94, $P < 0.0001$). The corresponding proportional increase in the three remaining categories of roundness (Cat 3, Cat 2 and Cat 1) is shown in Figure 4.38B. Each of these have a linear association $R^2 > 0.83$, $P < 0.0001$.

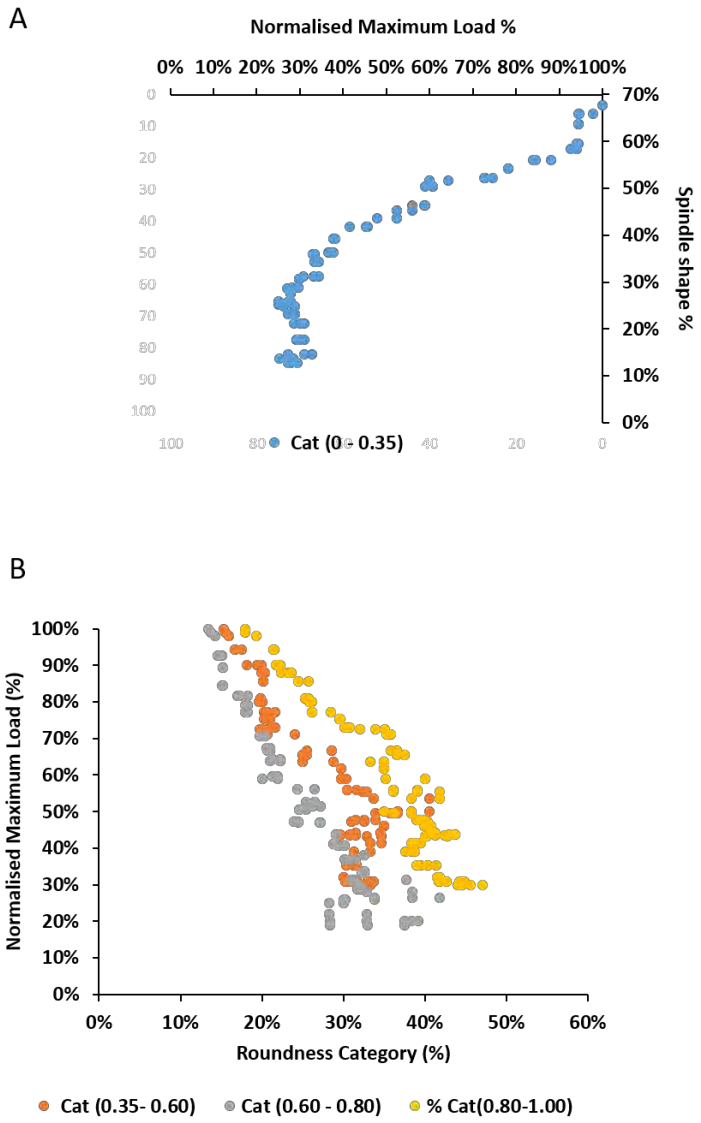

Figure 4.37. Changes in ML *vs* tenocyte roundness in the 9% strain group over four hours of cyclic loading. A shows the proportion of cells with a spindle shape (Cat 4) compared with ML. B shows the increase in proportion of cells in the three remaining categories of roundness (Cat 3, Cat 2 and Cat 1) compared with ML.

The following graphs show the changes in the mechanical profile[15] with the corresponding changes in fibre waviness for the prolonged-strain groups (3%, 6% and 9%) over the four hours of mechanical intervention.

- Waviness (3%)

Figure 4.38 shows the increased proportion of fibres (up to around 50%) in the samples that are wavy as the *k* declines (by around 30%). A rapid decrease in *k* with a slight increase in waviness exists at the beginning, followed by a greater increase in waviness. The two variables are significantly associated, with a polynomial correlation ($R^2 = 0.92$, $P < 0.0001$).

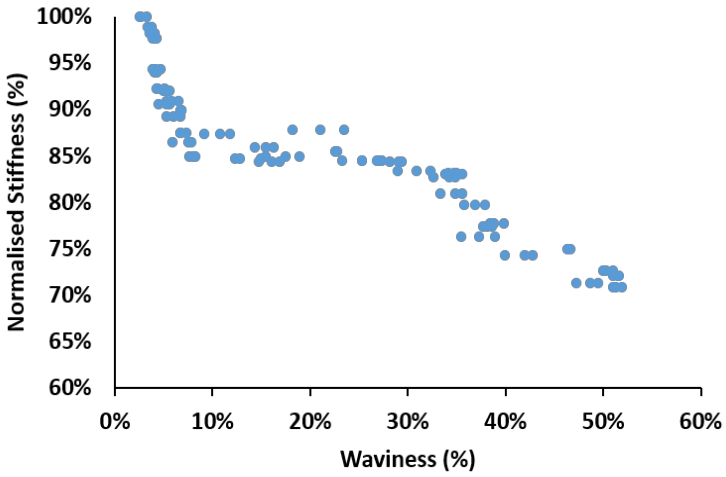

Figure 4.38. Changes in *k* versus waviness in the 3% group over four hours of cyclic loading.

Figure 4.39 shows the increased proportion of fibres (up to 50%) that are wavy as the *h* decreases (by around 40%). A rapid decrease in *h* with a slight increase in waviness

[15] All the data for stiffness assessments were found to be highly correlated. ($R^2 = 0.93$, 0.85 and 0.91, $P < 0.0001$) for the 3%, 6% and 9% strain groups respectively. The replication of the associations for loading stiffness (*k2*) are in Appendix 8.

exists at the beginning followed by a greater increase in waviness. The two variables are significantly associated, with a polynomial correlation ($R^2 = 0.80$, $P < 0.0001$).

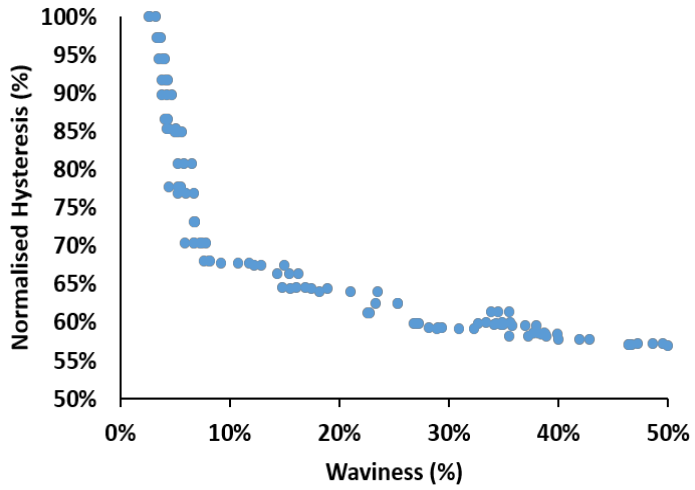

Figure 4.39. Changes in *h* versus waviness in the 3% strain group upon four hours of cyclic loading.

Figure 4.40 shows the increased proportion of fibres (up to around 50%) that are wavy as the ML declines (by around 30%). A rapid decrease in ML with a slight increase in waviness exists at the beginning followed by a greater increase in waviness. The two variables are significantly associated, with a polynomial correlation ($R^2 = 0.84$, $P < 0.0001$).

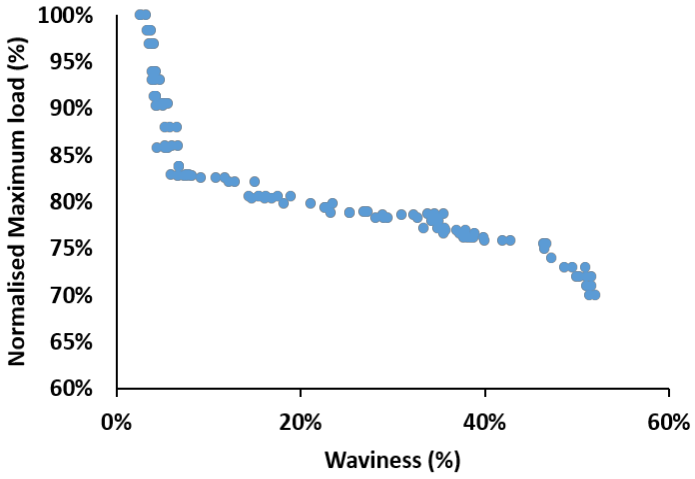

Figure 4.40. Changes in ML versus waviness in the 3% strain group upon four hours of cyclic loading.

- Waviness (6%)

Figure 4.41 shows the increased proportion of fibres (up to 70%) that are wavy as the *k* declines (by around 40%). The two variables are significantly associated, with a linear correlation ($R^2 = 0.97$, $P < 0.0001$).

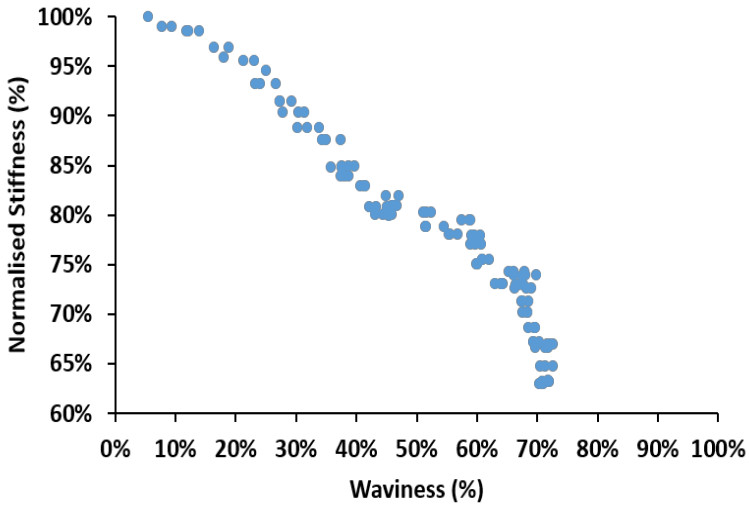

Figure 4.41. Changes in *k* versus waviness in the 6% strain group upon four hours of cyclic loading.

Figure 4.42 shows the increased proportion of fibres (up to around 70%) that are wavy as the *h* decreases (by around 70%). The two variables are significantly associated with a linear correlation ($R^2 = 0.99$, $P < 0.0001$).

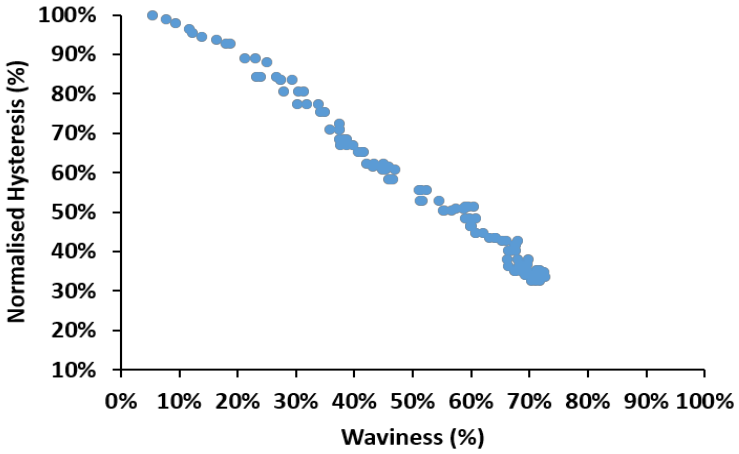

Figure 4.42. Changes in *h* versus waviness in the 6% strain group upon four hours of cyclic loading.

Figure 4.43 shows the increased proportion of fibres (up to around 70%) that are wavy as the ML declines (by around 60%). The two variables are significantly associated, with a linear correlation ($R^2 = 0.97$, $P < 0.0001$).

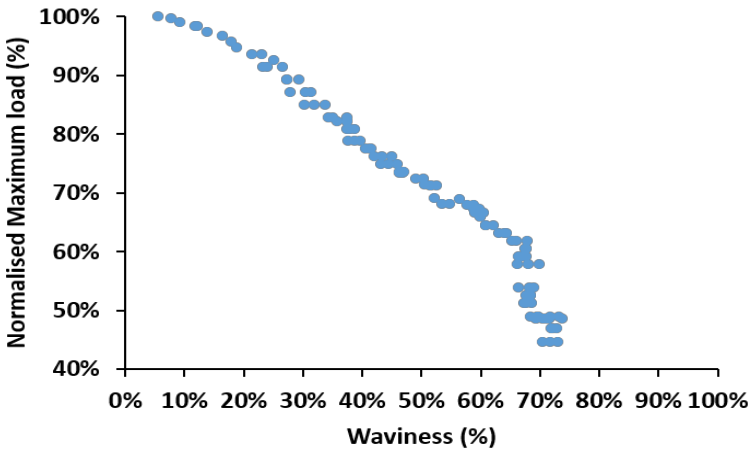

Figure 4.43. Changes in ML versus waviness in the 6% group upon four hours of cyclic loading.

- Waviness (9%)

Figure 4.44 shows the increased proportion of fibres (up to 95%) in the samples that are wavy as *k* declines (around 50%). The two variables are significantly associated, with a linear correlation ($R^2 = 0.97$, $P < 0.0001$).

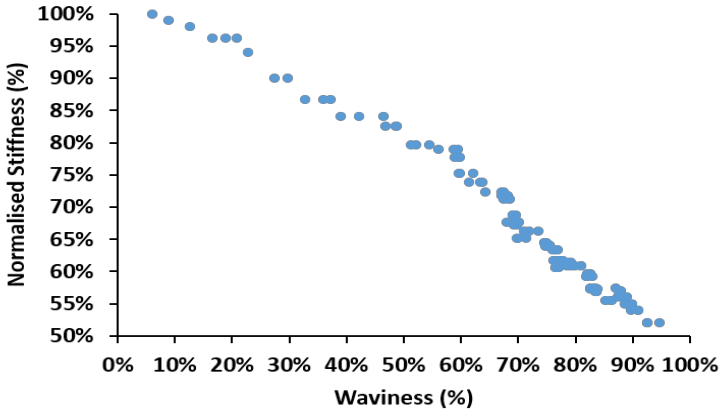

Figure 4.44. Changes in *k* versus waviness in the 9% strain group upon four hours of cyclic loading.

Figure 4.45 shows the increased proportion of fibres (up to 96%) in the samples that are wavy as *h* decreases (by around 82%). The two variables are significantly associated, with a linear correlation ($R^2 = 0.94$, $P < 0.0001$).

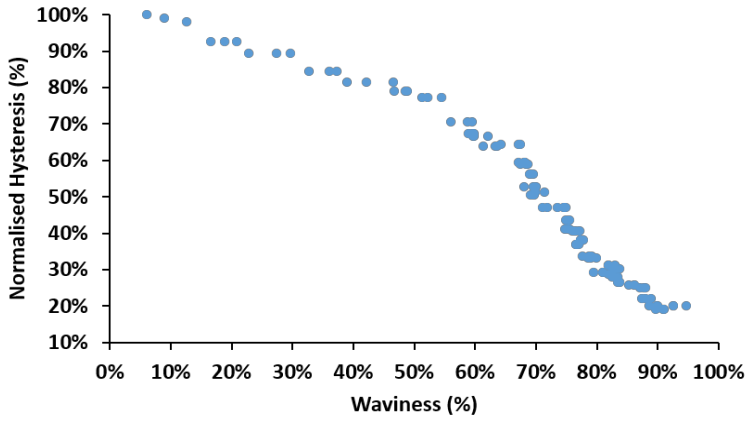

Figure 4.45. Changes in *h* versus waviness in the 9% strain group upon four hours of cyclic loading.

Figure 4.46 shows the increased proportion of fibres (up to 90%) in the samples that are wavy as the ML decreases (by 70%). The two variables are significantly associated, with a linear correlation ($R^2 = 0.93$, $P < 0.0001$).

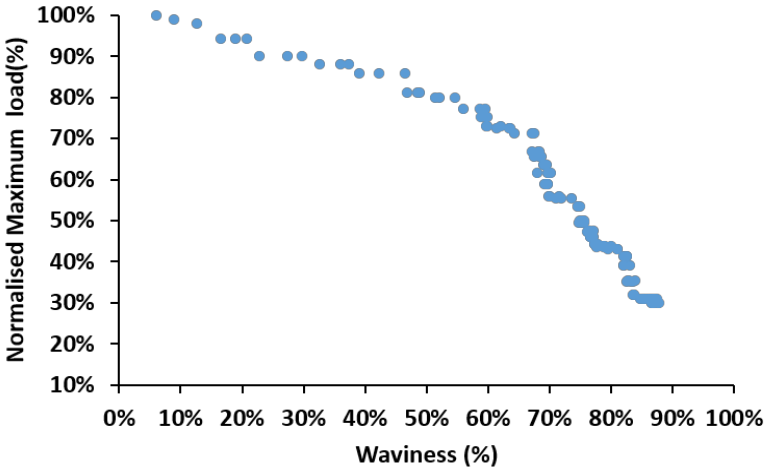

Figure 4.46. Changes in ML versus waviness in the 9% strain group upon four hours of cyclic loading.

Table 4.1. The correlation (R values) between changes in tenocyte roundness classification (spindle to roundness) and changes in mechanical characteristics for the different three strain levels (3%, 6% and 9%) over four hours of cyclic loading.

Variable	*Cat 4 (0.00–0.35)*	*Cat 3 (0.35–0.60)*	*Cat 2 (0.60–0.80)*	*Cat 1 (0.80–1.00)*
	Long spindle	Slightly rounded	Moderately rounded	Severely rounded
k				
3% strain	0.9742	0.8915	0.8820	0.9081
6% strain	0.8778	0.9399	0.9085	0.9101
9% strain	0.9594	0.8411	0.9264	0.9640
h				
3% strain	0.9616	0.9279	0.8727	0.9109
6% strain	0.9111	0.9534	0.9338	0.9337
9% strain	0.9141	0.7932	0.9328	0.9260
ML				
3% strain	0.9789	0.8893	0.8740	0.9477
6% strain	0.8479	0.9567	0.8844	0.9087
9% strain	0.9404	0.8322	0.9380	0.9414

Table 4.2. The correlation (R values) between changes in fibre waviness and changes in mechanical characteristics for the different strain levels (3, 6 and 9%) over four hours of cyclic loading.

Variable	*Waviness (0–1)*
k	
3% strain	0.9213
6% strain	0.9767
9% strain	0.9779
h	
3% strain	0.8083
6% strain	0.9928
9% strain	0.9498
ML	
3% strain	0.8467
6% strain	0.9762
9% strain	0.9364

4.7 Macro-morphological Outcomes in GAG-depleted Tendons (Study 2)

A. A semi-quantitative confocal and histological assessment of the observable structural changes in GAG-depleted tendons (6% strain for two hours)

- DMMB GAG quantification
- Assay Optimisation Part 1 (small tendon pieces)

The Chondroitin sulfate (Ch-SO_4) standards were graphed (concentration of standard *vs* absorbance at 525 nm) to create a standard curve (Figure 4.47B). The linear part of the curve was determined to be in the region between 0 mg/ml and 0.016 mg/ml Ch-SO_4. This region of the standard curve was regraphed (Figure 4.47A) and the linear equation of the line (eq 3.1) was obtained

$$y = 6.2612x + 0.0148 \quad \text{(eq 3.1)}$$

where y = absorbance and x = mg/ml Ch-SO_4. This equation was then rearranged (x = [y – 0.0148]/6.2612) so that the unknown (x) concentration of the test samples could be obtained from knowing y (absorbance at 525 nm) (Table 4.3). The final concentrations obtained from the equation were adjusted for the dilution factor (x 4 if a 20 µl sample was tested; x 8 if a 10 µl sample was tested). The percentage of GAGs remaining in the GAG-depleted samples was calculated relative to the control sample. A 40% reduction in GAG content was seen in the GAG-depleted samples. The control and two test samples were of equal dry weight in this experiment, so the final concentration of GAG did not have to be adjusted to reflect the amount of starting material. This was confirmed by measuring the absorbance of each sample at 260 nm for amino acid content. When using the 20 µl sample aliquots, the depleted samples A and B showed a similar reduction in GAG content, with GAG concentrations of 0.076 mg/ml and 0.088 mg/ml, compared to the control sample at 0.121 mg/ml (i.e. 71% and 73% compared to control). When using the smaller 10 µl aliquots, the variability was higher (72% and 58% compared to control). This may be due to the higher dilution (and thus higher multiplication factor). Overall, Ch-ABC depletion led to an approximately 27 – 42 % reduction in sulfated GAG content, as measured by the DMMB assay (Table 4.4).

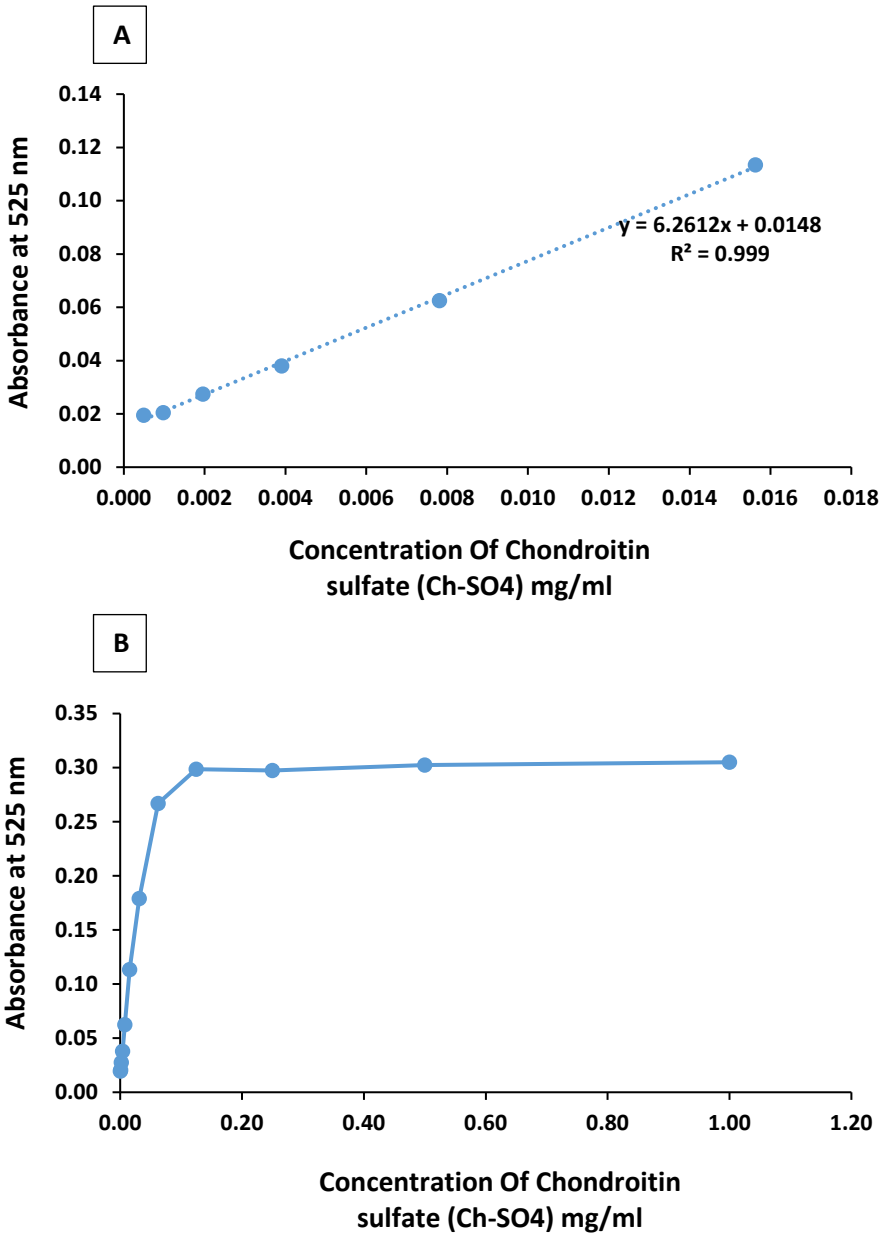

Figure 4.47. Ch-SO_4 standard curves (tendon pieces). A shows the linear range of the curve and the B shows the full standard curve.

Table 4.3. The Ch-SO_4 standard (mg/ml) of the tested samples.

	Absorbance											
	1	0.5	0.25	0.125	0.063	0.031	0.016	0.008	0.004	0.002	0.001	0
Standard 1	0.481	0.475	0.472	0.472	0.44	0.349	0.29	0.232	0.207	0.196	0.187	0.192
Standard 2	0.469	0.47	0.463	0.465	0.434	0.349	0.277	0.233	0.209	0.199	0.194	0.187
Mean	0.475	0.473	0.468	0.469	0.437	0.349	0.284	0.233	0.208	0.198	0.191	0.19
Minus Background	0.305	0.303	0.298	0.299	0.267	0.179	0.114	0.063	0.038	0.028	0.021	0.02

Table 4.4. The final concentration of Ch-SO_4 in the control and GAG-depleted samples (small tendon pieces).

Sample	*Absorbance (525 nm)*	*Corrected for background absorbance (– 0.17)*	*Ch-SO4 concentration (mg/ml)*	*Multiplied by dilution factor (x 4*; x 8**)*	*Percentage GAG remaining*
				20 µl samples, diluted 1:4	
Control	0.349	0.179	0.030	0.121 mg/ml*	
Sample A	0.303	0.133	0.021	0.086 mg/ml*	71 %
Sample B	0.306	0.136	0.022	0.088 mg/ml*	73 %
				10 µl samples, diluted 1:8	
Control	0.278	0.108	0.016	0.134 mg/ml**	
Sample A	0.252	0.082	0.011	0.095 mg/ml**	71 %
Sample B	0.241	0.071	0.009	0.079 mg/ml**	58 %

- Assay Optimisation Part 2 (whole tendon)

The Ch-SO_4 standard curves were obtained using similar procedures to those in Part 1 (Figure 4.48, Table 4.5). Samples were tested neat and diluted 1:2. Both the neat and 1:2 diluted samples fell in the linear range of the assay and gave the same results – thus only the values for the neat samples are shown. The whole tendon treated with Ch-ABC was found to have approximately 57% of the GAG content of the control tendon (i.e. a 43% reduction in GAG content); consistent with the data obtained for the small tendon pieces.

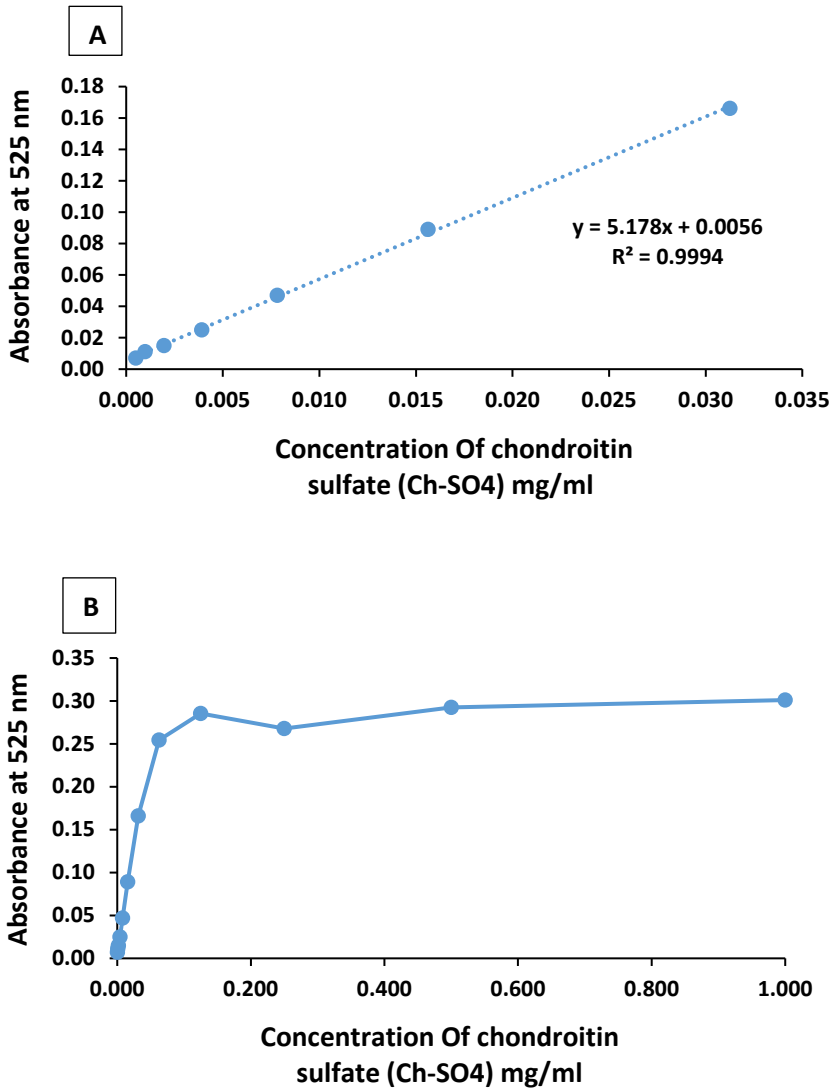

Figure 4.48. The chondroitin sulfate (Ch-SO_4) standard curves (whole tendon). A shows the linear range of the curve and B the full standard curve.

Table 4.5. The Ch-SO_4 standard (mg/ml) of the tested samples (whole tendon).

	Absorbance											
	1	0.5	0.25	0.125	0.063	0.031	0.016	0.008	0.004	0.002	0.001	0
Standard 1	0.481	0.458	0.414	0.462	0.431	0.34	0.266	0.223	0.201	0.19	0.186	0.18
Standard 2	0.475	0.481	0.476	0.463	0.432	0.346	0.266	0.225	0.203	0.194	0.19	0.174
Mean	0.478	0.469	0.445	0.465	0.431	0.343	0.266	0.224	0.202	0.192	0.188	0.177
Minus Background	0.301	0.292	0.268	0.285	0.254	0.166	0.089	0.047	0.025	0.015	1	0

Table 4.6. The final concentration of Ch-SO_4 in the control and GAG depleted samples (whole tendon).

Sample	*Absorbance (525 nm)*	*Corrected for background absorbance (– 0.17)*	*Ch-SO_4 concentration (mg/ml)*	*Multiplied by dilution factor (x 4*; x 8**)*	*Percentage GAG remaining and depleted*
				20 µl samples, diluted 1:4	
Control	0.304	0.127	0.024	2.988 mg/ml	
				10 µl samples, diluted 1:8	
GAG-depleted	0.231	0.054	0.0010	2.028 mg/ml	57.8%

- **GAG depletion in tendons undergoing mechanical testing**

Whole tendons for mechanical testing were prepared for GAG depletion as described in Section 4.7A. The whole tendon treated with Ch-ABC was found to have 57.7 – 73.3 % of the GAG content of the control tendons (i.e. a 26.7 – 42.3% reduction in GAG).

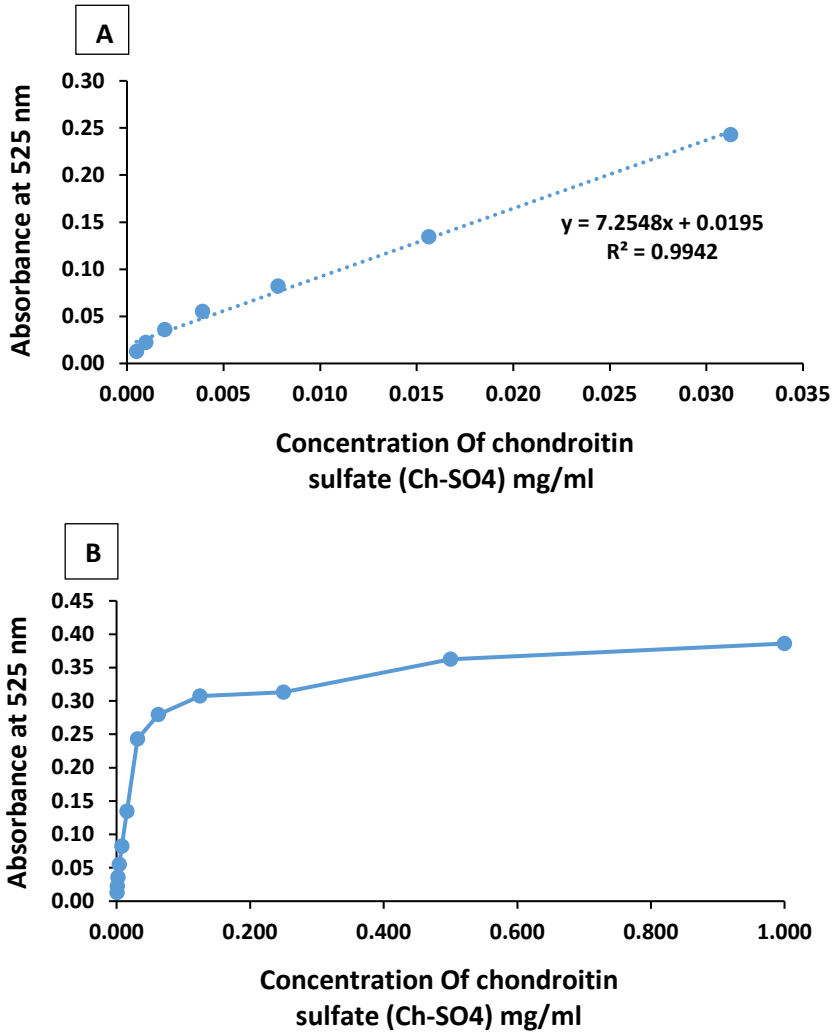

Figure 4.49. The chondroitin sulphate (Ch-SO4) standard curves obtained from experiment involved assessing the ability of Ch-ABC to deplete GAGs from a whole tendon that underwent mechanical testing. Figure (A) represents the linear range of the curve and the figure (B) represents the full standard curve. Where x axis = concentration of standard and y = absorbance at 525 nm.

Table 4.7. The Ch-SO_4 standard (mg/ml) of the tested GAG-depleted samples.

	Absorbance											
	1.000	0.500	0.250	0.125	0.063	0.031	0.016	0.008	0.004	0.002	0.001	0.000
Std Curve 1	0.58	0.56	0.50	0.53	0.47	0.43	0.32	0.27	0.26	0.23	0.21	0.20
Std Curve 2	0.55	0.52	0.48	0.44	0.44	0.41	0.31	0.25	0.20	0.19	0.19	0.18
Mean	0.56	0.54	0.49	0.48	0.46	0.42	0.31	0.26	0.23	0.21	0.20	0.19
Minus Background	0.39	0.36	0.31	0.31	0.28	0.24	0.13	0.08	0.06	0.04	0.02	0.01

Table 4.8. The final concentration of ChSO4 in the tested GAG depleted samples.

Sample	*Absorbance (525)*	*Corrected for background absorbance (– 0.17)*	*ChSO4 mg/ml (mean of diluted 20 and 10 µl Samples)*	*Adjusted GAG content relative to AA concentration*	*Percentage remaining*
1	0.586	0.409	0.137	0.0577	57.7 %
2	0.362	0.185	0.081	0.0404	70.0 %
3	0.353	0.176	0.069	0.0338	58.6 %
4	0.359	0.182	0.066	0.0363	62.9 %
5	0.328	0.151	0.052	0.0358	62.0 %
6	0.305	0.128	0.044	0.0343	59.5 %
7	0.438	0.261	0.112	0.0423	73.3 %
8	0.407	0.230	0.100	0.0392	68.0 %
9	0.396	0.219	0.075	0.0357	61.9 %
10	0.429	0.252	0.078	0.0411	71.3 %

GAG-depleted and undepleted tendons were given a dynamic and static repetitive cyclic loading of moderate-level strain (6%) over two hours. The semi-quantitative confocal assessment allowed for three-dimensional (3D) imaging of the tendon's microstructure. The tendon deformation that was induced by the repetitive loading was considered, in the same manner as shown in Section 4.3, to assess the cumulative progression of damage in GAG-depleted tendons.

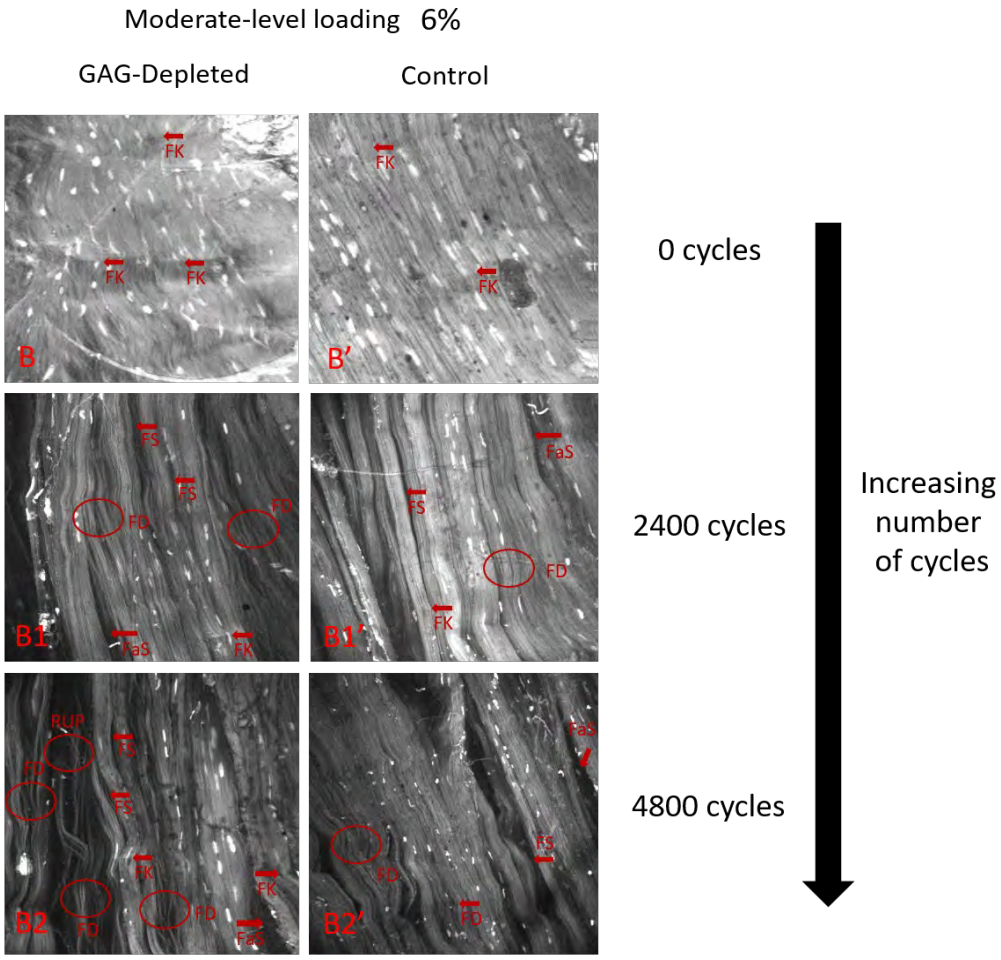

Figure 4.50. CA images demonstrating the progression of morphological changes of the unloaded and fatigued tendons that underwent 6% strain over two hours. Original magnification 475 μm.

The assessment demonstrated strain- and time-dependent morphological changes of the tendon microstructure. The morphology clearly shows distinct microdamage in the GAG-depleted tendons (Figure 4.50) which was also observed in the undepleted group (Section 4.5). However, the morphology was characterised by a progressively

increasing intensity and severity of microstructural damage in the GAG-depleted tendons as compared to the undepleted tendons.

Within the first hour of repeated loading (2,400 cycles), the GAG-depleted tendons demonstrated an increased disruption of fibre arrangement and orientation. The fibre orientation changed from parallel to a moderately loose and wavy orientation, and the fibres crossed each other and exhibited fibre kinks (FK in Figure 4.50:B1), a moderate separation and fragmentation of collagen fascicles and fibres (FaS and FD in Figure 4.50: B1,) and tenocyte morphological changes from long spindle cells (1B) to moderately rounded (2B) (Figure 4.50: B1). Whereas the control group exhibited a lower disruption of fibre arrangement and orientation, changing from parallel to slightly loose and wavy fibres exhibiting fibre kinks (FK in Figure 4.50 B1'), a slight separation and fragmentation of collagen fascicles and fibres (FaS and FD in Figure 4.50: B1') and slight tenocyte morphological changes from long spindle cells (1B) to oval-shaped cells (2B) (Figure 4.50: B1'). All of the above changes are consistent with Grade 4 in fibre structure, arrangement, orientation and cell roundness.

During the second hour of repetitive loading, the GAG-depleted group had increased in severity compared to the undepleted tendons (FD in Figure 4.50: B2'). During the second hour, severe fibre disruption, loss of alignment, significantly increased roundness of tenocytes, fibre thinning and significantly increased fragmentation (FS) and dissociation (FD) and fibre rupture patterns (RUP) between fibres became more evident in the GAG-depleted tendons (FS, FD and RUP in Figure 4.50: B2). For fibre structure, arrangement and orientation and cell roundness, the tendons graded 3 and 4 for the control and GAG-depleted groups respectively. During the second hour of loading, the distribution of damage areas continued to increase, and the damaged areas were microstructurally composed of ruptured fibres that subsequently seemed to form kinked patterns at the rupture sites (Figure 4.50: B2).

Similar results were found in the thick bulk histological sections stained with AB/PAS and H&E (Figure 4.51: B1, 1', B2, B2'). The Scanscope conventional histological images in Figure 4.51 rule out any ruptured areas of blurry thinned fibre discontinuities seen in the images taken by confocal arthroscopy. For both the control and GAG-depleted tendons, all assessments made for the CA and Scanscope histological images

throughout the mechanical intervention were consistent at the end-points of the two hours of cyclic loading. As shown in Figures 4.50 and 4.51, both the CA and Scanscope H&E histological assessments of fibre structure, arrangement and orientation and cell roundness, show that the GAG-depleted and control groups had a morphological grading of up to 3 for the first and 4 for the second hour of repetitive loading, indicating a moderate to severe damage effect.

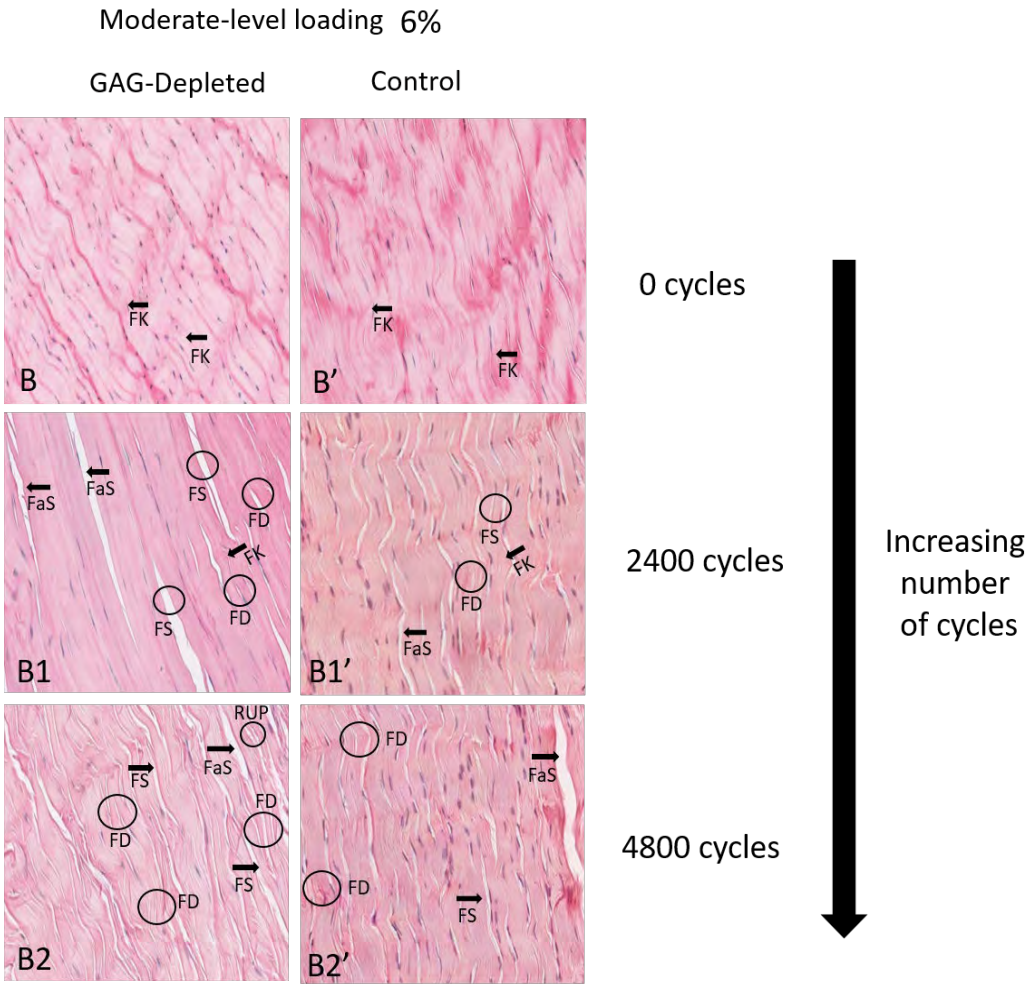

Figure 4.51. Scanscope H&E histological images of unloaded and loaded tendon groups demonstrating the progression of morphological changes of tendons underwent 6% strain over two hours. Original magnification 475 μm.

B. Quantitative confocal and histological assessment of the observable structural changes in GAG-depleted tendons

- Tenocyte shape, waviness and anisotropy

The controls and GAG-depleted samples both demonstrated a progressive change in tenocyte roundness and fibre waviness with fatigue loading characterised by a marked

decreasing categorical shift. However, the anisotropy of fibres did not demonstrate any marked changes.

Figure 4.52 illustrates the relative change in tenocyte morphology over two hours in the control and GAG-depleted groups. In both groups, the spindle shape declined over time with greater changes in the depleted tendon groups at the first and second hours. By the end of the first hour, on average 60% and 70 % of spindle tenocytes (Cat 4) had changed to slightly rounded (Cat 3) in the control and depleted groups respectively. Whereas, by the end of the second hour, on average 75% and 85% of spindle tenocytes (Cat 4) had changed to slightly rounded (Cat 3) in the control and depleted groups respectively.

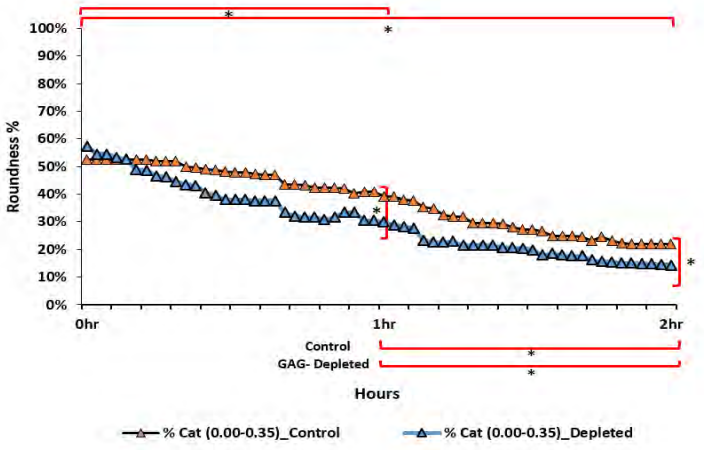

Figure 4.52. The effect of fatigue loading (6% strain) on tenocyte roundness in control and GAG-depleted groups over two hours. (Asterisks indicate a p-value < 0.05, NS denotes nonsignificant.)

There is a significant decline in the proportion of spindle-shaped tenocytes in both tendon groups ($p < 0.05$). The normalised changes from the beginning of the experiment to each hour and from the first to the second hour were significantly different in both groups ($p < 0.05$). There were significantly greater reductions in spindle-shaped tenocytes in the GAG-depleted tendons ($p < 0.05$) over the first and second hour.

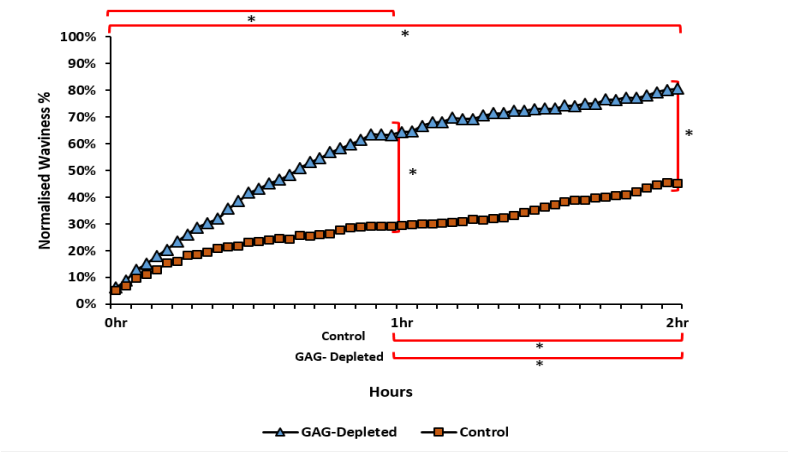

Figure 4.53. The effect of fatigue loading (6% strain) on fibre waviness in control and GAG-depleted groups over two hours. (Asterisks indicate a p-value < 0.05, NS denotes nonsignificant.)

Figure 4.53 illustrates the relative change in fibre waviness over the two hours (4,800 cycles) in the control and GAG-depleted groups. In both groups the fibre waviness increased over time with greater changes in the GAG-depleted tendon groups at the first and second hour. By the end of the first hour, on average there was a 25% and 60% increase in fibre waviness in the control and GAG-depleted groups, respectively. Whereas, by the end of the second hour, there was on average a 40% and 75% increase in fibre waviness in the control and GAG-depleted groups respectively.

There was a significant increase in the proportion of fibre waviness in both tendon groups ($p < 0.05$).The normalised changes from the beginning of the experiment to each hour and from the first to the second hour were significantly different in both groups ($p < 0.05$). There was a significantly greater increase in wavy fibres in the GAG-depleted tendons ($p < 0.05$) over the first and second hour.

Figure 4.54 illustrates the relative change in fibre anisotropy over two hours (4,800 cycles) in the control and GAG-depleted groups. There are no significant differences in the proportion of fibre anisotropy in both tendon groups ($p < 0.05$) at all-time points. The normalised changes from the beginning of the experiment to each hour and from the first to the second hour were not significantly different in both groups. There were no significant differences in fibre anisotropy between both tendon groups over the first

and second hour. This demonstrates that all anisotropic changes in both groups occurred during preconditioning.

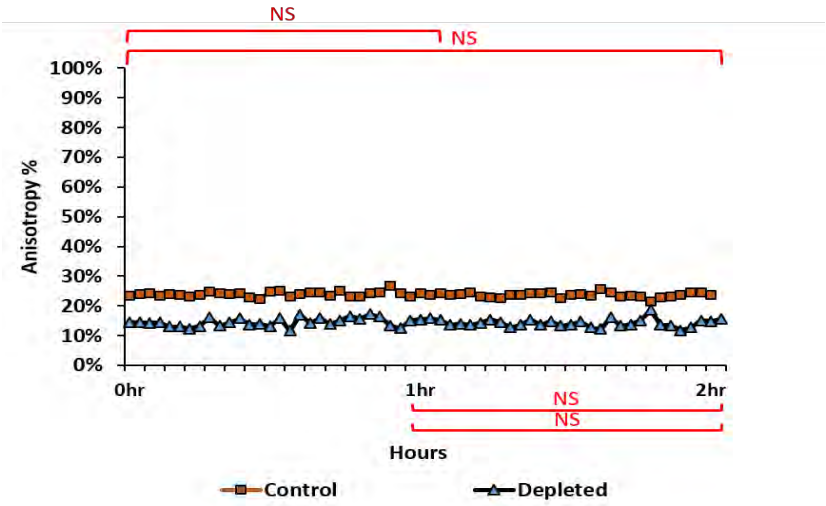

Figure 4.54. The effect of fatigue loading (6% strain) on fibre anisotropy in control and GAG-depleted groups over two hours. (NS denotes nonsignificant.)

4.8 The Association Between Mechanical and Macro-morphological Changes Over Time (Study 2)

A. Tenocyte Roundness for Controls

The following graphs show the changes in mechanical profiles[16] with the corresponding changes in cell morphology. All the tendons start with an average 100% of cells identified as spindle-like and over a time of repeated strain the proportion of spindles declines with an increase in the proportion of roundness in the remaining cells.

[16] All the data for stiffness assessments were found to be highly correlated (R = 0.94 for controls and 0.97 for GAG-depleted tendons, P < 0.0001). The replication of associations for of the loading stiffness (*k2*) is placed in the Appendix 9.

Figure 4.55A shows the decline in the proportion of spindle-shaped tenocytes (Cat 4) (on average 30%) as *k* declines (on average 30%), demonstrating a significant polynomial association (R^2 = 0.92, P < 0.0001). The corresponding proportional increase in the three remaining categories of roundness (Cat 3, Cat 2 and Cat 1) is shown in Figure 4.55B. Each of these have an increase with a polynomial association (R^2 > 0.13, all P < 0.0001).

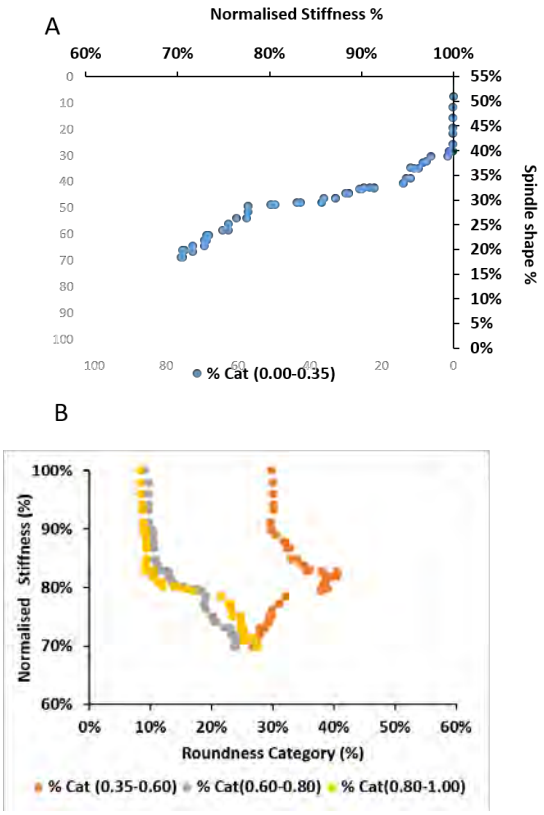

Figure 4.55. Changes (*k* vs tenocyte roundness) in the control group (6% cyclic loading over two hours). A shows the proportion of cells with a spindle shape (Cat 4) compared with *k* decline. B shows the increase in proportion of cells in the three remaining categories of roundness (Cat 3, Cat 2 and Cat 1) compared with *k* decline.

Figure 4.56A shows the declining proportion of tenocytes that are spindle shaped (Cat 4) (on average 30%) as *h* declines (on average 60%), demonstrating a significant polynomial association (R^2 = 0.74, P < 0.0001). The corresponding proportional increase in the three remaining categories of roundness (Cat 3, Cat 2 and Cat 1) is

shown in Figure 4.56B. Each of these have an increase with a polynomial association ($R^2 > 0.21$, all $P < 0.0001$).

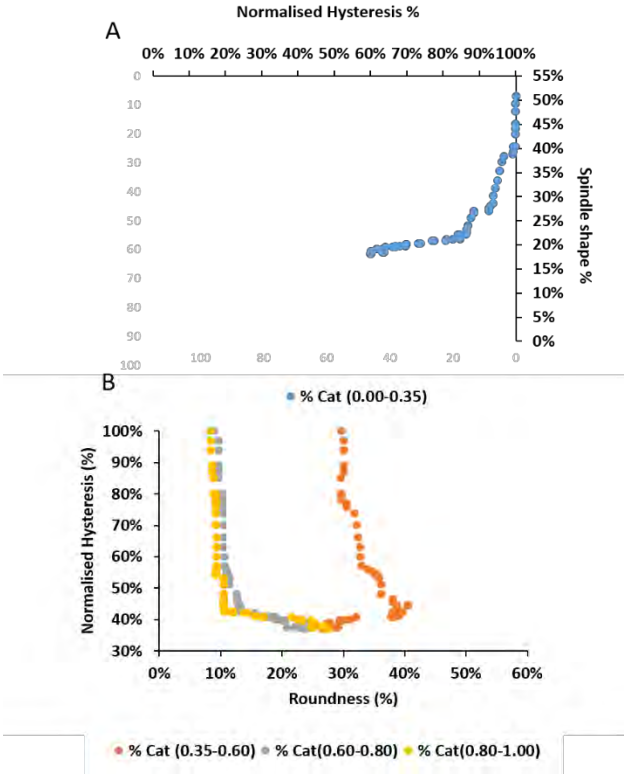

Figure 4.56. Changes (*h* vs tenocyte roundness) in the control group (6% cyclic loading over two hours). A shows the proportion of cells with a spindle shape (Cat 4) compared with *h* decline. B shows the increase in proportion of cells in the three remaining categories of roundness (Cat 3, Cat 2 and Cat 1) compared with *h* decline.

Figure 4.57A shows the declining proportion of cells in the samples (on average 30%) that are spindle-like (Cat 4) as the ML declines (on average 30%), demonstrating a significant polynomial association ($R^2 = 0.76$, $P < 0.0001$). The corresponding proportional increase in the three remaining categories of roundness (Cat 3, Cat 2 and Cat 1) is shown in Figure 4.57B. Each of these have an increase with polynomial associations ($R^2 > 0.16$, all $P < 0.0001$).

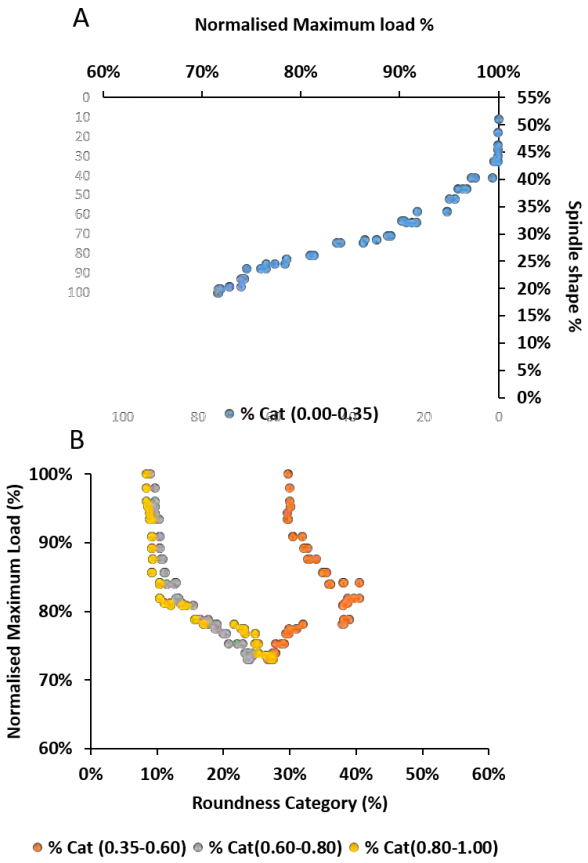

Figure 4.57. Changes (ML vs tenocyte roundness) in the control group (6% cyclic loading over two hours). A shows the proportion of cells with a spindle shape (Cat 4) compared with ML decline. B shows the increase in proportion of cells in the three remaining categories of roundness (Cat 3, Cat 2 and Cat 1) compared with ML decline.

B. Tenocyte Roundness for GAG-depleted Samples

The following graphs show the declines in the mechanical profiles with the corresponding changes in cell morphology for the GAG-depleted samples.

Figure 4.58A shows the decline in the proportion of spindle-shaped tenocytes (Cat 4) (around 45%) for the GAG-depleted samples as *k* declines (on average 55%), demonstrating a significantly polynomial association ($R^2 = 0.98$, $P < 0.0001$). The corresponding proportional increase in the three remaining categories of roundness (Cat 3, Cat 2 and Cat 1) is shown in Figure 4.58B. Each of these have an increase with a polynomial association ($R^2 > 0.42$, $P < 0.0001$).

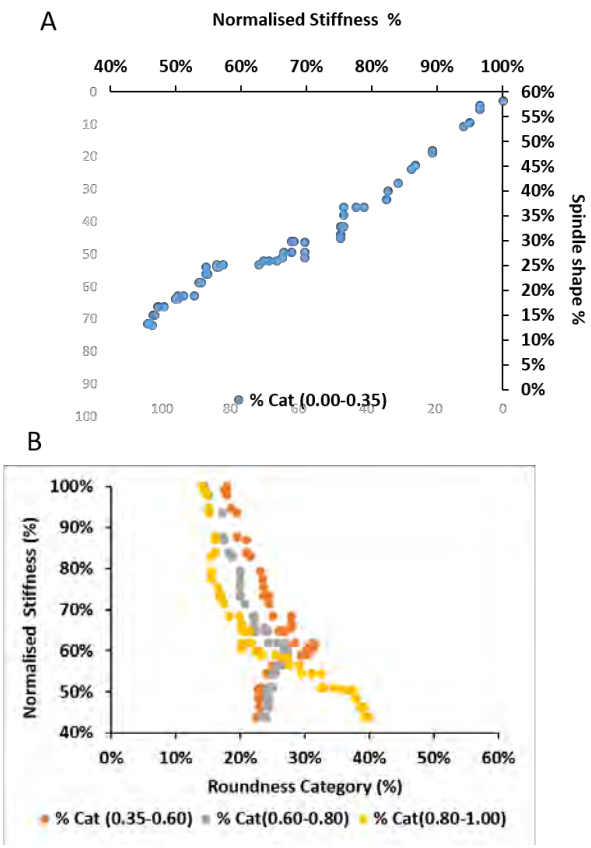

Figure 4.58. Changes (*k* vs tenocyte roundness) in the GAG-depleted group (6% cyclic loading over two hours). A shows the proportion of cells with a spindle shape (Cat 4) compared with *k* decline. B shows the increase in proportion of cells in the three remaining categories of roundness (Cat 3, Cat 2 and Cat 1) compared with *k* decline.

Figure 4.59A shows the decline in the proportion of spindle-shaped tenocytes (Cat 4) (around 45%) for the GAG-depleted samples as *h* declines (on average 70%), demonstrating a significantly polynomial association ($R^2 = 0.89$, $P < 0.0001$). The corresponding proportional increase in the three remaining categories of roundness (Cat 3, Cat 2 and Cat 1) is shown in Figure 4.59B. Each of these have an increase with a polynomial association ($R^2 > 0.65$, $P < 0.0001$).

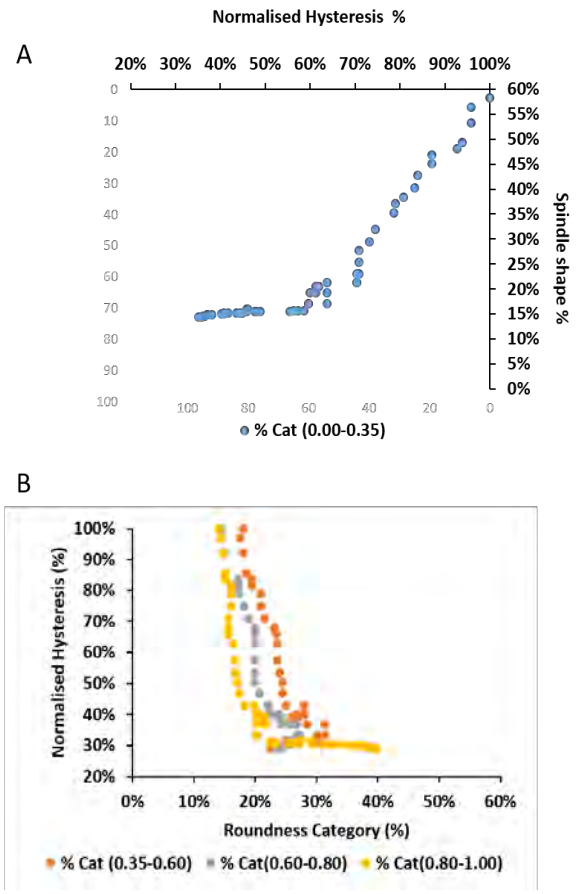

Figure 4.59. Changes (*h* vs tenocyte roundness) in the GAG-depleted group (6% cyclic loading over two hours). A shows the proportion of cells with a spindle shape (Cat 4) compared with *h* decline. B shows the increase in proportion of cells in the three remaining categories of roundness (Cat 3, Cat 2 and Cat 1) compared with *h* decline.

Figure 4.60A shows the decline in the proportion of spindle-shaped tenocytes (Cat 4) (on average 45%) for the GAG-depleted samples as the ML declines (on average 45%), demonstrating a polynomial association (R^2 = 0.98, P < 0.0001). The corresponding proportional increase in the three remaining categories of roundness (Cat 3, Cat 2 and Cat 1) is shown in Figure 4.60B. Each of these have an increase with a polynomial association (R^2 > 0.42, P < 0.0001).

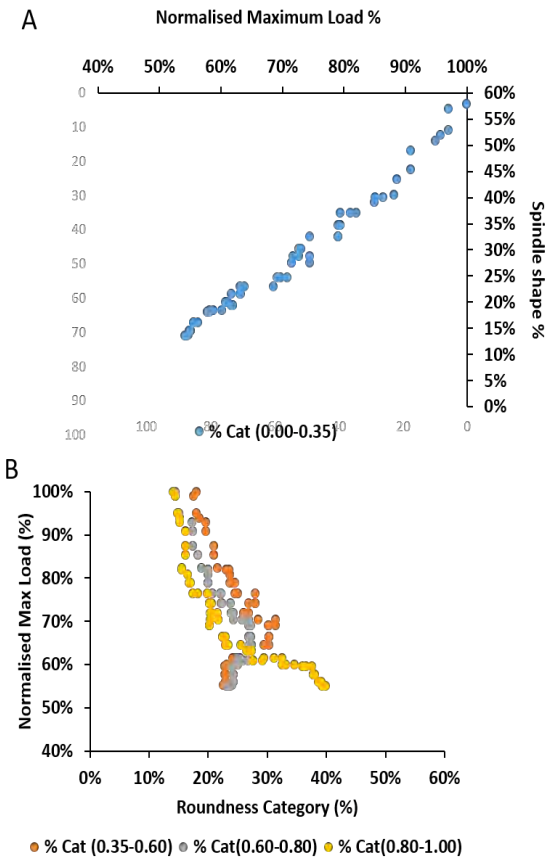

Figure 4.60. Changes (ML vs tenocyte roundness) in the GAG-depleted group (6% cyclic loading over two hours). A shows the proportion of cells with a spindle shape (Cat 4) compared with ML decline. B shows the increase in proportion of cells in the three remaining categories of roundness (Cat 3, Cat 2 and Cat 1) compared with ML decline.

The following graphs show the changes in the mechanical profile[17] with the corresponding changes in fibre waviness for the both control and GAG-depleted groups over the two hours of mechanical intervention.

- Waviness in Controls and GAG-depleted cells

Figure 4.61 shows the increase in the proportion of fibres that are wavy (up to 45% and 80% for the control and GAG-depleted groups, respectively). This corresponds with the decline in *k* (of 30% and 50% for the control and GAG-depleted groups, respectively). The two variables are significantly associated with a linear correlation (R^2 = 0.98, 0.97 and 0.97 for GAG-depleted, control (Study 2) and control (Study 1) respectively, P < 0.0001).

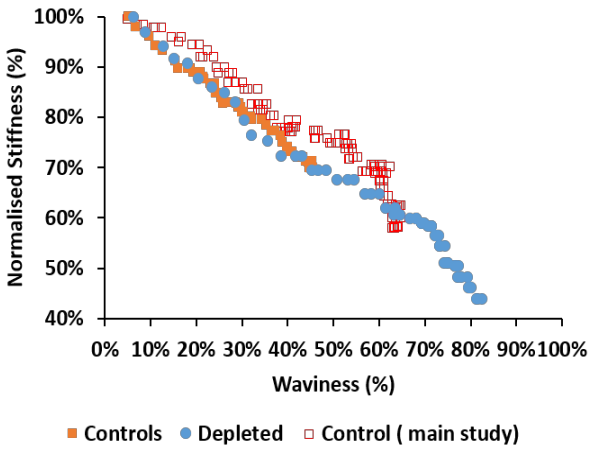

Figure 4.61. Changes in k vs waviness in controls[18] and GAG-depleted groups (6% cyclic loading over two hours).

[17] All the data for stiffness assessments were found to be highly correlated (0.80 for controls and 0.99 for GAG-depleted samples, P < 0.0001). The replication of the associations for loading stiffness (*k*2) is in Appendix 9.

[18] One control group uses data from the GAG-depletion study, and another the data from the main study.

Figure 4.62 shows the increased proportion of fibres that are wavy (up to 45% and 80% for control and GAG-depleted groups, respectively). This corresponds with a decrease in *h* (on average 50% and 70% for control and GAG-depleted groups, respectively). The two variables are significantly associated, with a linear correlation (R^2 = 0.94, 0.87 and 0.99 for GAG-depleted, control (Study 2) and control (Study 1) respectively, P < 0.0001).

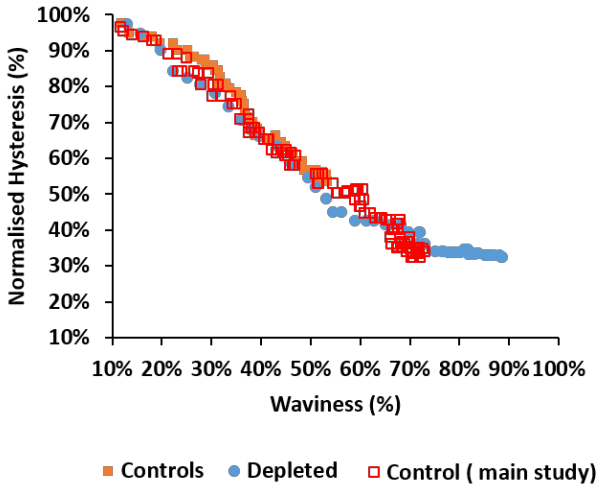

Figure 4.62. Changes in *h* vs waviness in control and GAG-depleted groups (6% cyclic loading over two hours).

Figure 4.63 shows the increase in the proportion of fibres that are wavy (up to 45% and for control and 80% for the GAG-depleted tendons). This corresponds with a decrease in ML (on average 30% for the control and 45% for the GAG-depleted samples). The two variables are significantly associated, with a linear correlation (R^2 = 0.98, 0.97 and 0.97 for GAG-depleted, control (Study 2) and control (Study 1) groups respectively, P < 0.0001).

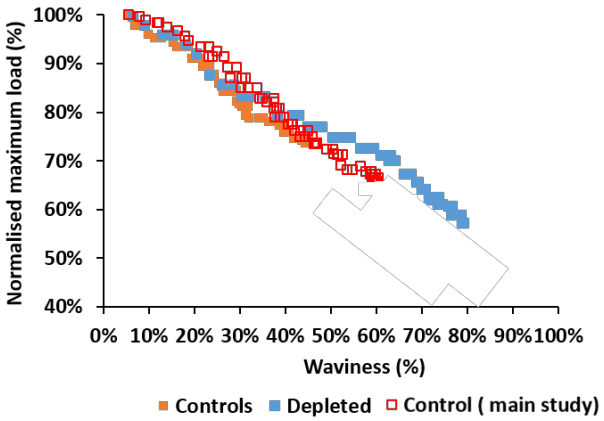

Figure 4.63. Changes in ML vs waviness in control and GAG-depleted groups (6% of cyclic loading over two hours).

Table 4.9. The correlation (R) between the changes of the tenocyte roundness classification (spindle to roundness) and mechanical characteristics over two hours of cyclic loading for the two control groups (from the main and GAG-depletion studies) and the GAG-depleted group.

Variable	*Cat 4 (0.00–0.35)*	*Cat 3 (0.35–0.60)*	*Cat 2 (0.60–0.80)*	*Cat 1(0.80–1.00)*
	Long spindle	Slightly rounded	Moderately rounded	Severely rounded
k				
GAG-depleted sample	0.9754	–0.4194	–0.8205	–0.8759
Control (Study 2)	0.9189	–0.1258	–0.8848	–0.7927
Control (Study 1)	0.8778	–0.9399	–0.9085	–0.9001
h				
GAG-depleted sample	0.8944	–0.6524	–0.9168	–0.6837
Control (Study 2)	0.7429	–0.2130	–0.6481	–0.5198
Control (Study 1)	0.9112	–0.9534	–0.9338	–0.9338
ML				
GAG-depleted sample	0.9867	–0.4213	–0.8407	–0.8780
Control (Study 2)	0.7552	–0.1553	–0.6727	–0.5591
Control (Study 1)	0.8480	–0.9567	–0.8844	–0.9087

Table 4.10. The correlation (R) between changes in waviness and the mechanical characteristics over two hours of cyclic loading for control and GAG-depleted groups.

Variable	*Waviness (0–1)*
k	R^2
GAG-depleted sample	0.9806
Control (Study 2)	0.9769
Control (Study 1)	0.9767
h	
GAG-depleted sample	0.9495
Control (Study 2)	0.8762
Control (Study 1)	0.9928
ML	
GAG-depleted sample	0.9890
Control (Study 2)	0.9828
Control (Study 1)	0.9762

4.9 Nano-morphological Outcomes in Strained Groups (3%, 6% and 9% strain) (Study 1)

A. Qualitative assessment – AFM assessments of tendons undergoing loading at three tensile strains (3%, 6% and 9%) over four hours

The qualitative AFM assessment of tendons that had been subject to dynamic and static repetitive cyclic loadings of low-, moderate- and high-level strain (3%, 6% and 9%) over one, two, three and four hours allowed for a three-dimensional (3D) imaging of tendon microstructure. Our study indicated that tendon deformation that is induced by cyclic loading can be studied to assess the cumulative progression of damage in tendons. Progressive increased intensity and severity of microstructural damage was observed as loading dose (both cycle and strain) were increased.

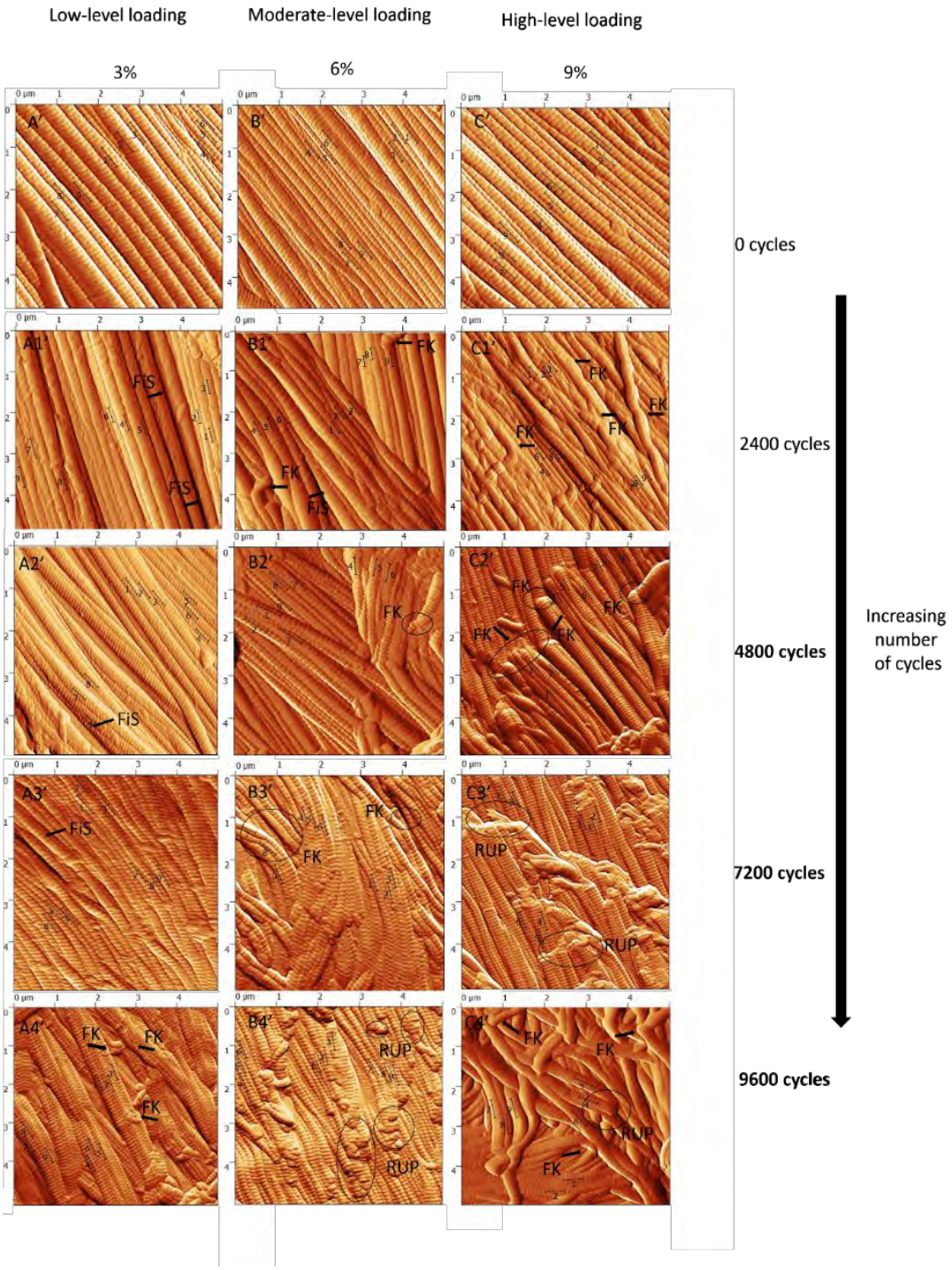

Figure 4.64. AFM images demonstrating the progression of morphological changes of tendons underwent strains (3%, 6% and 9%) over one, two, three and four hours of cyclic loading. Original magnification 5 μm.

The morphology clearly shows distinct different types of microdamage which are not observed in the nonloaded (preconditioned) tendons. Also, the assessment demonstrates a strain- and time-dependent effect on the morphological changes of the tendon's microstructure. At the end of the first hour, tendons subjected to the low-level loading (3%) demonstrated a slightly increased disruption of fibril arrangement and orientation and a slight separation of collagen fibrils (FiS in Figure 4.64: A1'). At the end of the second and third hours of repetitive loading, the tendons exhibited a continued progression of damage, with an increased separation and fragmentation of fibrils. However, a significant widening of the interfibril space and an increased disruption of fibre arrangement and orientation, exhibiting fibril kinks (FK in Figure 4.64:A3', A4') became more prominent and evident at the end of the fourth hour (FK in Figure 4.64: A4').

Tendons from the moderate-level (6%) repeated loading group exhibited similar damage changes to those seen in the low-level group (3%) but in a wider distribution, with an increased magnitude of damage that became evident at lower number of repeated cyclic loading (Figure 4.64: B1', B2', B3' and B4'). For example, an increased fibril kink (FK) and interfibril space (FiS) between fibrils was more prominent at the end of the second hour in the 6% group (Figure 4.64: B1'). Increased fibril kinks (FK) and fibril separation (FiS) with an increased disruption of fibril orientation that changed the direction of the fibrils from parallel to bended or twisted were observed after the first hour (Figure 4.64: B2', B3' and B4'). Marked areas of fibril ruptures (RUP) were prominent at the end of the fourth hour (Figure 4.64: B4).

Similar changes were observed in the 9% group but in a larger distribution with an increased severity of damage (Figure 4.64: C1', C2', C3' and C4'). Fibril kinks (FK) and fibril separation (FiS) with an increased disruption of fibril orientation that changed the direction of the fibrils from parallel to bended or twisted were observed as early as the end of the first hour (Figure 4.64: C1'). In addition, increased fibre disruption, loss of alignment, increased fibril kinks (FK) and fibril separation (FiS) were prominent at the end of the second hour. Out-of-plane discontinuity was only found in tendons from the 9% group, which were subjected to more than 4,800 repeated loading cycles (Figure 4.64: C4'). The high-level repeated loading (9%) group had increased and severe fibril rupture patterns (RUP) between fibrils that became more evident at the end of the third and fourth hours (RUP in Figure 4.64: C3', C4'). The distribution of damage continued to increase at the end of the third and fourth hour, microstructurally composed of ruptured fibrils that subsequently seemed to form a curl or kink pattern at the

rupture sites (Figure 4.64: C3' and C4'). Severe fibril disruption, loss of alignment, increased fibril kinks (FK) and fibril separation (FiS) were more prominent at the end of the fourth hour of cyclic loading.

B. Quantitative assessment – AFM assessment of tendons undergoing loading at three tensile strains (3%, 6% and 9%) over four hours

The 3%, 6% and 9% strain groups demonstrated a progression change in fibril D-periodicities characterised by a marked increase observed in WFB and BFB D-periodicities in tendons during the mechanical intervention.

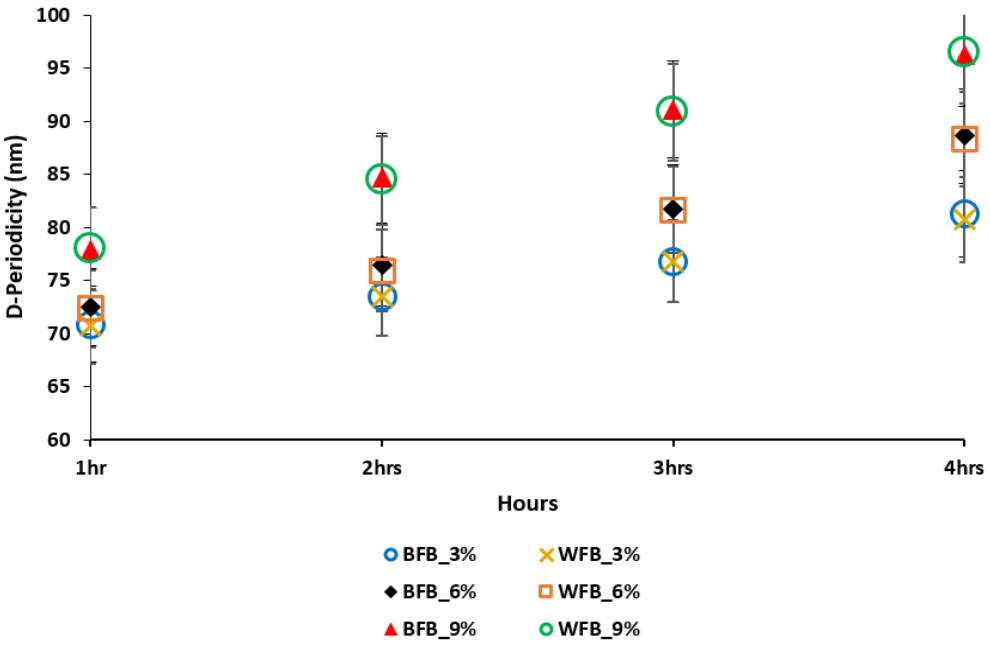

Figure 4.65. The effect of fatigue loading on tendon nano-structural properties (WFB and BFB D-periodicities).

The mean WFB D-periodicity of the native group was D0% = 67.43 ± 2.0 nm. At 3% strain the percentage change elongation of the WFB D-periodicity (from a starting periodicity of D3% = 75.50 ± 3.79 nm, P = 0.93), was 1.72%, 2.98%, 4.57% and 6.66% by the end of the first, second, third and fourth hour, respectively, corresponding to the toe region of the stress-strain curve (Table 4.10). The percent change elongation of the BFB D-periodicity (from a starting periodicity of D3%= 75.11 ± 3.76 nm, P = 0.93), was 1.49%, 2.80%, 4.51% and 6.36% by the end of the first, second, third and fourth hour, respectively, again corresponding to the toe region of the stress-strain curve.

At the 6% strain level, the percentage change of elongation of WFB D-periodicity (from a starting periodicity of D6% = 79.70 ± 6.1 nm, P = 0.98), was 1.20%, 2.14%, 3.53% and 5.24% by the end of the first, second, third and fourth hour, respectively, corresponding to the end of the toe region of the stress-strain curve. The percentage change of elongation of BFB D-periodicity (from a starting periodicity of D6% = 79.70 ± 6.1 nm, P = 0.98), was 1.22%, 2.16%, 3.52% and 5.23% by the end of the first, second, third and fourth hour, respectively, corresponding to the end of the toe region of the stress-strain curve.

At the 9% strain level, the percentage change of elongation of WFB D-periodicity (from a starting periodicity D9% = 87.36 ± 6.88 nm, P = 0.89) , was 1.74%, 2.81%, 3.84% and 4.72% by the end of the first, second, third and fourth hour, respectively, corresponding to the linear region of the stress-strain curve. The percentage change of elongation of BFB D-periodicity (from a starting periodicity D9% = 87.42 ± 6.90 nm, P = 0.89), was 1.74%, 2.82%, 3.88% and 4.72% by the end of the first, second, third and fourth hour, respectively, corresponding to the linear region of the stress-strain curve.

The WFB D-periodicities demonstrated highly significant differences between different strain groups at the fourth hour ($P < 0.0001$). There were no differences between the WFB and BFB D-periodicities for all groups at the fourth hour ($P > 0.05$).

Table 4.11. Summary of the structural characterisation of fibrils (WFB D-periodicities). Statistical differences between groups were calculated at the fourth hour (n = 12 for each of the strain groups and n = 9 for the native group).

Target tendon strain	0 % (native group) WFB	3% WFB	6% WFB	9% WFB
D-periodicity length increase at the 4th hour	67.43 ± 2.0 [A]	75.50 ± 3.7[B]	79.70 ± 6.1[C]	87.36 ± 6.8[D]
1st hour		3.5 nm	4.8 nm	10.6 nm
2nd hour		6.0 nm	8.6 nm	17.0 nm
3rd hour		9.2 nm	14.2 nm	23.3 nm
4th hour		13.4 nm	21.2 nm	28.6 nm
Total increase in D-periodicity length over the 1st, 2nd, 3rd and 4th hours		13.4 nm	21.2 nm	28.6 nm
Fibril elongation % 1st hour		1.72%	1.20 %	1.74 %
2nd hour		2.98%	2.14 %	2.81%
3rd hour		4.57%	3.53 %	3.84%
4th hour		6.66%	5.24%	4.72%
Total fibril elongation % over the 1st, 2nd, 3rd and 4th hours		15.93%	12.11%	13.11%

A, B, C, D statistically significant ($P < 0.0001$)

4.10 The Association Between Mechanical and D-periodicity Changes

The following graphs show the changes in the mechanical profiles[19] with the corresponding changes in D-periodicity (WFB and BFB) in the three prolonged strain groups (3%, 6% and 9%). In each of the figures, the starting D-periodicity length is different. The associations between the WFB and BFB D-periodicities are highly significant ($P < 0.0001$). The associations between the declines in mechanical profiles and the changes in D-periodicity (WFB and BFB) are close to linear with a rapid increase in D-periodicity length. The number of data points in the linear fit show that they are highly concordant in all cases (see Table 4.11).

A. D-periodicity – 3% strain

There is a linear association where a decline in *k* (of around 25%) correlates with an increase in D-periodicity (around 10 nm).

[19] All the data for stiffness assessments were found to be highly correlated ($R^2 = 0.88$ for samples of BFB D-periodicities and $R^2 = 0.90$ for samples of WFB D-periodicities, $P < 0.0001$). The replications of the associations for loading stiffness (*k2*) are in Appendix 9.

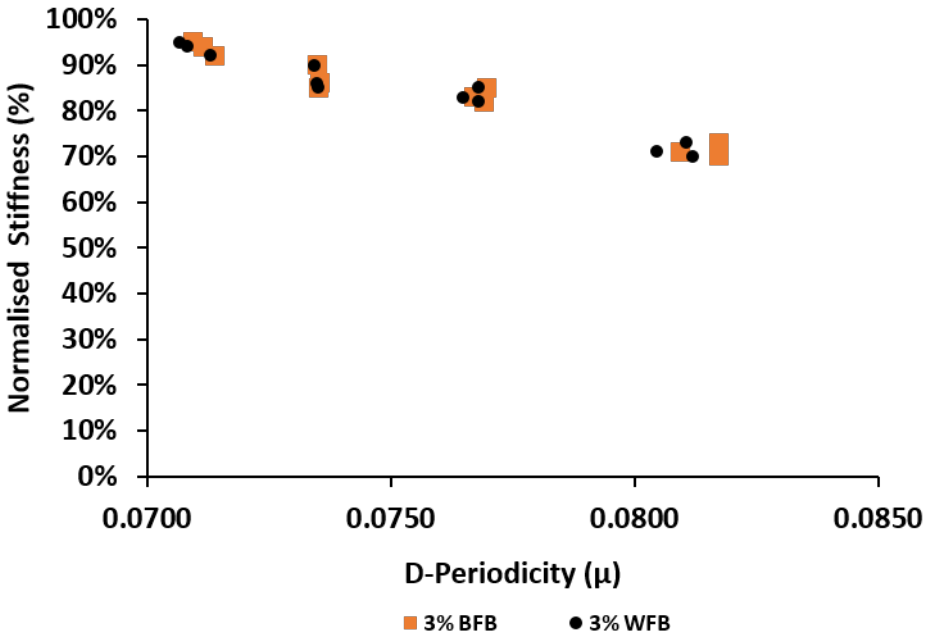

Figure 4.66. Changes in D-periodicity (WFB and BFB) versus *k*. The four clusters of data show the hourly measurements.

The decrease in *h* (around 40%) correlates with an increase (around 12 nm) in WFB and BFB D-periodicities.

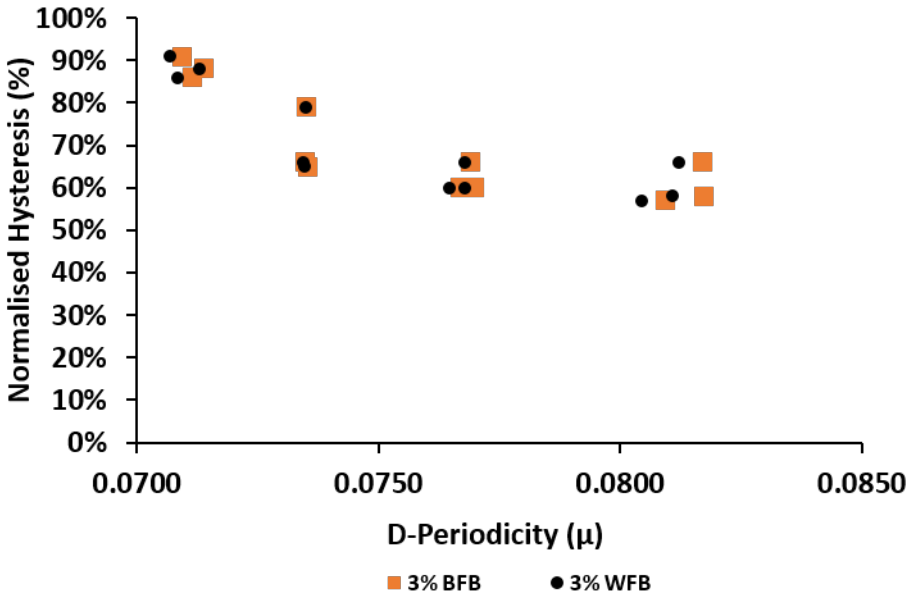

Figure 4.67. The change in D-periodicity (WFB and BFB) *vs h*. The four clusters of data show the hourly measurements.

The decline in ML (around 25%) correlates with an increase (around 12 nm) in WFB and BFB D-periodicities.

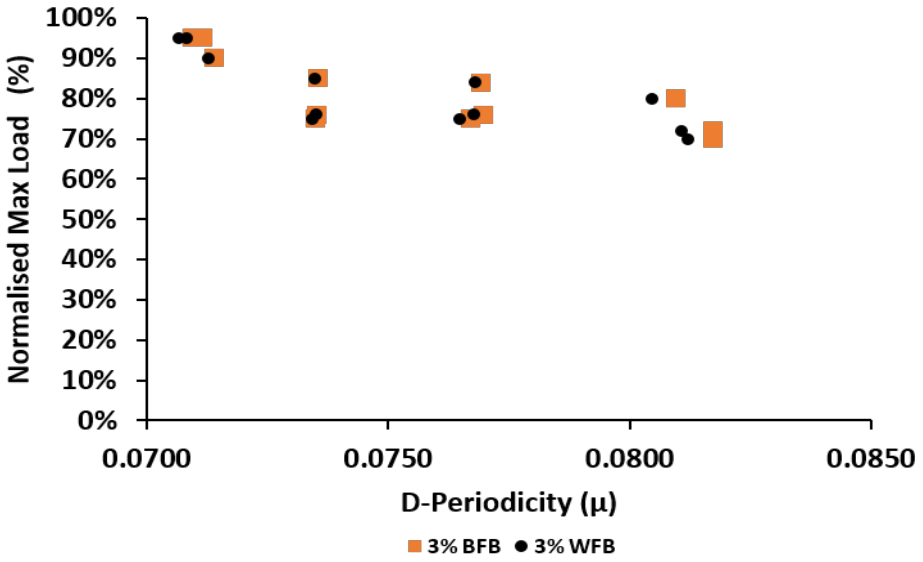

Figure 4.68. The change in D-Periodicity (WFB and BFB) *vs* the ML. The four clusters of data show the hourly measurements.

B. D-periodicity - 6% strain

The decline in *k* (around 30 %) correlates with an increase (around 18 nm) in WFB and BFB D-periodicities.

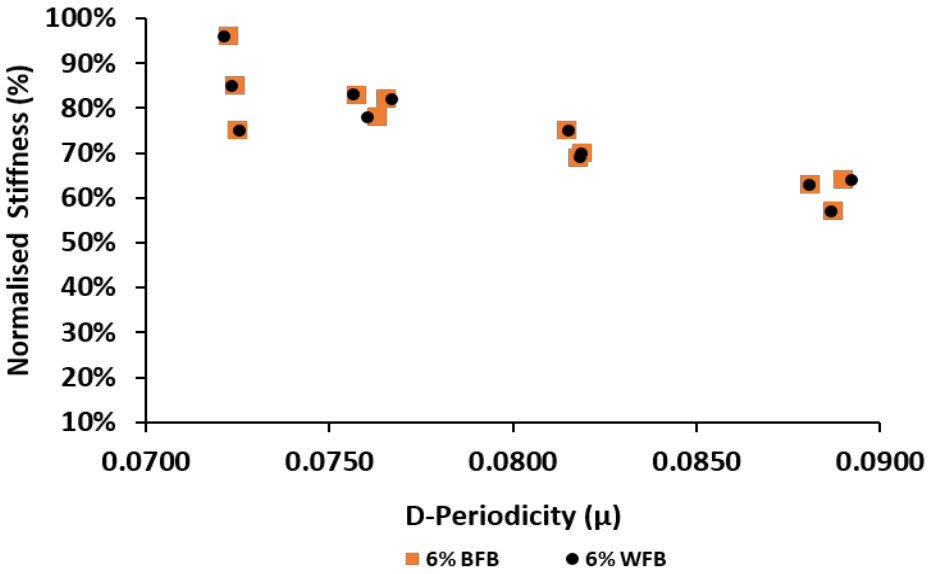

Figure 4.69. The change in D-periodicity (WFB and BFB) *vs* the *k*. The four clusters of data show the hourly measurements.

The decline in *h* (around 55%) correlates with an increase (around 18 nm) in WFB and BFB D-periodicities.

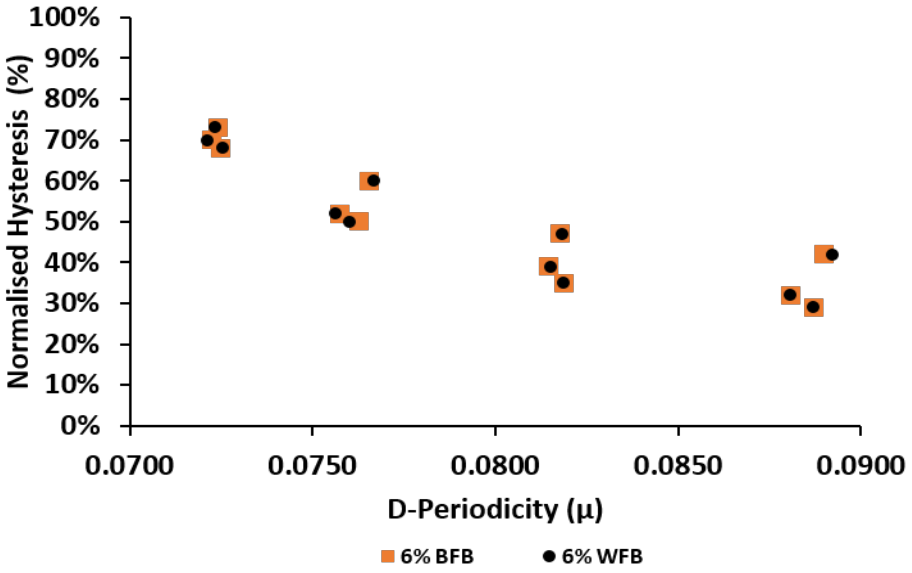

Figure 4.70. The change in D-Periodicity (WFB and BFB) *vs* the *h*. The four clusters of data show the hourly measurements.

The decline in ML (around 35%) correlates with an increase (around 16 nm) in WFB and BFB D-Periodicities.

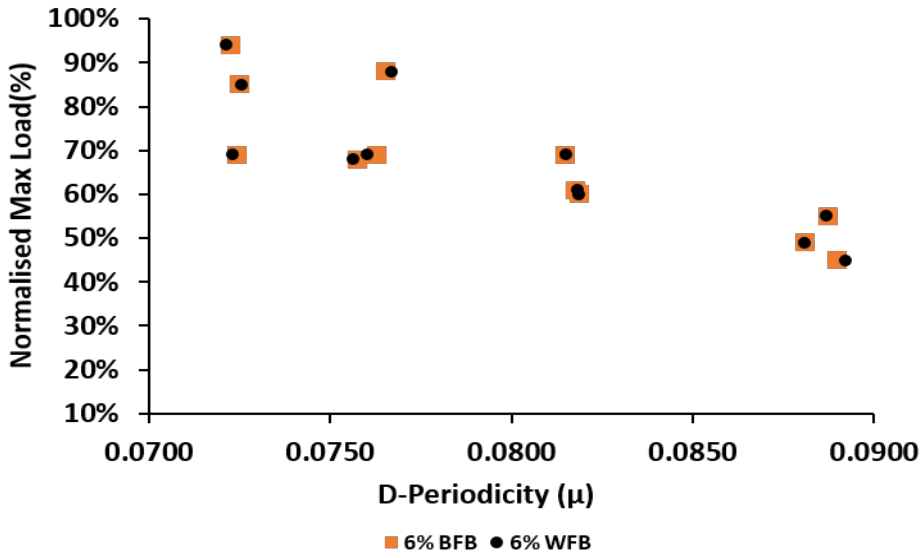

Figure 4.71. The change in D-periodicity (WFB and BFB) *vs* the ML. The four clusters of data show the hourly measurements.

C. D-Periodicity - 9% Strain

The decline in *k* (around 40%) correlates with an increase (around 20 nm) in WFB and BFB D-periodicities.

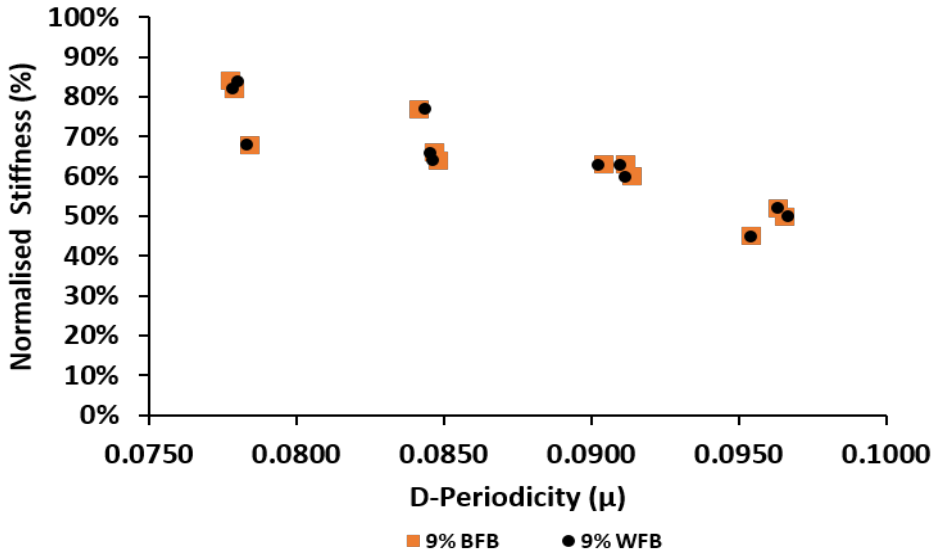

Figure 4.72. The change in D-Periodicity (WFB and BFB) *vs k*. The four clusters of data show the hourly measurements.

The decline in *h* (around 70%) correlates with an increase (around 20 nm) in WFB and BFB D-periodicities.

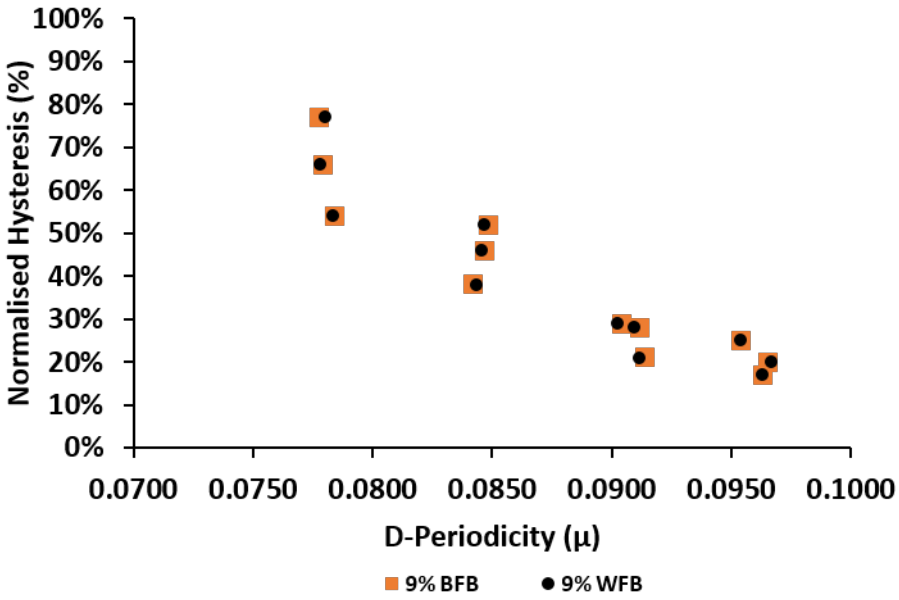

Figure 4.73. The change in D-Periodicity (WFB and BFB) *vs h*. The four clusters of data show the hourly measurements.

The decline in ML (around 70%) correlates with an increase (around 20 nm) in WFB and BFB D-periodicities.

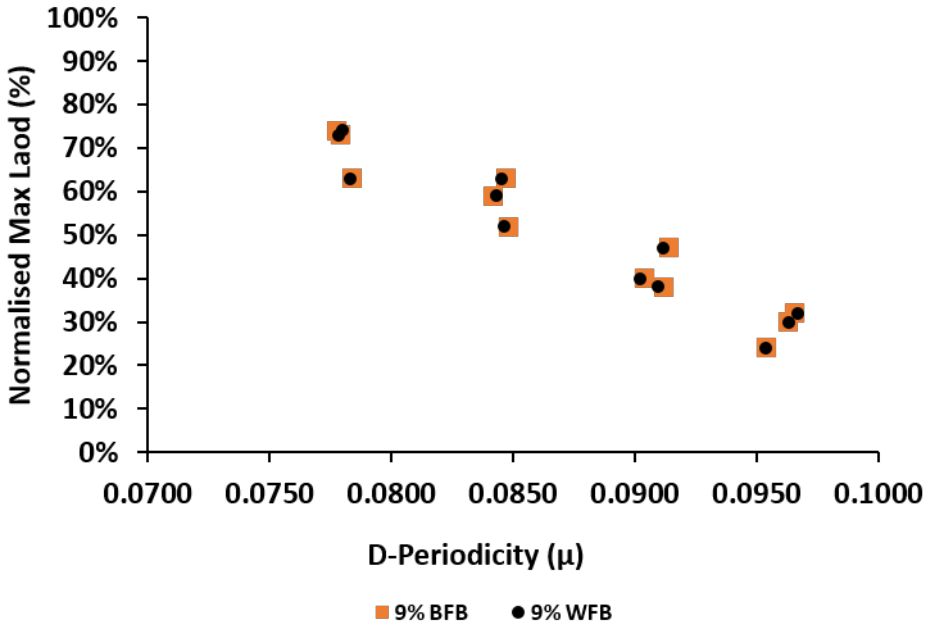

Figure 4.74. The change in D-Periodicity (WFB and BFB) *vs* the ML. The four clusters of data show the hourly measurements.

Table 4.12. The coefficients (R) for correlation between changes in D-periodicity (WFB and BFB) and mechanical characteristics for the 3%, 6% and 9% strain groups over one, two, three and four hours of cyclic loading.

Variable	*D-periodicity*	
	WFB	*BFB*
k		
3% strain	–0.97185	–0.97095
6% strain	–0.88935	–0.88919
9% strain	–0.89901	–0.90153
h		
3% strain	–0.81586	–0.80228
6% strain	–0.89405	–0.89868
9% strain	–0.93542	–0.93813
ML		
3% strain	–0.76138	–0.74766
6% strain	–0.85050	–0.85378
9% strain	–0.95874	–0.95978

4.11 Nano-morphological Outcomes in GAG-depleted Tendons (Study 2)

A. Qualitative assessment – AFM assessments of tendons undergoing loading

The semi-quantitative AFM assessment of tendons undergoing repetitive cyclic loading of 6% strain (in both control and GAG-depleted groups) over two hours allowed for three-dimensional (3D) imaging of the tendon's nanostructure. Our study characterised the progression of nanostructural damage indicating that tendon deformation that is induced by repetitive cyclic loading can be used to assess the cumulative progression of damage in tendons at the nanoscale level.

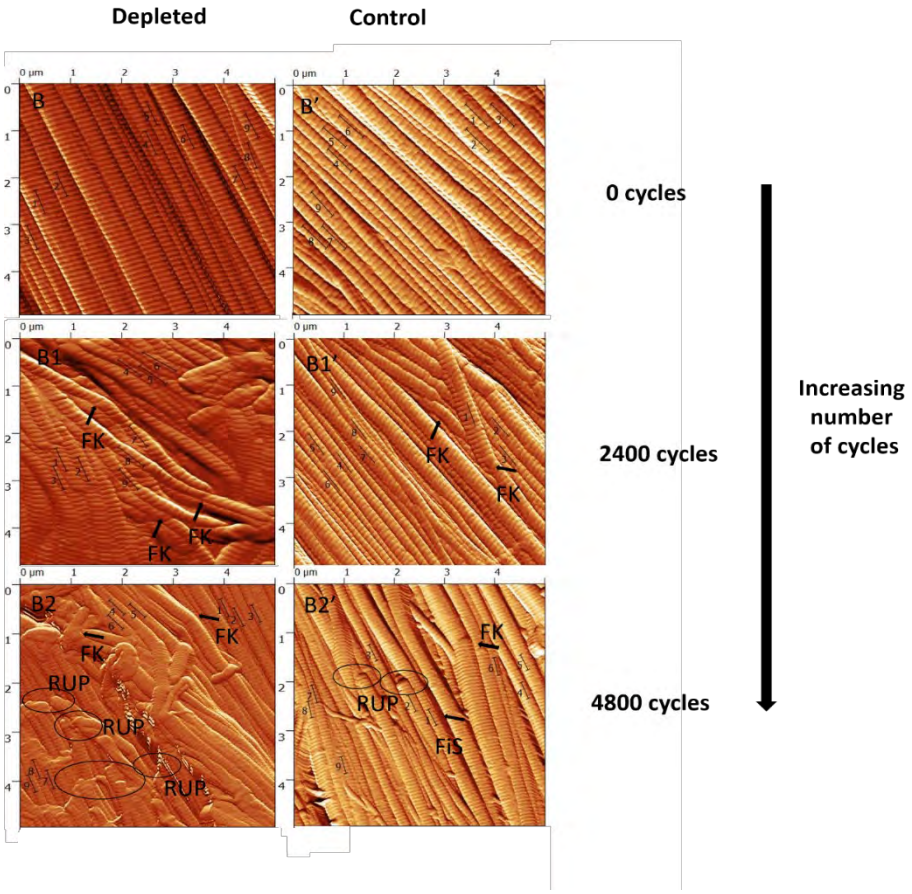

Figure 4.75. AFM images demonstrating the progression of morphological changes in tendons that underwent 6% strain over two hours of cyclic loading. Original magnification 5 μm.

At the end of the first hour of loading, the GAG-depleted group (Figure 4.75) demonstrated similar damage changes to those seen in the Study 1 9% group at the end of the second hour (see Figure 4.64). There was a marked widening of the interfibril space and an increased disruption of fibre arrangement and orientation. The latter changed to wavy fibrils exhibiting fibril kinks (FK in Figure 4.75: B1) that became more prominent and evident at the end of the second hour (FK in Figure 4.75: B2).

By the end of the second hour, the GAG-depleted group (Figure 4.75) exhibited similar damage changes seen in the Study 1 9% group at the end of the third and fourth hours (see Figure 4.64). Figure 4.75: B3 and B4 shows the damage in the GAG-depleted group, demonstrating a wider distribution and increased intensities of damage areas that are evident even with a lower number of repeated loadings (Figure 4.75: B1, B2).

For example, the GAG-depleted tendons show an increased fibril kink (FK) and the interfibril spaces (FiS) between fibrils are more prominent than those seen in the 6% group from the main study (Figure 4.75: B2, compared with Figure 4.64).

Furthermore, an increased disruption of fibril orientation (that changed the direction of the fibrils from parallel to bended or twisted) was also observed and marked areas of fibril rupture (RUP) were prominent in the GAG-depleted group (Figure 4.75: B2).

By the end of the first hour, the control group exhibited similar changes (Figure 4.75. B1) to those seen at the end of the first hour in the 6% group from the main study (Figure 4.64) but in a larger distribution. For example, an increased fibril kink (FK) and interfibril space (FiS) between fibrils was more prominent at the end of the first hour (Figure 4.75: B1, compared to Figure 4.64). However, at the end of the second hour of loading, the changes (RUP, FK and FiS) in the control group closely resemble the changes in the 6% group (from Study 1) that were seen at the end of the fourth hour (Figure 4.75: B2, compared with Figure 4.64).

B. Quantitative assessment – AFM assessments of control and GAG-depleted tendons undergoing loading (Study 2)

The control and GAG-depleted groups demonstrated a progression change in fibril D-periodicities characterised by a marked increase in WFB and BFB D-periodicities over the period of mechanical intervention. However, there were no marked differences between the WFB and BFB D-periodicities over the two hours of cyclic loading.

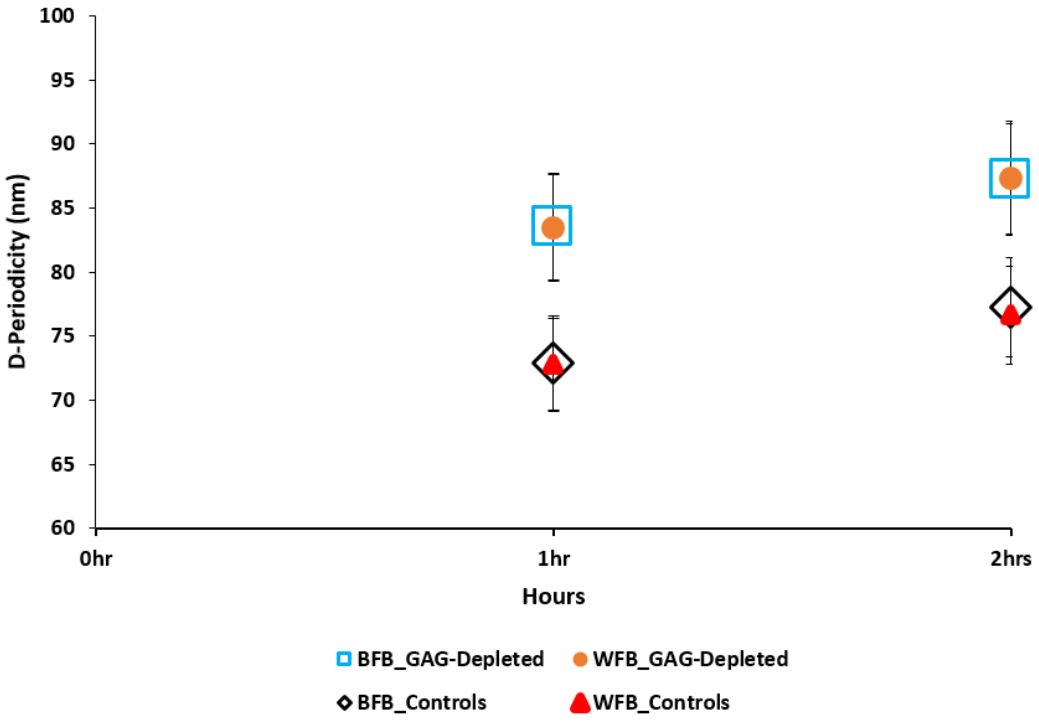

Figure 4.76. The effect of fatigue loading on tendon nanostructural properties (WFB and BFB D-periodicities) in the control and GAG-depleted tendon groups.

The mean WFB and BFB D-periodicities for the control group were D0% = 74.74 ± 1.95 nm and 75.10 ± 2.22 nm respectively, $P < 0.0001$. For the GAG-depleted group, the means were D_D% = 85.37 ± 1.82 nm, and 85.39 ± 18.47 nm respectively, $P = 0.08$. For the control group, the percentage changes of elongation for WFB and BFB D-periodicities were 1.39% and 2.44%, and 1.37% and 2.28% by the end of the first and second hours, respectively. For the GAG-depleted group, the percentage changes of elongation for WFB and BFB D-periodicities were 4.05% and 4.88%, and 4.04% and 4.88 % by the end of the first and second hours, respectively. This corresponds to the end of the toe region of the stress-strain curve.

There were significant differences in the D-periodicities between the control and GAG-depleted groups ($P < 0.0001$) at the second hour. Also, there were no significant differences between the WFB and BFB D-periodicities for either groups at the second hour ($P > 0.05$).

Table 4.13. Summary of the structural characterisation of fibril (WFB D-periodicities). Statistical differences between groups were calculated at the second hour (n = 10 for each group).

	Control WFB	GAG-depleted WFB
D-periodicity length increase at the second hour	74.74 ± 1.95 nm [A]	85.37 ± 1.82 nm [B]
First hour	5.6 nm	16.3 nm
Second hour	9.8 nm	19.7 nm
Total increase in D-periodicity length over first and second hours	15.4 nm	36.0 nm
Fibril elongation % first hour	1.39 %	4.05 %
Fibril elongation % second hour	2.44 %	4.88 %
Total fibril elongation over first and second hours	3.83%	8.93%

A and B denote statistical significance ($P < 0.0001$).

4.12 The Association Between Mechanical and D-periodicity Changes

The following graphs show the changes in the mechanical profiles[20] with the corresponding changes in D-periodicity (WFB and BFB) in the control and GAG-depleted tendon groups. In each of the figures, the starting D-periodicity length is different. The associations between WFB and BFB D-periodicities are highly significant ($P < 0.0001$). The association between the declines in mechanical profiles and the changes in D-periodicity (WFB and BFB) seem to be polynomial with a rapid increases in D-periodicity length. The number of data points in the polynomial fit shows that they are highly concordant in all cases (see Table 4.14).

A. D-periodicity - controls and GAG-depleted tendons

In Figure 4.77, there is a polynomial association of the two variables where a decline in *k* correlates with an increase in D-periodicity. This increase in periodicity up to around 10 nm corresponds with a decline in *k* of around 20% for controls and around 40% for GAG-depleted samples, respectively.

[20] All the data for stiffness assessments were found to be highly correlated ($R^2 = 0.96$ for WFB D-periodicities and $R^2 = 0.96$ for BFB D-periodicities, $P < 0.0001$). The replication of the associations for loading stiffness (*k2*) are in Appendix 9.

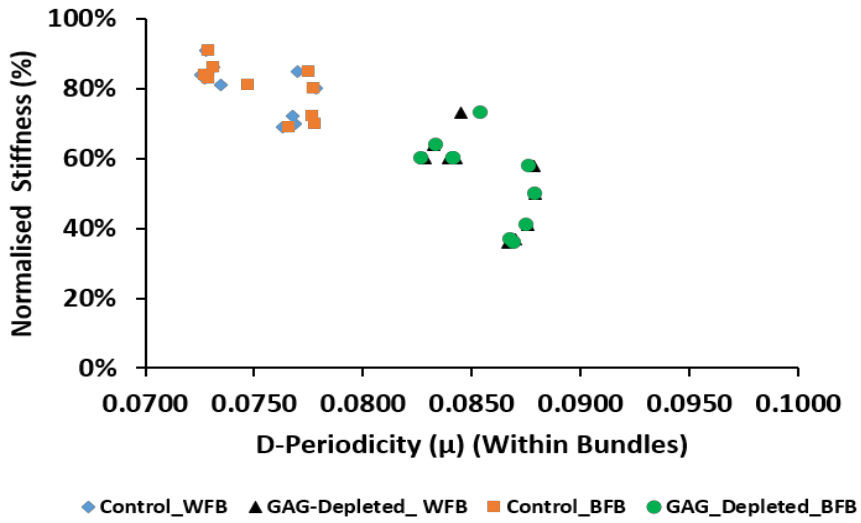

Figure 4.77. Changes in *k vs* WFB and BFB D-periodicity for 6% cyclic loading over two hours in both control and GAG-depleted tendons. The two clusters of data show the hourly measurements.

In Figure 4.78, there is a polynomial association of the two variables where a decline in *h* around 45 % for controls and around 60% for the GAG-depleted samples correlates with an increase in D-periodicity (WFB and BFB) of up to around 15 nm over the repeated testing cycle.

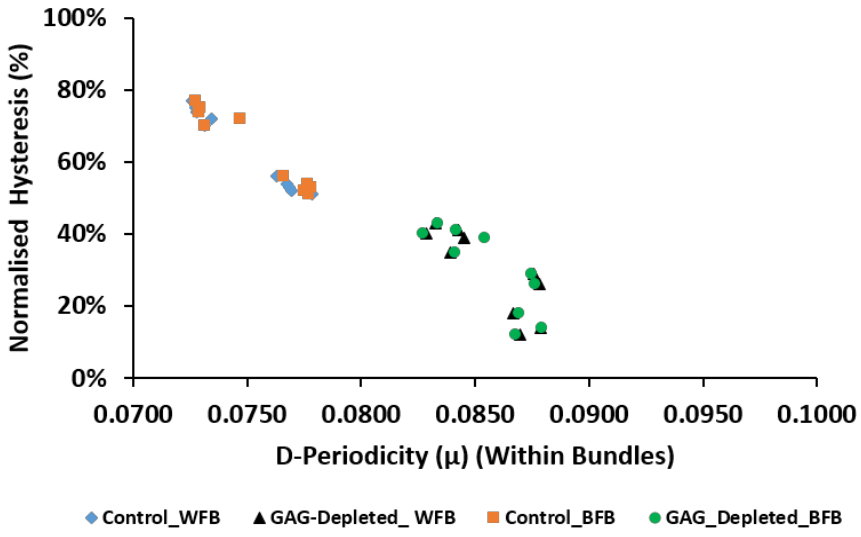

Figure 4.78. Changes in *h vs* WFB and BFB D-periodicity for 6% cyclic loading over two hours in both control and GAG-depleted tendons. The two clusters of data show the hourly measurements.

In Figure 4.79, there is a polynomial association of the two variables where a decline in ML of around 25% and 40% for controls and GAG-depleted samples respectively correlates with an increase in D-periodicity (WFB and BFB) of up to around 10 nm.

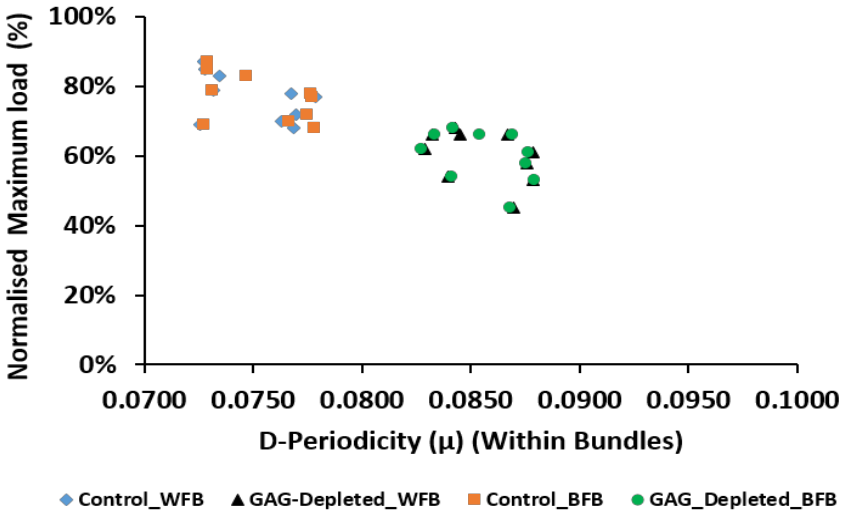

Figure 4.79. Changes in ML *vs* WFB and BFB D-periodicity for 6% cyclic loading over two hours in both control and GAG-depleted tendons. The two clusters of data show the hourly measurements.

Table 4.14. The correlation (R) between changes in D-periodicity (WFB and BFB) and changes in mechanical characteristics for controls (from Studies 1 and 2) and the GAG-depleted tendons over two hours of cyclic loading.

Mechanical Characteristic	*Correlation with D-periodicity changes*	
	WFB	*BFB*
k		
GAG-depleted	–0.6607	–0.6043
Control (Study 2)	–0.6888	–0.6325
Control (Study 1)	–0.5524	–0.5643
h		
GAG-depleted	–0.8165	–0.8348
Control (Study 2)	–0.9731	–0.9920
Control (Study 1)	–0.8670	–0.8633
ML		
GAG-depleted	–0.3938	–0.4427
Control (Study 2)	–0.5002	–0.5107
Control (Study 1)	–0.2825	–0.2844

4.13 Multiscale Association Between Macro- and Nano-morphological Changes

The following figures (4.80 to 4.82) show the association between the changes of tenocyte morphology (spindle shape) and fibre waviness with the corresponding changes in the WFB D-periodicities. In all of the figures, the starting D-periodicity length is different between all group samples. The associations between changes in WFB D-periodicities and changes in both the waviness and tenocyte morphology are highly significant ($P < 0.0001$). The association seems to be described well by a second-order polynomial (except for in the case of tenocyte morphology and fibre waviness *vs* WFB D-periodicity in the 3% strain group, which is a linear association) with a rapid increase in D-periodicity length. The number of data points in the polynomial fit shows high concordance in all cases (see Table 4.15).

A. D-periodicity - 3% strain

For the 3% strain group, Figure 4.80A shows the declining proportion of cells in the samples that are spindle-like as the WFB D-periodicity increases. Figure 4.80B shows the increasing proportion of fibre waviness in the samples as the WFB D-periodicity increases. It is clear that the figure shows a significant linear association between the variables ($P < 0.0001$).

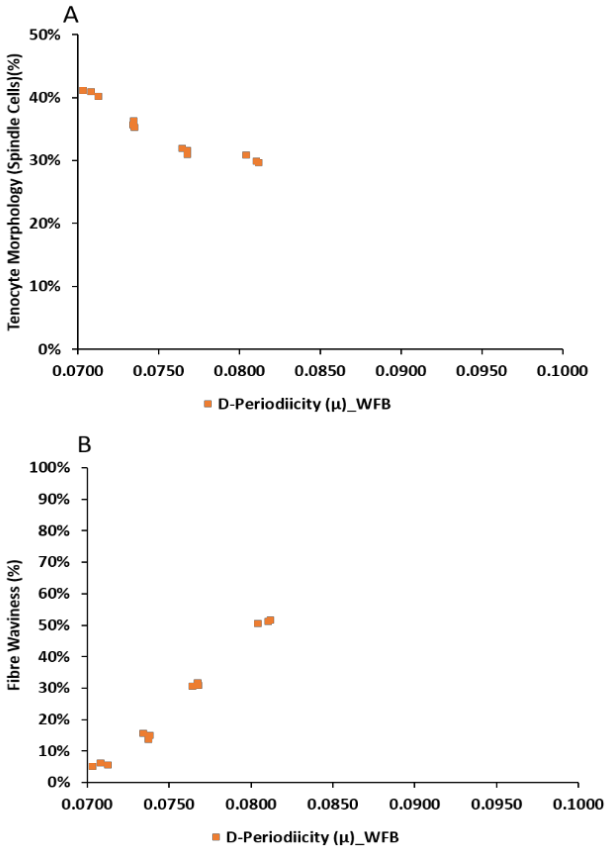

Figure 4.80. Changes in tenocyte morphology (spindle shape) (A) and fibre waviness (B) *vs* the corresponding changes of the WFB D-periodicities of samples under a 3% strain cyclic loading. The four clusters of data show the hourly measurements.

B. D-periodicity - 6% strain

For 6% strain group, Figure 4.81A shows the declining proportion of cells in the samples that are spindle-like as the WFB D-periodicity of fibrils increases. Figure 4.81B shows the increasing proportion of fibre waviness in the samples as the WFB D-periodicity increases. This figure shows significant polynomial associations between the variables ($P < 0.0001$).

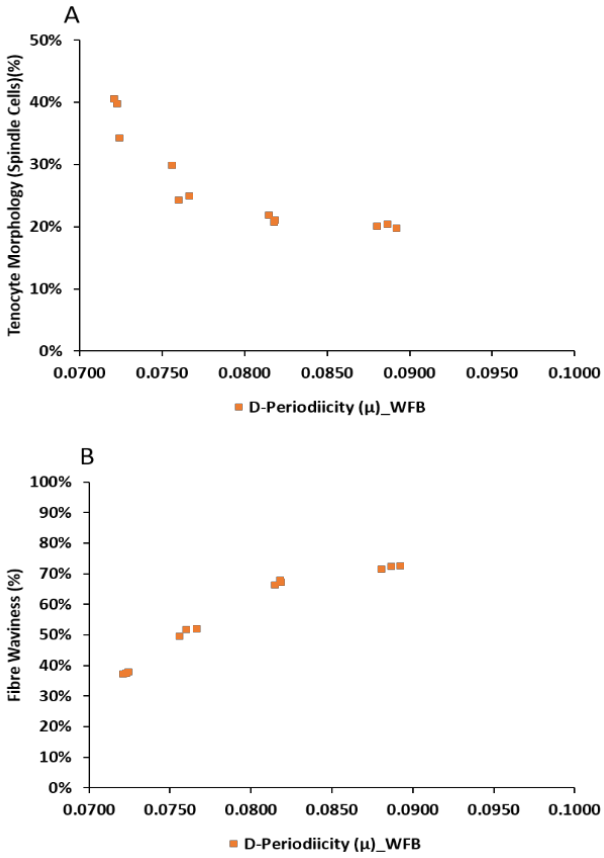

Figure 4.81. Changes in tenocyte morphology (spindle shape) (A) and fibre waviness (B) *vs* the corresponding changes of WFB D-periodicities of samples under a 6% strain cyclic loading. The four clusters of data show the hourly measurements.

C. D-Periodicity - 9% strain

For 9% strain group, Figure 4.82A shows the declining proportion of cells in the samples that are spindle-like as the WFB D-periodicity increases. Figure 4.82B shows the increasing proportion of fibre waviness in the samples as the WFB D-periodicity increases. This figure shows a significant polynomial association ($P < 0.0001$).

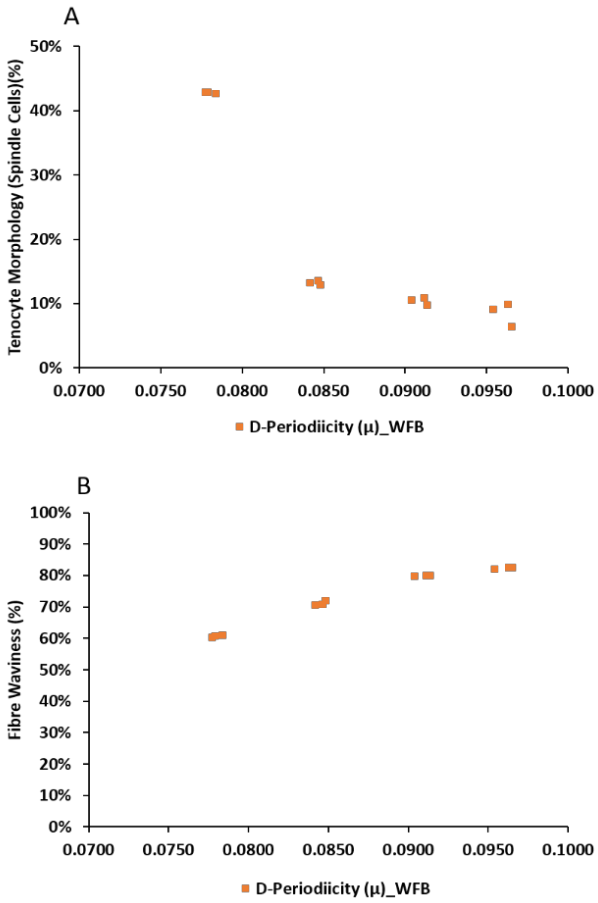

Figure 4.82. Changes of tenocyte morphology (spindle shape) (A) and fibre waviness (B) with the corresponding changes of the WFB D-periodicities of samples under 9% strain cyclic loading. The four clusters of data show the hourly measurements.

4.14 Multiscale Association Between Macro- and Nano-morphological Changes in the Control and GAG-depleted Groups (Study 2)

Figures 4.83 and 4.84 show the changes of tenocyte morphology (spindle shape) (A) and fibre waviness (B) with the corresponding changes in WFB D-periodicity of samples from the control and GAG-depleted groups. In all of the figures, the starting D-periodicity length is different between the controls and depleted samples. The associations between WFB D-periodicities and both the waviness and tenocyte morphology (spindle shape) are highly significant ($P < 0.0001$).

The association between the changes in the morphological profiles (waviness and tenocyte spindle shape) and the changes in D-periodicity (WFB) seems to be linear

with a rapid increase in D-periodicity length. The number of data points in the linear fits shows that they are highly concordant in all cases (see Table 4.15).

A. The control group

Figure 4.83A shows the proportion of cells in the samples that are spindle-like as the WFB D-periodicity increases. Figure 4.83B shows the proportion of fibre waviness in the samples as the WFB D-periodicity increases. This figure shows significant associations between the variables ($P < 0.0001$).

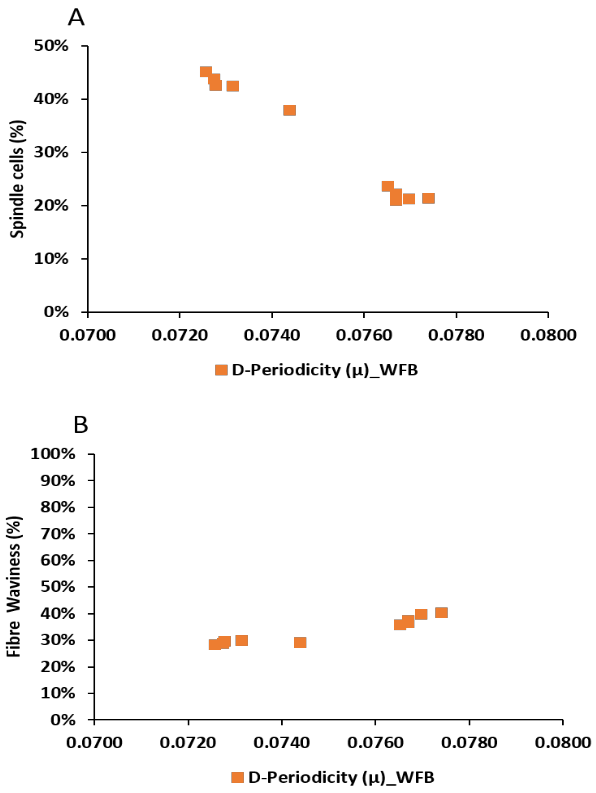

Figure 4.83. Changes of tenocyte morphology (spindle shape) (A) and fibre waviness (B) *vs* the corresponding changes of the WFB D-periodicities of the control samples. The two clusters of data show the hourly measurements.

B. The GAG-depleted group

Figure 4.84A shows the proportion of cells in the samples that are spindle-like as the WFB D-periodicity increases. Figure 4.84B shows the proportion of fibre waviness in

the samples as the WFB D-periodicity increases. The figure clearly demonstrates a significant association ($P < 0.0001$) between the variables.

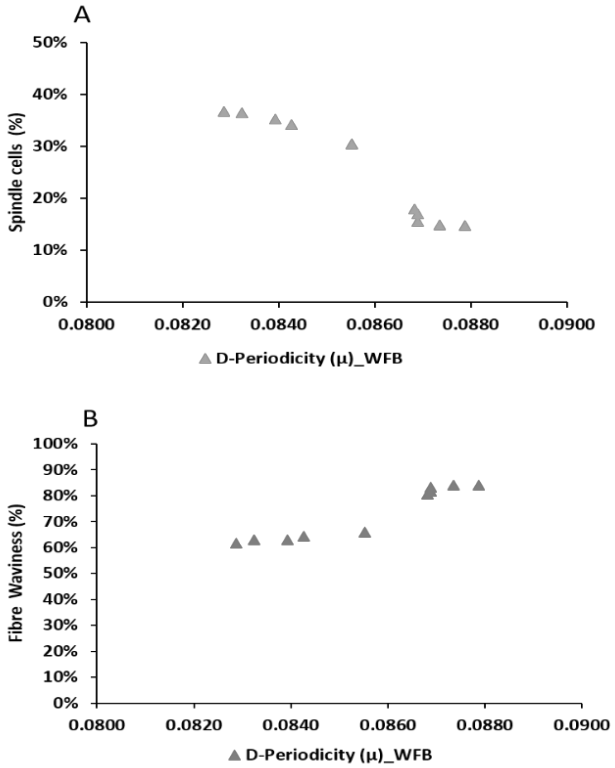

Figure 4.84. Changes in tenocyte morphology (spindle shape) (A) and fibre waviness (B) *vs* the corresponding changes of the WFB D-periodicities of the GAG-depleted samples. The two clusters of data show the hourly measurements.

Table 4.15. The multiscale correlation (R) between changes in WFB D-periodicities and tenocyte morphology (spindle shape) and fibre waviness for groups from Study 1 and Study 2.

Morphological variables	*Tenocyte morphology (spindle shape)*	*Fibre waviness*
D-Periodicity (WFB, Study 1)		
3% strain	–0.9429	0.9938
6% strain	–0.7323	0.9546
9% strain	–0.8491	0.9806
D-Periodicity (WFB, Study 2)		
Control group	–0.9936	0.9540
GAG-depleted group	–0.9658	0.9543

CHAPTER FIVE:
DISCUSSION

5.1 Introduction

The fatigue testing protocol developed in the current study is unique. This is the first study of the multiscale structural changes within the same non-viable intact/bulk tendon in response to prolonged cyclic and static loading protocols under controlled levels of strain. The examination of non-viable whole tendons is comparatively straightforward and has been reported to demonstrate the clearest data regarding the mechanical properties of tendons undergoing fatigue damage (Shepherd et al., 2013). This study is consistent with the literature in assessing the mechanical characteristics of tendons under repeated cyclic loading to three different strain levels (3%, 6% and 9%). Strain levels of less than or equal to 4% have been considered physiological in nature (Curwin, 1994; Kirkendall & Garrett, 1997) and other authors have proposed that strain levels from 6% to 8% may be within the physiological limit (Mcgough et al., 1996; Sheehan & Drace, 2000; Muramatsu et al., 2001; Magnusson et al., 2003). Beyond 8% strain, macroscopic failure exists and the load-supporting capacity of the tendon is almost completely lost (Butler et al., 1978; O'brien, 1992) and further stretching leads to rupture of the tendon (Weiss & Gardiner, 2001; Wren et al., 2001; Wang, 2006). These incremental strains (3%, 6% and 9%) were used in this study to represent low, normal and supra-normal strain levels.

The overall microstructural findings of this study concur with other controlled *in-vivo* studies that describe the stages of progression of micro- and nano- damage accumulation in response to repetitive loading (see Table 2.1). The novelty of this study is in demonstrating the evidence of strain and cycle-dependent mechanisms of tendon damage accumulation, including the progressive description of nano- and microstructural changes that are concurrently existing with changes in static and dynamic mechanical properties.

Tendinopathy is thought to be an originator of Achilles, patella and quadriceps tendon rupture. Indeed, cyclic loading and/or overuse is widely accepted to be a major cause of tendon failure. Most of the literature on *in-vitro* and *in-vivo* tendon loading consider models that focus on the relationship between the applied stress and the time or the number of cycles to failure (Backman et al., 1990; Archambault et al., 2001; Nakama et al., 2005; Fung et al., 2009; Fung et al., 2010; Andarawis-Puri et al., 2011; Neviaser et al., 2012). Furthermore, these studies have not quantified tendon damage, in part due to the lack of an accurate definition with a precise engineering context for tendons.

Previous studies have associated tendinopathy with structural micro-damage initiated by mechanical load (Tallon et al., 2001; Maquirriain, 2011) and others have addressed damage in the tendon (Fung et al., 2009; Fung et al., 2010; Thorpe et al., 2014). However, this thesis is original in that it has undertaken a research protocol that incorporates multi-scale assessments of both mechanical and structural observations by correlating concurrent quantified structural image-based measures with the mechanical characteristics of tendons to repeated sub-rupture loading, including both the strain extensions and the number of cycles. Few studies have combined these assessments concurrently.

The mechanical testing protocol included dynamic assessments of stiffness (k) and hysteresis (h) (Fung et al., 2009; Freedman et al., 2014; Thorpe et al., 2014; Freedman et al., 2015; Szczesny et al., 2018). Furthermore, this testing protocol also assessed changes of sustained static loading such as stress relaxation (SR) (Yamamoto et al., 1999; Shepherd & Screen, 2013). In this aspect, this is the first study to be able to correlate concurrent changes in dynamic mechanical assessments (i.e. k and h) and static sustained SR protocols.

The confocal assessment protocol used in this research program to examine tendon microstructure was similar to other research protocols such as that of Legerlotz et al. (Legerlotz et al., 2013; Shepherd et al., 2014). The variables derived from these are of interest within the literature and are commonly defined as the progression of change in cell morphology (spindle to round) (Matyas et al., 1994; Screen et al., 2003; Riley, 2008; Wang et al., 2013; Schochlin et al., 2014; Thorpe et al., 2015), fibre waviness

(Fung et al., 2009; Fung et al., 2010; Andarawis-Puri et al., 2011; Shepherd et al., 2014; Freedman et al., 2015) and fibre anisotropy (Wren et al., 2003; Screen et al., 2004; Williams et al., 2008; Lujan et al., 2009; Wallace et al., 2010; Sereysky et al., 2012; Szczesny & Elliot, 2014).

Atomic force microscopy (AFM) assessments were used to examine tendon nanostructure, similar to many other studies (Rigozzi et al., 2011; Fang et al., 2012; Erickson et al., 2013; Rigozzi et al., 2013; Szczesny et al., 2018). The derived variable from the AFM assessment is commonly defined as the axial D-periodicity, and is used as the metric measure of the morphological characteristics of collagen fibrils (Wallace. et al., 2010; Fang et al., 2012; Erickson et al., 2013), and a function of fibril strain (Rigozzi et al., 2011; Rigozzi et al., 2013). The axial D-periodicity of fibrils is measured within fibril bundles (WFB) and between bundles of fibrils (BFB) (Fang et al., 2012; Erickson et al., 2013).

With the viscoelasticity of tendons, the recovery of a tendon's mechanical properties after loading can partially be possible (Duenwald et al., 2009; Maquirriain, 2011; Thorpe et al., 2014) and has also been part of investigations of tendon mechanical profiles. Previous studies quantified the mechanical response immediately after loading, without dissociating the permanent effects of change from time-dependent recovery (Thorpe et al., 2013; Kondratko-Mittnacht et al., 2015). With the use of our unique mechanical protocol, we have quantified the mechanical response of the tendon microstructure and clearly dissociated these changing effects by the evaluation of the effect of a one-minute resting period following 240 dynamic cycles of the loading protocol. In this sense, this is also a unique element of the full research testing protocol utilised in this study.

Our loading protocol has demonstrated that the recovered strain of the loaded tendon was muted within the first 60 cycles of the following repetitive fatigue loading phase. Therefore, our loading protocols are damaging, and we believe that our measures of non-recoverable variables in our assessments are mechanical damaging metrics that are similar to those suggested by previous studies (Fung et al., 2010; Hansen et al., 2010; Riggin et al., 2013). Further, our assessment of the progression in the tendon's structural changes with fatigue loading provided a better description of mechanics than

other measures such as the damage area fraction used in previous studies (Fung et al., 2009; Fung et al., 2010). The observed microstructural changes throughout the fatigue loading intervention were more dramatic compared to previous studies investigating degenerative changes of tissue under load (Parent et al., 2011; Shepherd et al., 2013).

This study is unique as it is the first mixed-methods approach, assessing and mixing both quantitative and qualitative data in a series of connected studies. The derived variables of quantitative and qualitative nano- and microstructural change have been assessed in the same domains that were subjected to the mechanical intervention. Therefore, our mixed-methods research could potentially counterbalance the weaknesses and harness the strengths of both approaches, especially when addressing and interpreting the concurrent mechanical and complex hierarchical structural changes in the tendons that were subjected to cyclic loading.

The research protocol for this thesis was undertaken over an extended period of time (four hours); however, the sample size was gradually depleted as the destructive testing protocols destroyed the tendons. The quantitative statistical analysis of the nano- and macro-changes was undertaken on effect sizes since the sample sizes were low during the third and fourth hour of the mechanical intervention. Therefore, the inferential statistics of the quantitative studies were primarily focused on the changes over the first two hours of loading.

The complementary qualitative assessments were employed for the ongoing two hours (hours three and four) to provide a trend analysis and description of the estimated trajectory of tendon changes under such extreme loading cycles. Therefore, the usage of both approaches has provided comprehensive interpretations and conclusions about the progression of mechanical and hierarchical structural changes in tendons that were subject to such extreme loading cycles.

A major aspect of this research was to repeat these mechanical and structural assessments from Study 1 in a set of glycosaminoglycan (GAG)-depleted tendons (Study 2). GAG depletion is a recognised experimental protocol commonly used to investigate the mechanisms of the GAG sidechains in regulating fibril load sharing. The protocol used Ch-ABC to perform enzymatic GAG depletion.

The structural response of the GAG-depleted and control groups was quantified by assessing the fibril D-periodicities (Rigozzi et al., 2011) and fibre structure (Lynch et al., 2003; Fessel & Snedeker, 2009; Rigozzi et al., 2009; Legerlotz et al., 2013) and the mechanical response was quantified by assessing *k* (Screen et al., 2005; Rigozzi et al., 2009; Svensson et al., 2011) and SR (Legerlotz et al., 2013) among the tested tendons from both groups.

5.2 Mechanical Loading Outcomes (Study 1)

A. Dynamic and static cyclic loading: hysteresis (h), stiffness (k) and maximum load (ML)

The response of all mechanical properties in the strain groups (3%, 6% and 9%) were consistent over the first, second, third and fourth hour of the mechanical intervention. The overall trend of the tendons from the three groups demonstrated a decline in *k*, *h* and ML throughout the entire period of loading. However, there was a rapid decline in *h*, *k* and ML within the first hour (see Figures 4.3 and 4.6). Consistent with previous reports, a significant change was observed in the mechanics with increasing cyclic loading and different levels of strain, demonstrating the interaction of dose and repetition (Devkota et al., 2007; Connizzo et al., 2013). For example, significant changes in *k* and *h* were observed among the high fatigue group (9%) (Fung et al., 2009; Andarawis-Puri et al., 2011), and a decrease in *h* was evident among the groups with an increased number of cycles of fatigue loading throughout the mechanical intervention (Figures 4.3 and 4.6) (Freedman et al., 2014; Freedman et al., 2015).

An increasing prevalence of observed ruptured fibres were observed in tendon samples with greater strain and number of repetitions (Figures 4.16 and 4.17). Since concurrent mechanical changes were recorded reflecting a similar model, then the mechanical findings (*k*, *h* and ML) of this study could be explained by a reduction in the number of load-bearing fibres. This is consistent with the hypothesis of Andarawis-Puri & Flatow (2011) and Fung et al. (2010) who attribute the changes in mechanical properties to the reduction in elasticity, decrease in the number of load-bearing fibres

and the increasingly obvious damage of fibres (Fung et al., 2010; Andarawis-Puri & Flatow, 2011).

While the rupture of the Achilles tendon seem to be a sudden event, there is a cited contrastive hypotheses in the literature that also purports that the intact fibres develop pathology prior to rupture caused by a gradual micro-damage accumulation and degeneration that also reflected a decline in mechanical integrity and performance (Wren et al., 2003; Kongsgaard et al., 2005; Kujala et al., 2005; Wang, 2006).

The rapid decrease in *k*, *h* and ML in both the 6% and 9% groups compared to the 3% group and observed within the first hour (Figures 4.3 and 4.6), concurs with the attribution suggested by Andarawis-Puri et al. (2011) and Fung et al. (2010). In line with this, in comparison to the 6% and 9% groups, the slow decrease in *k*, *h* and ML that was evident in the 3% group with no evidence of fibre ruptures (from confocal arthroscopy (CA) observations, Figure 4.16) is likely attributed to the higher number of load-bearing fibres. Furthermore, the evidence of some fibre rupture observed in the 6% and 9% groups has likely accounted for the poorer elastic response of fibre to load. This is likely attributed to the lower number of load-bearing fibres in the 6% and 9% strain groups (Figures 4.20 and 4.22).

The presented assessment of morphological changes during different strains over repeated loading supports the hypothesis of progression to damage accumulation (Fung et al., 2009; Fung et al., 2010; Andarawis-Puri et al., 2011; Ros et al., 2019). Any minor fluctuated increase and decrease in stiffness percentages between the assessments may describe the redistributed loads from damaged fibres (that cannot bear the applied load) to undamaged fibres. The concomitant morphological changes that occur during the mechanical intervention are discussed later in detail.

The most sensitive measure to increasing strain and numbers of cycles was the decline in *h* (Figure 4.3). This highlights the importance of *h* in assessing tendon damage accumulation. Knowledge that the change in the measured *h* was larger compared to the measured *k* and ML (Figures 4.5 and 4.6) for the same number of cycles and strain level of the intervention is important. This demonstrates that assessing only tendon *k* and ML may return an incomplete characterisation of the mechanical properties of the

assessed tendons. The mechanical properties in this study were highly correlated, therefore, they are all interrelated to a common domain of mechanical function in the tendon.

The presented results generated from three controlled levels of fatigue (low (3%), moderate (6%) and high (9%) level strain groups), provide insights at the macrostructural level into failure mechanisms and damage processes in tendons. Specifically, the results show which micro-damage accumulates and leads to a tendon's deterioration and rupture, supporting a pathology that is caused by a gradual accumulation of micro-damage (Wren et al., 2003; Wang, 2006).

The findings support those reported by Wren et al. (2003) and Schechtman and Bader (1997). For instance, Wren et al. (2003) have examined the effects of cyclic and static creep loadings on the mechanical characteristics of human Achilles tendons and reported that the initial strain (as measured at first loading to a predetermined stress level) is the best predictor of cycles or time to failure (Wren et al., 2003). The data in the current study appears to parallel this finding and also concurs with the suggestion that strain is the primary mechanical variable controlling the accumulation of tendon damage (Schechtman & Bader, 1997; Wren et al., 2003).

5.3 Mechanical Loading Outcomes (Study 2)

A. Dynamic and static testing – k, h and ML

The outcomes for the GAG-depleted and control tendons are also compared with the data from Study 1 showing a high concordance and replication of findings. Consistent with previous studies and the main study, there was a rapid decline in *k*, *h* and ML within the first hour of testing of the GAG-depleted group throughout the fatigue loading test compared to the control groups (the controls from both Study 1 and Study 2) (Figures 4.7–4.9) (Fessel & Snedeker, 2009; Rigozzi et al., 2009; Legerlotz et al., 2013). Within the first hour, the GAG-depleted group demonstrated a change in mechanical adaptation to repetitive loading. The overall declining trends throughout the intervention demonstrated the interaction of the dose and frequency effect of cyclic repetitions, reflecting similar findings in another GAG-based study by Fessel & Snedeker (2009).

Both control and GAG-depleted groups initially experienced fibre elongation which is consistent with the literature that suggests that this is associated with fibre recruitment, crimp straightening and the alignment of these fibres (Abrahams, 1967; Diamant et al., 1972; Cribb et al., 1995; Hansen et al., 2002; Screen et al., 2004; Franchi et al., 2007). At 6% applied strain in the control and GAG-depleted groups, the sliding mechanism (as suggested previously) was then recruited to allow and facilitate further elongation of fibres (Screen et al., 2004; Bruehlmann et al., 2005; Provenzano & Vanderby, 2006; Cheng & Screen, 2007).

By the end of the first hour of testing, it appears that the control group concurs with the literature on fibre elongation and sliding mechanisms. It seems that this group recruited a balance between fibre elongation and fibre sliding, resulting in better mechanical properties (higher *k* and *h*) compared to those in the GAG-depleted group. However, with the increased number of cycles (beyond the first hour), the balance between fibre elongation and sliding seems to be impaired in the control group, possibly by a change in the fascicles' force-strain response (Screen et al., 2005) and irreversible damage (as inter-fibrillar sliding) occurred at the nanoscale level and resulted in altered *k, h* and ML (Krajcinovic, 1985; Lee et al., 2017). This possibly explains the decline observed by the end of the second hour in *k, h* and ML of the control group that is analogous to the main study group.

Taking all comparisons between the GAG-depleted and control groups together, it appears that the findings of this study concur with the literature that purports that the fundamental role of GAGs is to control the elongation and sliding mechanisms between collagenous units at different hierarchal levels (fascicles, fibres and fibrils) (Minns et al., 1973; Ruggeri et al., 1984; Birk et al., 1989; Cribb et al., 1995; Sasaki & Odajima, 1996; Fratzl et al., 1998; Puxkandl et al., 2002; Raspanti et al., 2002; Redaelli et al., 2003; Scott, 2003; Screen et al., 2005; Vesentini et al., 2005; Screen et al., 2006; Liao & Vesely, 2007; Fratzl, 2008; Legerlotz et al., 2013). The presented findings do not concur with literature refuting the contributing role of interfibrillar GAGs in the elongation and sliding mechanisms (Screen et al., 2004; Bruehlmann et al., 2005; Screen et al., 2005; Provenzano & Vanderby, 2006; Cheng & Screen, 2007; Franchi et al., 2010). Compared to the control group, the depletion of GAGs seemed to influence both the elongation and sliding mechanisms in local and gross matrix

mechanical properties as observed by the outcomes from the first hour of testing of the GAG-depleted group (Study 2).

However, previous biomechanical studies on fascicles from rat-tail tendon (Screen et al., 2005) and fascicles from the anterior part of human patellar tendon (Svensson et al., 2011) have reported higher stiffness outcomes than those measured in this study and a previous study by Rigozzi et al. (2009). This inconsistency in *k* measurements from our study and from Rigozzi et al. (2009) compared to those from the above counterintuitive cited studies is perhaps, partially, due to the experimental setup, the biomechanical testing machine used and the condition and heterogeneity of the treated tendon samples.

One factor could be the differences in buffering techniques. For example, the experiment using fascicles from human patellar tendon was carried out in phosphate buffered saline solution (PBS) at 37°C using a mechanical micro-tensile tester while the other cited studies on rat-tail fascicles were carried out at room temperature and the tendon sprayed lightly with PBS using a custom-designed rig. However, the whole Achilles tendons used in our study and in the study by Rigozzi et al. (2009) were sufficiently moistened with PBS throughout the entire mechanical testing using universal testing machines.

Interestingly, our findings and those reported by Rigozzi et al. (2009) have indicated that removal of 40% and 50% of the total GAG from whole Achilles tendons results in a significant loss (about 50% and 46%) in *k*, respectively. Whereas, the other reports by Svensson et al. (2011) and Screen et al. (2005) have reported no differences in fascicle stiffness when about 90% of GAG was removed from the tested fascicles (Screen et al., 2005; Svensson et al., 2011). The GAG content of the tendons in this study and the aforementioned studies was measured by a spectrophotometric GAG assay as described by Farndale et al. (1986). Therefore, the differences are not likely to be due to differences in the GAG assay methods.

The absolute assessment of the effect of GAG removal from whole or a small specimen of tendon on the mechanical behaviour of the tested tissue appears to be muddied by the fact that the GAG depletion is typically incomplete (ranging from 40%

to 90% in the aforementioned studies). Consequently, an argument could be made that depleted tissue samples with higher percentages of remaining GAGs would be sufficient to sustain the tissue mechanics. However, the inconsistencies in the mechanical outcome between studies using whole tendon (this study and Rigozzi et al. (2009)) and those studies that have used only fascicles in their GAG assays are, perhaps, due to the heterogeneity of the mechanical response of different hierarchies (tendon *vs* fascicle). For example, it has been reported previously that tensile stiffness of a whole tendon is lower than that of a small specimens of tendon (Stouffer et al., 1985; Butler et al., 1987). Furthermore, the increased fascicle stiffness could also be attributed to the decreased amount of areolar connective tissue in smaller tendon specimens (Danylchuk et al., 1978; Yahia & Drouin, 1988).

Danylchuk et al. (1978) has previously suggested that the relative contributions of connective sheaths and collagen fasciculi should be included in calculations to rule out the different tissues contributing to the whole tissue mechanical characteristics (Danylchuk et al., 1978).

However, similarly to the findings of the current study, a study by Legerlotz et al. (2013) has reported a significant increase in SR of fascicles that had 77% of their GAGs removed (Legerlotz et al., 2013), contradicting the findings by Svensson et al. (2011). Consequently, it seems that the role of hierarchical heterogeneity between the depleted tendon and fascicle on the mechanical response of the tested tissue does not explain the inconsistency between the reports supporting or rejecting the role of PG and GAG in the mechanical properties of tendons.

Interestingly, several studies on the same hierarchy in ligaments and tendons suggested different concentrations of GAGs between the mid and insertion zones may alter the mechanical characteristics of tendons (Merrilees & Flint, 1980; Koob & Vogel, 1987; Vogel & Koob, 1989; Kannus et al., 1992). However, one study has shown that cultured tendon fascicles with greater GAG concentrations have increased stiffness (Abreu et al., 2008). This warrants further investigation on the role of the concentration and distribution of GAGs in contributing to the mechanical characteristics of the tendon.

Although there was a consistent decline in the mechanical characteristics when there was evidence of GAG depletion, few studies have documented the level or magnitude of GAG depletion precisely. Therefore, future research is required to understand if there is a linear decline in mechanical behaviour related to the amount of depletion of GAG in a tendon.

Other studies have suggested that tissue hydration during testing may mediate the role of decorin (Koob, 1989; Paavola et al., 2002). For example, increased stiffness has been observed in rat-tail tendon fascicles after the removal of GAG (Screen et al., 2006), indicating that GAG may have a lubricating effect. It is likely that the buffer used has reduced the swelling of the fascicles, leading to an increase in stiffness to the level seen under ambient conditions. Therefore, this possibly explains why the effect of buffer on stiffness was not observed in other studies in which the buffer swelling effect was controlled by polyethylene glycol (Fessel & Snedeker, 2009). Reconciling the results found in another study (Lujan et al., 2009) with our results, is difficult since the swelling in their study was not successfully controlled or fixed.

The buffer used in our study for the control group reflected closely the *in-vivo* environment. All tendons from the control group that were incubated in the buffer compared with the data from the main study have shown high concordance and replication of trends for *k*, *h* and ML that were similar to the 6% group in Study 1 (see Figures 4.7 and 4.9) . This likely indicates that the buffer did not affect the mechanics of the tendon samples in either study.

5.4 The Association Between Mechanical Loading Outcomes in Strained, Control and GAG-depleted Groups

This study has demonstrated that the mechanical variables are strongly associated with each other. This is reflected in all strain levels across a wide range of cycles. Therefore, in general, all the mechanical values are assessing a similar domain or characteristic. This was found to be true in the GAG-depleted groups, therefore GAG depletion

would seem to have an overall impact on all the mechanical properties. In summary, independent of strain and the GAG-depletion effect, the results have demonstrated a strong significant linear correlation between *k*, *h* and ML ($P < 0.0001$) (see Figures 4.3, 4.6, 4.7 and 4.9). Although this study assessed multiple variables we note consistency with previous studies that have shown strong correlations between *k* and *h* (Fung et al., 2009; Farris et al., 2011; Foure et al., 2012; Neviaser et al., 2012; Freedman et al., 2015).

The significant linear correlation between all mechanical variables in both studies may be attributable to the increase in fibre disorganisation followed by damage (see Figures 4.16 and 4.50) that resulted in decreased *k*, *h* and ML (see Figures 4.3, 4.6, 4.7 and 4.9). Shepherd et al. (2014) would argue that the strong relationship between *h* and ML may be attributed to the microstructural rearrangement that may have facilitated a stress redistribution (Shepherd et al., 2014). This would also seem plausible for the findings in this study.

It has been reported that SR is larger when larger portions of the tendon are loaded (Atkinson et al., 1999). In this context, our findings in the strain (6% and 9%), control and GAG- depleted groups show a dramatic decrease in ML with higher strain and number of cycles (see Figures 4.6 and 4.9). It seems that at strains or doses applied to pre-conditioned tendons that have been preconditioned, the strength differences of different fascicles or fibre locations are exposed during the increase in SR. This may suggest that during the SR, there is a differential loading and elongation of the fibres within the tendon. As some fibres elongate, the internal stressors may be transferred to other fibres over time. There are relatively new clinical hypotheses that stress shielding may be a mechanism of sustained tendinopathy in humans after repeated cyclic loading (Orchard et al., 2004). It could be that loading in different ranges or sustained holds may be a methods of altering the overall loading profile.

The variables incorporated in this study are comprehensive compared to other studies and also have been studied concurrently. In addition, the significant correlations (see Figures 4.10, 4.11, 4.12, 4.13, 4.14, and 4.15 & see Tables 4.2, 4.3, 4.9 and 4.10) between the mechanical properties clearly show that these are dependent on each other, suggesting that such metrics should be considered and incorporated in any

fatigue loading assessment to provide a complete investigation of tendon behaviour. Additionally, since these properties are all related, measuring only a couple of them could be sufficient to get a general view. But equally so, this may provide an avenue for future investigations in examining if these are similarly correlated when tested in *in-vivo* or in rehabilitation settings.

Such strong correlations between the mechanical properties may provide a better understanding of mechanisms to improve the functional behaviour of the muscle-tendon complex (MTC) for improvement in movement performances (Bosco et al., 1982; Bosco & Rusko, 1983).

5.5 Macro-morphological Outcomes in Undepleted Tendons

A. Quantitative and qualitative - confocal and histological assessments

There are a limited number of observational (i.e. morphology) (Fung et al., 2009; Fung et al., 2010; Shepherd et al., 2013) and quantitative studies (Freedman et al., 2014; Freedman et al., 2015) in the area of the mechanical assessment of tendons. Therefore, the present research was designed to utilise a hybrid model of both quantitative and qualitative analysis to investigate the effect of cyclic loading on the tendon's structural and mechanical properties at the microscale level. This thesis has described tendon response to repetitive loading using different variables and how these variables are correlated, with the intent to increase the understanding of the early stages of tendinopathy.

The subjective and objective assessments in the same domains accurately showed reproducible morphological changes during the mechanical intervention. Although there were minor differences in the proportional category shifts in each of three structural domains during all time points of the loading test, all results from both subjective and objective assessments have demonstrated similar progressive category changes in tendon structural morphology (see Figures 4.16, 4.17, 4.20, 4.21, 4.22, 4.26, 4.27). Subjective assessments of categorisation of tenocyte shapes and other fibre characteristics have been limited in the literature. The subjective classifications

used in the quantitative scoring system were valid and reproducible with the classification of objective observation described in the current study.

The test re-test reliability results as weighted Kappa showed an excellent level of inter-rater reliability and a very good intra-rater reliability for the measured domains: fibre arrangement and orientation, fibre structure and tenocyte roundness (The inter-rater reliability was > 0.82; 95% CI > (0.87 to 1.00) , the intra-rater reliability was > 0.76; 95% CI > (0.65-0.90). The observational assessment on Scanscope conventional histological images has validated and ruled out any ruptured areas of blurry fibre discontinuities seen in the images taken by CA.

All CA and conventional histological assessments were consistent and reproducible. The histological images in this study (see Figures 4.18) are consistent with previous studies that reported a significant change in the GAG amounts with a change in magnitude of the load (Devkota et al., 2007), and an increased GAG concentration in tendons that were subjected to cyclic loading (Abreu et al., 2008).

The progressive damage seen as morphological changes in the histological and confocal morphological findings (see Figures 4.16 and 4.17), (such as fibre kink deformation, separation, fragmentation and dissociation of collagen fibres) are consistent with those histological findings in previous studies (Fung et al., 2009; Fung et al., 2010; Andarawis-Puri et al., 2011). Furthermore, these observations are parallel to the pathohistological observations in human tendons including fibril denaturing, stretching, fraying, fragmenting, splitting of the collagen fibrils and fibre and finally resulting in rupture as reported by others (Kastelic & Baer, 1980; Kannus & Jozsa, 1991; Sonnabend et al., 2001; Jarvinen et al., 2004; Fung. et al., 2009; Sereysky et al., 2012).

Quantitative analysis of the low (3%), moderate (6%) and high (9%) level strain groups demonstrated a progression change in tenocyte morphology (roundness) and fibre waviness and no change in anisotropy (see Figure 4.28). The changes in the structural domains (except for anisotropy) clearly exhibited distinctive levels of micro-damage in the tendon which were not observed in the nonloaded (preconditioned) tendons. The results obtained are consistent with the presented hypothesis that there is

a sequential dose and strain effect on the variables of the examined macroscale domains in the loaded tendons.

The strong quantitative relationships in the current study between a broad range of microstructural measures and mechanical properties (see Tables 4.1 and 4.2) have not been reported previously, with the exception of one study by Freedman et al. (2015). In that study, significant relationships between crimp amplitude and both strain (R = 0.53) and laxity (R = 0.72–0.89) were reported (Freedman et al., 2015). The vast majority of previous studies have demonstrated qualitative relationships between structural and mechanical changes (Fung et al., 2009; Fung et al., 2010; Ros et al., 2013; Thorpe et al., 2014). Furthermore

Further, the structural changes found in the present study are in line with those reported by Parent et al. (2011) that showed that changes progressed non-linearly, increased rapidly and preceded rupture (Parent et al., 2011).

Shepherd et al. (2014) have suggested that the early fatigue micro-damage occurs at the weakest point – the inter-fascicle space. In this study, this was observed in the early period (first hour) of the lowest strain (3%) in the absence of other evidence of damage (see Figures 4.16 and 4.17). Therefore the findings of this study seem to support the observations of Shepherd et al. (2014).

The level of additional micro-damage observed, particularly by the end second hour in the 6% group (see Figures 4.16 and 4.17), is consistent with various previous reports (Järvinen et al., 1997; Waterston et al., 1997; Woo, 2000; Maffulli & Kader, 2002; Hamilton et al., 2008). Sivaguru et al. (2014) commented on these studies and suggested that all of these changes are markers of lateral tension or tertiary structure loss (Sivaguru et al., 2014). The current study supports this inference in that the loss of mechanical integrity was observed as the frequency and extent of the micro-damage increased. The fatigue damage represented by fibre waviness has been related to a specific mechanism by various authors (Fung et al., 2009; Andarawis-Puri et al., 2011; Neviaser et al., 2012). This mechanism is suggested to result from the stretching of a small group of fibres into their plastic deformation range (Pingel et al., 2014). Then upon unloading, they are compressed and kinked due to the shortening of the parallel

elongated elastic fibres (Herod & Veres, 2018). The formation of such micro-damage allows a further elongation with consequent repeated loading on both groups. The presented findings supports the studies by Maytas et al. (1994) and Screen et al. (2003) who found a correlation between strain and nucleus deformation of tenocytes, in which they found that the nuclei became thinner and longer in the viable loaded tendon fascicles (Matyas et al., 1994; Screen et al., 2003).

The quantitative assessment demonstrated a progressive change in tenocyte morphology from spindle to slightly round with a higher strain and an increased number of cycles of mechanical loading. This category shift was found mainly in regions where micro-damage was seen generally in the form of kinked (wavy) fibres, fibre dissociation and fascicle widening (see Figures 4.16 and 4.17). This appears to supports the view that the change in cell morphology is a secondary physical effect following the loss of integrity of the fibrous matrix.

Since 1995, the volume and shape of the chondrocyte nucleus has been reported to be sensitive to changes induced by compression (Guilak, 1995). However, it was not until 2002 that the nuclei of rat-tail tendon tenocytes were first seen to be responsive to strain (Arnoczky et al., 2002). Interestingly, our findings are not congruent with those reported by Ros et al. (2019) on progressive change in tenocyte morphology. They reported that tenocyte morphological changes were less disrupted with the progressed structural damage in higher strain groups when compared with lower damage in lower strain groups, and did not increase in severity with increased cycle numbers. The inconsistency is, perhaps, attributed to the significant lower levels of strain (3%, 6% and 9% *vs* 0.5%, 1.0%, 1.5% and 2.5%) and the number of cycles (up to 9,600 *vs* 500 cycles only) used in the assessments. It seems that the strain level and number of cycles in the study by Ros et al. did not reach the threshold at which significant change in tenocyte morphology may occur. Our data shows that this threshold was seen by the end of the first hour for all strained groups (see Figure 4.26).

These changes are consistent with other qualitative studies, which have observed tenocytes having more round nuclei in overloaded and tendinopathy tendons and ligaments (Matyas et al., 1994; Tallon et al., 2001; Sharma & Maffulli, 2005; Scott et al., 2007; Hamilton et al., 2008; Magra & Maffulli, 2008; Riley, 2008; Fung et al.,

2009; Shepherd et al., 2013; Thorpe et al., 2015) and suggest that matrix change is usually seen along with cell change (Shepherd et al., 2013). The change from spindle shape (Cat 4) to slightly round (Cat 3) was the most obvious change for all groups over all time points. All significant changes for spindle shape (Cat 4) occurred within the first two hours (see Figure 4.26). The other three categories (Cat 3, 2, and 1) all increased during the loading (see Figures 4.23, 4.24, and 4.25) and were not definitively different across the different forms of differentiation.

Clearly, in terms of association with other obersved and mechcncial profiles changes the utility of the 4 categories as widely reported by (Schochlin et al., 2014) is limited. The predictive value in the tenocyte shape is the early loss of the spindle stucture to reflect roundness, rather than degrees of roundness (Cat 3,2 &1). Since the objective assessments of the spindle shape using Image-J was derived from work with cancer cells (Schochlin et al., 2014) then future research clearly needs to determine if the (0.0-0.35) threshold for roundness could be improved to validate mechanical changes and pathology.

Not only are the microstructural changes in the three strained groups generally consistent with those in fatigue models in the literature, the presented findings also concur with the findings by Szczesny et al. (2017; 2018) and Chao & Tseng (2014) who observed other structural changes (e.g collagen fibre kinking and molecular denaturation) to precede tenocyte morphological changes (Chao & Tseng, 2014; Szczesny et al., 2017; Szczesny et al., 2018) and that fibre waviness may affect the mechanical and structural behaviour of tenocytes (Szczesny et al., 2018). For example, proportional changes in fibre waviness were higher and occurred earlier with lower strain levels than the proportional changes seen in tenocyte morphology. The findings of this study may also be useful for fibre recruitment models (Peltz et al., 2010) for the modelling of the response of tendons to fatigue loading.

In contrast to our findings, Lavagnino et al. (2017) found waviness in tendons to be reflected by cellular tension and governed, in part, by the contraction mechanism of the cells (Mehdizadeh et al., 2017). The force that induced the cellular contraction mechanism that can alter the crimp or waviness of the tendon (Lavagnino et al. 2017),

is miniscule compared to the applied load to the tendons in this study. The contraction mechanism may work as a reset of cyclically loaded induced loss of waviness.

Further, the contradiction between the presented work and the findings of Lavagnino et al. (2017) is perhaps due to the variability between the continuous and categorical variables used in the current study. Since the waviness is a continuous variable (0-1) and tenocyte morphology is a categorical value (Cat 4, Cat 3, Cat 2, Cat 1), it may not be the proportional change of both domains but the sensitivity of having a categorical classification for tenocyte roundness that perhaps caused the contradiction between the contradictive findings. Therefore, the loss of spindle shape seems a very sensitive measure and one must consider that the four categories of morphology may warrant further research, although there is a systematic change in the level of roundness during the loading phases. It is also noted that the roundness categories had greater variability and noise in the assessment, especially in the higher strain cohorts (see Figures 4.23, 4.24, and 4.25). Given that the loss of the spindle characteristic is the key observation then this is a critical marker for morphological changes in tendons following micro-damage and is likely related to the failure of the integrity of specific associated fibres causing reduction in the mechanical properties. Future research may wish to examine if there are sub-categories of spindle like thresholds that reflect mechanical impact on tenocytes than the threshold use in this study. After all, the threshold of loss of spindle like Cat 4 was based on a cancer research model and used for the first time in tenocyte methodology.

Although tenocytes are known as mechanosensitive (Lavagnino et al., 2015; Wang et al., 2018), the governing mechanisms that change the cell strain environment and disturb the cell-matrix interactions are still unclear. However, the sensitivity of tenocytes to mechanical stimuli may have triggered the structural changes and behaviour in tenocyte morphology from spindle to round shape as a response to loading. Findings of changes in tenocyte morphology with fatigue loading may have vital implications about local cell behaviour for clinical studies, providing justification for alterations in gene expression and cell imaging observed in other studies.

Future research may examine live cells to determine if these structural changes mediate the failure of tenocyte mechano-transduction in the cell-matrix interactions

under different loading protocols. Furthermore, this study highlights the significance of the tenocyte morphological characteristics and their contribution to important information associated with the mechanisms of tendinopathy. Fatigue micro-damage may play a vital role in the initial tenocyte response to damage as the tenocyte category changes. Therefore, understanding the interactions between tendon cells, fibres and the surrounding matrix and the fatigue damage mechanisms by which these are influenced warrants further investigation.

For the entire period of the mechanical intervention, there was no difference in fibre anisotropy between any of the strain groups. No marked difference was observed between all groups for all time points. All the differences in fibre anisotropy existed during the preconditioning of the samples. This warrants a specific discussion on the role of preconditioning.

Firstly, the anisotropy of fibres slightly declined in the three groups during preconditioning. However, as expected, the anisotropy for the 3% group was twice as high as both the 6% and 9% groups for all time points (see Figure 4.28). This is attributable to the excessive loading (Wren et al., 2003; Sereysky et al., 2012) and higher strain levels that can cause disruption to collagen fibres and their anisotropy, which then can adversely affect the mechanical behaviour of the bulk tendon. However, our results are not in line with previous reports (Lujan et al., 2009; Miller et al., 2012; Thomas et al., 2012) and suggest that anisotropy is likely a non-significant metric for any fatigue damage in tendons that undergoes prolonged loading regimes. For example, Ros et al ((Fung et al., 2010; Ros et al., 2019) did a study of 500 cycles whereas the preconditionong of this study was 720 cycles.

The current findings are not consistent with the work by Fung et al. (2010) that reported more anisotropic fibres in the high-level damage group and a statistically significant correlation between anisotropy and high levels of damage (Fung et al., 2010). It seems that differences in anisotropy among groups are only remarkable in stress-mediated and not strain-mediated repeated loading. Early changes may happen but unless the stress is increased then the differences in anisotropy in the different groups remains unchanged.

The current findings concur with a previous report on the role of preconditioning in explaining the realignment of fibres (becoming anisotropic) reporting that most of the collagen realignment seem to be caused by preconditioning (Miller. et al., 2012). This may explain the lack of anisotropic differences between all groups observed in the preconditioned and highly aligned three groups. Consistent with the suggestion by Miller et al. (2012), this indicates a tissue structural response to load that can occur after applying a small amount of load and not due to a large number of cycles.

5.6 Macro-morphological Outcomes in GAG-depleted Tendons During Mechanical Loading (Study 2)

A. Quantitative and qualitative - confocal and histological assessments

It was difficult to run reliable GAG-depletion and nondepletion testing protocols concurrently so this thesis undertook a second study that addressed the impact of depletion of GAG from tendons. The testing protocol repeated a subset of dose (6% strain for the two hours) for control and GAG-depleted tendon groups. The control group in the GAG-depleted study was compared with the Study 1 tendons with the same loading profile. As a result, this model was able to compare the reliability of all variables for this loading profile. This contributes significantly to the robustness of the data and shows the repeatability of the overall testing protocol.

Data generated from the quantitative assessments demonstrated structural changes that seem broadly consistent with changes observed in tendinopathic tendons reported by previous GAG- depletion-based studies (Lynch et al., 2003; Fessel & Snedeker, 2009; Rigozzi et al., 2009; Legerlotz et al., 2013). Similarly to the qualitative and quantitative outcomes in the main study, the results obtained are consistent with the presented hypothesis that there is a sequential dose change effect on the tested derived variables of the examined macroscale domains in the fatigue-loaded GAG-depleted tendons.

This is the first study that has quantified the relationship between microstructural characteristics (waviness, tenocyte morphology and fibre anisotropy) and broad viscoelastic mechanical measures (ML, *h* and *k*) in GAG-depleted tendons. The quantitative relationships between microstructural and mechanical measures have been reported previously in only one previous study (Robinson et al., 2004). Interestingly, the work of Robinson et al. (2004) demonstrated GAG content as a strong marker for mechanical properties and showed that it was strongly correlated with mean collagen fibril diameter and tendons collagen content. Although they have shown strong correlations between structural and mechanical measures, the structural measure (fibril diameter) used was not within the scope of our tested structural domains. This may warrant further investigation.

However, only a few studies have examined the qualitative structural relationships of GAG-depleted tendons with (Screen et al., 2005; Screen et al., 2006; Svensson et al., 2011) and without their mechanical properties (Franchi et al., 2010). In the current study, the quantitative analysis of the GAG-depleted group and the control group demonstrated a progressive change in tenocyte morphology (roundness) and fibre waviness. These changes clearly exhibited distinctive levels of damage in the GAG-depleted tendons and their controls (see Figures 4.52 and 4.53), whereas there were no marked changes in the anisotropy of fibres, in agreement with the findings of Study 1.

The 6% strain group and the control group were very similar in their structural and mechanical changes (see Figures 4.7, 4.9, 4.32, 4.33, 4.34, 4.55, 4.56, 4.57, 4.61, 4.62 and 4.63). Removal of the GAG from tendons impacted on both the form (morphology) and function (mechanics) of the tendons. The control group replicated the data from the matched tendon from Study 1 and therefore this suggests that these changes are specifically related to the GAG depletion. The GAG-depleted tendons had damage profiles that were significantly increased in magnitude compared to the control tendons and these changes happened at earlier time points. This parallels the observations of tendons exposed to a greater strain (i.e. 9%) in the main study.

This damage suggests that the balance between fibre elongation and sliding was more impaired in the GAG-depleted group than the control group, possibly due to the

removal of the GAG cross-linkages. This supports the literature which suggests the important role of GAGs in the tendon's structural integrity, and their mechanical function as nano-connecters in transferring the load across adjacent fibrils (Screen et al., 2005). With an increased number of repetitive loadings, by the end of the second hour, the damage in the GAG-depleted group (see Figures 4.76, 4.77, 4.78, 4.79) was in line with the suggestions reported by Krajcinovic (1985), Lee et al. (2017) and (Screen et al., 2005) and may be explained by the proposed model that this reflects more irreversible damage (as inter-fibrillar sliding) at the nanoscale level (Krajcinovic, 1985; Screen et al., 2005; Lee et al., 2017).

It is proposed that with the increased response of the GAG-depleted fascicles to load and the consequential impact on the macroscopic properties, the mechanical properties of the tendon may be more heavily impacted in the GAG-depleted group than the control group (Screen et al., 2005). Although there were and a significant decrease in *h, k* and ML in the control and GAG-depleted groups (see Figures 4.7 and 4.9), the damage intensities and damage fractions seen in the GAG-depleted group were greater by the end of all time points. This would suggest that the structural damage in the control group did not affect the tensile characteristics of the fibres. Therefore, the increased waviness and inter-fibre space seen in the disorganised collagen fibres existing in the control group was perhaps governed by other mechanisms. However, the increased intensities and damage fractions seen in the GAG-depleted group would suggest that these were caused by the removal of GAGs from the tendons. Further, the increase in damage seen for the GAG-depleted groups might be largely caused by lower inter- and intrafascicular water content following their removal. And to some extent the effects of decreased water content may have been exacerbated by not conducting testing in solution.

The clinical literature attributes similar patterns of damage to be governed by degeneration and repair with repeated loading. This is sometimes related to an acute inflammatory response, and also to an imbalance existing between the degeneration and repair cycle. There is limited objective data showing such multiple-scale changes in a clinical setting and therefore it is unclear if clinical observations are consistent with *in-vivo* or *ex-vivo* models. The current study paradigm opens an opportunity to examine such models to validate this assumption in the clinical context.

Taking all comparisons between the GAG-depleted and control groups together, the current findings support the suggestion in the literature that GAGs play a fundamental role in controlling the elongation and sliding mechanisms between collagenous units at different hierarchal levels (fascicles, fibres and fibrils) that consequently influence both local and gross matrix mechanical properties (Minns et al., 1973; Ruggeri et al., 1984; Cribb et al., 1995; Sasaki & Odajima, 1996; Fratzl et al., 1998; Redaelli et al., 2003; Screen et al., 2005; Liao & Vesely, 2007; Legerlotz et al., 2013) and facilitate the structural integrity of the collagen matrix. These observations are supported by the results from the current AFM-based study (more detail in Section 5.8) that showed higher levels of strain (elongation) expressed as higher D-periodicity values in fibrils (≥ 10 nm) were seen in the GAG-depleted group compared to the control group (see Figures 4.76, 4.77, 4.78, 4.79).

With the increased damage magnitude and distribution as observed by the end of the first hour in the GAG-depleted group, a significant rapid decrease in *h* and *k* was observed as early as the end of the first 30 min. During this stage, there seemed to be a change in the mechanical adaptation that had been impacted by the removal of GAGs. It is clear that *h* was the most sensitive measure to GAG depletion.

The transverse network of fibrillar linkages that are likely to facilitate the transfer of load to the neighbouring fibres (Scott, 1988), may be adversely influenced by a heavily impaired load-sharing mechanism. The removal of the GAG crosslinks, may heavily impair the redistribution of local strain among various portions of fibres to other fibre portions in the tendon. This perhaps leads to the dramatic changes observed in the mechanical properties.

Quantitative assessment has demonstrated a progression change in tenocyte morphology from spindle-shaped to slightly round in both the GAG-depleted and control groups (see Figures 4.55, 4.56, 4.57, 4.58, 4.59 and 4.60). The changes in the control group are consistent with the changes seen in the moderate (6%) strain group in the main study thereby asserting that the measurements were repeatable.
Significant progressive categorical shifts were observed in tenocyte morphology (from spindle to round) in the control groups with an increased number of cycles of

mechanical loading (see Figures 4.52, 4.55, 4.56, and 4.57). The findings in this study concur with the findings by Szczesny et al. (2017, 2018) and Chao & Tseng (2014) who observed other structural changes (e.g collagen fibre kinking and molecular denaturation) to precede tenocyte morphological changes (Chao & Tseng, 2014; Szczesny et al., 2017; Szczesny et al., 2018). For example, the proportional change in fibre waviness was higher than proportional change in tenocyte morphology for both control and GAG-depleted groups (see Figures 4.52 and 4.53). However, the proportional changes of the same domains were greater and occurred earlier in the GAG- depleted group for all time points.

These findings concur with the literature on the remodelling activities of tenocytes (Riley, 2008; Spiesz et al., 2015). Based on this, our findings, perhaps, are attributed to GAG depletion slowing the timescale of remodelling activities of the tenocytes. These remodelling activities may be influenced by the impaired load transfer between adjacent fibrils. The removal of GAGs may lead to an impaired pericellular integrity and cell-matrix interaction. This, therefore, can impact the ability of the resident tenocytes to interact with and respond to their native tissue environment, impacting the ability of these tenocytes to trigger reactive tendinopathy (Cook et al., 2009) and tissue remodelling through mechanotransduction pathways (Screen et al., 2003). This, however, is hypothetical in the fact that this study is undertaken on non-viable tendons and therefore the changes in GAGs in the biological recovery and repair models also warrants further investigation.

Taking into account the vital role of facilitating the load transfer between adjacent fibrils and preserving the tissue integrity of the loaded tendons in the control group, the GAGs role perhaps has assisted the resident tenocyte activities in their native tissue environment. Consequently, the assistance of tenocytes may lead to loading at the microscale rather than over-stimulating the matrix (Lavagnino et al., 2006; Arnoczky et al., 2007; Hakimi et al., 2017; Mehdizadeh et al., 2017) causing later changes in the mechanical properties compared to the GAG-depleted group. It may be conjecture, but possibly the GAG in biological tissue may be a mechanism to transfer or mediate load to other parts of the tendons and therefore future research may examine how these loading profiles may alter when GAG depletion occurs unevenly within the full tendon structure.

5.7 Nano-morphological Outcomes in Study 1

A. Quantitative AFM assessment

The highly accurate morphometric imaging of AFM, together with the experimental approach used in this study allowed precise imaging of the strained fibrils in their nanostructural network. This provided a unique insight into the effect of load-bearing on the tendon's fibrils. To assess fibril elongation, the axial D-periodicity of collagen fibrils was assessed after different loading protocols. To the best of our knowledge, this work is novel, being the first to quantify the relationship between the nano-morphological changes (D-periodicity changes) and the macro-mechanical viscoelastic properties of tendons.

As hypothesised based on the prior work of others (Sasaki & Odajima, 1996; Puxkandl et al., 2002; Gupta et al., 2010; Rigozzi et al., 2011; Connizzo et al., 2014; Connizzo et al., 2015), this study demonstrated that there is a sequential dose and strain change effect on the D-periodicity values. The D-periodicity increased under strain with statistically smaller D-periodicities observed in lower strain groups compared to higher strain groups with a lower number of repetitive loadings (see Figures 4.65 and 4.53 and see Table 4.11).

The strain modulation protocol used showed that strain is an overall driver for D-periodicity changes. The strain remaining constant also means that after a while the load is significantly reduced and yet the D-periodicity still continued to change (Figure 5.1). Our findings also concur with previous reports that the overall fibre strain is higher than the overall fibril strain (Misof et al., 1997; Fratzl et al., 1998; Puxkandl et al., 2002).

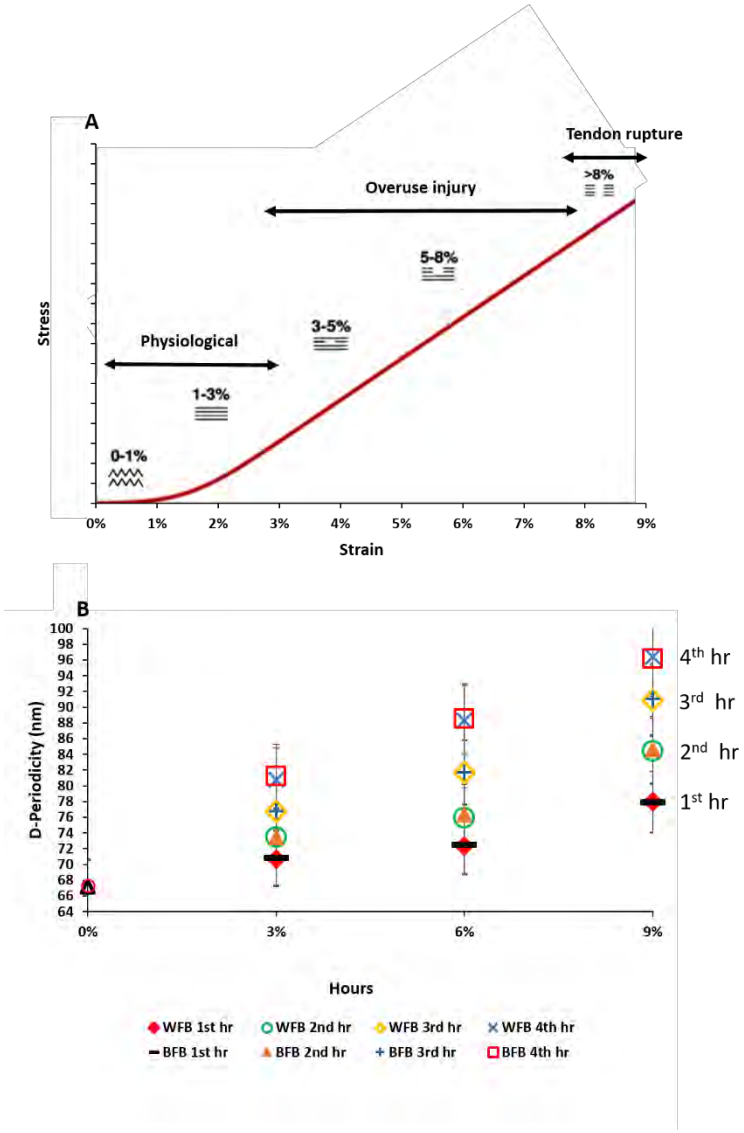

Figure 5.1. The change in D-Periodicity as a function of the macroscopic strain in the 3%, 6% and 9% strain groups at the first, second, third and fourth hour of repetitive cyclic loading. (A) The macroscopic applied load for the whole tendon. Modified from (Józsa & Kannus, 1997; Arnoczky et al., 2007). (B) The measured length of WFB and BFB D-periodicities. At 6% and 9% strains, the increase in the WFB and BFB D-periodic length is statistically significant (asterisks indicate a p-value < 0.0001, NS denotes non-significant). No significant differences were found between the 0% (control) and each of the three strained groups 3%, 6% and 9% over the duration of loading.

Collagen fibres are composites, consisting of stiff fibrils embedded in a soft matrix of hydrated PGs and their associated GAG side chains including chondroitin sulfate and

dermatan sulfate. The GAGs, which are mainly dermatan sulfate (DS) in tendons (Minns et al., 1973; Ruggeri et al., 1984; Koob & Vogel, 1987; Cribb et al., 1995; Sasaki & Odajima, 1996; Fratzl et al., 1998; Redaelli et al., 2003; Screen et al., 2005; Liao & Vesely, 2007; Legerlotz et al., 2013) is attached covalently to the core protein decorin , demonstrating an orthogonal structure aligning relative to the collagen fibrils (Weber et al., 1996) supporting the notion that GAGs are considered to be extended chains connecting the neighbouring fibrils and acting mainly as a shear load transmitter from one fibril to its neighbouring fibrils (Scott, 1992; Cribb et al., 1995; Redaelli et al., 2003; Liao & Vesely, 2007). Therefore, these crosslinks between the fibrils of the low strain group (3%), may facilitate the inter-fibrillar sliding suggesting that the tissue's resistance to load is derived mainly from inter-fibril elongation and sliding mechanisms (Puxkandl et al., 2002; Silver et al., 2002) protecting fibrils from overstrain. The inelastic deformation assists the tendon to elongate further at higher hierarchies without provoking complete failure of the fibrils.

This is in line with a previous attribution of this behaviour as the macroscopic crimp elongation that seem to disappear almost after 5% strain in tendon fibres (Misof et al., 1997; Fratzl et al., 1998). The tendon structure in this study in the 6% group seemed to be complete under load and a rapid decline was observed afterwards in *k*, *h* and ML in both the 6% and 9% groups over the first, second, third and fourth hour of repetitive cyclic loadings (see Figures 4.3 and 4.6). Concomitantly, the fibrils began to incrementally bear the increased number of repetitive cyclic loadings over the same duration of mechanical loading. This is attributed by the incrementally significant increase seen in the WFB and BFB D-periodicities at 6% and 9% targeted strains (Figure 5.1B) and by the increased density and severity of kink patterns of local fibrils, and increased marked areas of fibril rupture and recoiling evident from AFM images of the 6% and 9% groups (Figure 4.64). These nanostructural and mechanical concomitant changes are likely attributed to an exceeded physiological strain limit (Józsa & Kannus, 1997; Arnoczky et al., 2007) (Figure 5.1A) and to the loss of load-bearing capacity (Fung et al., 2010; Ros et al., 2019) among various portions of fibril bundles. Critically however, the loading protocol was a controlled strain protocol; therefore, the damage relates to the transfer of stress across the tendons sub-units in combination with the number of cycles. Since fibrils slide past one another (Mosler et al., 1985; Folkhard et al., 1987; Sasaki & Odajima, 1996; Puxkandl et al., 2002; Silver

et al., 2002) some fibrils are bearing increased nonuniform stress concentrations, inducing abnormal/higher load concentrations (Maffulli, 2011) and a higher number of overloaded fibrils in the loading areas in the 6% and 9% groups.

As a protection mechanism from overstrain, the contribution from fibrillar sliding is represented as a relative stretching of tropocollagen molecules and a change in the length of the gap zone. With increased number of cycles in both 6% and 9% groups, parts of or complete GAG sidechains have become detached from the fibrils and are therefore inactive (Figure 5.2). The remaining load transmitters continue to transfer load from one fibril to its neighbouring fibril, until complete macroscopic failure occurs, when load descends to zero instantly. Figure 5.2 shows this proposed model of deformation as a schematic illustration.

This is in good agreement with results reported in our study that the AFM analysis demonstrates higher intensity and severity of damage in the 9% group as larger WFB and BFB D-periodicities are concomitant with a greater density and severity of kink patterns in local fibrils, increased marked areas of fibril rupture and recoiling than seen in the 6% group (Figure 4.64).

The damage progression demonstrated here is similar to the fibre-reinforced composite behaviour, where failure exists from the formation of concentrated stresses at the local aggregations of fibre rupture (Okabe et al., 2001).

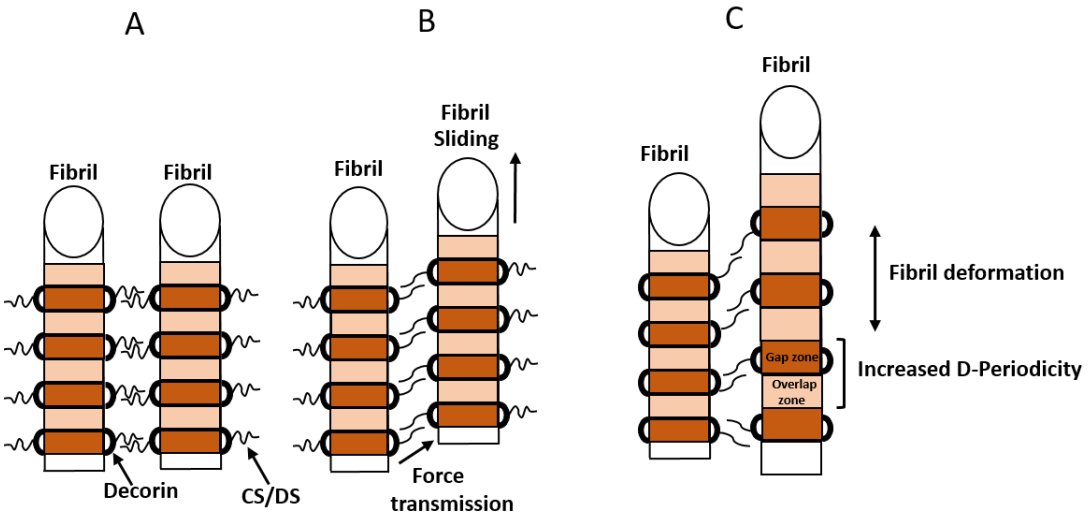

Figure 5.2. A schematic representation of the deformation and failure model at the fibrillar level. (A) Two unloaded fibrils connected with GAG side chains (black zigzag pattern). (B) Elastic linear region (< 5 % strain) – sliding of fibrils and the removal of kinks in the molecular gap regions. (C) Inelastic linear region (> 5% strain) – tropocollagen molecules start to slide past one another. Strained cross links (GAGs) are attached to the fibrillar surface via their core protein Decorin at the D-periodicity molecular gap zones).

The number of cyclic loadings was a significant factor in increasing the WFB and BFB D-periodicities in all strained groups (Figure 5.1). As tendons were strained dynamically to 3%, 6% and 9% of the stress-strain curve (Figure 5.1A), these strained groups demonstrated a statistically significant increase in the WFB and BFB D-periodicity length with the increased duration of repetitive cyclic loading (see Figure 4.65 and Table 4.11) ($P < 0.0001$).

These findings are in line with the clinical literature that states that similar patterns, governed by repetitive accumulation of microtrauma, may lead to an imbalance in the equilibrium between the cellular rate of repair and the rate of damage (Archambault, 2003; Archambault et al., 2005; Maffulli, 2011). There is limited objective data showing such changes in the clinical setting and therefore it is unclear if these clinical observations are being influenced by *in-vivo* or *ex-vivo* models. The current study paradigm opens the opportunity to examine such models to validate this assumption in the clinical context.

Our findings also concur with previous reports on the difference between fibril strain and applied strain at the macroscale level where the overall fibre always seems to have a higher strain than the individual fibril (Fratzl et al., 1998; Puxkandl et al., 2002; Rigozzi et al., 2011) suggesting the occurrence of relative movements within the matrix. Beyond 5% strain, the elongation of D-periodicity is suggested to explain nearly 40% (Puxkandl et al., 2002) and 50% (Fratzl et al., 1998) of the measured elongation of the applied fibre strain. Similarly, the findings in this study (Figures 5.1B and Table 4.11) also suggests that the WFB and BFB D-periodicities significantly increased at 6% strain. However, the increase in WFB and BFB D-

periodicities accounted for ~31% (in the current study) and 20% (in Rigozzi et al., 2011) of the incrementally applied tendon strain.

The differences between our findings and those of Rigozzi et al. (2011) compared to those by Puxkandl et al. (2002) and Fratzl et al. (1998) are likely attributed to the various applied methodological approaches used to quantify strain under mechanical load (Brodsky et al., 1980; Sasaki et al., 1999; Kukreti & Belkoff, 2000; Franchi et al., 2010). For example, the studies of Puxkandl et al. (2002) and Fratzl et al. (1998) were based on a stress modulation and employed scattering X-ray spectroscopy for measurement. Whereas the current study and that of Rigozzi et al. (2011) are based on a strain modulation and use AFM for measurement.

Furthermore, the differences in study outcomes are likely attributed to the different hierarchical complexity between the tested whole tendons used in our study and that of Rigozzi et al. (2011) and the isolated fascicles used in other studies (Screen et al., 2005; Svensson et al., 2011). Therefore, the mechanism by which the structural hierarchy in tendons is related to the variation in mechanical strain warrants further investigation.

Statistical analysis in previous reports suggests that the D-periodicity distribution is 10 nm at the bundle level (Wallace. et al., 2010; Fang et al., 2012; Erickson et al., 2013); however, another recent study has suggested a smaller distribution, only 2.5 nm (Su et al., 2014). However, the singular D-periodicity value of 67 nm is broadly established as the normal D-periodicity value. If the large range of distribution is true, it can challenge the widely accepted knowledge about collagen. But, the distribution of the D-Periodicity populations varies in the literature – +/-10nm (Erickson et al., 2013) to 2.5nm (Su et al., 2014) . For example, several detailed Type I collagen models of fibrils and their sub-content in various tissues are based on the singular D-periodicity value of 67 nm (Piez & Trus, 1981; Holmes et al., 1998; Orgel et al., 2001; Orgel et al., 2006). Importantly, the studies that suggest the large distribution of D-periodicities did not consider the technical error resulting from thermal drifts in imaging.

However, other important potential and technical factors may result in a larger variation in the D-periodicity values including the hydration of the scanned sample, the resolution of an image and different scanning angles of the image (Su et al., 2014). A recent conflicting work by Erickson et al (2013) has shown that thermal drift and various angles of image scanning are negligible as reflecting a minimal variation of only 2 nm between different fibrils scanned at different angles (Erickson et al., 2013). Their work suggested that a large distribution of D-periodicity values (up to 10 nm) existed in different tissues that did not undergo any mechanical intervention (Erickson et al., 2013).

The hypothesised difference between the WFB or BFB D-periodicities was not supported by the results of this study. The inconsistency between our findings and those that reported a large D-periodicity distribution (up to 10 nm) among different fibre bundles existing in different tissues (teeth, bone, tendons and skin) (Wallace et al., 2010; Fang et al., 2012; Erickson et al., 2013) is likely attributed to effects of repetitive loading on the non-uniformity of the fibrils of the loaded tendons. These fibril bundles are likely to demonstrate a non-uniform (Arndt et al., 2012; Slane & Thelen, 2014) regional strain behaviour during passive elongation, with the maximum strain found in the superficial layer (Bogaerts et al., 2016). In line with this, the fibril bundle distribution in the current study was larger with a higher level of strain and number of cycles among the three groups. In other words, the differences in the WFB and BFB D-periodicity would be expected to significantly increase with higher strain levels and larger amount of repeated cyclic loading. However, there were no differences observed between the WFB and BFB D-periodicities among all groups. This is likely attributed to the maintained preconditioning effect. It is possible that the preconditioning in our mechanical protocol, prior to the prolonged mechanical intervention, may have reduced the overall non-uniform strain distribution across the structural hierarchies of the tendon and therefore, affected the non-uniform behaviour of fibrils. This concurs with the previous suggestion by Miller et al. (2012) and Quinn et al. (2012) that the realignment (anisotropy) of the fibrils and the fibril bundles may occur in the loading direction through a progressive fibril or fibril bundle recruitment. The anisotropy data in the current study clearly shows that all the changes occurred in the preconditioning stage.

Therefore, it appears that the fibrils from the same fibre bundle and others from different bundles have deformed homogeneously and behaved uniformly (a continuous increase in D-periodicities among higher strain levels with higher number of cyclic and static fatigue loading). This is further supported by previous studies that have shown significant changes in the transverse morphology (e.g. the antero-posterior diameter of the tendon) following contractions in non-preconditioned Achilles tendons (Fahlstrom & Alfredson, 2010; Grigg et al., 2012; Wearing et al., 2013) while other reports have shown minimal or no effect (e.g. in the cross-sectional area) when the tendons were preconditioned (Farris et al., 2012; Lichtwark et al., 2013; Obst et al., 2016).

Realignment is the main mechanism of preconditioning, explaining the increased tendon stiffness observed after preconditioning in the highly ordered fascicles and fibres of the tendon (Connizzo et al., 2013). This indicates that tendons may structurally respond after applying a minimal amount of load. However, this response seems to be associated with communication between fibrils where they play a vital role in controlling the load transfer process across tendon structural hierarchies. The non-uniformity of different fibre/fascicle bundles is influenced by preconditioning. The ability of fibrils to rearrange and reorient themselves somehow indicates a connection between them, whether through hydrostatic forces or friction between them or their attached GAG chains (Connizzo et al., 2013). Our data on the anisotropy of the three strained groups that shows only non-significant differences between these groups over the entire course of mechanical intervention, clearly supports the rearrangement of the fibril bundle non-uniform behaviour.

Qualitative AFM assessment

Three-dimensional (3D) AFM imaging of the tendon's microstructure allowed qualitative assessment of the tendons (see Figure 4.64). The morphology clearly showed distinct types of damage which were not observed in the non-loaded (preconditioned) tendons. The progression of markers of observed damage that were associated with changes in the mechanical properties may provide a better understanding of the physical progression from overused tendons to tendinopathy at the nanoscale level.

As expected, in the first hour of loading the 3% strain group did not show any damage, in agreement with the lack of significant changes in the mechanical properties (*k*, *h* and ML) of this group in the first hour. This is evidenced by the AFM images that demonstrated highly aligned collagen fibrils with no fibril kinks except a few minor occurrences of fibril separation (see Figure 4.64). This indicates that this loading is within the elastic linear region and is in line with the suggestion that strain levels less than or equal to 4% are physiological in nature (Curwin, 1994; Kirkendall et al., 1997).

As expected, after four hours of loading, the 3% group showed cycle-dependent damage with concomitant increased changes in the mechanical properties. The damage is evidenced by the AFM images that demonstrated increased fibril kinks (see Figure 4.64). The 6% and 9% strain groups showed strain-dependent severity of damage when the nano-damage was compared to that seen in the 3% group. Furthermore, cycle number-dependent damage was also evident in the 6% and 9% groups (see Figure 4.64).

For the 6% group, the cycle number-dependent damage is evidenced by the increased accumulation of fibril kinks and fibril separations seen by the end of the first hour and the increased severity and damage area with the higher number of cycles (as seen by the end of the second, third and fourth hours) with some ruptured areas by the end of the fourth hour (see Figure 4.64). Evidence of kink accumulation and increased fibril separations suggest that some fibril sub-sets are unloaded and other subsets are overloaded (Bojsen-Møller et al., 2019). The fibril kinks had disruptions seen as localised points, similar to those reported previously by Herod and Veres (2018). Mostly, these disruptions at the fibril kinks did not seem to have discrete plasticity patterns as seen over the whole fibril length. These findings are similar to disruptions seen in previous studies (Veres & Lee, 2012; Veres et al., 2013, 2014). For the 9% group, the damaged area, density and severity were larger than for the 6% group for all time points. The increased serial density of kinks seen as severe kink patterns on locally damaged fibrils with the disappearance of D-periodicity was evident by the end of the second and third hours. The increased groups of elastic recoil of damaged fibrils were also observed at the ruptured sites by the end of the fourth hour.

In comparison with the 3% group, the increased damage area, density and severity seen in the AFM for the 6% and 9% groups corresponded with significant changes in mechanical properties. This indicates that prolonged over-loading of the 6% and 9% groups that caused nano-damage can be attributed to an exceedance of the physiological strain limit that is concomitant with the damage and rupture seen at the macroscale level in the main study. Critically however, the loading protocol was one of controlled strain. Therefore, the damage relates to the transfer of stress across the tendon sub-units through the number of cycles.

This study demonstrates that structural changes, mechanisms of fatigue damage, and the increased intensity and severity of nanostructural damage accumulation in Achilles tendon are all dependent on the strain level and number of cycles. Since the elongation changes in fibres are dependent on the changes in the fibre kink, our results propose that the nanoscale kink changes were both cycle- and strain-dependent. The strong changes in stiffness with the corresponding increase in density, severity and area of damage of fibrils, reflects that mechanical outputs (function) are a manifestation of these changes in structure (form).

Early kink formation and increased interfibril spacing as observed in the 3% group are indicative that some fibrils are loaded and others are not. The 3% group had minimal nanostructural changes – non-disrupted collagen fibrils with only minimal widening of the interfibril space (see Figure 4.64) and the existence of a low density of fibril kinks with the concomitant mechanical decline – and these are likely attributed to the redistribution of load from damaged to undamaged fibril bundles at the microscale level (Thornton et al., 2003).

However, nanostructural changes (increased density and severity of kink patterns of local fibrils, increased marked areas of fibril rupture and recoiling) as observed in the 6% and 9% groups with the concomitant significant mechanical decline, are likely attributed to a loss of load-bearing capacity (Fung et al., 2010; Ros et al., 2019) among various portions of fibril bundles.

Since fibrils are sliding past one another, some fibrils are bearing high local strain leading to severe deformations and ruptures. This is supported by the fact that in the

6% and 9% groups with an increased number of cycles, the severity of damage increases, with a higher number of fibril kinks and some complete rupture of fibrils seen by AFM (see Figure 4.64). The increased severe damage associated with the increased number of cycles may cause higher stress concentrations in the loading areas or impair localised cells outside these damage areas. The damage progression demonstrated here is similar to fibre-reinforced composite behaviour, where failure exists from the formation of concentrated stresses at the local aggregations of fibre rupture (Okabe et al., 2001).

Our results provide evidence of the novel strain- and cycle-dependent mechanism of damage accumulation in fibrils including nanostructural characterisations of density and severity of damaged areas and the corresponding mechanical changes.

5.8 Nano-morphological Outcomes in GAG-depleted Tendons (Study 2)

A. Quantitative AFM assessment

Our previous quantitative assessment on the macroscale level shows the importance of the role and contribution of PG-GAGs to tendon mechanical and microstructural properties. Here we use AFM and enzymatic GAG depletion using Ch-ABC to investigate the mechanisms by which GAG sidechains regulate fibril load sharing. The nanostructural response of the GAG-depleted and control groups was quantified by assessing the fibril D-periodicities among different fibre bundles (BFB) and WFB.

The observed structural differences generated from our data, measured as differences in D-periodicities between the GAG-depleted and control groups, are likely attributable to the functional differences resulting from differences in GAG content between both groups. The control and GAG-depleted groups demonstrated a progressive change in WFB and BFB D-periodicities characterised by marked increases in length over the periods of mechanical intervention (see Figure 4.76 and Table 4.13). However, there were no marked differences between the WFB and BFB D-periodicities over the two hours of the intervention.

The GAG-depleted group had ~40% fewer GAGs than the control group. Our results show that by the end of the second hour, there are significant higher D-periodicity values (higher fibril strain ~10 nm) in the GAG-depleted group than in the control group. Our findings are in the line with others that have demonstrated that fibril elongation and sliding contributed 10–40% of the full macroscopic elongation (Diamant et al., 1972; Misof et al., 1997; Fratzl et al., 1998; Puxkandl et al., 2002; Birch, 2007; Rigozzi et al., 2011). This percentage reflects the higher D-periodicity values in fibrils (≥ 10 nms) from the GAG-depleted group compared to the lower D-periodicities found in the control group that experienced the same mechanical intervention (Figure 5.3). Clearly the GAG-depleted group had significantly increased D-periodicity after the preconditioning. As a result, studies that have various GAG depletion levels would need to consider if the preconditioning is actually a standardisation or in some circumstances increases the variance across sample cohorts.

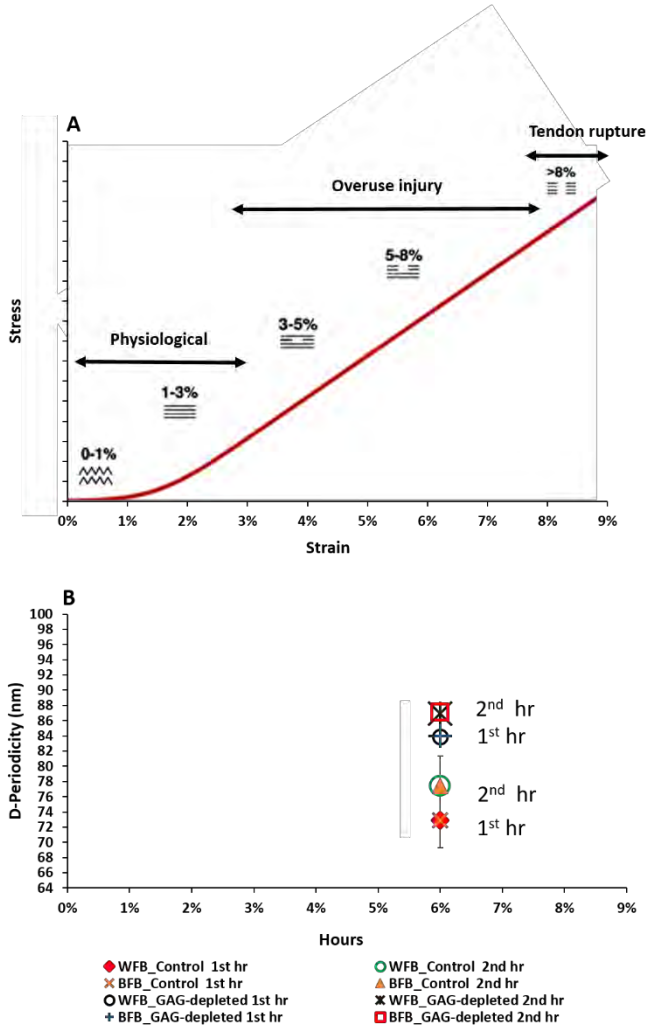

Figure 5.3. The change in D-Periodicity as a function of the macroscopic strain in the control and GAG-depleted groups at the first and second hour of repetitive cyclic loading. (A) The macroscopic applied load for the whole tendon. Modified from (Józsa & Kannus, 1997; Arnoczky et al., 2007). (B) The measured length of WFB and BFB D-periodicities.

In each of the two groups, the increase in the WFB and BFB D-periodicity is statistically significant from the first to the second hour ($P < 0.0001$). In both WFB and BFB, there are significant differences between the control and GAG-depleted group at the first and second hour ($P < 0.0001$). No significant differences were found between WFB and BFB D-periodicities in either of the two groups at the first and second hour of loading ($P > 0.05$).

Beyond 5% strain, the elongation of D-periodicity is suggested to explain nearly 40% (Puxkandl et al., 2002) and 50% (Fratzl et al., 1998) of the measured elongation of fibres. However, the increase in WFB and BFB D-periodicity lengths accounted for only nearly 29% of the applied tendon strain in our study and 20% in the study of Rigozzi et al. (2011).

The relatively lower increase of percentages in D-periodicity strains measured in both the current work and the work by Rigozzi et al. (2011) is likely attributed to the different methods used in measuring the fibril strain in our experiments (AFM) and the methods used in other studies (X-ray diffraction) (Fratzl et al., 1998; Puxkandl et al., 2002). Furthermore, the tendons assessed in our study and those by Rigozzi et al. (2011) have a more complex structure than those assessed in the study by Puxkandl et al. (2002) since the use of fibres mirrors a less realistic supposition of tendon homogeneity. Therefore, the difference is also likely attributed to different hierarchical level that was measured for the gross strain of tissue, presented as whole tendon in the current work and work by Rigozzi et al. (2011), and as measured fibres in the work by Puxkandl et al. (2002). This is supported by the suggestion that the fibrils, fibres and fascicles slide relative one to the other (Puxkandl et al., 2002; Screen et al., 2004; Thorpe et al., 2012; Ahmadzadeh et al., 2013; Szczesny & Elliot, 2014) and therefore, the total strain of each hierarchal level is different. Clarifying how the structural

hierarchies in tendons are related to the variation in mechanical strain of these hierarchies warrants further study.

Our findings are in agreement with the suggestion in the literature that the GAGs of the PG decorin play a vital role as mechanical connectors facilitating the load transfer between the fibrils (Minns et al., 1973; Ruggeri et al., 1984; Cribb et al., 1995; Sasaki & Odajima, 1996; Fratzl et al., 1998; Redaelli et al., 2003; Screen et al., 2005; Provenzano & Vanderby, 2006; Liao & Vesely, 2007; Legerlotz et al., 2013).

Our findings also support the suggestion in the literature that GAGs have a hydrophilic role in facilitating fibril sliding and probably protecting fibrils from overstrain (Koob, 1989; Kannus, 2000; Screen et al., 2006), and that the tissue's resistance to load is derived mainly from inter-fibril elongation and sliding mechanisms (Puxkandl et al., 2002; Silver et al., 2002). This is further supported by the observations in this study (and consistent with Rigozzi et al. (2010)) that lower GAG concentrations in the GAG-depleted group are positively and strongly related with reduced stiffness. Furthermore, this relationship was also seen with *h* and ML in the current study.

It seems that GAGs facilitate the shear load transfer across the fibrillar network. This is directly supported by the fact that depleting the GAG from the fibrillar network has clearly led to an increase in the WFB and BFB D-periodicities in the GAG-depleted group compared to control groups (Figure 5.3), although the fibrils from both groups bore the same strain (6%) and the same increased number of repetitive cyclic loadings over the first and second hour of mechanical loading.

In both variables, the WFB and in BFB D-periodicities, there are significant differences between the control and GAG-depleted groups at the first and second hour ($P < 0.0001$) (see Figures 4.76 and Table 4.13). These findings are in line with the notion of GAG as an extended chain of the binding decorin core protein, allowing the fibrils to assume an orthogonal structure, aligning relative to each other and bridging with the neighbouring fibrils (Scott, 1992; Cribb et al., 1995; Weber et al., 1996; Redaelli et al., 2003). With the removal of these structures from the core proteins, the fibrils in the GAG-depleted groups perhaps lost their viability in connecting and transferring forces to their neighbouring fibrils (Figure 5.4).

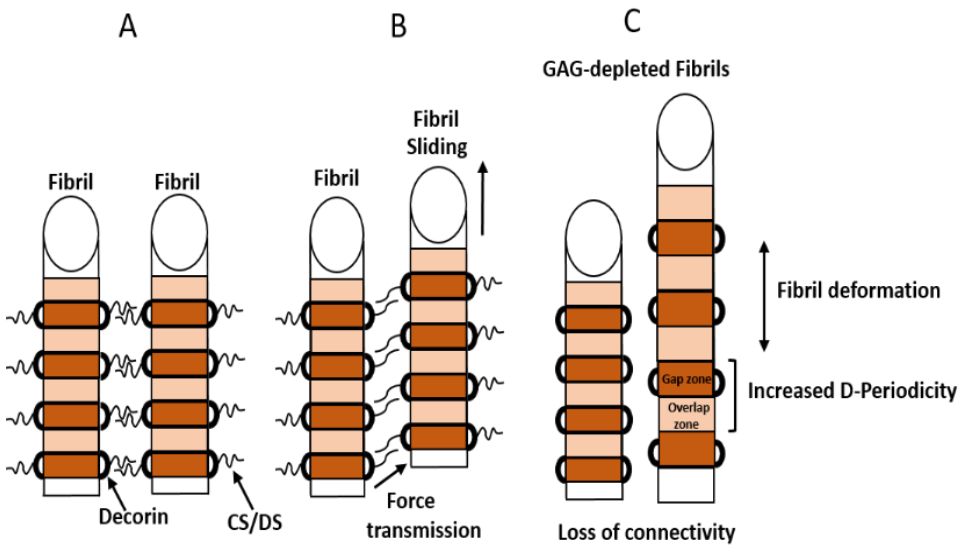

Figure 5.4. Schematic representation of the theoretical force transmission mechanism. Unloaded fibrils with their core protein decorin and attached glycosaminoglycan (GAG) (CS/DS) (A). Representation of force transmission via GAG (CS/DS) (B). One fibril is strained and started to slide in the direction of force (right fibril); through non-covalent interactions the connecting GAG transmits the force to the neighbouring fibril. (C). The GAG-depleted fibrils have loss of connectivity and are deformed with increased elongation in their D-periodicities (right fibril) with increased repetitive cyclic loading.

Since fibrils slide past one another (Mosler et al., 1985; Folkhard et al., 1987; Sasaki & Odajima, 1996; Puxkandl et al., 2002; Silver et al., 2002) as a protection mechanism from overstrain, the GAG-depleted fibrils would lose their connectivity or force transmission and the hydrophilic properties required to facilitate their sliding process as a result of the removal of the force transmitting-structures (GAGs). Consequently, these GAG-depleted fibrils bear more friction forces and increased nonuniform stress concentrations inducing abnormal or higher load concentrations (Maffulli, 2011) and a higher number of overloaded GAG-depleted fibrils in the loading areas. This may explain the higher severity of deformations and ruptures that existed in the GAG-depleted group.

These findings are supported by the fact that with an increased number of cycles, the AFM analysis showed a greater intensity and severity of damage in the GAG-depleted

group (demonstrated as larger WFB and BFB D-periodicities compared to the control). These fibril length changes were concomitant with a greater density and severity of kink patterns in local fibrils, and increased marked areas of fibril rupture and recoiling than seen in the control group (Figure 4.75).

The number of cyclic loadings was a significant factor in increasing the WFB and BFB D-periodicities (Figure 5.3). As tendons were strained dynamically to 6% of the stress-strain curve (Figure 5.3), all groups demonstrated a statistically significant increase in the WFB and BFB D-periodicities from the first to the second hour ($P < 0.0001$). However, the WFB and BFB D-periodicity lengths in the GAG-depleted group were significantly longer ($\geq$ 10 nm, $P < 0.0001$) at both the first and second hour of repetitive cyclic loading.

From the nano-morphological changes of the GAG-depleted tendons, we can confidently conclude that our findings support previous studies (Koob, 1989; Paavola et al., 2002; Screen et al., 2006) on the vital role of GAGs in force transmission, and the hydrophilic role of GAG, facilitating fibril sliding and probably protecting fibrils from overstrain. Therefore, the mechanical properties of different hierarchical tissue structures (fibres and fascicles) are likely to depend on the GAG content as it regulates the fibril sliding mechanism (Minns et al., 1973; Ruggeri et al., 1984; Cribb et al., 1995; Sasaki & Odajima, 1996; Fratzl et al., 1998; Redaelli et al., 2003; Screen et al., 2005; Liao & Vesely, 2007; Legerlotz et al., 2013).

B. Qualitative AFM assessment

As expected, both the control and GAG-depleted groups (6% strain) have shown a strain and cycle-dependent severity and area of damage as observed in the AFM images (see Figure 4.75). The nanostructural changes observed were similar to those seen in the main study. However, there was increased severity and intensity of damaged areas for the GAG-depleted tendons. Furthermore, the damage in the GAG-depleted group concurs with the generalised mode of fibril damage observed in previous studies (Veres & Lee, 2012; Veres et al., 2013).

A generalised mode of fibril damage was evident with increased serial density of kinks in the GAG-depleted tendons seen as severe kink patterns on local damaged fibrils. Also, the disappearance of the D-periodicities was evident and increased groups of elastic recoil of damaged fibrils were observed at the ruptured sites by the end of the second hour. In comparison with the control group, in the GAG-depleted group increased damage area, density and severity was seen under the AFM that showed concomitantly significant changes in mechanical properties (see Figure 4.75).

In addition to the increased density and severity of kink patterns of local fibrils, and recoiling, the nanostructural changes exhibited the focal damage mode as increased marked areas of fibril breakages and ruptures that are similar to the changes reported by Provenzano et al. (2005) (Provenzano et al., 2005). The focal damage observed with the concomitant decline in mechanical properties, is in line with a previous report by Ros et al. (2019) on the bearing capacity of fibres. The loss of load-bearing capacity among various portions of fibres means that load is likely to be redistributed to other healthy fibre portions in the tendon. Together, tendon assessments using CA (as in Study 1) and AFM (as in Study 2) on the role and contribution of PG-GAGs in mechanical and structural properties, provided new insights into the progression mechanisms of accumulation of damage in fatigue-loaded Achilles tendons.

The patterns and associations between the observed and mechanical profiles were similar to Study 1 but with a greater magnitude of decline in function (mechanics) and a concomitant decline in form (structure). Hence GAGs are important in in the maintenance of form and function in tendons.

5.9 The Association Between Mechanical and Macro-morphological Changes in Strained and GAG-depleted Tendons

Study 1

For the 3%, 6% and 9% strain groups

For all strains, the declining proportion of cells that are spindle-like and the increasing fibre waviness demonstrated a highly significant correlation with all mechanical properties (*k*, *h* and ML) (see Figure 4.80, 4.81, 4.82).

The non-linearity in waviness changes observed in the 3% group (see Figures 4.38, 4.39 and 4.40) is likely attributed to the existence of crimp angles that may influence the straightening rate of crimp and fibre recruitment (Screen et al., 2003). This suggests that the straightening rate of crimp and fibre recruitment were higher in the 6% and 9% groups since both groups have demonstrated a linearity in waviness changes during all-time points.

The changes in fibre waviness and tenocyte roundness properties observed in this study throughout the mechanical intervention were more dramatic than previous reports evaluating structural changes of tendon tissue with fatigue loading (Fung et al., 2010; Parent et al., 2011; Shepherd et al., 2013). Our study demonstrated a stronger association between these variables than other studies. For example, the correlations between the mechanical properties and the structural domains were highly significant regardless of the different magnitude of strain or duration (see Tables 4.1 and 4.2). This may be associated with the significant pre-conditioning undertaken in this study.

Possibly, the assessment of changes in fibre waviness and tenocyte roundness with fatigue loading mechanics in tendons offers a better mechanistic description than other measures reported previously, such as the damage area fraction (Fung et al., 2010). This is probably because our study mediated the load by strain not stress (to rupture). The strong relationship between the observed structural and mechanical changes in tendons demonstrates the significance of the use of *k*, *h* and ML as parameters for modelling the response of Achilles tendons to fatigue loading. Also, it shows the significance of the use of the structural changes as indicators for tendon failure progression. Future *in-vivo* research may examine if there are biological markers (e.g. ultrasound markers) that correlate with these changes to consider if these could be markers for specific damage and progression of injury (Torriani & Kattapuram, 2003; Hodgson et al., 2012; Purohit & King, 2015).the using

Study 2

For all control and GAG-depleted groups, the declining proportion of cells in the samples that are spindle-like and the increasing proportions of fibre waviness, demonstrated a highly significant correlation with all mechanical properties (*k*, *h* and

ML) regardless of the different magnitudes of strain and dose (see Tables 4.9 and 4.10).

The lag effect of the detection of the spindle change and mechanical drop off may be partly explained by the category measurement and the threshold of the decision to change from Cat 4 (spindle tenocyte) to Cat 3 (slightly round). This may suggest that a more objective assessment of spindle shape may provide some improvement in the threshold of mechanical failure. Dropped percentages perhaps reflects the maladaptive mechanical loading that the damage (as the categorical shift from Cat 4 to Cat 3) is progressed through. Biological models as described by Archambault (2003) have suggested that damage accumulation progressed through a maladaptive loading and/or non-equilibrium between the driven rate of cell repair and the rate of damage (Archambault, 2003). It is unclear if the changes in the mechanical profile would also be reflected by changes in spindle tenocyte prevalence.

Furthermore, all the correlations between the mechanical properties (*k*, *h* and ML) and roundness categories Cat 3, 2 and 1 were not clearly linear (polynomial) and showed weak associations for both the controls and GAG- depleted groups (see Figures 4.55, 4.56, 4.57, 4.58, 4.59 and 4.60). However, the GAG-depleted group showed stronger associations than those seen in the control group. It is likely that there is a threshold in the number of tenocytes that shift from spindle to round, at which the shift plays a prominent role in influencing adversely the pericellular matrix surrounding tenocytes. The number of rounder cells (particularly severely round cells (Cat 1)) were higher in the GAG-depleted group, and seems that this threshold was reached faster in the GAG-depleted group, due to the effect of the removal of GAG on both the elongation and sliding mechanisms that consequently affected the local and gross matrix mechanical properties. As more cells may become rounder, they may play a larger role in facilitating a larger damage distribution to the integrity of associated fibrils and fibres causing more significant changes in the mechanical properties. However, it is unclear if the changes in the mechanical profile would also be caused by changes in spindle tenocyte prevalence.

5.10 The Association Between Mechanical and Nano-morphological Changes (D-periodicity Changes) in Study 1 and Study 2

As hypothesised, all mechanical properties (*k*, *h* and ML) for the 3%, 6% and 9% strain, GAG-depleted and control groups have exhibited statistically significant correlations with the D-periodicity changes (WFB and BFB) regardless of the different magnitude of strain and dose (see Tables 4.12 and 4.14). For the 3%, 6% and 9% strain groups, the correlations have been linear. However, both the control and GAG-depleted groups demonstrated polynomial associations with the mechanical properties. In all groups, there was a significant decline in mechanical properties with increased strain and dose and a rapid increase in D-periodicity (WFB and BFB).

The strong correlation between the tendon nanostructure and the mechanical properties of the macro-structure indicates that the main facilitation of tendon mechanics and damage in fibres and fascicles occurs at the fibril scale. Our findings are consistent with the theories reported previously by Szczesny & Elliot (2014) and Lee et al. (2017) that the structural nanoscale (in fibril) damage is related to the changes in microscale (in fibre and fascicle) mechanical properties. Furthermore, nanoscale sliding mechanisms suggested in the literature and representing shear between nanoscale structures (fibrils and sub-fibrils), are likely associated with both loading (Szczesny & Elliot, 2014) and tissue damage (Lee et al., 2017) mechanisms at fascicle and fibre scales. The strong relationship between the nanostructural and the mechanical changes in our study demonstrates the significance of the use of *k*, *h* and ML as parameters for modelling the response of the Achilles tendon to fatigue loading. Also, it shows the significance of the use of the structural changes in the tendons as an indicator of the progression of tendon failure.

Taking together all the above mechanical and multiscale structural strong correlations, this is the first study to be able to correlate concurrent changes in a broad dynamic and static sustained mechanical assessments (i.e. *k*, *h*, and ML) with macro- and nanostructural changes (i.e. tenocyte spindle shape, fibre anisotropy and waviness and fibril D-periodicity) in tendons from strained, control and GAG-depleted groups.

The SR in this study is expressed as the decline in the stress over the static held length at three different points (SR1, SR2 and SR3). The SR at the maximum load was used to represent the total SR since these three cohort points (maximum, halfway and end) were highly correlated (R^2 = 0.87–0.99, P < 0.0001) for all tendons from all groups at all-time points. More detail is in Appendix 7. Since the maximum load SR was highly correlated with all macro- and nanostructural changes, this may provide an avenue for future investigations to examine whether SR is similarly correlated with nano- and macrostructural changes in tendons when tested in an *in-vivo* or *ex-vivo* static mechanical intervention.

5.11 The Multiscale Association Between Macro and Nano-morphological Changes

The WFB strains observed at the nanoscale level and measured for the 3%, 6% and 9% strain, GAG-depleted and control groups demonstrated a strong significant correlation with fibre waviness and tenocyte morphology (Cat 4) (see Figures 4.80, 4.81, 4.82, 4.83, 4.84 & see Table 4.15). For all groups, the WFB strains increased with increasing and declining proportions of fibre waviness and spindle-like shape (Cat 4), respectively. Most of the nano- and macro-morphological variables were associated in a linear pattern for all groups. In the strained groups, the strong correlations (R^2 = 0.74–0.91, P < 0.0001) demonstrate the strong relationship between the nano- and the macrostructural changes, consistent with our hypothesis that nanostructural changes in the three strain groups contribute to the macrostructural changes in Achilles tendons that were subjected to four hours of repetitive loading. It seems that the structural changes occur concurrently at multiple scales. The macroscale changes (as increased fibre waviness and change in tenocyte spindle shape) that affected tendon mechanical properties were influenced by changes at the nanoscale level (as changes in fibril D-periodicities that were used as a function for fibril elongation).

Our study demonstrated the interfibrillar structural damage as fibril kinks and discontinuities seen after applying fatigue loading. This is inconsistent with a previous study suggesting that the first stage of damage caused by inter-fibrillar sliding is not

related to fibril damage (Lee et al., 2017). Our findings parallel others of Fung et al. (2010) and Veres et al. (2013). In their studies, tendons were also subjected to lower applied strains and lower numbers of cyclic loadings. Damage of fibrils is likely to follow after interfibrillar sliding damage, when the interfibrillar network cannot bear any more load and cannot transmit the shear loads. This is clearly seen in the AFM images that show fibril damage (a high density and severity of fibril kinks, localised fibril rupture and recoiling of ruptured fibrils at the rupture sites) that were observed at higher strains (6% and 9%) with higher number of cycles (beyond the second hour). These AFM findings mirror the macro-damage observed by CA at the fascicle and fibre levels for the same strain levels and number of cycles. These observations of tendon damage support the purported mechanism that damage first exists by interfibrillar sliding followed by irreversible intrafibrillar sliding and damage in fibrils.

A recent report has suggested that sub-rupture nano-changes observed as the repetitive fibril kinking exists at distinct repeated intervals on the fibril surface (Veres et al., 2013). These nano-changes are in line with changes in waviness seen at the fibre and fascicle levels in the different strain groups in the current study. Therefore, this provides support that fatigue loading induced changes concurrently at multiscale structural levels in tendons. The correlations between the nano- and macroscale parameters were similar in GAG-depleted ($R^2 = 0.91$, $P < 0.001$) and the control groups ($R^2 = 0.87$, $P < 0.001$) even though the GAG-depleted group had a much greater decline in both structure and function. This maintains the association between these two domains further proving the strong role of the GAG matrix network in the function of tendons. This highlights integrating both the form and function of the tendon. In other words, the association between changes in the structural domain (observations) and the changes in the mechanical domains (stiffness etc) are maintained independent of the GAG depletion or not. That said the rate of these changes under different strain and cycle loading are protected by the GAG matrix. This is observed in the increased density and severity of nano- and macro-changes and damage seen in the GAG-depleted group, which results from the removal of GAG from fibrils. GAG is suggested to contribute to the integrity of fibres by connecting adjacent fibrils (Scott, 1992; Cribb et al., 1995). Such merging of the inter-fibrillar structure is important for preserving the collagen fibrils and therefore keeping the triple helices in a tight cohesive structure (Redaelli et al., 2003; Vesentini et al., 2005). Since the mechanisms

of elongation and sliding of the collagen triple helices do not occur concurrently (Folkhard et al., 1987), it seems that the nanostructural response to load has a sequential process beginning with uncrimping, then elongation (observed as an increase in fibrillar D-periodicities), then the sliding of fibrils.

For example, in both controls and GAG-depleted tendons, no significant D-periodicity increase was detected until 6% applied strain, which corresponded to the loss of collagen fibre crimping at the macroscale (Misof et al., 1997). Nevertheless, higher levels of fibril strains (measured as increased D-periodicities) in the GAG-depleted tendons were observed compared to control groups. This perhaps suggests the effect of removing of GAG on the elongation and sliding mechanisms in fibrils. Thus, the removal of these GAGs from the tendons, perhaps, led to weakening of the localised fibrils that could not bear the excessive loads. Consequently, impairment of the load transfer across to adjacent fibrils occurred resulting in the impaired integrity of fibres and consequently fibre damage.

Consistent with our hypothesis, the significant relationship in the GAG-depleted group between nano- and macrostructural measures indicated that macroscale mechanically induced changes (observed as higher percentages of fibre waviness and rounder tenocytes) affected the tendon stiffness (observed as higher percentages of changed mechanical properties). These macrostructural and mechanical changes in the GAG-depleted group were driven by changes at the nanoscale level, observed as broader changes in WFB D-periodicities compared to the control group.

CHAPTER SIX:

LIMITATIONS

This study was an ambitious program of research that examined multiscale levels of change (using objective and subjective assessments) during cyclic loading across three strain levels and four different durations of loading. Additionally, a glycosaminoglycan (GAG) depletion study was performed. The study was undertaken using harvested rabbit tendons and therefore the generalisations and conclusions are limited within this parameter. Following the basic principle of maximising the repeatability of the research methods and research integrity, the following section provides a clear narrative of methodological issues for the replication of the work undertaken in this thesis. On this basis, the following limitations are acknowledged:

7.1 Tissue samples

Examining non-viable whole tendon tissue in *in-vitro* testing, as used in this study, is relatively direct and allows for the clearest information regarding the mechanical properties of tendons undergoing fatigue damage. For instance, this study uncovered the importance of strain as the main mechanical measure controlling the accumulation of tendon damage. Although *in-vitro* testing can demonstrate the natural course of tendon damage due to mechanical loading, it cannot demonstrate the matrix processes of tissue healing and remodelling that occur at many biological substrate levels and across different timelines. The difference between *ex-vivo* and *in-vivo* testing models is acknowledged as a limitation of the generalisability of the results. Therefore, the multiscale form (morphology) and function (mechanics) assessments within this thesis set up a basis for future *in-vivo* research to consider the biological implications and the direct clinical implications for tendinopathy and the management of conditions within the therapeutic setting.

7.2 The testing instrumentation

A multiscale analysis of the structure of the Achilles tendon and its response to mechanical loading required an assessment of the tissue using different devices (Instron, confocal arthroscopy (CA) and atomic force microscopy (AFM)). This has

created some technical limitations due to the fact that each device has its own assessment methodology, outcome specialty and scale limitations (from macro to nanoscales). This may affect the multiscale assessment of the tested samples in terms of correlating the outcomes of each device with each other.

CA and AFM assess different levels of damage. CA allows assessment of tendon structure at the microscale while AFM is at the nanoscale (molecular-scale) level. This means that a tissue that is observed to have no damage or change in the structure by CA will not necessarily be observed to be undamaged in the AFM observation and *vice versa*. It is likely that before structural damage is observed in CA, the tissue will show damage at the level of AFM.

Clearly, there is an interaction between the scale of magnification and the field of view of each instrument. Since damage may not be homogeneous especially in the early loading phase, tracing similar morphological characteristics of the tested variables by CA with AFM and *vice versa* was labour intensive and time-consuming. As a result, there was a trade-off between the repeated sampling frequency and the total number of tendons used in the study.

It is now clear from this study that tendon damage happens at different scales and therefore the literature needs to be reviewed in the context of the scale of the assessments that have been undertaken. Some commentary in the literature refers to presumptions of damage at scales other than those that were actually measured. This is a general limitation in the literature review, since to criticise the narrative within the tendinopathy literature with this repeated caveat makes writing the literature review difficult. The reader should therefore consider this a limitation within the narrative.

A. Confocal Arthroscopy (CA)

The first experiment used the arthroscope probe to take images of the tissues mechanically loaded by the Instron. During the course of the experiment, the presence of image artefacts adversely impacted some images. The images taken by the probe of

the arthroscope during the mechanical tensile testing may have some technical resolution issues due to common artefacts affecting the quality of images.

Unfortunately, in order to reveal the images, the coverslip glass of the probe has to be in contact with the targeted tissue surface at various angles to the surface of the tissue. Obtaining the best imaging angle of the probe against the surface was a challenge due to the short imaging time allowed in the experimental protocol (one minute at zero strain). Some poor-quality images possibly contained artefacts including residual contrast agents and water droplets that accumulated on the coverslip of the probe, or the quality may have been reduced by hand vibration and/or motion of the probe during the acquisition of the image.

It was also challenging to overcome these problems during the repetitive image acquisition at zero strain stages for the long periods of tensile testing by the Instron (from one to four hours). To minimise this limitation multiple photos were taken on each testing window (up to 10).

Contrasting fluorophore agents such as the fluorophore sodium fluorescein stain tenocytes as negative images which can make it very challenging to distinguish the cells from the collagenous components in CA images. A major complication with fluorophores is that they may irreversibly fade when exposed to exciting light. Although this process is poorly understood, it is thought in some cases that the fluorophore molecule reacts with oxygen and/or oxygen radicals and changes to become non-fluorescent (Wang & Wolfbeis, 2014). The reaction can occur after a fluorophore molecule changes from the single excitation to the triple excitation state. This can cause a significant photo-bleaching.

Furthermore, most confocal microscopes require 0.1–1 s to produce a single image. This rate may be too slow for various dynamic processes, specifically if three-dimensional stacks of images are needed. Even for a single two-dimensional image,

slow frame rates translate into long exposure periods of the sample to intensive laser light, which may also cause damage or photo-bleaching.

Suitable contrasting agent fluorophores (acridine orange (AO) or sodium fluorescein) were selected for the best penetration of the tendon tissue as this controls the penetration capacity of CA. Sodium fluorescein is approved for direct systemic application in human and animal tissues and AO, a common contrast fluorescent in animal assessments, can distinguish specific RNA and DNA in the cytoplasm and nuclei. However, another issue is the potential hazard that may exist using these fluorophores. Also, the combination of the potential fluorophore toxicity and intense light illumination of the laser may cause tissue damage that is interpreted as mechanical in origin during tensile testing.

B. Atomic force microscopy (AFM)

A disadvantage of AFM was the single scan image size. AFM can only image a maximum height of 10–20 μm and a maximum scanning area of about 150 × 150 μm. The scanning speed of the AFM was also an issue. Traditionally, an AFM scans relatively slowly and requires four to six minutes for a typical scan. The relatively slow scanning rate during AFM imaging often caused image drifts that showed some distortion and resulted in moved, elongated or compressed images. This drift is an unavoidable and common factor that introduces technical errors into AFM measurements (Ricci & Braga, 2004; Mokaberi & Requicha, 2006; Rahe et al., 2010). The AFM scanner's piezoelectric ceramic is subtle for the AFM environment, and even minimal changes in temperature can introduce drift on the images. According to (Ricci & Braga, 2004; Mokaberi et al., 2006; Rahe et al., 2010; Su et al., 2014), the drift effect could be due to either thermal (internal or external) or instrumental reasons (hysteresis of the piezoelectric material and crosses between the x, y, and z axes). Similarly to any other imaging technique, image artefacts are possible, which could be prompted by poor operating procedures and conditions or an unsuitable AFM tip. Different methods are often applied to reduce the effect of image drifts, such as increasing the scanning rate or adjusting the AFM environmental conditions.

Since the effect of drift on the slow scanning axis (y) is comparatively clear, the fast scanning axis (x) was adapted in all AFM assessments. Therefore, when the D-periodicities were measured, the scanning angle was fixed to allow the tip to scan along the fast scanning x-axis to reduce errors and to produce much more precise D-periodicity values. Consequently, the D-periodicity values of the measured fibrils from images with the drifting effect were within the range of ± 2 nm and exhibited very small to negligible imaging effects

C. Strain mediation and preconditioning

The findings of this study on the impact of repeated loading may not necessarily match other research protocols because this study set the fatigue control variable as strain. This means that the tendons were elongated to a set strain on each cycle. This resulted in a declining force loading of the tendon over time. Other studies have used stress (force) as the control parameter. Such studies load the tendon to the same amount and as the tendon fails the strain increases to a point of rupture. Also, a limitation of the current study is that each tendon cohort had a preconditioning of 720 cycles at the strain level of the cohort. This had an effect particularly on the anisotropy measurement, which was clearly mediated by stress and for which all the major changes occurred in the preconditioning phase.

D. Stress relaxation represented as maximum load

The stress relaxation (SR) in this study is expressed as the decline in the stress over the static held length at three different points (Max, halfway and End). The ML were considered to represent the SR since these three cohort points were highly correlated (R^2= 0.87-0.99, P<.0001) for all tendons from all groups at all-time points. Greater details are under appendix 7. Since the Max load was highly correlated with all macro and nanostructural changes, this may provide an avenue for future investigations in examining if (SR) is similarly correlated with nano and macrostructural changes in tendons when tested in an in-vivo/or ex-vivo static mechanical intervention.

E. Repeatability of observed classifications of tendon morphology

While the literature has a number of papers reporting methods for the identification of tendon morphology from observations, few, if any, follow valid statistical models. For

example, the ordinal classification of cell type or fibre disruption is indeed ordinal and therefore calculating the statistical inferential parameters such as mean and standard deviation suggests that there are a few statistical assumptions being made.

Furthermore, there are no studies published reporting the blind test-retest reliability of the observer and although the protocols describing the classification are well reported, these address the validity of the assessments, not the source of errors of bias or reliability. The current study incorporated a test-retest between and within observations of the tester who was blind to the conditioning of the imaged tendons. This thesis, therefore, is the only reported case where the reliability of the assessments has been quantified. This study also reported intra-tester reliability. The limitation of the study is that the assessment of the histological slides was not validated in any way. The frameworks of the observed slide characteristics were discussed with other colleagues but like many histological research papers, they are somewhat descriptive in nature.

F. Statistical analysis

As described in the statistical section in Chapter 3 the research design used in this study was undertaken as an observational (qualitative) study of trends as much as the inferential (quantitative) statistical analysis. The duality of the method raises limitations in both the statistical alpha level and the statistical power.

First, only the results of the data points at each hour were assessed in the paired comparison. The data, however, were plotted for all assessments to create a trend and observational changes. The sample sizes were small and declined at each destructive sample period for the histology and nanoscale assessments. All the variables proposed in the study have been reported. The loading stiffness (stiffness assessed at the first cycle of the repeated loading cycle) had a duplicate assessment at the start of the static one-minute hold. This was removed from the detailed analysis because it was highly correlated ($R^2 > 0.96$) with the ramping stiffness. The results are in the appendices for clarity. These two assessments demonstrated a very high level of reliability across the testing protocol.

G. Effect size calculations provided – no alpha-level adjustments

The inferential statistics were kept simple and the effect sizes reported. The *a priori* estimates of the sample size were made for the first two hours of assessment with the intention of providing the third and fourth hour as observational assessments only. However, our *a priori* estimates underestimated the actual effect size, and therefore the third hour was reported. No alpha level adjustments were made. That said, the discussion and narrative of the conclusion were mostly associated with common outcomes of the overall domains and not a single strain, hour, or variable.

The primary limitation of this is that the discussion reflects on the changes in the domains of assessments and the associations between the variables. The p values for any individual paired difference should not be considered in isolation. Finally, the use of the effect size comparison has limited clinical interpretation; however, it can be used for future researchers as a basis for the future optimal research design.

CHAPTER SEVEN:
CONCLUSION AND THE AREAS OF FUTURE RESEARCH

From the literature review and research in this thesis, the following conclusions and suggestions for areas for future research are made:

- This study provides a robust assessment of the testing protocol by replicating the mechanical and morphological changes in two control groups (from the glycosaminoglycan (GAG)-depletion study (Study 2) and Study 1). Moreover, the inter- and intra-tester observational damage classification was shown to be reliable.

- Both strain and cycles impact on the mechanical and morphological changes in tendons. In this study the differential strains (3%, 6%, and 9% strain) reflected significant differences across most derived variables over the first , second , third and fourth hour of the mechanical intervention.

- Static mechanical changes are highly correlated with dynamic mechanical changes (for example, maximum load *vs* stiffness) throughout the repeated loading protocol.

- Hysteresis was the most sensitive mechanical assessment to increased strain and numbers of cycles. This highlights the importance of hysteresis in assessing tendon damage accumulation.

- By two hours of strain-mediated mechanical loading all significant changes had occurred. Therefore, any future research validating the outcomes for stress-mediated loading protocols would warrant restricting the duration of the cycles under a strain-mediated model. This would allow reallocation of testing time and resources to increase sample size and research design.

- Tenocyte spindle morphology change is a sensitive marker for mechanical and other morphological changes. The loss of spindle shape, rather than just increasing roundness, is the key marker. The predictive value in the tenocyte shape is the early loss of the spindle stucture to reflect roundness, rather than degrees of roundness (Cat 3,2 &1). The lag effect between the detection of the spindle change and the mechanical drop off may be partly explained by the categorical measurement and the threshold of the boundary between changes from Cat 4 to Cat 3 (from spindle-shaped to slightly rounded tenocytes). Since the usage of Image J on cell shape categories was derived from work on cancer cell morphology, then future research clearly needs to determine if the (0.0-0.35) threshold of roundness could be improved to validate mechanical failure or structural damage. Future *in-vivo* research may warrant the examination of biological markers for shape change and concurrent mechanical decline.

- The depletion of GAGs resulted in increased damage and mechanical failure compared with matched control tendons. This clearly shows that GAGs provide an improved mechanical and structural elasticity.

- The association between the mechanical and morphological changes remained relatively constant whether measured in control or GAG-depleted tendons. Therefore, this study shows that mechanical and morphological changes in tendons happen concurrently.

- Not only are the microstructural changes in the three strained and GAG-depleted tendon groups generally consistent with those in fatigue models reported in the literature, but in our findings these. These changes have also been revealed to, however precede tenocyte morphological changes, supporting the theory that fibre waviness can affect the mechanical and structural behaviour of tenocytes.

- The form and function of tendons is highly correlated at multiple hierarchical scales. This is reflected by the very strong associations between the mechanical variables and the observations of structural damage. For instance, fibril elongation is a tendon damage mechanism that contributes to changes in mechanical properties at the macroscale level of the tendon. Furthermore, mechanical changes – especially in hysteresis – reflect structural damage at different scales. Future research would be

warranted to examine if stress-mediated fatigue loading would maintain these strong associations.

- After repeated loading, damage occurs concurrently at the nano- and macroscale (i.e. nano and macrostructural changes). There are strong correlations between tendon nanostructure (as changes in D-periodicity) and mechanical properties of macrostructure (fibre waviness and tenocyte roundness).

- Mechanical changes at low numbers of cycles and amounts of strain were observed in the absence of gross morphological changes (i.e. high density and severity of fibril kinks, localized fibril rupture and recoiling of ruptured fibrils at the rupture sites). At higher cycles and strains the damage at the fibril level increased. This supports the construct that initially intra-fibrillar sliding occurs followed by irreversible inter-fibrillar sliding and clear damage in fibrils.

APPENDIXES

Appendix 1

The origin of D-Periodicity variability

Non-mechanical factors

Intracellular determinants

In these studies, the reversal of the weak acid buffers – used to break down the collagen linkages - have demonstrated that the reconstructed repeated Tc depict the same D-periodicities as in tissue fibrils (Kadler et al., 1996; Canty et al., 2004). The self-assembly structure, however, results in a semi-rigid gels that differ from fibrils as they have unspecific orientation. This suggests cellular involvement in vivo modulates the orientation and serial alignment of the collagen subunits. Therefore, the formation of collagen fibrils is likely controlled by the molecular intrinsic characteristics, however, also mediated by cell regulation mainly in developing or healing tissues (Kadler et al., 1996).

Although there are competing theories on the formation of fibril bundle in fibrillogenesis models, the observations from EM proposed a nucleation, growth and coalescence (NGC) sequential formation of collagen fibrils and fibril bundles. For example, in chick embryonic tendon, single or small clusters of fibrils were found in membrane projections near the surfaces of the fibroblast, known as fibripositors (Trelstad & Hayashi, 1979; Canty & Kadler, 2005). Based on their findings, it is suggested that nucleation and axial growth of the fibrils occur in these fibripositors. Tip-to-tip joining (Graham et al., 2000; Kadler et al., 2008) and side-to-side joining (Birk & Trelstad, 1986; Prockop &, 1994; Canty & Kadler, 2005) of fibrils has also been reported, which could explain the formation of the D-Periodicity bundle. This is consistent with the strong evidence demonstrating that genetic intracellular information can modulate the fibril function and therefore the D-Periodicity (Wallace et al., 2011).

Environmental determinants

Although AFM based studies have reported the importance of dehydration in changing the D-Periodicity (Habelitz et al., 2002; Kemp et al., 2012), there is inconclusive evidence that dehydration can impact on the D-Periodicity distribution reported in the literature. For instance, Habelitz and his co-workers (2002) reported that the reduced D-Periodicity may be due to a dehydrated structure resulted from a disorder and diminished crystallinity and suggested a narrow D-Periodicity distribution (67-68 nm in hydrated fibrils) and a division of the D-Periodicity distribution into three groups at 67, 62, and 57 nm in dehydrated fibrils (Habelitz et al., 2002). In contrast, another AFM based study by Erickson et al (2013) did not find any significant correlation between the average of fibril D-Periodicity of hydrated (62.2 ± 2.0 nm) and the dehydrated (63.1 ± 1.9) imaged fibrils (Erickson et al., 2013). Although the averages in D-Periodicity may be affected by surface dehydration, still the averages of both refuting studies do not explain the full range of D-Periodicity distribution (60 and 70nm) that are frequently found in tissues which suggests that this distribution does not seem to be as an artefact of surface dehydration.

Measurement artefact has also been considered in the assessment of D-Periodicity using AFM to investigate the systematic errors which may be caused by thermal drift and scanning angle. Erickson et al (2013) studied thermal drift beam angulation and scan rates and found a variation in D- periodicity of individual fibrils less than 2 nm showing no systematic changes in D-Periodicity (Erickson et al., 2013). They also have found that the thermal drift would have an insignificant impact on D-Periodicity even at a slower rate of 0.5 Hz during a single scan and the systematic errors which may be caused by thermal drift and scanning angle do not seem to influence the measurements of D-Periodicity. Su et al (2014) have refuted this conclusion and suggested a variation about 2nm and an impact of thermal drift that was found more obviously on the slow scanning axis (Su et al., 2014).

The non-consensus between the two studies on the effect of thermal drift visualised on the slow scanning axis is possibly attributed to the difference between tested samples that been used as tissue samples or collagen fascicles (Erickson et al., 2013)

and single collagen fibrils on mica (Su et al., 2014). Further, these samples are affected by different impacts of thermal drift and scanning angle on both samples that may lead to the systematic errors. In the images of collagen fibrils on mica, it is noticeable that the surface of substrates are not parallel to the surfaces of collagen fascicles (Fang et al., 2012). When curved collagen surfaces were imaged, there were fewer points to measure that were parallel to the x–y plane. Such measurements can increase the measured D-Periodicity variation. Further studies are needed to clarify the difference of measured D-Periodicity values between within fibrils and between fibrils of same and different fibril bundles taking into consideration the impacts of thermal drifts on the D-Periodicity variation. Kemp et al (2012) investigated whether the relationship between the morphology and mechanics can change the phenotype of the diseased tendons (Kemp et al., 2012). This study has shown the dried Brtl/+ fibrils with higher mean differences of D-Periodicity accompanied by significant increases in elastic modulus (MPa), adhesion force and decreased indentation depth (nm) in compared to WT group that shown the D-Periodicity were not accompanied by any nanoscale mechanical changes.

The inconsistency on the suggested potential sources and mechanisms for the variability in the D-Periodicity in reviewed previous studies may be attributed to variations in the tissue samples and/or dehydration-dependent artefacts from tissue sample preparation (Bear, 1944; Brodsky et al., 1980; Stinson & Sweeny, 1980; Eikenberry et al., 1982; Habelitz et al., 2002), the method of analysis, experimental procedure and calibration of the instrument used in the assessment (Wallace et al., 2010; Erickson et al., 2013; Su et al., 2014). However, these potential sources for the variability do not seem to solely explain the D-Periodicity distribution (+/- 10nm) within and between collagen fibril bundles. To date few studies have examined sequential changes during experiments.

Biological determinants

Some aspects of the literature suggest that variations of collagen fibril D-Periodicity is associated with some diseases (Wallace et al., 2010; Wallace et al., 2011; Fang et al., 2012; Hammond et al., 2014). This is evident in bone diseases where variation on D-Periodicity has been associated with alterations in nano/microstructure of collagen

(Bear, 1944; Brodsky et al., 1980; Fraser et al., 1983; Fraser et al., 1987; Odetti et al., 2000; Reed & Iozzo, 2002). An AFM based study has reported a 63–73nm distribution of D-Periodicity in the mice bone, dentin and tendon by using a 2D Fast Fourier Transform (FFT) (Wallace et al., 2010). This study has shown that this distribution of D-Periodicity was present without the existence of cellular, mineral origin or anatomical location or mechanical function. However, the distributions measured from samples of mice bone were statistically indistinctive.

Similar results have reported alterations in type I collagen nanomorphology in an ovariectomy-induced estrogen depletion study on Sh and OVX ovine radius bone and skin (Wallace et al., 2010; Fang et al., 2012). It was found in these studies that the percentage of OVX bone and dermis collagen fibrils with D-periodicities below 64 nm existed about four times higher than fibrils in the Sh groups. There is evidence that genetic modifications identified with known pathological phenotypes can alter the D-Periodicity. Osteogenesis Imperfecta (OI) phenotypes are predominantly related to mutant genes encoding the a1 or a2 chains of type I collagen or proteins related in type I collagen intracellular trafficking and post-translational modification(Cundy, 2012).

A recent study by Wallace et al (2011) used a heterozygous (Brtl/+) mouse model of type IV (OI) to quantitatively analyse the D-Periodicity of type I collagen fibrils in fermora from heterozygous (Brtl/+) mice (Wallace et al., 2011). The distribution of D-Periodicity values was distinctive between the two genotypes. Their results have shown that this bone disease has a well-characterized changes in the col1a1 allele resulted from Glycine 349 to Cysteine substitution in one col1a1 allele and led to a characterized more heterogeneity of D-Periodicity distribution (56-75 nm) compared to wild type (WT) animals (63-74nm). The change in D-periodicities in dried Brtl/+ fibrils from tendon have shown different results (Kemp et al., 2012). However, the D-Periodicity mean of Brtl/+ fibrils was shifted downward versus WT when imaged wet, (Brtl/+ wet: 67.5 ± 1.4 nm versus WT wet: 68.2 ± 1.2 nm). This downward shift was driven by a greater number of fibrils with shorter D-periodicities. 30% of Brtl/+fibrils had D-periodicities less the mean minus 1 standard deviation of the WT group. The difference could be due to the difference in tissue used, the existence or absence of mineral or animal age between the studies. Such studies have shown statistically significant variations in the D-Periodicity distributions in the presence of OI bone,

proposing the biological importance of the D-Periodicity distribution (Wallace et al., 2010; Wallace et al., 2011; Fang et al., 2012). These studies suggest that such distribution values may be a marker at the nanoscale level that is associated with bone pathology.

Intrafibrillar determinants

Intra and inter fibril variation of D-Periodicity is rarely documented in the literature. This is critical in understanding the sequential development of ultrastructural damage in the presence of pathology or acute injury. There is some evidence that variant intrafibrillar interactions such as crosslinks on hydroxylysines (Hyl) and Hyp, hydrophobic and electrostatic interactions and hydrogen bonding may contribute to the D-Periodicity variations at the bundle level. This contribution may take place when Hyl sites are joined between neighbouring fibrils during an enzymatic reaction at the cross-links that leads to an overlapping between gap and overlap zones (Orgel et al., 2011).

It was further expressed that non-enzymatic glycation (NEG) that take place with aging and diabetes (Vashishth et al., 2001) is independent of collagen fibril D-Periodicity using *in vitro* D-ribose ovine bones (Fang et al., 2012). In the light of fibrillogenesis models that offered views on the formation of fibril bundle, other researchers have suggested that the mechanistic pathways for the nucleation, growth and coalescence (NGC) and Liquid Crystalline (LC) models are consistent with the results of their study on the relationship between fibril D-Periodicity and bundle ultrastructure (Fang et al., 2012). Comparable conclusions are provided by Odetti and co-workers(Odetti et al., 2000). It is also possible that D-Periodicity distribution form the super twisting between the fibril's constituents, supported by the assumption used to explain the 64 versus 67nm D-Periodicity in various tissues. Moreover, Bozec et al (Bozec et al., 2007) exhibited intertwined rope characteristics of the digital tendon fibrils and suggested a rope-like model of fibril periodicity, that also accounted for fibril D-Periodicity variation within fibrils (69.6 ± 2.9 nm) regardless of fibril dimensions or overall topology. It is further added that D-Periodicity distribution within and between fibril bundles can be predicted by more developed theoretical

models such as (NGC) and Liquid Crystalline (LC) containing collagen molecular and microfibril assemblies.

Appendix 2

THE UNIVERSITY OF WESTERN AUSTRALIA

Animal Ethics

Office of Research Enterprise

The University of Western Australia
M459, 35 Stirling Highway
Crawley WA 6009 Australia

T +61 8 6488 2516 / 7887
F +61 8 6488 8775
E aeo@uwa.edu.au

CRICOS Provider Code: 00126G

Our Ref: RA/3/200/547 27 April 2015

Dr Peter McFawn
School of Anatomy, Physiology and Human
Biology MBDP: M311

Dear Doctor McFawn

ANIMAL ETHICS TEACHING PROTOCOL AMENDMENT - APPROVED

Physiology of cardiovascular and respiratory systems PHYL3002

Addition of multiple surgical support procedures

On behalf of the Animal Ethics Committee (AEC), I am pleased to inform you that your application for an amendment to the above teaching protocol has been approved from the date of this letter to **01 April 2017**.

A copy of the approval will be circulated under separate cover.

Approval Number:	RA/3/200/547
Approval Period:	08 April 2014 - 01 April 2017
Authorised Personnel:	Dr Peter McFawn

Associate Professor Shane Maloney
Dr Gavin Pinniger
Dr Anthony Bakker Ms Caroline Chi
Mr Matthew Kenrick
Dr Christina Bojarski
Mr Nikitas Economou
Mrs Beatrice Birkner

Species Name	Approved
Cane Toad	306
Rabbit, NZ White	174

The approval of this project is conditional upon you adhering to the conditions outlined in this letter and your continuing compliance with the Animal Welfare Act (2002) and the *Australian code for the care and use of animals for scientific purposes* (8th edition 2013).

Investigators must maintain records of the care and use of animals, and must provide to the AEC an Annual Report and State Government Annual Animal Use Report for an approved project, regardless of the duration of AEC approval for the project (see Australian Code clauses 2.4.32 and 2.4.34). Reports are due in January each year

Special Conditions that Apply to this Amendment

Thank you for extending a standing invitation to the AWO to attend any or all of the practical teaching sessions on this protocol. If you have any concerns regarding animal wellbeing or welfare, one of following must be notified immediately:

Animal Welfare Officer
awo@uwa.edu.au;
T: (08) 6488 7882 M: 042 802 1529
Veterinary Services
staff-vetservices@uwa.edu.au;
T: (08) 6488 4549 / 4700 / 6638

Conditions of Approval Applicable to All Projects

Any changes to the protocol must be submitted on an Amendment form and approved by the AEC before proceeding with changes. This includes any changes to: personnel, source of animals, animal numbers, location of animals and experimental procedures.

The Amendment forms are available on the Animals and Research website at http://www.research.uwa.edu.au/staff/forms/animals .All cages/pens/tanks/paddocks used for holding animals must be clearly labelled with the Chief Investigator's name, approval number, title of project and cage/pen/tank number. A copy of this approval letter, together with all relevant monitoring records, must be kept in the facility where your animals are housed. All unexpected deaths or unplanned euthanasia must be reported immediately to the Animal Welfare Officer. This also refers to all animal deaths in field research projects and wildlife projects. Completion of a 'Notification of Unexpected Death or Unplanned Euthanasia' form is required. See http://www.research.uwa.edu.au/staff/forms/animals. It is a requirement of the Australian Code that when an animal dies unexpectedly, or is euthanized due to unforeseen complications, an autopsy should be performed by a person with appropriate qualifications and/or experience. All personnel working with animals must be named on the protocol and have a valid Permission to Use Animals (PUA). The AEC would like to remind all investigators using animals that while animal technicians are responsible for the daily care of animals, and play a major role in alerting investigators should an emergency arise, the ultimate responsibility for animal welfare lies with the investigator.

Please contact the Manager, Animal Ethics should you require further information or clarification. Yours sincerely

Emeritus Professor D'Arcy Holman

Chair Animal Ethic Committee

Appendix 3

The processes were undertaken according to the bio-protocol lab processes (bio-protocol.org) and are outlined as the following:

Dimethylmethylene Blue Assay (DMMB)

Materials and Reagents

1. Dimethylmethylene blue (DMMB) (Sigma-Aldrich, catalog number: 341088)
2. NaCl
3. Glycine (Sigma-Aldrich, catalogue number: 410225)
4. Glacial acetic acid (Sigma-Aldrich, catalogue number: S7653)
5. Tris-Base (Merck KGaA, catalogue number: 648310)
6. Bovine chondroitin 4-sulfate as standard (Sigma-Aldrich, catalogue number: C9819)
7. DMMB reagent (see Recipes)

Equipment

1. Plate mixer (VWR International, catalogue number: 89202-332)
2. Cover adhesive (R&D Systems, catalogue number: DY992)
3. Microplate reader with 525 nm (BioTek Instruments, catalogue number: 11-120-531)
4. 96 well microplate spectrophotometer with 525 nm filter set (Thermo Fisher Scientific, catalogue number: 51119200)
5. Microplate shaker (VWR International, catalogue number: 97043-608)

Procedure

1. Prepare DMMB reagent and paper filter using Whattman® 3MM. The pH of this solution is around 3.0. To prepare 1 L dye solution, dissolve 16 mg DMMB in 1 L water containing 3.04 g glycine, 1.6 g NaCl and 95 ml of 0.1 M Acetic Acid.
2. Prepare standard solution of chondroitin 4 sulphate (500 µg/ml in H_2O). Prepare standard curve as stated in the table below.
3. Pipet the standard stock solution and complete the volume to 20 µl with H_2O into the 96 well microplate.
4. Pipet 20 µl of each sample into the microplate.
5. Add 200 µl of DMMB to each sample and shake the plate of a plate shaker for 5 sec.
6. Read the absorbance using a plate reader at 525 nm immediately.

Std (µg/ml)	Vol (µl) of 500 µg/ml std	vol H_2O (µl)	vol DMMB (µl)
0	0	20	200
1.25	2.5	17.5	200
2.5	5	15	200
5	10	10	200
7.5	15	5	200
10	20	0	200

Recipes

DMMB reagent
Dissolve 16 mg DMMB, 3.04 g glycine, 1.6 g NaCl and 95 ml of 0.1 M acetic acid and complete the volume to 1 L
Filter (0.45 µm)
Protect from light
Do not use if precipitate is present in the solution

Appendix 4

The processes were undertaken according to the CELLCentral lab protocols at the School of Anatomy Physiology & Human Biology, University of Western Australia and are outlined as the following:

1. Paraffin Processing

1.1. Fixation of tissues

The tissue fixed in buffered formalin was fixed at room temperature, For 2 - 24 hrs, the fixative were used 10 times to the volume of the specimen.

1.2. Preparation of block

Paraffin embedding was used. Once fixation has occurred, a representative area of approximately 5mm thickness was processed, along with an accompanying label, to infiltrate the tissue with wax. This was performed on an automated tissue processor.

1.3. Dehydration

Dehydration was commenced by ascending concentrations of alcohols as using 70% ethanol, progressing to absolute alcohol. For example, 70%, 80%, 90%, 100% to avoid the sudden change from water to absolute ethanol that can lead to excessive shrinkage and hardening with subsequent problems in section cutting.

1.4 Clearing

Clearing agents used were xylene and toluene that tend to harden tissue if left in contact for extended periods.

1.5. Wax infiltration

A suitable paraffin wax MP 54-58°C was used. Tissue was kept in heated wax for the minimum time consistent with complete infiltration (2 to 4 hours). The wax was retained in a liquid condition below 60°C while tissue was infiltrated.

1.6. Embedding

Following infiltration, tissues were cast in fresh wax in a mould. The blocks were labelled so that they could be identified. To make a complete bond between infiltrating and embedding wax, both were liquefied. The solid block was hard and allows thin sectioning of the tissue. Rapid cooling of the mould on a cold block was applied. In order to make ribboning easy when cutting sections, the moulds were not left to cool for too long and so avoided to produce planes of crystallisation within the block that lead to cracking.

1.7. Operation of an automated tissue processor

The automated rotary tissue processor consists of 12 available solution stations. The fixed tissue was placed in baskets, which were then rotated at suitable time intervals through the dehydration and clearing agents and finally the waxes. Electronically, controlled agitation was employed in the machine with a keypad. The available solutions were moved into and out of the processing chamber, and the selection of heat, vacuum and pressure were allowed. The total number of solutions available was between 12 and 14. The pressure and vacuum replaced the need for agitation used in rotary processors.

2. Cutting sections

2.1. Preparation of samples for Paraffin wax sectioning

Paraffin wax sections were cut on a rotary microtome. Sections were usually cut at 20-50 µm.

2.1.1 Floating out sections

Once ribbons were cut, they were floated out on a water bath heated to about 45°C and picked up onto slides. To assist the tissue section to adhere to the glass slide the slides were coated with wood glue (Araldite), gelatine dichromate or horse serum. Sections mounted on slides were incubated overnight in ovens set at 37-45°C and were ready for staining the following day.

2.2 Preparation of samples for cryo-sectioning

Samples were fixed in BFS immediately. After appropriate fixation (about 24 hours) sample were placed into PBS for rinsing (x2 15 mins each).Samples were then removed from PBS and placed into 30% sucrose solution made up in PBS. When samples sunk to the bottom of the container they were adequately cryoprotected. Next, a 50:50 solution of 30% sucrose (in PBS) with OCT was made, samples were placed into solution. After a few hours or overnight, sample was placed into pure OCT to remove any sucrose. Samples were frozen on to specimen chuck and sectioning was carried out.

3. Staining of sections

3.1. Staining technique (Hematoxylin and Eosin for morphology)

Sections are agitated 10 times in each of the Hematoxylin and Eosin solutions. For immersion times 2 minutes or longer, samples were agitated again before removing the slides. The slides were drained well, before placing into the next solution in order to avoid contamination in the following solutions. The complete staining protocol was applied at the CELLcentral histology at UWA according to standard procedures (Luna, 1968; Bancroft et al., 2008).

3.1.1. Dewaxing and Hydration of sections

Before staining the sections, using aqueous stains they are dewaxed. This is achieved using toluene. The sections were then “taken to water” using graded alcohols and were subsequently ready for staining. This involved steps 1 – 6 of the Haematoxylin and Eosin method.

3.1.2. Water wash of sections

The facility at UWA has two-tier washing system where freshwater flows into the top container and then makes its way into the lower container. The slides are first rinsed using the lower container and then are washed efficiently using the top container. Water is flown at a moderate rate and all traces of haematoxylin in the bottom container are gone by the time the slides have had their last wash before dehydration.

If the water refused to obey gravity and flow down, the air bubble was removed by elevating the outlet tube a little until the water commences to flow.

3.1.3. Dehydration and clearing of sections

The instructions 'dehydrate, clear and mount' involve steps 13 and 15 – 21 of the H&E staining method. Slides can be left in the final toluene before mounting without affecting the staining. Clearing refers to the action of these solutions to optically clear the sections making them transparent, due to the solutions high refractive index.

3.1.4. Mounting of sections

Sections are mounted using the smallest suitable sized coverslip and DPX to protect the section from damage and resolve the image under the microscope. DPX is a plastic dissolved in xylene to a specific optical density, rather than viscosity. The DPX is dispensed from a small plastic bottle, located in the fume hood, onto a coverslip.

3.1.5. Storage of sections

Slides are appropriately labelled and then allowed to dry horizontally for at least a week before storing upright in trays, files or boxes for histological assessment.

3.1.6. Histological assessment of sections

Blind general histological scoring is performed by two individuals as previously described (Chen et al., 2011; Wang et al., 2013). The qualitative derived- variables included in the scale for the analysis of tendon macrostructure , are assessed using a scoring scale of 0–3, as described previously (Chen et al., 2011; Wang et al., 2013) . The average score of each parameter are used for comparison. Greater details are showed under appendix 5, Briefly, Cellularity: Scale of 0–3, 0 represents acellular, and 3 represents high density. Tenocyte morphology: Scale of 0–3, 0 represents Acellular, and 3 represents predominately spherical. Fibre structure: scale of 0–3, 0 represents continue, long fibre, and 3 represents severely fragmented. Fibre arrangement and orientation: scale of 0–3, 0 represents compacted and parallel, and 3

represents no identifiable pattern. Fibre Visibility: scale of 0–3, 0 represents highly fibrous, and 3 represents no fibres.

3.2. Staining technique (Alcian blue for GAG and PG content)

The total GAG and PG content are assessed by obtaining a specific stain for mucopolysaccharides (GAG and PG content) (Gagliano et al., 2013). The sections are stained with Alcian blue in sodium acetate buffer, pH 5.8 containing different MgCl2 concentration in order to selectively stain different mucopolysaccharides. In particular, in 0.025M MgCl2 all acid mucopolysaccharides stain blue; using 0.3 and 0.65g MgCl2, respectively, sulphated acid mucopolysaccharides and strongly sulphated acid mucopolysaccharides can be observed. The slides are examined under a light microscope.

3.2.1. Storage of sections

Slides are appropriately labelled and then allowed to dry horizontally for at least a week before storing upright in trays, files or boxes for histological assessment.

3.2.2. Histological assessment

The qualitative derived- variables included in the scale for the analysis of tendon macrostructure - total GAG and PG content, are assessed using scoring scale of 0–3, where 0 is normal and 3 severely abnormal and are analysed in blind by two different operators using a four-point quantitative scoring system as described by Gagliano et al (Gagliano et al., 2013), where 0 indicates normal appearance, 1 slightly abnormal appearance, 2 moderately abnormal appearance, and 3 markedly abnormal appearance. The degree of staining (The total GAG and PG content) is assessed using a similar quantitative score based on four-point scoring system, using scoring scale of 0–3, where 0 is normal and 3 severely abnormal. Scale of 0–3, 0 represents very strong staining, and 3 represents faint staining. The results of the scoring system are expressed as means. The average score of each parameter is used for comparison.

HAEMATOXYLIN AND EOSIN STAINING

Paraffin sections

REAGENTS:

Harris' Haematoxylin 500ml

Oxidant, add oxidant to haematoxylin then invert 6-8 times or use a magnetic stirrer for better mixing. Allow to stand for 8 hours prior to use.

1% Acid Alcohol

Alcohol	70 ml
Distilled water	30 ml
Hydrochloric acid	1 ml

Alkaline rinse

Tap water	300 ml
Strong ammonia 28%	3 drops OR Lithium carbonate approx. 0.15g Tap water 300 ml

Eosin / Phloxine

Stock Eosin		
Eosin Y	1.0 g	
Distilled water	100 ml	
Stock Phloxine		
Phloxine B	1.0 g	
Distilled water	100 ml	
Working solution		
Stock Eosin		40 ml
Stock Phloxine	10 ml	
Ethanol	330 ml	
Distilled water		20 ml
Glacial acetic acid	1.6 ml	

METHOD:

DEWAXING

1. Toluene, 2 min, drain.
2. Toluene, 2 min, drain.

HYDRATING

3. 100% Ethanol, Agitate 10 times, drain.
4. 100% Ethanol, Agitate 10 times, drain
5. 70% Ethanol, Agitate 10 times, drain.
6. Tap water wash, Agitate 10 times, drain.

NUCLEAR STAINING

7. Haematoxylin solution, 1.5 min, drain.
8. Rinse well in running tap water.
9. Dip, quickly into acid/alcohol, DON'T DRAIN.
10. Rinse in running tap water.
11. Alkaline rinse, agitate 10 times, drain.
12. Rinse well in running tap water.

DEHYDRATING

13. 70% Ethanol, Agitate 10 times, drain

CYTOPLASMIC STAINING

14. Eosin, 45secs

DEHYDRATING

15. 100% Ethanol, Agitate 10 times, drain.
16. 100% Ethanol, Agitate 10 times, drain.
17. 100% Ethanol, Agitate 10 times, drain.

CLEARING

18. Toluene, Agitate 10 times, drain.
19. Toluene, Agitate 10 times, drain.
20. Toluene, Agitate 10 times

MOUNTING

22. Mount and coverslip in DPX.

RESULTS:

Nuclei : blue
Cytoplasm: various shades of pin

Appendix 5

Semi-quantitative four-point scoring system in Tendons

(Movin et al 1997, 1998 and 2000, Svensson et al 2005, Kartus et al 2000, Chen et al 2011, Meknas et al 2012, Wang et al 2013, Gagliano et al 2013)

Blinded image scoring instructions

The below system is the grading of the Confocal Arthroscopy (CA) images based on the following four main parameters:

1) Fibre structure
2) Fibre arrangement and orientation
3) Tenocyte roundness

This scoring system aims to provide some quantifiable measure to assess the collagen damage induced by repeated cyclic loading and to provide a measure by which the CA images can be reasonably compared via an overall grading system to conventional histological assessment (*according to the scoring methods adapted by the above-listed references*).

1. Fibre structure

A. Continuous and long fibres with no interruption	4
B. Slight separation and fragmentation of fibres , waviness	3
C. Marked waviness , separated and fragmented fibres	2
D. Increased waviness, separated and fragmented fibres	1

2. Fibre arrangement and orientation

A. Compacted ,parallel , regular and well-ordered	4
B. slightly loose and wavy	3
C. Increased loose , wavy and cross to each other	2
D. Moderately loose , wavy crossing each other with some unidentified pattern	1

3. Tenocyte roundness

A. Long spindle shape cells	4
B. Slightly rounding	3
C. Moderately rounding	2
D. Severely rounding	1

4= normal appearance, 3 = slightly abnormal appearance, 2= moderately abnormal appearance, 1 = severely abnormal appearance.

Therefore, a perfectly normal tendon would score 12, and a maximally abnormal tendon would score 3.

Examples on the CA grading system:

(A) Grade 1 :

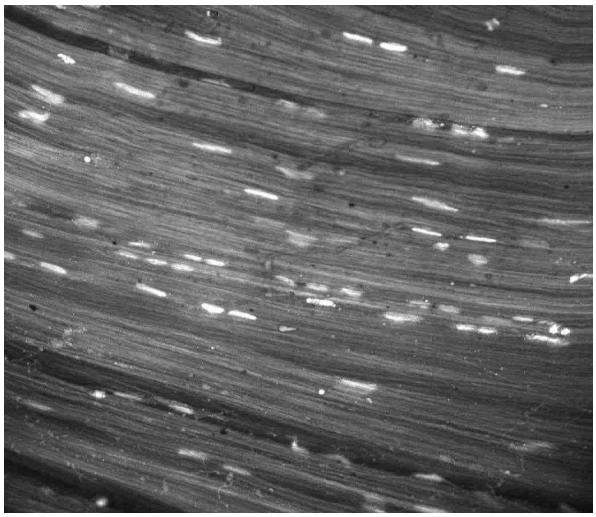

Acridine orange 0.5g/L at 30 mins. 475µm x 475 µm

1)	Fibre structure	4
2)	Fibre arrangement and orientation	4
3)	Tenocyte roundness	4
	Total:	**12**

(B) Grade 2 :

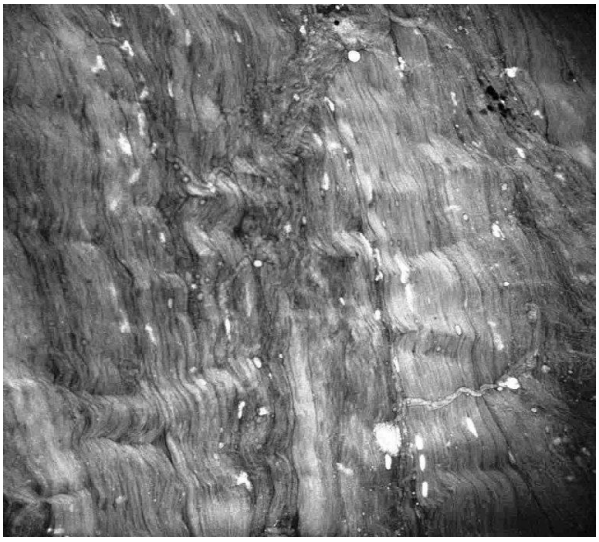

Acridine orange 0.5g/L at 30 mins. 475µm x 475 µm

1)	Fibre structure	3
2)	Fibre arrangement and orientation	3
3)	Tenocyte roundness	3
	Total:	**9**

(C) Grade 3:

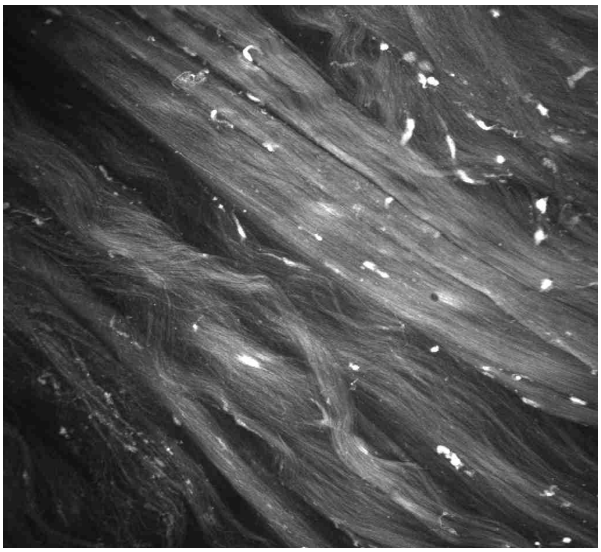

Acridine orange 0.5g/L at 30 mins. 475µm x 475 µm

1)	Fibre structure	2
2)	Fibre arrangement and orientation	2
3)	Tenocyte roundness	2
	Total:	**6**

(D) Grade 4:

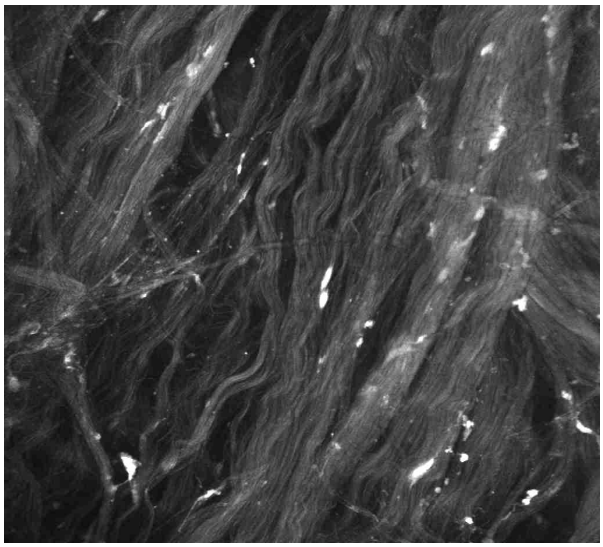

Acridine orange 0.5g/L at 30 mins. 475µm x 475 µm

1)	Fibre structure	1
2)	Fibre arrangement and orientation	1
3)	Tenocyte roundness	1
	Total:	**3**

Appendix 6

Nanoscale imaging protocol – AFM

Tissue specimens were imaged in air using a *Dimension FastScan* AFM in tapping mode (TM). The topographic images were revealed by tapping the surface lightly with an oscillated probe tip. The Stage Controller, the Nanoscope V controller, and the HV Amplifier were all turned on and the Nanoscope software consequently started. The type of experiment was chosen through the first window seen. Then “Tapping mode” Followed by “Tapping in air” were chosen. The next window allowed the loading of the probe and aligning the optical beam deflection setup.

Then, the probe was loaded by clicking the button “Change Probe”, then the scanner was removed after the High Voltage indicator on the head was turned off. The collagen fibrils, subfibrils, fascicles and fibres were imaged in air, using “Fast Scan-A” Bruker probes; silicon nitride cantilevers with nominal tip radius 8 nm, force constant 40 N/m, resonance frequency 800 – 2000 kHz). The probe was inserted into the right spot on the scanner head and then positioned in place with a tweezer. After the probe was loaded, the scanner was located back in its position. By clicking the focus control buttons, the camera was focused on the tip.

- The laser was then quickly aligned by moving the laser spot with the arrows indicated in the window “Align Laser” or by double-clicking on the tip with the mouse courser in the camera image (See Figure 1). Optimisation of the Aligning Detector as well as the laser position can be achieved automatically by clicking “Auto-align Detector” or “Optimize Laser Position”.

- The tip location was optionally specified, and therefore tuning of the cantilever was completed. Optimal resolution for images was achieved with very sharp probes. To avoid the damage of the specimen when the probe was scanned at a fixed height, the tip was adjusted to the specimen distance by using a feedback system which assisted the system to keep a constant force between the probe and the specimen.

- A vertical piezoelectric scanner holds the cantilever and to maintain constant force. It moved the probe in the Z direction at the same time using another

piezoelectric block that scanned the specimen in the X and Y directions. The outcome was a topography represented by a map of the area $S= F (X, Y)$. A small area scan was scanned only at the beginning of the imaging procedure (about 500 nm) and the feedback gain was set as ≤ 1.

- The "Z Range" was set to its maximum value, as well as the "Deflection Limit" and "Amplitude Range". The probe moved slowly to the specimen surface. However, at the stage, there isn't any deflection since the tip and the specimen surface were still apart. At large distances (the right of the image), weak attractive forces occur between atoms at the apex of the probe and those at the surface of the specimen.
- The more the distance in the interatomic separation decreases the more increase exists in the attractive force.

- The cantilever was positioned very near to its resonance frequency and the amplitude of the oscillated stiff cantilever was set between 100-200 nm and was generally large enough to overcome the tip - specimen adhesion that may occur in contact mode (CM). At the time the probe was very close to the specimen, the attractive surface tension force pulls the probe to the specimen surface. This continued until the electrons of the atoms started to interact and repel each other electrostatically. The repulsive force weakens the total attraction with further decrease in this separation distance, until the forces reach a net force of zero (See Figure 2). At this stage, the distance between the atoms was nearly the length of a chemical bond and on the order of 2–3 Å. Finally the scanner was engaged and it started to scan the surface of the specimen.

- The height of the cantilever above the specimen's surface was controlled by the AFM electronic servo usage of a piezoelectric actuator to keep particular oscillation amplitude for the cantilever. The advantage of tapping the surface was a better friction resolution on the samples. Friction forces such as drag, which is common in CM, were drastically minimized since the tip that is in contact with the surface, barely taps or touches the specimen for a small fraction of its tapping period. Therefore, weakly adsorbed single fibrils were imaged. Furthermore, the energy loss that causes specimen degradation was quite smaller (Putman et al., 1994; You & Yu,

1999). It also reduced the degradation on the surface and the tip compared to the damage that may exist in the CM. Furthermore, TM was employed since it has a better resolution results(Putman et al., 1994; Hansma et al., 1995).

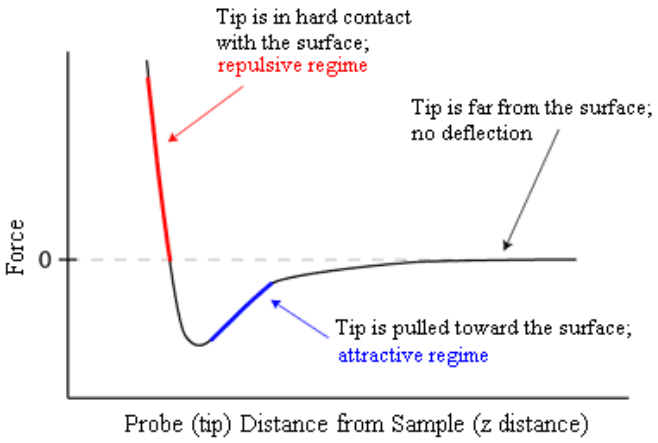

Figure1. The van der Waals energy curve representing the main systems during probe approach and retraction (Wallace, 2012).

- With lesser separation, the interactive forces became positive (repulsive). The repulsive force pulled away the probe from the surface and the retraction phase started when the probe was in a firm contact with the specimen's surface. The atoms were described to be in contact. In the contact area, the slope of the curve is quite sharp. Hence, the repulsive forces balance nearly any forces pushing the atoms closer together. In the case of AFM, the cantilever deflected when the cantilever attempted to push the probe against the specimen. Therefore, the force was measured indirectly by calculating the deflection of the cantilever. However, this force was directly relative to the force applied to the cantilever. The type of specimen, operation modes and the surrounding environment decides the probe's types.

- There were a set of parameters and settings that been adjusted to obtain a high resolution of the image (See Figure 3). Initially, the specimens/line value was increased to its maximum level and then the amplitude setpoint was increased incrementally until the tip was no longer tracing the surface of the specimen. This was noticeable when the retrace and trace lines were no longer placed over and appeared

as straight lines. The piezo moved up to its maximum height to remain in contact with the probe. Consequently the amplitude set point was lowered again until the tip has resumed tracking again. A good amplitude setpoint value was slightly lowered after the tip started tracking. This was to reduce the imaging force on the specimen.

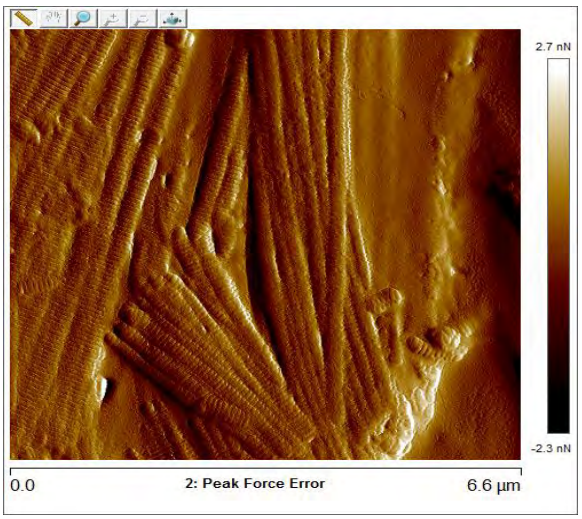

Figure 2. An AFM topography and amplitude images in tapping mode of collagen fibrils (measuring 6 x 6 µm) in the histological tendon sample of white New Zealand rabbits. Figure shows the circled bundles of collagen fibrils with their characteristic D-periodicity pattern. The fibrils form a network-like structure. Some of them overlap one another. The amplitude image (right) shows the fibril contours in more detail.

- In order to retain a constant force between the specimen and the probe, a feedback controller was used with a third piezoelectric actuator. This actuator keeps a chosen set point force between the probe and the specimen by moving the specimen up or down (Bruker) . The triggered z-piezo by a voltage moved the probe away from or towards the surface, if the measured force was smaller or larger than this set point. This brought the force back to its chosen set point. Topographic images were produced when the probe scans or taps across the surface of the specimen in the X-direction. The cantilever on which the probe was mounted, measured the interaction force between the specimen and the probe. An array of photodiodes position detector (Bruker) measured interaction force between the specimen and the probe and finally then displayed the deflection of a laser beam from the back of the oscillated cantilever onto a computerised system (See Figure 4).

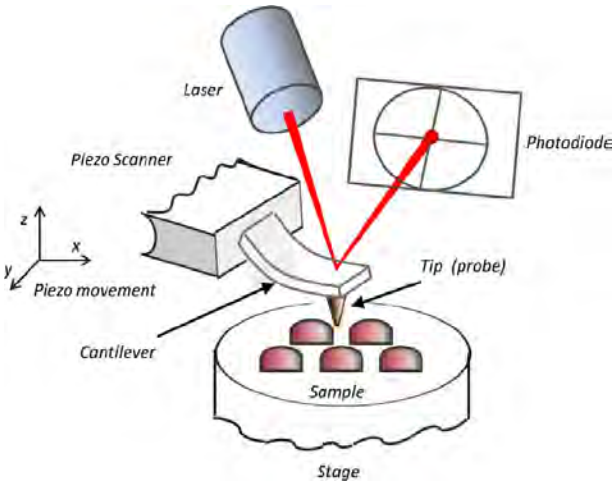

Figure 3. A laser beam and photodiodes position detector used to measure the beam position (Vidal & Mello, 1984). During scanning, the tip was adjusted very close to the specimen surface. Since the cantilever acts like a linear spring, the force was determined from Hooke's Law (F=−KX, where K is the cantilever's spring constant and X, is the deflection). AFM can generate high atomic and molecular resolution images beyond the light diffraction limit. The images was done in air, conductive and non-conductive surfaces. The lateral resolution was controlled by the specific specimen conditions required. However, it ranged from 1nm to the molecular scale up to 100 nm which was controlled by the resolution of the XYZ scanner stage (Santos et al., 2011).

- Modification of the Proportional and Integral gains has further improved the quality of the picture (See Figure 3). First, the Integral gain value was increased in small steps until the system resonated. The resonance was identified in the Amplitude window as an increased noise. The value dropped again to a set point where the system did not resonate any further. The same procedure was done with the Integral gain. As soon as the surface was properly tracked, the scan size was increased to several micrometres to obtain a general idea of the scanned fibre network and so the picture was captured. Next, a single fibre bundle area was zoomed into and high-resolution images were taken (See Figure 3) where one fibre bundle was oriented vertically in the software (along the slow scan axis) and the other bundles were tilted from it. The

fibre bundles are quite big structures compared to single fibrils, therefore, the engagement scanning was started at a random location.

Appendix 7

Main study (3, 6 and 9%): The association between the cohorts of the stress relaxation (SR) (SR1, SR2 and SR3) over time

The following graph shows the association between the concomitant changes in the normalised SR1 with the corresponding SR2 and SR3 and the concomitant changes in the SR2 with the SR3 during prolonged 3% strain. The three variables are significantly associated with a linear correlation of (R^2= 0.95, 0.97 and 0.97, P<.0001).

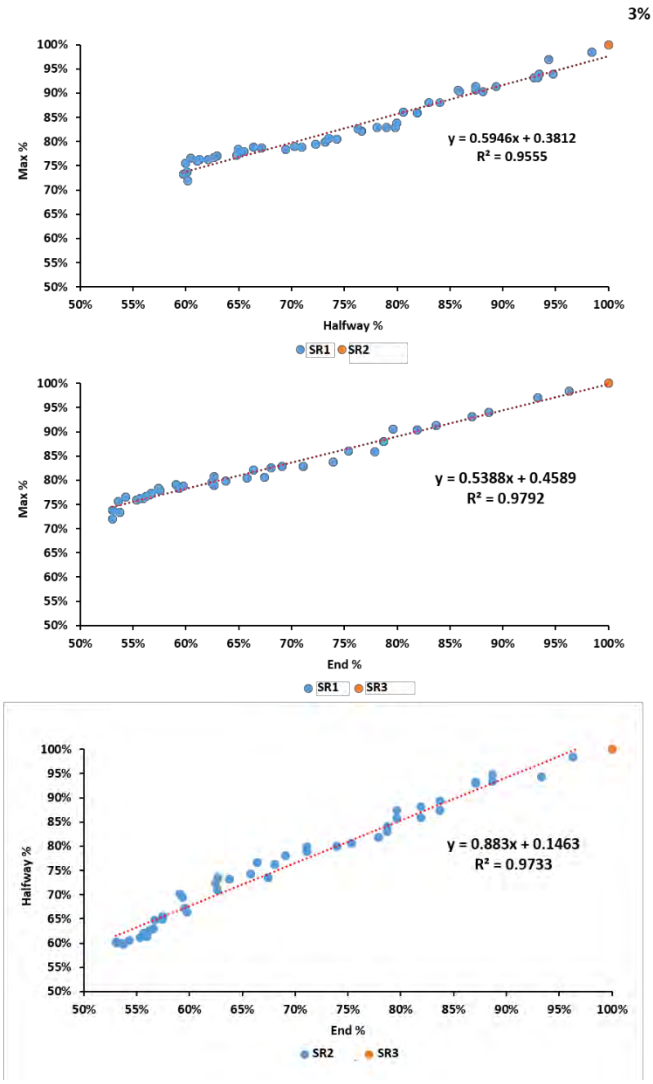

Figure 4. The graph shows the association between the cohorts of the stress relaxation (SR) (SR1, SR2 and SR3) over time from the 3% strain group.

The following graph shows the association between the concomitant changes in the normalised SR1 with the corresponding SR2 and SR3 and the concomitant changes in the SR2 with the SR3 during prolonged 6% strain. The three variables are significantly associated with a linear correlation of (R^2= 0.98, 0.95 and 0.97, P<.0001).

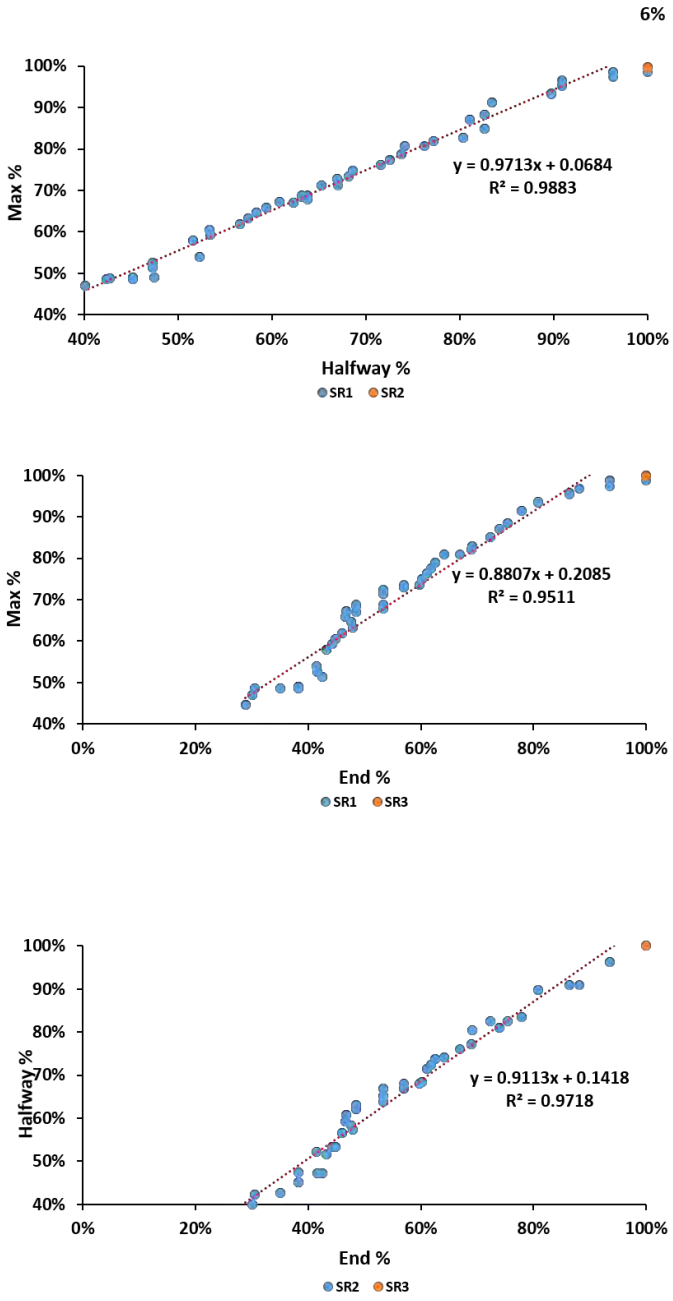

Figure 5. The graph shows the association between the cohorts of the stress relaxation (SR) (SR1, SR2 and SR3) over time from the 6% strain group.

The following graph shows the association between the concomitant changes in the normalised SR1 with the corresponding SR2 and SR3 and the concomitant changes in

the SR2 and SR3 during prolonged 9% strain. The three variables are significantly associated with a linear correlation of (R^2= 0.97, 0.93 and 0.96, P<.0001).

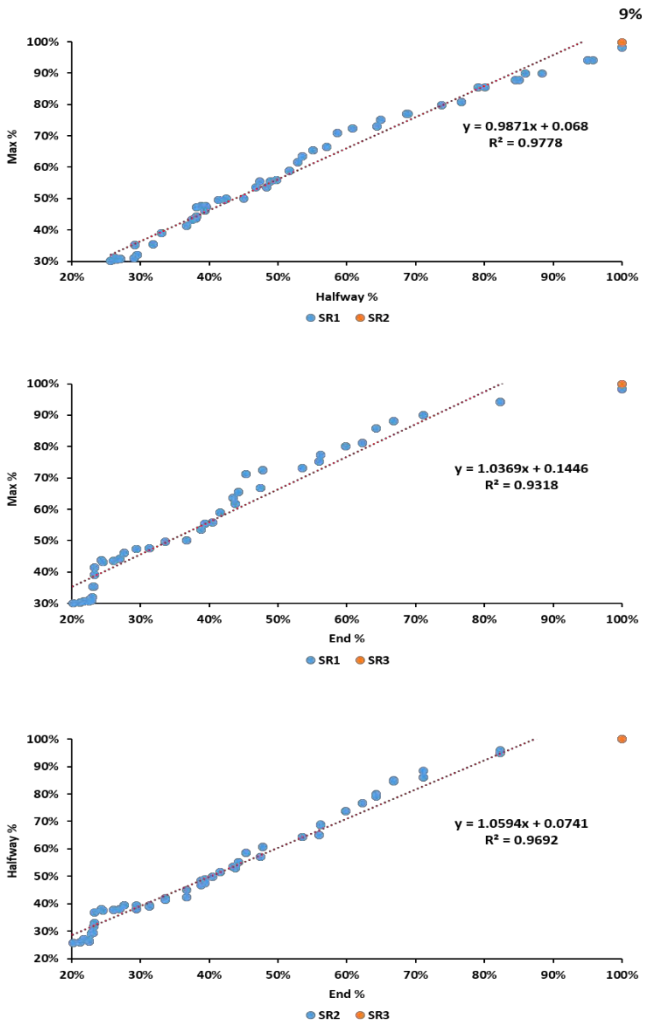

Figure 6. The graph shows the association between the cohorts of the stress relaxation (SR) (SR1, SR2 and SR3) over time from the 9% strain group.

Main study (3, 6 and 9%): The association between mechanical and macro-morphological changes over time

Ramping and Loading stiffness

The following graph shows the association between the concomitant changes in the tendon ramping stiffness with the corresponding loading stiffness during three prolonged different strains. Figure 1 demonstrates a decrease in ramping and loading stiffness over the repeated testing cycle. This corresponds with the decline around 30,

40 and 50% for 3, 6 and 9 % respectively. The two variables are significantly associated with a linear correlation of (R^2 = 0.97, 0.86 and 0.90, P<.0001 for 3, 6 and 9% respectively).

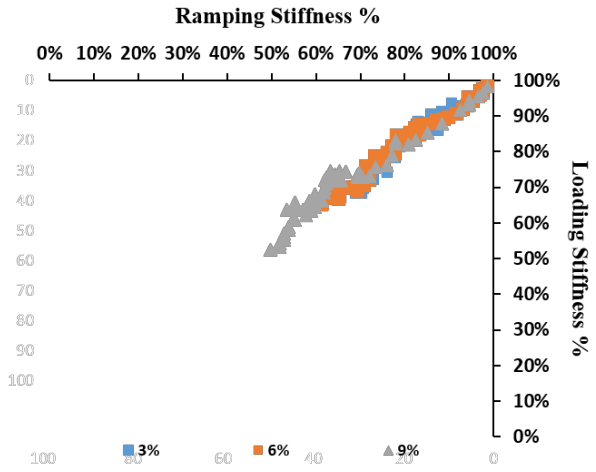

Figure 7. The change in the normalised ramping stiffness versus loading stiffness, this shows the association for three strain levels.

Loading stiffness and hysteresis

The following graph shows the association between the concomitant changes in the normalised tendon loading stiffness with the corresponding hysteresis during three prolonged different strains. There is a decrease in loading stiffness and hysteresis over the repeated testing cycle. At 3, 6 and 9 %, this corresponds with the average decline of 40, 70 and 90% respectively. The two variables are significantly associated with a linear correlation of (R^2 = 0.93, 0.97 and 0.94, P<.0001 for 3, 6 and 9% respectively).

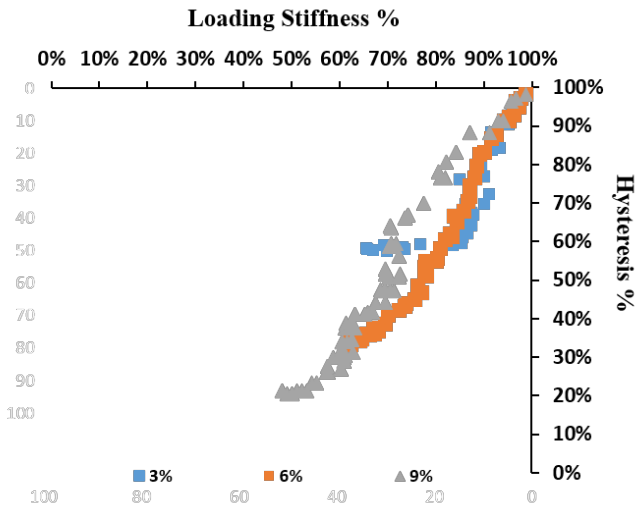

Figure 8. The change in the normalised loading stiffness versus hysteresis, this shows the association for three strain levels.

Loading stiffness and maximum load

The following graph shows the association between the concomitant changes in the normalised tendon loading stiffness with the corresponding maximum load during three prolonged different strains. In Figure 10, the figure demonstrates a linear decrease in loading stiffness and maximum load over the repeated testing cycle. At 3, 6 and 9 %, this corresponds with the average decline of 50, 70 and 80% respectively. The two variables are significantly associated with a linear correlation (R^2 = 0.94, 0.99 and 0.96, P<.0001 for 3, 6 and 9% respectively).

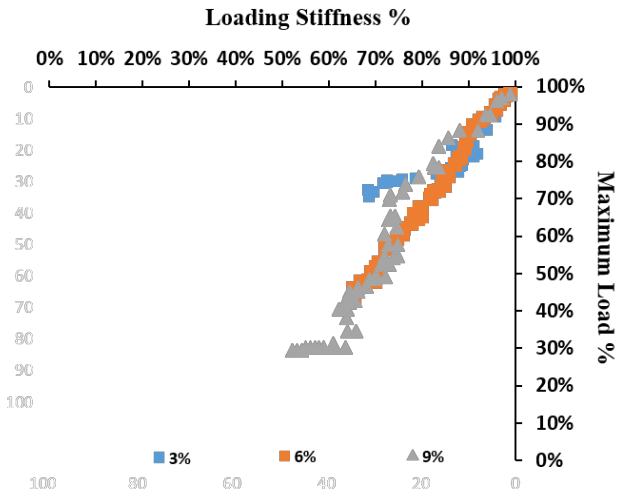

Figure 9. The change in the normalised loading stiffness versus max load, this shows the association for three strain levels.

<u>The GAG depleted study (6% for 2 hours) :The association between the cohorts of the stress relaxation (SR) (SR1, SR2 and SR3) over time from the control and GAG depleted groups.</u>

The following graph shows the association between the concomitant changes in the normalised SR1 with the corresponding SR2 and SR3 and the concomitant changes in the SR2 with the SR3 during prolonged 6% strain of the control group. The three variables are significantly associated with a linear correlation of (R^2= 0.97, 0.90 and 0.93, P<.0001).

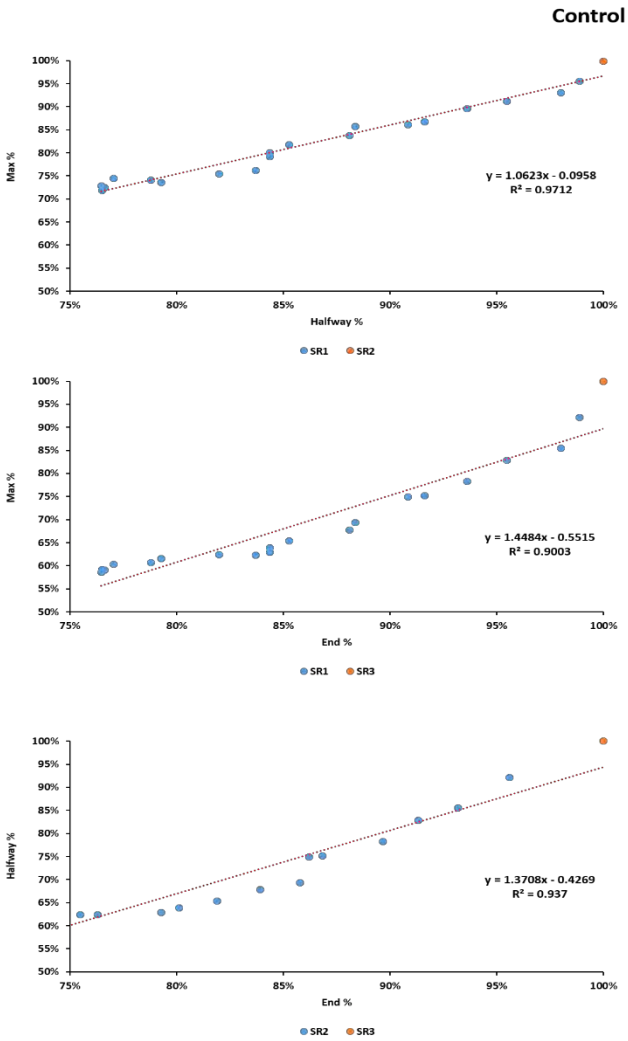

Figure 10. The graph shows the association between the cohorts of the stress relaxation (SR) (SR1, SR2 and SR3) over time from the control groups.

<u>The GAG depleted study (6% for 2 hours): The association between the cohorts of the stress relaxation (SR) (SR1, SR2 and SR3) over time from the control and GAG depleted groups.</u>

The following graph shows the association between the concomitant changes in the normalised SR1 with the corresponding SR2 and SR3 and the concomitant changes in the SR2 with the SR3 during prolonged 6% strain of the control group. The three variables are significantly associated with a linear correlation of (R^2= 0.99, 0.87 and 0.87, P<.0001).

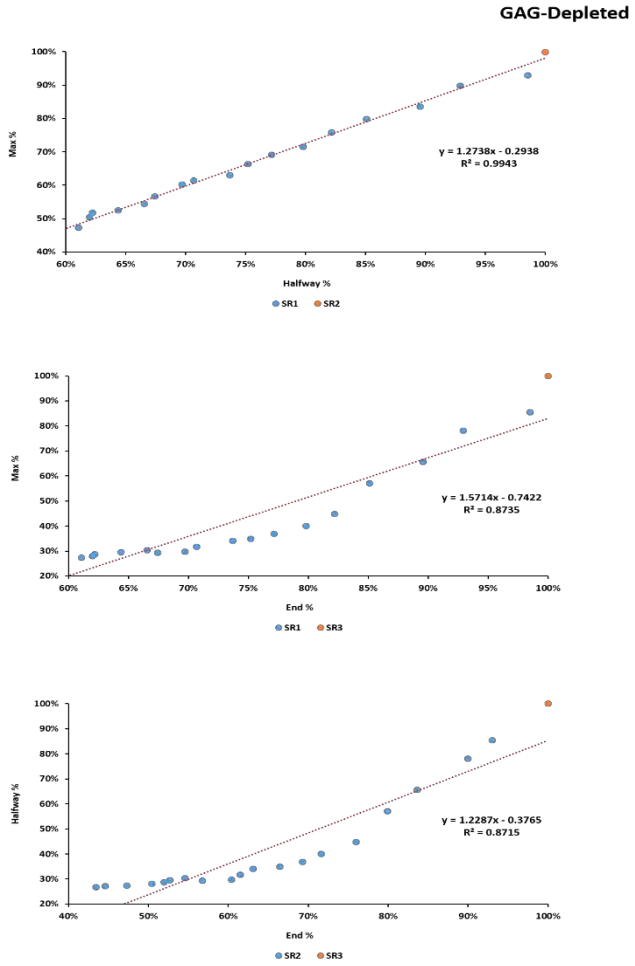

Figure 11. The graph shows the association between the cohorts of the stress relaxation (SR) (SR1, SR2 and SR3) over time from the GAG-depleted group.

The GAG depleted study (6% for 2 hours) : The association between mechanical Loading outcomes in control and GAG-depleted samples (6 % over 2 hours)

Ramping and Loading stiffness

The following graph shows the association between the concomitant changes in the tendon ramping stiffness with the corresponding loading stiffness during three prolonged different strains. There is a decrease in ramping and loading stiffness over the repeated testing cycle. For the control and GAG-depleted groups, this corresponds

with the decline by around 30% and 50% respectively. The two variables are significantly associated with a linear correlation of (R^2 = 0.95 for controls and 0.98 for GAG-depleted, P<.0001).

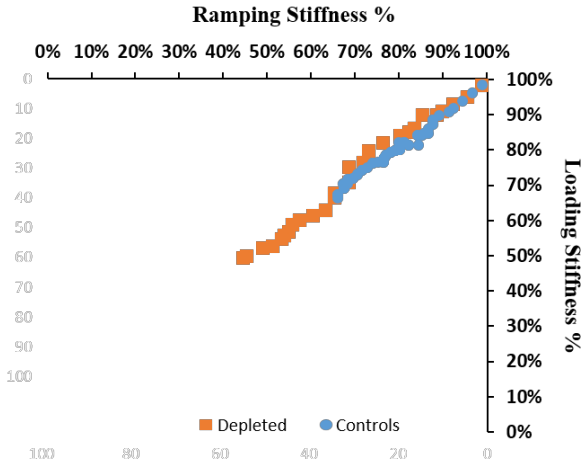

Figure 12. The change in ramping stiffness versus loading stiffness, this shows the association for three strain levels.

Loading stiffness and hysteresis

The following graph shows the concomitant changes in the tendon loading stiffness with the corresponding hysteresis during three prolonged different strains. There is a decrease in loading stiffness and hysteresis over the repeated testing cycle. For the control and GAG-depleted groups, this corresponds with the decline by around 50% and 70% respectively. The two variables are significantly associated with a linear correlation (R^2 = 0.97 for controls and 0.97 for GAG-depleted, P<.0001).

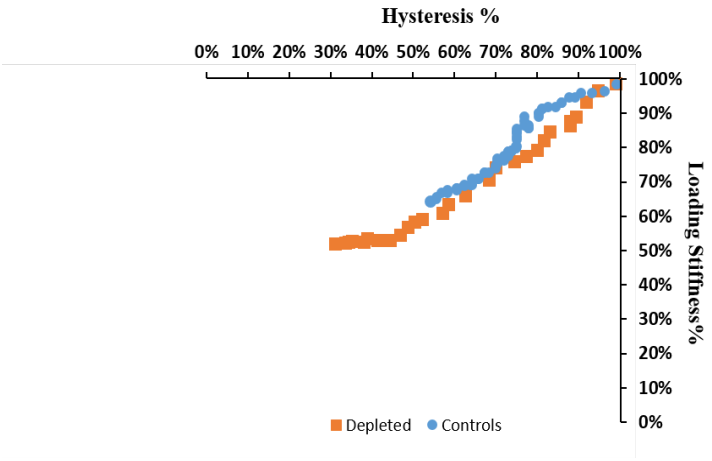

Figure 13. The change in loading stiffness versus hysteresis, this shows the association for three strain levels.

Loading stiffness and maximum load

The following graph shows the association between the concomitant changes in the tendon loading stiffness with the corresponding maximum load during three prolonged different strains. There is a decrease in loading stiffness and maximum load over the repeated testing cycle. For the control and GAG-depleted groups, this corresponds with the decline by around 30% and 40% respectively. The two variables are significantly associated with a linear correlation (R2 = 0.97 for controls and 0.97 for GAG-depleted, P<.0001).

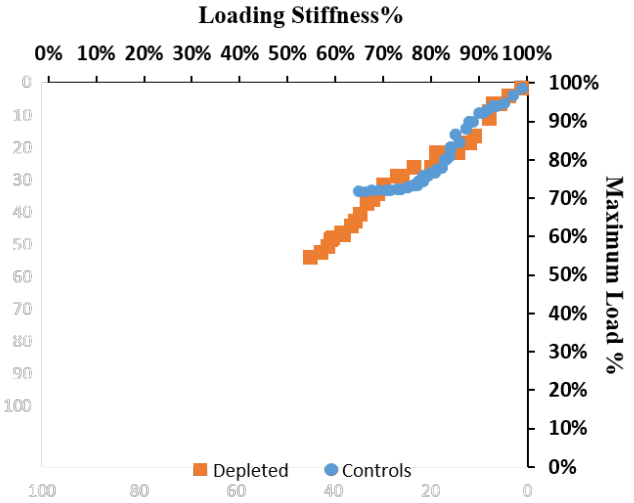

Figure 14. The change in loading stiffness versus maximum load, this shows the association for three strain levels.

Appendix 8

Main study: The association between mechanical and macro-morphological changes over time

Tenocyte Roundness (3%) – Loading Stiffness

Figure 16.A shows the proportion of cells in the samples that are spindle-like Cat (0 to 0.35). The figure demonstrates a linear decline from around 60% of cells to around 30% of cells. This corresponds with the decline in loading stiffness over the repeated testing cycle. The two variables are significantly associated with a linear correlation of (R^2 = 0.94, P<.0001). The corresponding proportional increase in the three remaining categories of roundness Cat I (0.35 – 0.60), Cat II (0.60 to 0.80) and Cat III (0.80 to 1.00) is shown in Figure 16.B. Each of these have a decline with polynomial associations of greater than R^2 = 0.87, all P<.0001.

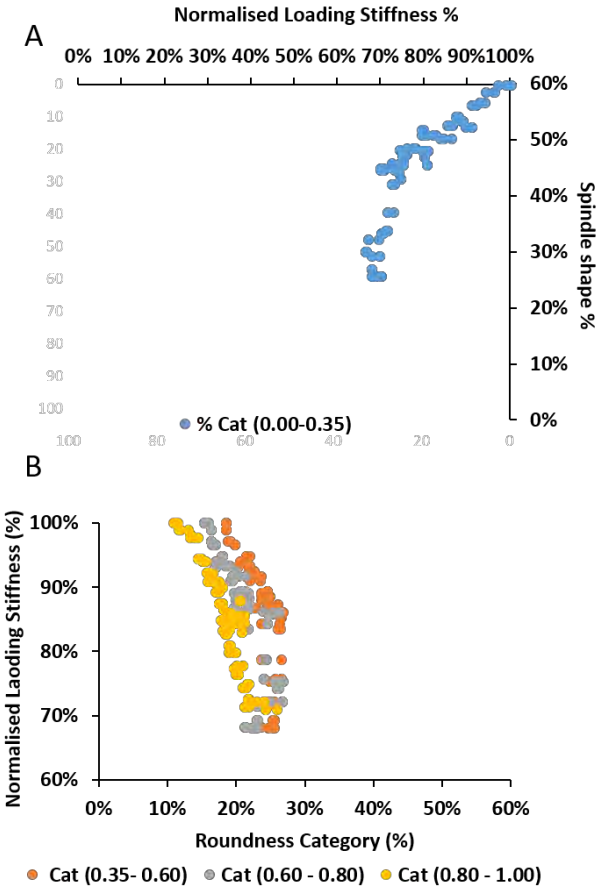

Figure 15. The scatter plots for changes (loading stiffness versus tenocyte roundness) in 3% group underwent of cyclic loading over 4 hours. Figure (A) represents the change in spindle shape [Cat 4 (0.00-0.35)] and figure (B) represents the changes in three remaining categories of roundness Cat 3 (0.35 – 0.60), Cat 2 (0.60 to 0.80) and Cat 1 (0.80 to 1.00).

Tenocyte Roundness (6%) – Loading Stiffness

Figure 17. A shows the proportion of cells in the samples that are spindle-like Cat (0 to 0.35). The figure demonstrates a linear decline from around 60% of cells to around 20% of cells. This corresponds with the decline in loading stiffness over the repeated testing cycle. The two variables are significantly associated with a linear correlation of (R^2 = 0.84, P<.0001). The corresponding proportional increase in the three remaining categories of roundness Cat I (0.35 – 0.60), Cat II (0.60 to 0.80) and Cat III (0.80 to 1.00) is shown in Figure 17.B. Each of these have a linear decline with associations of greater than R^2 = 0.89, all P<.0001.

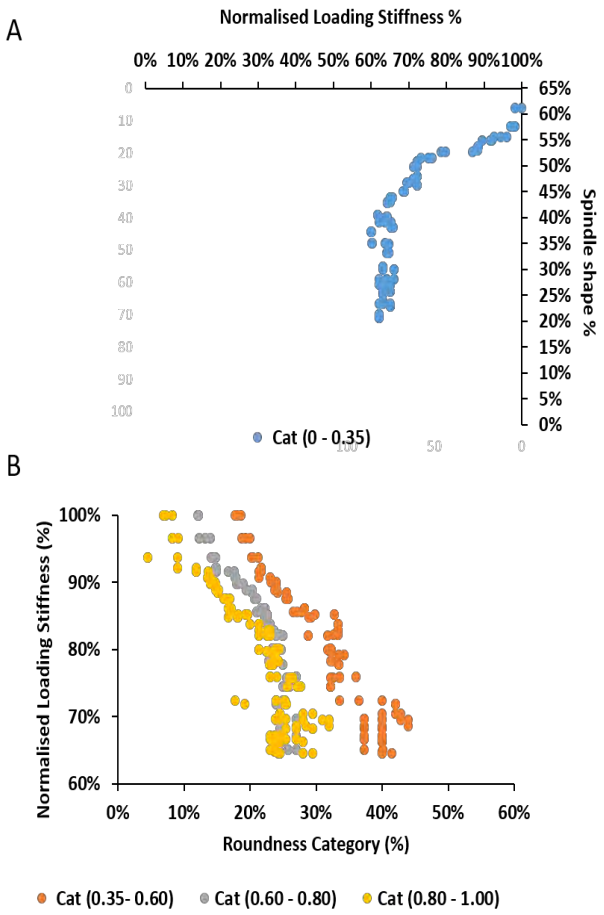

Figure 16. The scatter plots for changes (loading stiffness versus tenocyte roundness) in 6% group underwent of cyclic loading over 4 hours. Figure (A) represents the change in spindle shape [Cat 4 (0.00-0.35)] and figure (B) represents the changes in three remaining categories of roundness Cat 3 (0.35 – 0.60), Cat 2 (0.60 to 0.80) and Cat 1 (0.80 to 1.00).

Tenocyte Roundness (9%) – Loading Stiffness

Figure 18.A shows the proportion of cells in the samples that are spindle-like Cat (0 to 0.35). The figure demonstrates a linear decline from around 60% of cells to around 20% of cells. This corresponds with the decline in loading stiffness over the repeated testing cycle. The two variables are significantly associated with a linear correlation of (R^2 =0.93, P<.0001). The corresponding proportional increase in the three remaining categories of roundness Cat I (0.35 – 0.60), Cat II (0.60 to 0.80) and Cat III

(0.80 to 1.00) is shown in Figure 18.B. Each of these have a linear decline with associations of greater than $R^2 = 0.84$, all P<.0001.

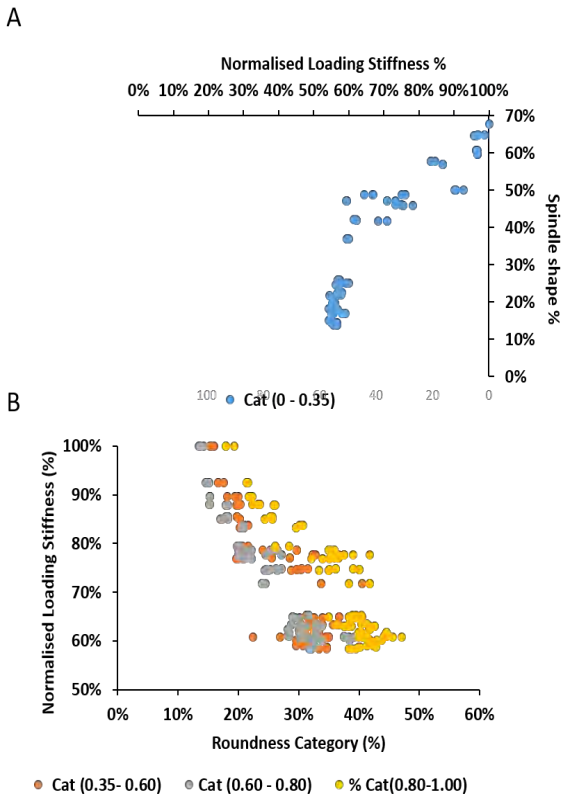

Figure 17. The scatter plots for changes (loading stiffness versus tenocyte roundness) in 9% group underwent of cyclic loading over 4 hours. Figure (A) represents the change in spindle shape [Cat 4 (0.00-0.35)] and figure (B) represents the changes in three remaining categories of roundness Cat 3 (0.35 – 0.60), Cat 2 (0.60 to 0.80) and Cat 1 (0.80 to 1.00).

Fibre waviness (3%) – Loading Stiffness

The following figures show the concomitant changes in fibre waviness with the decline of tendon's loading stiffness during three prolonged different strains.

Figure 19 shows the proportion of fibres in the samples that are wavy like as the loading stiffness declines. The figure demonstrates an increase (around 50%) in the waviness of fibres. This corresponds with the decline in loading stiffness (around

30%) over the repeated testing cycle. The two variables are significantly associated with a linear correlation of (R^2 = 0.93, P<.0001).

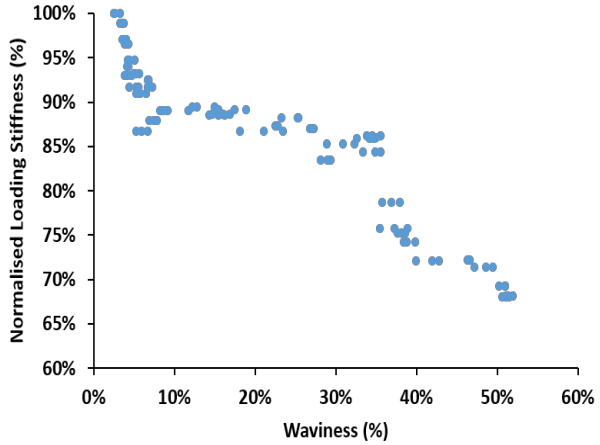

Figure 18. The scatter plots for changes (ramping stiffness versus waviness) in 3% group underwent 4 hours of cyclic loading.

Fibre waviness (6%) – Loading Stiffness

The following figures show the concomitant changes in fibre waviness with the decline of tendon's loading stiffness during three prolonged different strains.

Figure 20 shows the proportion of fibres in the samples that are wavy like as the loading stiffness declines. The figure demonstrates an increase (around 50%) in the waviness of fibres. This corresponds with the decline in loading stiffness (around 15%) over the repeated testing cycle. The two variables are significantly associated with a linear correlation of (R^2 = 0.85, P<.0001).

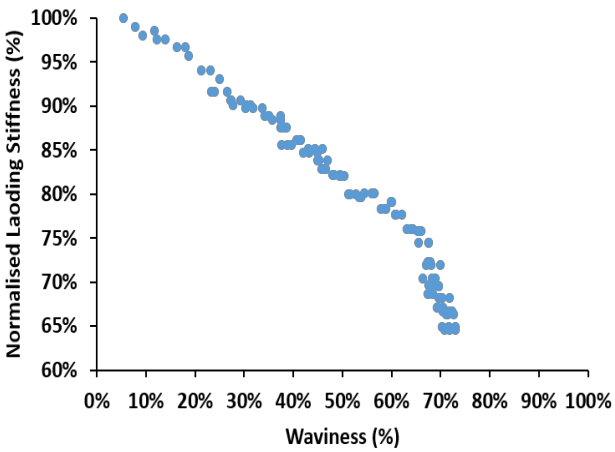

Figure 19. The scatter plots for changes (loading stiffness versus waviness) in 6% group underwent 4 hours of cyclic loading.

Fibre waviness (9%) – Loading Stiffness

The following figures show the concomitant changes in fibre waviness with the decline of tendon's loading stiffness during three prolonged different strains.

Figure 21 shows the proportion of fibres in the samples that are wavy like as the loading stiffness declines. The figure demonstrates an increase (around 90%) in the waviness of fibres. This corresponds with the decline in loading stiffness (around 50%) over the repeated testing cycle. The two variables are significantly associated with a linear correlation ($R^2 = 0.91$, $P<.0001$).

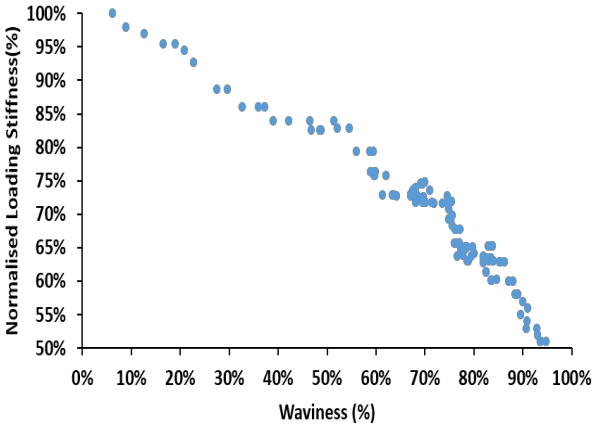

Figure 20. The scatter plots for changes (loading stiffness versus waviness) in 9% group underwent 4 hours of cyclic loading.

Appendix 9

GAG-Depleted study: The association between mechanical and macro-morphological changes over time

Tenocyte Roundness (6%) - Control – Loading Stiffness

Figure 21. A shows the proportion of cells in the samples that are spindle-like Cat (0 to 0.35) as the loading stiffness declines. The data demonstrates a significant association ($R^2 = 0.94$, P<.0001). The corresponding proportional increase in the three remaining categories of roundness Cat I (0.35 – 0.60), Cat II (0.60 to 0.80) and Cat III (0.80 to 1.00) is shown in Figure 21.B. Each of these have a decline with associations of greater than $R^2 = 0.15$, all P<.0001.

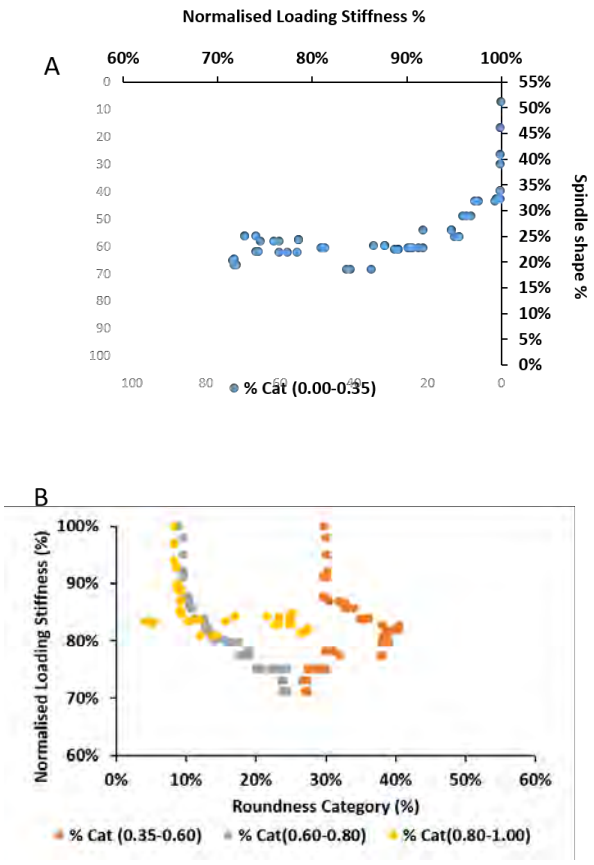

Figure 21. The scatter plots for changes (loading stiffness versus tenocyte roundness) in control group underwent 6% of cyclic loading over 2 hours. Figure (A) represents the change in spindle shape [Cat 4 (0.00-0.35)] and figure (B) represents the changes

in three remaining categories of roundness Cat 3 (0.35 – 0.60), Cat 2 (0.60 to 0.80) and Cat 1 (0.80 to 1.00).

Tenocyte Roundness (6%)-Depleted – Loading Stiffness

Figure 22. A shows the proportion of cells in the samples that are spindle-like Cat (0 to 0.35) as the loading stiffness declines. The data demonstrates a significant linear association ($R^2 = 0.97$, P<.0001). The corresponding proportional increase in the three remaining categories of roundness Cat I (0.35 – 0.60), Cat II (0.60 to 0.80) and Cat III (0.80 to 1.00) is shown in Figure 22.B. Each of these have a decline with associations of greater than $R^2 = 0.49$, all P<.0001.

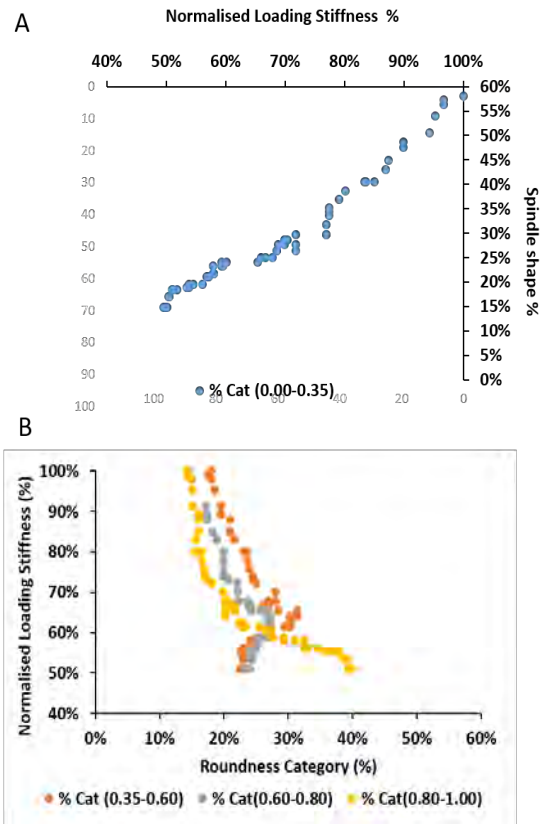

Figure 22. The scatter plots for changes (loading stiffness versus tenocyte roundness) in GAG- depleted group underwent 6% of cyclic loading over 2 hours. Figure (A) represents the change in spindle shape [Cat 4 (0.00-0.35)] and figure (B) represents the changes in three remaining categories of roundness Cat 3 (0.35 – 0.60), Cat 2 (0.60 to 0.80) and Cat 1 (0.80 to 1.00).

Fibre waviness (6%) – Depleted and Controls - Loading Stiffness

The following figures show the concomitant changes in fibre waviness with the decline of tendon's loading stiffness during three prolonged different strains.

Figure 23 shows the proportion of fibres in the samples that are wavy like as the loading stiffness declines. The figure demonstrates an increase (around 50% for control and 80% for depleted) in waviness of fibres. This corresponds with the decline in loading stiffness around 30% for controls and around 50% for depleted samples over the repeated testing cycle. The two variables are significantly associated with a linear correlation (R^2 = 0.80 for controls and 0.99 for GAG-depleted, P<.0001).

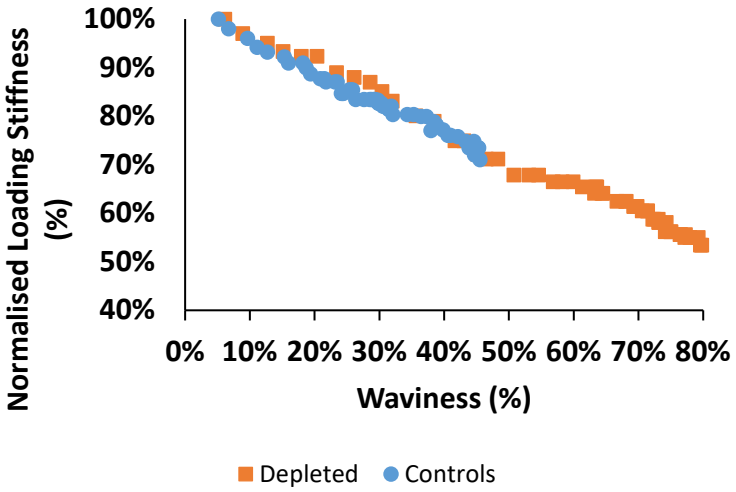

Figure 23. The scatter plots for changes in loading stiffness versus waviness for 6% cyclic loading for 2 hours for control and GAG-depleted tendons.

D-Periodicity (Within bundles and fibrils) 3%_Loading stiffness

The following graph shows the association between the changes in the tendon loading stiffness (declining) with the corresponding changes in D-Periodicity within bundles and within fibrils from the 3% group.

Figure 24 shows the proportional changes in within bundles and fibrils as the ramping stiffness declines. The figure demonstrates a linear increase (around 12 nm) in bundle and fibril D-Periodicities. This corresponds with the decline in ramping stiffness (around 25%) over the repeated testing cycle. The two variables are significantly associated with a linear correlation (R^2 = 0.88 for samples of within bundles D-Periodicities and R^2 = 0.90 for samples of within Fibrils D-Periodicities, P<.0001).

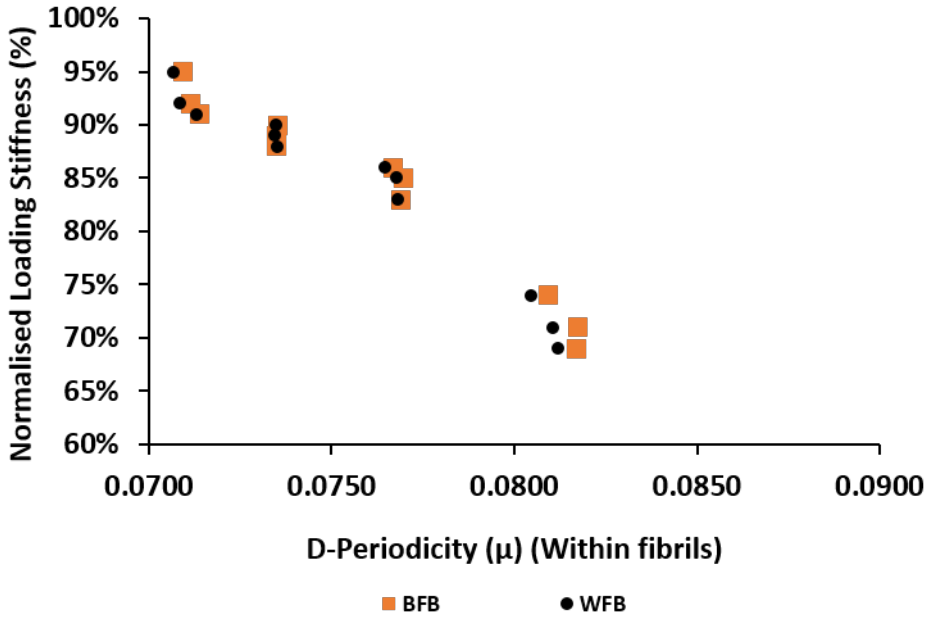

Figure 24. The scatter plots for changes in D-Periodicity (within bundles and within fibrils) versus the loading stiffness. The association/XY plot is demonstrated as four clusters of data representing hourly change.

D-Periodicity (Within bundles and fibrils) _ 6%_Loading stiffness

The following graph shows the association between the changes in the tendon loading stiffness (declining) with the corresponding changes in D-Periodicity within bundles and within fibrils from the 6% group

Figure 25 shows the proportional changes in within bundles and fibrils as the ramping stiffness declines. The figure demonstrates a linear increase (around 18 nm) in bundle and fibril D-Periodicities. This corresponds with the decline in loading stiffness

(around 30%) over the repeated testing cycle. The two variables are significantly associated with a linear correlation (R^2 = 0.96 for samples of within bundles D-Periodicities and R^2 = 0.96 for samples of within fibrils D-Periodicities, P<.0001).

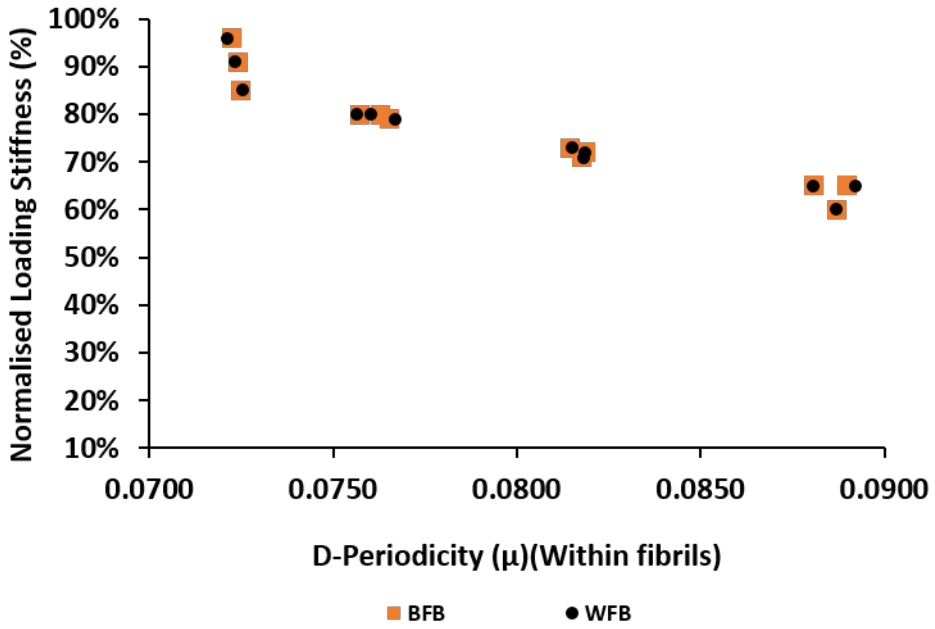

Figure 25. The change in D-Periodicity (within bundles and within fibrils) versus the loading stiffness. The association/XY plot is demonstrated as four clusters of data representing hourly change.

D-Periodicity (Within bundles and fibrils) _ 9%_Loading stiffness

The following graph shows the association between the changes in the tendon loading stiffness (declining) with the corresponding changes in D-Periodicity within bundles and within fibrils.

Figure 26 shows the proportional changes in within bundles and fibrils as the loading stiffness declines. The figure demonstrates an increase (around 20 nm) in bundle and fibril D-Periodicities. This corresponds with the decline in loading stiffness (around 40%) over the repeated testing cycle. The two variables are significantly associated with a linear correlation (R^2 = 0.92 for samples of within bundles D-Periodicities and R^2 = 0.92) for samples of within Fibrils D-Periodicities, P<.0001).

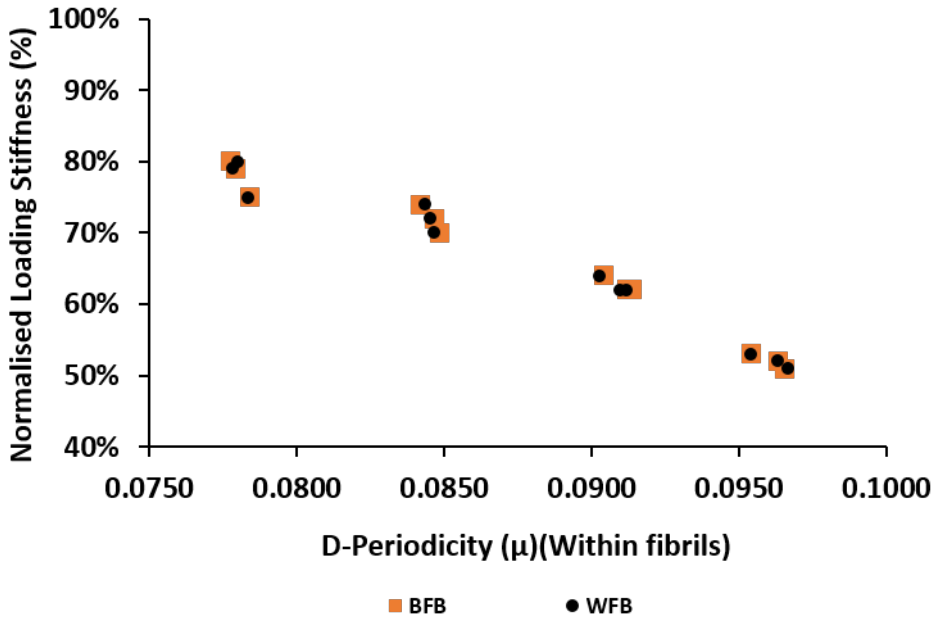

The figure 26. The change in D-Periodicity (within bundles and within fibrils) versus the loading stiffness. The association/XY plot is demonstrated as four clusters of data representing hourly change.

D-Periodicity (Within bundles and fibrils) _ 6% Controls and GAG-Depleted _ Loading stiffness

The following graph shows the association between the changes in the tendon loading stiffness (declining) with the corresponding changes in D-Periodicity (within bundles and within fibrils) from controls and depleted samples.

The figure 27 shows the proportion of changes in D-Periodicity (within bundles and within fibrils) as the loading stiffness declines. The figure demonstrates an increase (around 12 nm) in D-Periodicity. This corresponds with the decline in loading stiffness around 20% for controls and around 35% for depleted samples over the repeated testing cycle. The two variables are significantly associated with a correlation (R^2 = 0.90 for control samples of within bundles D-Periodicities and R^2 = 0.89 for GAG-depleted samples of within fibrils D-Periodicities, P<.0001).

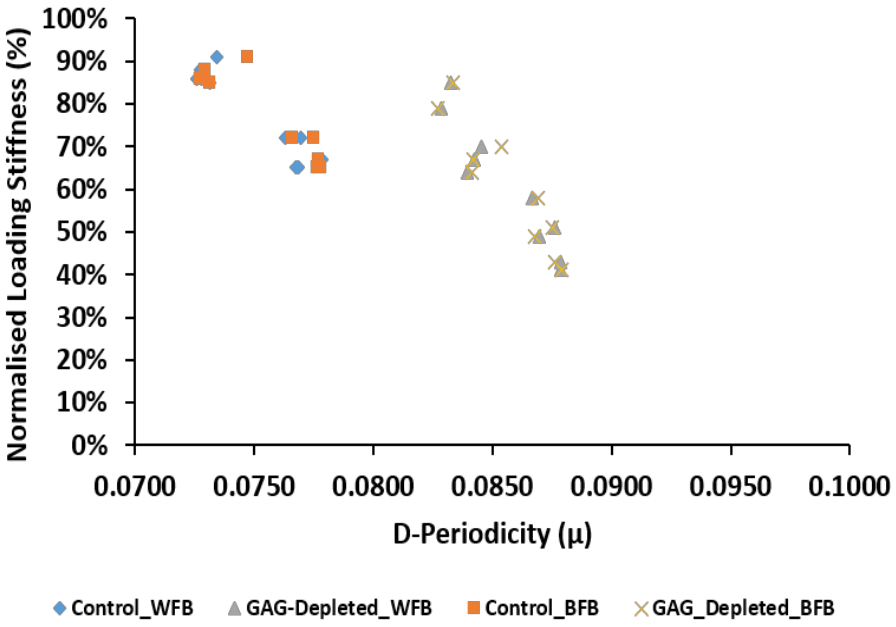

Figure 27. The scatter plots for changes in loading stiffness versus D-Periodicity (within bundles and within fibrils) for 6% cyclic loading over 2 hours for control and GAG-depleted tendons. The association/XY plot is demonstrated as two clusters of data representing hourly change.

Appendix 10

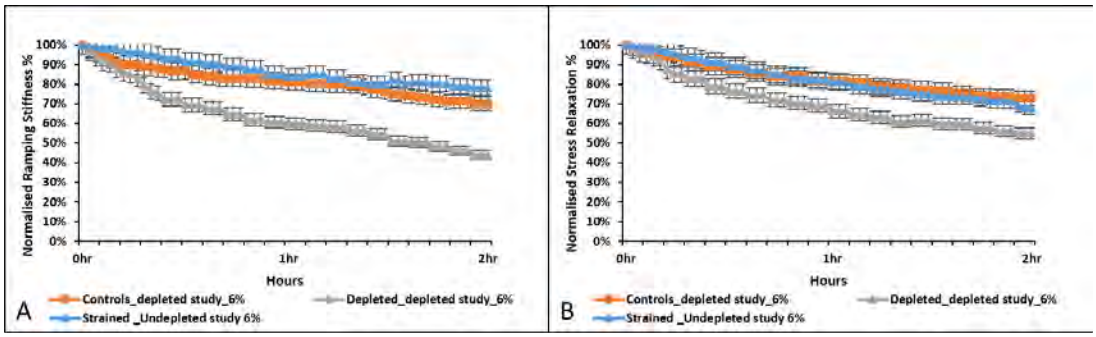

Figure 28. The normalised Stiffness (k) [A] and Stress relaxation (SR) [B] of tendons from the depleted study underwent 6% strained group over 2 hours of dynamic repetitive cyclic loading.

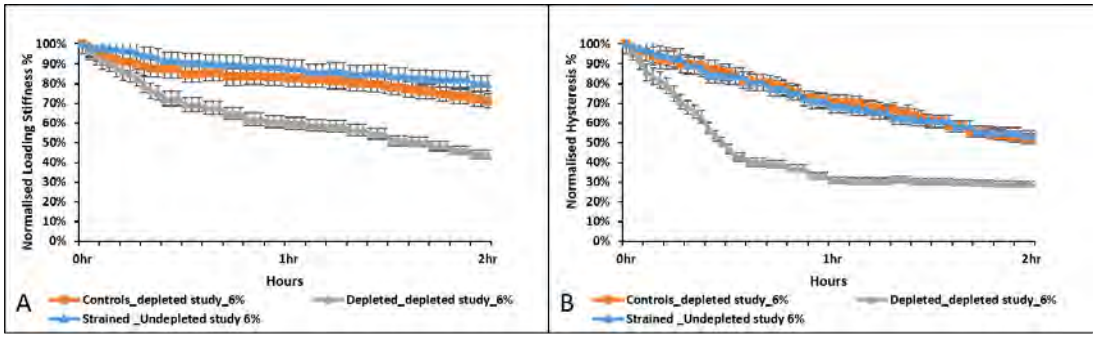

Figure 29. The normalised Loading Stiffness (LS) [A] and Hysteresis (H) [B] of tendons from the depleted study underwent 6% strained group over 2 hours of dynamic repetitive cyclic loading.

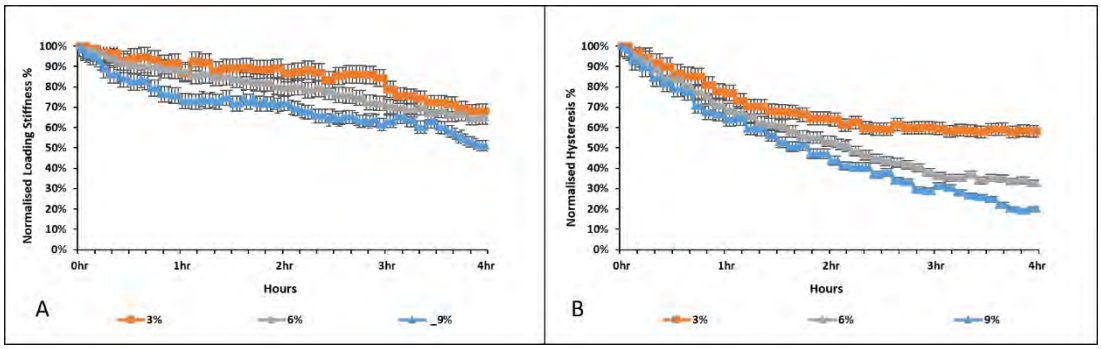

Figure 30. The normalised Loading Stiffness (LS) [A] and the normalised Hysteresis (h) [B] of tendons from 3, 6, and 9% strained groups over 1, 2, 3 and 4 hours of dynamic repetitive cyclic loading.

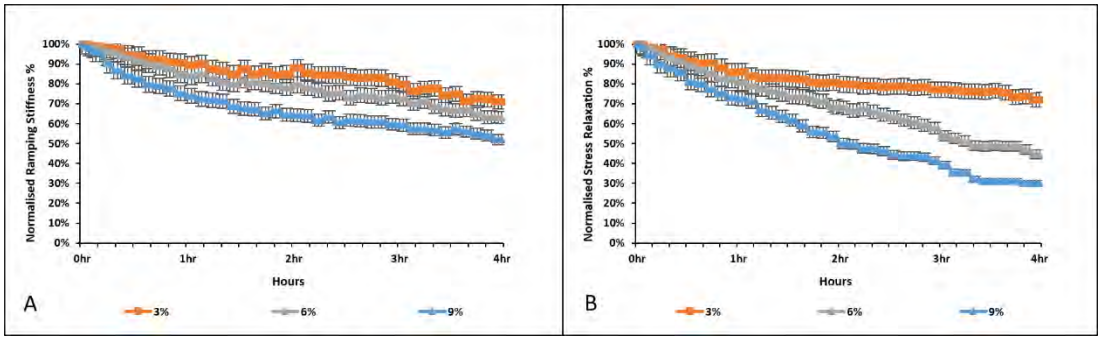

Figure 31. The normalised Stiffness (k) [A] and normalised stress relaxation (SR) [B] of tendons from 3, 6, and 9% strained groups over 1, 2, 3 and 4 hours of static repetitive cyclic loading.

Appendix 11

Reliability results and Summary

Observational classification of tendon morphology

The following two tables are the test-retest contingency tables for all the observation paired data between weeks. The within test blind repetition were consistent with the between sessions assessments.

Table 1. Cohen's weighted Kappa values for pairwise comparison of the inter-tester for within-session and between sessions for qualitative evaluation of fibre structure (A) and fibre arrangement and orientation (B).

A

		Week 2.			
	Category	I	II	III	IV
Week 1	I	0	0	0	0
	II	0	23	0	0
	III	0	0	53	2
	IV	0	0	0	37

Weighted Kappa	St Error	Lower Limit	Upper Limit
0.9724	0.0193	0.9345	1

B

		Week 2.			
	Category	I	II	III	IV
Week 1	I	0	0	0	0
	II	0	22	0	0
	III	0	0	57	0
	IV	0	1	2	34

Weighted Kappa	St Error	Lower Limit	Upper Limit
0.9314	0.03	0.8726	0.9902

Table 2. Cohen's weighted Kappa values for pairwise comparison of the intra-tester for qualitative evaluation of fibre structure (A) and fibre arrangement and orientation (B).

A

		1st tester			
	Category	I	II	III	IV
	I	0	0	0	0
2nd tester	II	0	25	0	0
	III	0	4	45	7
	IV	0	0	5	30

Weighted Kappa	**St Error**	**Lower Limit**	**Upper Limit**
0.8245	0.0422	0.7419	0.9071

B

		1st tester			
	Category	I	II	III	IV
	I	0	0	0	0
2nd tester	II	0	17	0	0
	III	0	4	52	9
	IV	0	0	6	28

Weighted Kappa	**St Error**	**Lower Limit**	**Upper Limit**
0.7659	0.0514	0.6652	0.8666

REFERENCES

Abate, M., Silbernagel, K.G., Siljeholm, C., Di Iorio, A., et al. (2009). Pathogenesis of tendinopathies: inflammation or degeneration? *Arthritis research & therapy, 11*(3), 235.

Abrahams, M. (1967). Mechanical behaviour of tendon in vitro. A preliminary report. *Med Biol Eng, 5*(5), 433-443. doi:10.1007/bf02479137

Abràmoff, M.D., Magalhães, P.J., & Ram, S.J.J.B.i. (2004). Image processing with ImageJ. *11*(7), 36-42.

Abramowitch, S., Zhang, X., Curran, M., & Kilger, R. (2010). A comparison of the quasi-static mechanical and non-linear viscoelastic properties of the human semitendinosus and gracilis tendons. *Clinical biomechanics, 25*(4), 325-331.

Abreu, E.L., Leigh, D., & Derwin, K.A. (2008). Effect of altered mechanical load conditions on the structure and function of cultured tendon fascicles. *J Orthop Res, 26*(3), 364-373. doi:10.1002/jor.20520

Abu-Abdeen, M. (2010). Single and double-step stress relaxation and constitutive modeling of viscoelastic behavior of swelled and un-swelled natural rubber loaded with carbon black. *Materials & Design, 31*(4), 2078-2084. doi:https://doi.org/10.1016/j.matdes.2009.10.006

Ahmadzadeh, H., Connizzo, B.K., Freedman, B.R., Soslowsky, L.J., et al. (2013). Determining the contribution of glycosaminoglycans to tendon mechanical properties with a modified shear-lag model. *J Biomech, 46*(14), 2497-2503. doi:10.1016/j.jbiomech.2013.07.008

Aisenberg, J. (2008). Gastrointestinal endoscopy nears “the molecular era”. In: Mosby.

Aladin, D.M., Cheung, K.M., Ngan, A.H., Chan, D., et al. (2010). Nanostructure of collagen fibrils in human nucleus pulposus and its correlation with macroscale tissue mechanics. *J Orthop Res, 28*(4), 497-502. doi:10.1002/jor.21010

Alexander, R.M. (2002). Tendon elasticity and muscle function. *Comp Biochem Physiol A Mol Integr Physiol, 133*(4), 1001-1011.

Alfredson, H., Ohberg, L., & Forsgren, S. (2003). Is vasculo-neural ingrowth the cause of pain in chronic Achilles tendinosis? An investigation using ultrasonography and colour Doppler, immunohistochemistry, and diagnostic injections. *Knee Surg Sports Traumatol Arthrosc, 11*(5), 334-338. doi:10.1007/s00167-003-0391-6

Andarawis-Puri, N., & Flatow, E.L. (2011). Tendon fatigue in response to mechanical loading. *J Musculoskelet Neuronal Interact, 11*(2), 106-114.

Arampatzis, A., Karamanidis, K., Mademli, L., & Albracht, K. (2009). Plasticity of the human tendon to short- and long-term mechanical loading. *Exerc Sport Sci Rev, 37*(2), 66-72. doi:10.1097/JES.0b013e31819c2e1d

Archambault, J. (2003). Tendon micromechanics and research methods in tendinopathy. *J Musculoskelet Neuronal Interact, 3*(4), 326-328; discussion 333-324.

Archambault, J.M., & Banes, A.J. (2005). Research Methodology and Animal Modeling in Tendinopathy. In Maffulli, Renström & Leadbetter (Eds.),

Tendon Injuries: Basic Science and Clinical Medicine (pp. 279-286). London: Springer London.

Archambault, J.M., Hart, D.A., & Herzog, W. (2001). Response of rabbit Achilles tendon to chronic repetitive loading. *Connect Tissue Res, 42*(1), 13-23.

Arndt, A., Bengtsson, A.S., Peolsson, M., Thorstensson, A., et al. (2012). Non-uniform displacement within the Achilles tendon during passive ankle joint motion. *Knee Surg Sports Traumatol Arthrosc, 20*(9), 1868-1874. doi:10.1007/s00167-011-1801-9

Arner, O. (1959). Subcutaneous rupture of the Achilles tendon. A study of 92 cases. *Acta. Chir. Scandinavica Supplementum., 239*.

Arnoczky, S.P., Lavagnino, M., & Egerbacher, M. (2007). The mechanobiological aetiopathogenesis of tendinopathy: is it the over-stimulation or the under-stimulation of tendon cells? *Int J Exp Pathol, 88*(4), 217-226. doi:10.1111/j.1365-2613.2007.00548.x

Arnoczky, S.P., Lavagnino, M., Whallon, J.H., & Hoonjan, A. (2002). In situ cell nucleus deformation in tendons under tensile load; a morphological analysis using confocal laser microscopy. *J Orthop Res, 20*(1), 29-35. doi:10.1016/s0736-0266(01)00080-8

Arya, S., & Kulig, K. (2010). Tendinopathy alters mechanical and material properties of the Achilles tendon. *J Appl Physiol (1985), 108*(3), 670-675. doi:10.1152/japplphysiol.00259.2009

Ashby, D. (1991). Practical statistics for medical research. Douglas G. Altman, Chapman and Hall, London, 1991. No. of pages: 611. *Statistics in medicine, 10*(10), 1635-1636.

Aström, M., Rausing, A.J.C.o., & research, r. (1995). Chronic Achilles tendinopathy. A survey of surgical and histopathologic findings. (316), 151-164.

Atkinson, T.S., Ewers, B.J., & Haut, R.C. (1999). The tensile and stress relaxation responses of human patellar tendon varies with specimen cross-sectional area. *J Biomech, 32*(9), 907-914.

Backman, C., Boquist, L., Friden, J., Lorentzon, R., et al. (1990). Chronic achilles paratenonitis with tendinosis: an experimental model in the rabbit. *J Orthop Res, 8*(4), 541-547. doi:10.1002/jor.1100080410

Bancroft, J.D., & Gamble, M. (2008). *Theory and practice of histological techniques*: Elsevier Health Sciences.

Bannerman, A., Paxton, J.Z., & Grover, L.M. (2014). Imaging the hard/soft tissue interface. *Biotechnol Lett, 36*(3), 403-415. doi:10.1007/s10529-013-1374-4

Baselt, D.R., Revel, J.P., & Baldeschwieler, J.D. (1993). Subfibrillar structure of type I collagen observed by atomic force microscopy. *Biophysical Journal, 65*(6), 2644-2655.

Bear, R.S. (1944). X-Ray Diffraction Studies on Protein Fibers. I. The Large Fiber-Axis Period of Collagen. *Journal of the American Chemical Society, 66*(8), 1297-1305. doi:10.1021/ja01236a027

Bell, R., Boniello, M.R., Gendron, N.R., Flatow, E.L., et al. (2015). Delayed exercise promotes remodeling in sub-rupture fatigue damaged tendons. *33*(6), 919-925. doi:10.1002/jor.22856

Beniash, E., Traub, W., Veis, A., & Weiner, S. (2000). A Transmission Electron Microscope Study Using Vitrified Ice Sections of Predentin: Structural

Changes in the Dentin Collagenous Matrix prior to Mineralization. *J Struct Biol, 132*(3), 212-225. doi:http://dx.doi.org/10.1006/jsbi.2000.4320
Benjamin, M., Kaiser, E., & Milz, S. (2008). Structure-function relationships in tendons: a review. *J Anat, 212*(3), 211-228.
Bennett, M.B., Ker, R.F., Imery, N.J., & Alexander, R. (1986). Mechanical properties of various mammalian tendons. *Journal of Zoology, 209*(4), 537-548. doi:10.1111/j.1469-7998.1986.tb03609.x
Birch, H. (2007). Tendon matrix composition and turnover in relation to functional requirements. *Int J Exp Pathol, 88*(4), 241-248. doi:10.1111/j.1365-2613.2007.00552.x
Birk, D.E., Southern, J.F., Zycband, E.I., Fallon, J.T., et al. (1989). Collagen fibril bundles: a branching assembly unit in tendon morphogenesis. *Development, 107*(3), 437-443.
Birk, D.E., & Trelstad, R.L. (1986). Extracellular compartments in tendon morphogenesis: collagen fibril, bundle, and macroaggregate formation. *J Cell Biol, 103*(1), 231-240.
Bogaerts, S., Desmet, H., Slagmolen, P., & Peers, K. (2016). Strain mapping in the Achilles tendon - A systematic review. *J Biomech, 49*(9), 1411-1419. doi:10.1016/j.jbiomech.2016.02.057
Bojsen-Møller, J., & Magnusson, S.P. (2019). Mechanical properties, physiological behavior, and function of aponeurosis and tendon. *126*(6), 1800-1807. doi:10.1152/japplphysiol.00671.2018
Bosco, C., & Rusko, H. (1983). The effect of prolonged skeletal muscle stretch-shortening cycle on recoil of elastic energy and on energy expenditure. *Acta Physiol Scand, 119*(3), 219-224. doi:10.1111/j.1748-1716.1983.tb07331.x
Bosco, C., Viitasalo, J.T., Komi, P.V., & Luhtanen, P. (1982). Combined effect of elastic energy and myoelectrical potentiation during stretch-shortening cycle exercise. *Acta Physiol Scand, 114*(4), 557-565. doi:10.1111/j.1748-1716.1982.tb07024.x
Bozec, L., Groot, J.d., Odlyha, M., Nicholls, B., et al. (2005). Atomic force microscopy of collagen structure in bone and dentine revealed by osteoclastic resorption. *Ultramicroscopy, 105*(1–4), 79-89. doi:http://dx.doi.org/10.1016/j.ultramic.2005.06.021
Bozec, L., & Horton, M. (2005). Topography and Mechanical Properties of Single Molecules of Type I Collagen Using Atomic Force Microscopy. *Biophysical Journal, 88*(6), 4223-4231. doi:http://dx.doi.org/10.1529/biophysj.104.055228
Bozec, L., van der Heijden, G., & Horton, M. (2007). Collagen Fibrils: Nanoscale Ropes. *Biophysical Journal, 92*(1), 70-75. doi:10.1529/biophysj.106.085704
Brandes, G., & Reale, E. (1990). The reaction of Acridine Orange with proteoglycans in the articular cartilage of the rat. *The Histochemical Journal, 22*(2), 106-112. doi:10.1007/bf01885789
Brodsky, B., Eikenberry, E.F., & Cassidy, K. (1980). An unusual collagen periodicity in skin. *Biochimica et Biophysica Acta (BBA) - Protein Structure, 621*(1), 162-166. doi:http://dx.doi.org/10.1016/0005-2795(80)90072-0
Bromage, T.G., Goldman, H.M., McFarlin, S.C., Warshaw, J., et al. (2003). Circularly polarized light standards for investigations of collagen fiber

orientation in bone. *Anat Rec B New Anat, 274*(1), 157-168. doi:10.1002/ar.b.10031
Bruehlmann, S., Kelly, E., & Duncan, N. (2005). In situ tendon damage occurs within the interfibril matrix. *Trans Orthop Res Soc, 30*, 389.
Bruker. https://www.bruker.com/products/surface-and-dimensional-analysis/atomic-force-microscopes/afm-application-notes/an133-introduction-to-brukers-scanasyst-and-peakforce-tapping.html.
Burkhardt, D., Hwa, S.Y., & Ghosh, P. (2001). A novel microassay for the quantitation of the sulfated glycosaminoglycan content of histological sections: its application to determine the effects of Diacerhein on cartilage in an ovine model of osteoarthritis. *Osteoarthritis Cartilage, 9*(3), 238-247. doi:10.1053/joca.2000.0381
Butler, D., Noyes, F., Walz, K., & Gibbons, M. (1987). Biomechanics of human knee ligament allograft treatment. *Trans Orthop Res Soc, 12*(128), 55-60.
Butler, D.L., Grood, E.S., Noyes, F.R., & Zernicke, R.F. (1978). Biomechanics of ligaments and tendons. *Exerc Sport Sci Rev, 6*, 125-181.
Canty, E.G., & Kadler, K.E. (2005). Procollagen trafficking, processing and fibrillogenesis. *J Cell Sci, 118*(Pt 7), 1341-1353. doi:10.1242/jcs.01731
Canty, E.G., Lu, Y., Meadows, R.S., Shaw, M.K., et al. (2004). Coalignment of plasma membrane channels and protrusions (fibripositors) specifies the parallelism of tendon. *J Cell Biol, 165*(4), 553-563. doi:10.1083/jcb.200312071
Carpinteri, A., & Pugno, N.M. (2008). Mechanics of hierarchical materials. *International Journal of Fracture, 150*(1-2), 221.
Carvalho, F.A., Martins, I.C., & Santos, N.C. (2013). Atomic force microscopy and force spectroscopy on the assessment of protein folding and functionality. *Arch Biochem Biophys, 531*(1-2), 116-127. doi:10.1016/j.abb.2012.11.007
Chao, Hsu, H., & Tseng, H. (2014). Electrospun microcrimped fibers with nonlinear mechanical properties enhance ligament fibroblast phenotype. *Biofabrication, 6*(3), 035008. doi:10.1088/1758-5082/6/3/035008
Chen, J., Song, S.K., Liu, W., McLean, M., et al. (2003). Remodeling of cardiac fiber structure after infarction in rats quantified with diffusion tensor MRI. *Am J Physiol Heart Circ Physiol, 285*(3), H946-954. doi:10.1152/ajpheart.00889.2002
Chen, J., Yu, Q., Wu, B., Lin, Z., et al. (2011). Autologous tenocyte therapy for experimental Achilles tendinopathy in a rabbit model. *Tissue Engineering Part A, 17*(15-16), 2037-2048.
Cheng, V.W.T., & Screen, H.R.C. (2007). The micro-structural strain response of tendon. *Journal of materials science, 42*(21), 8957-8965. doi:10.1007/s10853-007-1653-3
Connizzo, B.K., Freedman, B.R., Fried, J.H., Sun, M., et al. (2015). Regulatory role of collagen V in establishing mechanical properties of tendons and ligaments is tissue dependent. *Journal of Orthopaedic Research, 33*(6), 882-888.
Connizzo, B.K., Han, L., Birk, D.E., & Soslowsky, L.J. (2016). Collagen V-heterozygous and -null supraspinatus tendons exhibit altered dynamic mechanical behaviour at multiple hierarchical scales. *Interface Focus, 6*(1). doi:10.1098/rsfs.2015.0043

Connizzo, B.K., Sarver, J.J., Han, L., & Soslowsky, L.J. (2014). In situ fibril stretch and sliding is location-dependent in mouse supraspinatus tendons. *J Biomech, 47*(16), 3794-3798. doi:http://dx.doi.org/10.1016/j.jbiomech.2014.10.029

Connizzo, B.K., Yannascoli, S.M., & Soslowsky, L.J. (2013). Structure–function relationships of postnatal tendon development: A parallel to healing. *Matrix Biology, 32*(2), 106-116. doi:http://dx.doi.org/10.1016/j.matbio.2013.01.007

Cook, J.L., Khan, K.M., & Purdam, C. (2002). Achilles tendinopathy. *Man Ther, 7*(3), 121-130.

Cook, J.L., & Purdam, C.R. (2009). Is tendon pathology a continuum? A pathology model to explain the clinical presentation of load-induced tendinopathy. *British Journal of Sports Medicine, 43*(6), 409. doi:10.1136/bjsm.2008.051193

Copeland, N.G., Jenkins, N.A., Gilbert, D.J., Eppig, J.T., et al. (1993). A genetic linkage map of the mouse: current applications and future prospects. *Science, 262*(5130), 57-66. doi:10.1126/science.8211130

Corsi, A., Xu, T., Chen, X.D., Boyde, A., et al. (2002). Phenotypic effects of biglycan deficiency are linked to collagen fibril abnormalities, are synergized by decorin deficiency, and mimic Ehlers-Danlos-like changes in bone and other connective tissues. *J Bone Miner Res, 17*(7), 1180-1189. doi:10.1359/jbmr.2002.17.7.1180

Coulson-Thomas, V.a.G., T. F. . (2014). Dimethylmethylene Blue Assay (DMMB). *Bio-protocol 4*(18), e1236.

Craig, A.S., Birtles, M.J., Conway, J.F., & Parry, D.A. (1989). An estimate of the mean length of collagen fibrils in rat tail-tendon as a function of age. *Connect Tissue Res, 19*(1), 51-62.

Cribb, A.M., & Scott, J.E. (1995). Tendon response to tensile stress: an ultrastructural investigation of collagen:proteoglycan interactions in stressed tendon. *Journal of Anatomy, 187*(Pt 2), 423-428.

Cundy, T. (2012). Recent advances in osteogenesis imperfecta. *Calcif Tissue Int, 90*(6), 439-449. doi:10.1007/s00223-012-9588-3

Curwin, S. (1994). The aetiology and treatment of tendinitis. In *Oxford textbook of sports medicine* (pp. 512-528): Oxford University Press, Oxford.

Cusack, S., & Miller, A. (1979). Determination of the elastic constants of collagen by Brillouin light scattering. *Journal of Molecular Biology, 135*(1), 39-51. doi:http://dx.doi.org/10.1016/0022-2836(79)90339-5

Dallas, S.L., Chen, Q., & Sivakumar, P. (2006). Dynamics of assembly and reorganization of extracellular matrix proteins. *Curr Top Dev Biol, 75*, 1-24. doi:10.1016/s0070-2153(06)75001-3

Danylchuk, K., Finlay, J.B., & Krcek, J. (1978). Microstructural organization of human and bovine cruciate ligaments. *Clinical orthopaedics and related research*(131), 294-298.

de Vet, H.C., Terwee, C.B., Knol, D.L., & Bouter, L.M. (2006). When to use agreement versus reliability measures. *J Clin Epidemiol, 59*(10), 1033-1039. doi:10.1016/j.jclinepi.2005.10.015

Derwin, K.A., Soslowsky, L.J., Kimura, J.H., & Plaas, A.H. (2001). Proteoglycans and glycosaminoglycan fine structure in the mouse tail tendon fascicle. *J Orthop Res, 19*(2), 269-277. doi:10.1016/s0736-0266(00)00032-2

Devkota, A.C., Tsuzaki, M., Almekinders, L.C., Banes, A.J., et al. (2007). Distributing a fixed amount of cyclic loading to tendon explants over longer periods induces greater cellular and mechanical responses. *J Orthop Res, 25*(8), 1078-1086. doi:10.1002/jor.20389

Diamant, J., Keller, A., Baer, E., Litt, M., et al. (1972). Collagen; Ultrastructure and Its Relation to Mechanical Properties as a Function of Ageing. *Proceedings of the Royal Society of London. Series B, Biological Sciences, 180*(1060), 293-315. doi:10.2307/76283

Dirks, R.C., & Warden, S.J. (2011). Models for the study of tendinopathy. *J Musculoskelet Neuronal Interact, 11*(2), 141-149.

Doral, M.N., Alam, M., Bozkurt, M., Turhan, E., et al. (2010). Functional anatomy of the Achilles tendon. *Knee Surg Sports Traumatol Arthrosc, 18*(5), 638-643. doi:10.1007/s00167-010-1083-7

Dowling, B.A., & Dart, A.J. (2005). Mechanical and functional properties of the equine superficial digital flexor tendon. *The Veterinary Journal, 170*(2), 184-192. doi:http://dx.doi.org/10.1016/j.tvjl.2004.03.021

Drury, N.J. (2008). *Evaluating the anterior stability provided by the glenohumeral capsule: a finite element approach.* University of Pittsburgh,

Drury, R.A.B., & Wallington, E. (1967). Carleton's histological technique.

Duenwald-Kuehl, S., Kondratko, J., Lakes, R.S., & Vanderby, R., Jr. (2012). Damage mechanics of porcine flexor tendon: mechanical evaluation and modeling. *Ann Biomed Eng, 40*(8), 1692-1707. doi:10.1007/s10439-012-0538-z

Duenwald-Kuehl, S.E., Kondratko, J., Vanderby, R., & Lakes, R. (2011). *Characterization of Tendon Mechanics Following Subfailure Damage*, New York, NY.

Duenwald, S.E., Vanderby, R., Jr., & Lakes, R.S. (2009). Viscoelastic relaxation and recovery of tendon. *Ann Biomed Eng, 37*(6), 1131-1140. doi:10.1007/s10439-009-9687-0

Eaton, P., & West, P. (2010). Atomic force microscopy. Oxford Univ Press.

Eikenberry, E.F., Brodsky, B., & Parry, D.A.D. (1982). Collagen fibril morphology in developing chick metatarsal tendoms: 1. X-ray diffraction studies. *International Journal of Biological Macromolecules, 4*(6), 322-328. doi:http://dx.doi.org/10.1016/0141-8130(82)90063-0

Einhorn, T.A., Buckwalter, J.A., & O'Keefe, R.J. (2007). *Orthopaedic basic science: foundations of clinical practice*: Amer Academy of Orthopaedic.

Elliott, D.M., Robinson, P.S., Gimbel, J.A., Sarver, J.J., et al. (2003). Effect of Altered Matrix Proteins on Quasilinear Viscoelastic Properties in Transgenic Mouse Tail Tendons. *Ann Biomed Eng, 31*(5), 599-605. doi:10.1114/1.1567282

Eppell, S.J., Smith, B.N., Kahn, H., & Ballarini, R. (2006). Nano measurements with micro-devices: mechanical properties of hydrated collagen fibrils. *Journal of the Royal Society Interface, 3*(6), 117-121. doi:10.1098/rsif.2005.0100

Erickson, B., Fang, M., Wallace, J.M., Orr, B.G., et al. (2013). Nanoscale structure of type I collagen fibrils: quantitative measurement of D-spacing. *Biotechnol J, 8*(1), 117-126. doi:10.1002/biot.201200174

Espinosa, H.D., Zhu, Y., & Moldovan, N. (2007). Design and Operation of a MEMS-Based Material Testing System for Nanomechanical Characterization. *Microelectromechanical Systems, Journal of, 16*(5), 1219-1231. doi:10.1109/JMEMS.2007.905739

Ezura, Y., Chakravarti, S., Oldberg, Å., Chervoneva, I., et al. (2000). Differential Expression of Lumican and Fibromodulin Regulate Collagen Fibrillogenesis in Developing Mouse Tendons. *J Cell Biol, 151*(4), 779-788.

Fahlstrom, M., & Alfredson, H. (2010). Ultrasound and Doppler findings in the Achilles tendon among middle-aged recreational floor-ball players in direct relation to a match. *Br J Sports Med, 44*(2), 140-143. doi:10.1136/bjsm.2008.047316

Fang, Goldstein, E.L., Turner, A.S., Les, C.M., et al. (2012). Type I Collagen D-spacing in Fibril Bundles of Dermis, Tendon and Bone: Bridging Between Nano- and Micro-Level Tissue Hierarchy. *ACS nano, 6*(11), 9503-9514. doi:10.1021/nn302483x

Fang, & Holl, M.M.B. (2013). Variation in type I collagen fibril nanomorphology: the significance and origin. *BoneKEy Rep, 2*. doi:10.1038/bonekey.2013.128

Fang, Liroff, K., Turner, S., Les, M., et al. (2012). Estrogen depletion results in nanoscale morphology changes in dermal collagen. *J Invest Dermatol, 132*(7), 1791-1797. doi:10.1038/jid.2012.47

Farndale, R.W., Buttle, D.J., & Barrett, A.J. (1986). Improved quantitation and discrimination of sulphated glycosaminoglycans by use of dimethylmethylene blue. *Biochim Biophys Acta, 883*(2), 173-177.

Farris, D.J., Trewartha, G., & McGuigan, M.P. (2011). Could intra-tendinous hyperthermia during running explain chronic injury of the human Achilles tendon? *J Biomech, 44*(5), 822-826. doi:10.1016/j.jbiomech.2010.12.015

Farris, D.J., Trewartha, G., & McGuigan, M.P. (2012). The effects of a 30-min run on the mechanics of the human Achilles tendon. *Eur J Appl Physiol, 112*(2), 653-660. doi:10.1007/s00421-011-2019-8

Fessel, G., & Snedeker, J.G. (2009). Evidence against proteoglycan mediated collagen fibril load transmission and dynamic viscoelasticity in tendon. *Matrix Biol, 28*(8), 503-510. doi:10.1016/j.matbio.2009.08.002

Fessel, G., & Snedeker, J.G. (2011). Equivalent stiffness after glycosaminoglycan depletion in tendon--an ultra-structural finite element model and corresponding experiments. *J Theor Biol, 268*(1), 77-83. doi:10.1016/j.jtbi.2010.10.007

Finni, T., Peltonen, J., Stenroth, L., & Cronin, N.J. (2013). Viewpoint: On the hysteresis in the human Achilles tendon. *J Appl Physiol (1985), 114*(4), 515-517. doi:10.1152/japplphysiol.01005.2012

Folkard, W., Geercken, W., Knorzer, E., Mosler, E., et al. (1987). Structural dynamic of native tendon collagen. *J Mol Biol, 193*(2), 405-407.

Folkhard, W., Mosler, E., Geercken, W., Knörzer, E., et al. (1987). Quantitative analysis of the molecular sliding mechanisms in native tendon collagen — time-resolved dynamic studies using synchrotron radiation. *International Journal of Biological Macromolecules, 9*(3), 169-175. doi:http://dx.doi.org/10.1016/0141-8130(87)90047-X

Foure, A., Cornu, C., & Nordez, A. (2012). Is tendon stiffness correlated to the dissipation coefficient? *Physiol Meas, 33*(1), N1-9. doi:10.1088/0967-3334/33/1/n1

Franchi, De Pasquale, V., Martini, D., Quaranta, M., et al. (2010). Contribution of glycosaminoglycans to the microstructural integrity of fibrillar and fiber crimps in tendons and ligaments. *The Scientific World Journal, 10*, 1932-1940.

Franchi, Fini, M., Quaranta, M., De Pasquale, V., et al. (2007). Crimp morphology in relaxed and stretched rat Achilles tendon. *Journal of Anatomy, 210*(1), 1-7. doi:10.1111/j.1469-7580.2006.00666.x

Franchi, Quaranta, M., Macciocca, M., Leonardi, L., et al. (2010). Collagen fibre arrangement and functional crimping pattern of the medial collateral ligament in the rat knee. *Knee Surg Sports Traumatol Arthrosc, 18*(12), 1671-1678. doi:10.1007/s00167-010-1084-6

Franchi, Raspanti, M., Dell'Orbo, C., Quaranta, M., et al. (2008). Different crimp patterns in collagen fibrils relate to the subfibrillar arrangement. *Connect Tissue Res, 49*(2), 85-91. doi:10.1080/03008200801913635

Franchi, M., Ottani, V., Stagni, R., & Ruggeri, A. (2010). Tendon and ligament fibrillar crimps give rise to left-handed helices of collagen fibrils in both planar and helical crimps. *Journal of Anatomy*, *216*(3), 301-309. doi:10.1111/j.1469-7580.2009.01188.x

Fraser, R.D., MacRae, T.P., & Miller, A. (1987). Molecular packing in type I collagen fibrils. *J Mol Biol, 193*(1), 115-125.

Fraser, R.D., MacRae, T.P., Miller, A., & Suzuki, E. (1983). Molecular conformation and packing in collagen fibrils. *J Mol Biol, 167*(2), 497-521.

Fratzl, Gupta, H., Paschalis, E., & Roschger, P. (2004). Structure and mechanical quality of the collagen–mineral nano-composite in bone. *Journal of materials chemistry, 14*(14), 2115-2123.

Fratzl, Misof, K., Zizak, I., Rapp, G., et al. (1998). Fibrillar structure and mechanical properties of collagen. *J Struct Biol, 122*(1-2), 119-122. doi:10.1006/jsbi.1998.3966

Fratzl, P. (2008). Collagen: Structure and Mechanics, an Introduction. In Fratzl (Ed.), *Collagen* (pp. 1-13): Springer US.

Freedman, B.R., Sarver, J.J., Buckley, M.R., Voleti, P.B., et al. (2014). Biomechanical and structural response of healing Achilles tendon to fatigue loading following acute injury. *J Biomech, 47*(9), 2028-2034. doi:10.1016/j.jbiomech.2013.10.054

Freedman, B.R., Zuskov, A., Sarver, J.J., Buckley, M.R., et al. (2015). Evaluating changes in tendon crimp with fatigue loading as an ex vivo structural assessment of tendon damage. *J Orthop Res, 33*(6), 904-910. doi:10.1002/jor.22875

Fung, D.T., Sereysky, J.B., Basta-Pljakic, J., et al. (2010). Second harmonic generation imaging and Fourier transform spectral analysis reveal damage in fatigue-loaded tendons. journals of biomedical engineering, 38(5), 1741-1751. https://doi.org/10.1007/s10439-010-9976-7

Fung, D.T., Wang, V.M., Andarawis-Puri, N., Basta-Pljakic, J., et al. (2010). Early response to tendon fatigue damage accumulation in a novel in vivo model. *J Biomech, 43*(2), 274-279.

Fung, D.T., Wang, V.M., Laudier, D.M., Shine, J.H., et al. (2009). Subrupture tendon fatigue damage. *Journal of Orthopaedic Research, 27*(2), 264-273.

Gagliano, N., Menon, A., Martinelli, C., Pettinari, L., et al. (2013). Tendon structure and extracellular matrix components are affected by spasticity in cerebral palsy patients. *Muscles Ligaments Tendons J, 3*(1), 42-50. doi:10.11138/mltj/2013.3.1.042

Gautieri, A., Vesentini, S., Redaelli, A., & Buehler, M.J. (2011). Hierarchical Structure and Nanomechanics of Collagen Microfibrils from the Atomistic Scale Up. *Nano Letters, 11*(2), 757-766. doi:10.1021/nl103943u

Gautieri, A., Vesentini, S., Redaelli, A., & Buehler, M.J. (2012). Viscoelastic properties of model segments of collagen molecules. *Matrix Biol, 31*(2), 141-149. doi:10.1016/j.matbio.2011.11.005

Ge, J., Cui, F.-Z., Wang, X., & Wang, Y. (2007). New evidence of surface mineralization of collagen fibrils in wild type zebrafish skeleton by AFM and TEM. *Materials Science and Engineering: C, 27*(1), 46-50. doi:http://dx.doi.org/10.1016/j.msec.2006.01.006

Gimbel, J.A., Van Kleunen, J.P., Mehta, S., Perry, S.M., et al. (2004). Supraspinatus tendon organizational and mechanical properties in a chronic rotator cuff tear animal model. *J Biomech, 37*(5), 739-749. doi:10.1016/j.jbiomech.2003.09.019

Graham, H.K., Holmes, D.F., Watson, R.B., & Kadler, K.E. (2000). Identification of collagen fibril fusion during vertebrate tendon morphogenesis. The process relies on unipolar fibrils and is regulated by collagen-proteoglycan interaction. *J Mol Biol, 295*(4), 891-902. doi:10.1006/jmbi.1999.3384

Graham, J.S., Vomund, A.N., Phillips, C.L., & Grandbois, M. (2004). Structural changes in human type I collagen fibrils investigated by force spectroscopy. *Exp Cell Res, 299*(2), 335-342. doi:10.1016/j.yexcr.2004.05.022

Grigg, N.L., Wearing, S.C., & Smeathers, J.E. (2012). Achilles tendinopathy has an aberrant strain response to eccentric exercise. *Med Sci Sports Exerc, 44*(1), 12-17. doi:10.1249/MSS.0b013e318227fa8c

Gross, J., & Schmitt, F.O. (1948). The Structure of Human Skin Collagen As Studied with The Electron Microscope *The Journal of Experimental Medicine, 88*(5), 555-568. doi:10.1084/jem.88.5.555

Guilak, F. (1995). Compression-induced changes in the shape and volume of the chondrocyte nucleus. *J Biomech, 28*(12), 1529-1541. doi:10.1016/0021-9290(95)00100-x

Gupta, H.S., Seto, J., Krauss, S., Boesecke, P., et al. (2010). In situ multi-level analysis of viscoelastic deformation mechanisms in tendon collagen. *Journal of structural biology, 169*(2), 183-191. doi:http://dx.doi.org/10.1016/j.jsb.2009.10.002

Gupta, H.S., Seto, J., Wagermaier, W., Zaslansky, P., et al. (2006). Cooperative deformation of mineral and collagen in bone at the nanoscale. *Proceedings of the National Academy of Sciences, 103*(47), 17741-17746.

Gupta, S., Wagermaier, W., Zickler, G.A., Raz-Ben Aroush, D., et al. (2005). Nanoscale Deformation Mechanisms in Bone. *Nano Letters, 5*(10), 2108-2111. doi:10.1021/nl051584b

Gutsmann, T., Fantner, G.E., Kindt, J.H., Venturoni, M., et al. (2004). Force Spectroscopy of Collagen Fibers to Investigate Their Mechanical Properties and Structural Organization. *Biophysical Journal, 86*(5), 3186-3193.

Habelitz, S., Balooch, M., Marshall, S.J., Balooch, G., et al. (2002). In situ atomic force microscopy of partially demineralized human dentin collagen fibrils. *J Struct Biol, 138*(3), 227-236. doi:http://dx.doi.org/10.1016/S1047-8477(02)00029-1

Hakimi, O., Ternette, N., Murphy, R., Kessler, B.M., et al. (2017). A quantitative label-free analysis of the extracellular proteome of human supraspinatus tendon reveals damage to the pericellular and elastic fibre niches in torn and aged tissue. *PLoS One, 12*(5), e0177656. doi:10.1371/journal.pone.0177656

Hamilton, B., Remedios, D., Loosemore, M., & Maffulli, N. (2008). Achilles tendon rupture in an elite athlete following multiple injection therapies. *J Sci Med Sport, 11*(6), 566-568. doi:10.1016/j.jsams.2007.03.008

Hammond, M.A., Gallant, M.A., Burr, D.B., & Wallace, J.M. (2014). Nanoscale changes in collagen are reflected in physical and mechanical properties of bone at the microscale in diabetic rats. *Bone, 60*(0), 26-32. doi:http://dx.doi.org/10.1016/j.bone.2013.11.015

Hansen, K.A., Weiss, J.A., & Barton, J.K. (2002). Recruitment of tendon crimp with applied tensile strain. *J Biomech Eng, 124*(1), 72-77.

Hansen, P., Haraldsson, B.T., Aagaard, P., Kovanen, V., et al. (2010). Lower strength of the human posterior patellar tendon seems unrelated to mature collagen cross-linking and fibril morphology. *J Appl Physiol (1985), 108*(1), 47-52. doi:10.1152/japplphysiol.00944.2009

Hansma, H.G., Laney, D.E., Bezanilla, M., Sinsheimer, R.L., et al. (1995). Applications for atomic force microscopy of DNA. *Biophys J, 68*(5), 1672-1677. doi:10.1016/s0006-3495(95)80343-7

Harvey, A., Cornell, H., Hulley, P., Cochlin, L., et al. (2010). *Functional imaging of tendon extracellular matrix*.

Hayes, A. (2017). Mechanical Behaviour of Tendinopathic Tendon: *An Engineering Perspective*. Curtin University,

Heinemeier, K.M., & Kjaer, M. (2011). In vivo investigation of tendon responses to mechanical loading. *J Musculoskelet Neuronal Interact, 11*(2), 115-123.

Henninger, H.B., Maas, S.A., Shepherd, J.H., Joshi, S., et al. (2009). Transversely isotropic distribution of sulfated glycosaminoglycans in human medial collateral ligament: a quantitative analysis. *J Struct Biol, 165*(3), 176-183. doi:10.1016/j.jsb.2008.11.013

Hernández-Jiménez, A., Hernández-Santiago, J., Macias-García, A., & Sánchez-González, J. (2002). Relaxation modulus in PMMA and PTFE fitting by fractional Maxwell model. *Polymer Testing, 21*(3), 325-331. doi:https://doi.org/10.1016/S0142-9418(01)00092-7

Herod, T.W., & Veres, S.P. (2018). Development of overuse tendinopathy: A new descriptive model for the initiation of tendon damage during cyclic loading. *J Orthop Res, 36*(1), 467-476. doi:10.1002/jor.23629

Hjelle, K., Solheim, E., Strand, T., Muri, R., et al. (2002). Articular cartilage defects in 1,000 knee arthroscopies. *Arthroscopy, 18*(7), 730-734.
Hodgson, R.J., O'Connor, P.J., & Grainger, A.J. (2012). Tendon and ligament imaging. *Br J Radiol, 85*(1016), 1157-1172. doi:10.1259/bjr/34786470
Holmes, D.F., Graham, H.K., & Kadler, K.E. (1998). Collagen fibrils forming in developing tendon show an early and abrupt limitation in diameter at the growing tips. *J Mol Biol, 283*(5), 1049-1058. doi:10.1006/jmbi.1998.2153
Holzapfel, G.A., & Ogden, R.W. (2009). On planar biaxial tests for anisotropic nonlinearly elastic solids. A continuum mechanical framework. *Mathematics and Mechanics of Solids, 14*(5), 474-489.
Hurschler, C., Provenzano, P.P., & Vanderby Jr, R. (2003). Scanning electron microscopic characterization of healing and normal rat ligament microstructure under slack and loaded conditions. *Connect Tissue Res, 44*(2), 59-68.
Iozzo, R.V. (1998). Matrix proteoglycans: from molecular design to cellular function. *Annu Rev Biochem, 67*, 609-652. doi:10.1146/annurev.biochem.67.1.609
Järvinen, M., Józsa, L., Kannus, P., Järvinen, T.L.N., et al. (1997). Histopathological findings in chronic tendon disorders. *Scand J Med Sci Sports, 7*(2), 86-95. doi:10.1111/j.1600-0838.1997.tb00124.x
Jarvinen, T.A., Jarvinen, T.L., Kannus, P., Jozsa, L., et al. (2004). Collagen fibres of the spontaneously ruptured human tendons display decreased thickness and crimp angle. *J Orthop Res, 22*(6), 1303-1309. doi:10.1016/j.orthres.2004.04.003
Jones, C.W., Keogh, A., Smolinski, D., Wu, J.P., et al. (2004). Histological assessment of the chondral and connective tissues of the knee by confocal arthroscope. *Journal of Musculoskeletal Research, 08*(02n03), 75-86. doi:doi:10.1142/S0218957704001247
Józsa, L.G., & Kannus, P. (1997). Human Tendons: Anatomy, Physiology and Pathology . Human Kinetics, Champaign, IL.
Jozsa, Kannus, Balint, & Reffy. (1991). Three-dimensional ultrastructure of human tendons. Acta Anat (Basel), 142(4), 306-312. https://doi.org/10.1159/000147207
Kadler, K.E., Hill, A., & Canty-Laird, E.G. (2008). Collagen fibrillogenesis: fibronectin, integrins, and minor collagens as organizers and nucleators. *Curr Opin Cell Biol, 20*(5), 495-501. doi:10.1016/j.ceb.2008.06.008
Kadler, K.E., Holmes, D.F., Trotter, J.A., & Chapman, J.A. (1996). Collagen fibril formation. *Biochem J, 316 (Pt 1)*, 1-11.
Kannus, P. (2000). Structure of the tendon connective tissue. *Scand J Med Sci Sports, 10*(6), 312-320.
Kannus, P., & Jozsa, L. (1991). Histopathological changes preceding spontaneous rupture of a tendon. A controlled study of 891 patients. *J Bone Joint Surg Am, 73*(10), 1507-1525.
Kannus, P., Sievänen, H., Järvinen, M., Heinonen, A., et al. (1992). A cruciate ligament injury produces considerable, permanent osteoporosis in the affected knee. *Journal of bone and mineral research, 7*(12), 1429-1434.

Kartus, J., Movin, T., Papadogiannakis, N., Christensen, L.R., et al. (2000). A Radiographic and Histologic Evaluation of the Patellar Tendon after Harvesting Its Central Third. *The American journal of sports medicine, 28*(2), 218-226.

Kastelic, J., & Baer, E. (1980). Deformation in tendon collagen. *Symp Soc Exp Biol, 34*, 397-435.

Kastelic, J., Galeski, A., & Baer, E. (1978). The multicomposite structure of tendon. *Connect Tissue Res, 6*(1), 11-23. doi:10.3109/03008207809152283

Kato, M., Takada, S., Kashida, Y., & Nomura, M. (1995). Histological examination on Achilles tendon lesions induced by quinolone antibacterial agents in juvenile rats. *Toxicologic pathology, 23*(3), 385-392. doi:10.1177/019262339502300315

Kelly, D.W., Carter, V.S., Jobe, F.W., & Kerlan, R.K. (1984). Patellar and quadriceps tendon ru p tures— jumper's knee. *The American journal of sports medicine, 12*(5), 375-380. doi:doi:10.1177/036354658401200508

Kemp, A.D., Harding, C.C., Cabral, W.A., Marini, J.C., et al. (2012). Effects of tissue hydration on nanoscale structural morphology and mechanics of individual Type I collagen fibrils in the Brtl mouse model of Osteogenesis Imperfecta. *Journal of Structural Biology, 180*(3), 428-438. doi:http://dx.doi.org/10.1016/j.jsb.2012.09.012

Ker, F. (1981). Dynamic tensile properties of the plantaris tendon of sheep (Ovis aries). *Journal of Experimental Biology, 93*(1), 283-302.

Ker, R.F. (2002). The implications of the adaptable fatigue quality of tendons for their construction, repair and function. *Comp Biochem Physiol A Mol Integr Physiol, 133*(4), 987-1000.

Ker, R.F., Wang, X.T., & Pike, A.V. (2000). Fatigue quality of mammalian tendons. *J Exp Biol, 203*(Pt 8), 1317-1327.

Khan, K.M., Cook, J.L., Bonar, F., Harcourt, P., et al. (1999). Histopathology of common tendinopathies. Update and implications for clinical management. *Sports Med, 27*(6), 393-408.

Kiesslich, R., & Neurath, M.F. (2006). Chromoendoscopy and Other Novel Imaging Techniques. *Gastroenterology Clinics of North America, 35*(3), 605-619. doi:http://dx.doi.org/10.1016/j.gtc.2006.07.004

Kilts, T., Ameye, L., Syed-Picard, F., Ono, M., et al. (2009). Potential roles for the small leucine-rich proteoglycans biglycan and fibromodulin in ectopic ossification of tendon induced by exercise and in modulating rotarod performance. *Scand J Med Sci Sports, 19*(4), 536-546. doi:10.1111/j.1600-0838.2009.00909.x

Kirkendall, D.T., & Garrett, W.E. (1997). Function and biomechanics of tendons. *Scand J Med Sci Sports, 7*(2), 62-66. doi:10.1111/j.1600-0838.1997.tb00120.x

Kjaer, M., Langberg, H., Heinemeier, K., Bayer, M., et al. (2009). From mechanical loading to collagen synthesis, structural changes and function in human tendon. *Scandinavian journal of medicine & science in sports, 19*, 500-510. doi:10.1111/j.1600-0838.2009.00986.x

Knorzer, E., Folkhard, W., Geercken, W., Boschert, C., et al. (1986). New aspects of the etiology of tendon rupture. An analysis of time-resolved dynamic-

mechanical measurements using synchrotron radiation. *Arch Orthop Trauma Surg, 105*(2), 113-120.
Kondratko-Mittnacht, J., Lakes, R., & Vanderby, R., Jr. (2015). Shear loads induce cellular damage in tendon fascicles. *J Biomech, 48*(12), 3299-3305. doi:10.1016/j.jbiomech.2015.06.006
Kongsgaard, M., Aagaard, P., Kjaer, M., & Magnusson, S. (2005). Structural Achilles tendon properties in athletes subjected to different exercise modes and in Achilles tendon rupture patients. *Journal of applied physiology, 99*(5), 1965-1971.
Konig, K. (2000). Multiphoton microscopy in life sciences. *J Microsc, 200*(Pt 2), 83-104.
Koob, T.J. (1989). Effects of chondroitinase-ABC on proteoglycans and swelling properties of fibrocartilage in bovine flexor tendon. *J Orthop Res, 7*(2), 219-227. doi:10.1002/jor.1100070209
Koob, T.J., & Vogel, K.G. (1987). Site-related variations in glycosaminoglycan content and swelling properties of bovine flexor tendon. *Journal of Orthopaedic Research, 5*(3), 414-424.
Kottner, J., Audige, L., Brorson, S., Donner, A., et al. (2011). Guidelines for Reporting Reliability and Agreement Studies (GRRAS) were proposed. *J Clin Epidemiol, 64*(1), 96-106. doi:10.1016/j.jclinepi.2010.03.002
Krajcinovic, D. (1985). Continuous Damage Mechanics Revisited: Basic Concepts and Definitions. *Journal of Applied Mechanics, 52*(4), 829-834. doi:10.1115/1.3169154
Kujala, U.M., Sarna, S., & Kaprio, J. (2005). Cumulative incidence of achilles tendon rupture and tendinopathy in male former elite athletes. *Clinical Journal of Sport Medicine, 15*(3), 133-135.
Kukreti, U., & Belkoff, S.M. (2000). Collagen fibril D-period may change as a function of strain and location in ligament. *J Biomech, 33*(12), 1569-1574. doi:http://dx.doi.org/10.1016/S0021-9290(00)00150-0
Lake, S.P., Ansorge, H.L., & Soslowsky, L.J. (2008). Animal models of tendinopathy. *Disabil Rehabil, 30*(20-22), 1530-1541. doi:10.1080/09638280701785460
Lake, S.P., Miller, K.S., Elliott, D.M., & Soslowsky, L.J. (2009). Effect of fiber distribution and realignment on the nonlinear and inhomogeneous mechanical properties of human supraspinatus tendon under longitudinal tensile loading. *J Orthop Res, 27*(12), 1596-1602. doi:10.1002/jor.20938
Lake, S.P., Miller, K.S., Elliott, D.M., & Soslowsky, L.J. (2010). Tensile properties and fiber alignment of human supraspinatus tendon in the transverse direction demonstrate inhomogeneity, nonlinearity, and regional isotropy. J Biomech, 43(4), 727-732. https://doi.org/10.1016/j.jbiomech.2009.10.017
Lanir, Y. (1978). Structure-Function Relations in Mammalian Tendon - Effect of Geometrical Nonuniformity. *Journal of Bioengineering, 2*(1-2), 119-128.
Lavagnino, M., Arnoczky, S.P., Egerbacher, M., Gardner, K.L., et al. (2006). Isolated fibrillar damage in tendons stimulates local collagenase mRNA expression and protein synthesis. *J Biomech, 39*(13), 2355-2362. doi:10.1016/j.jbiomech.2005.08.008

Lavagnino, M., Wall, M.E., Little, D., Banes, A.J., et al. (2015). Tendon mechanobiology: Current knowledge and future research opportunities. *J Orthop Res, 33*(6), 813-822. doi:10.1002/jor.22871

Lavker, R.M., Zheng, P.S., & Dong, G. (1987). Aged skin: a study by light, transmission electron, and scanning electron microscopy. *J Invest Dermatol, 88*(3 Suppl), 44s-51s.

Lee, A.H., Szczesny, S.E., Santare, M.H., & Elliott, D.M. (2017). Investigating mechanisms of tendon damage by measuring multi-scale recovery following tensile loading. *Acta Biomater, 57*, 363-372. doi:10.1016/j.actbio.2017.04.011

Legerlotz, K., Riley, G.P., & Screen, H.R. (2013). GAG depletion increases the stress-relaxation response of tendon fascicles, but does not influence recovery. *Acta Biomater, 9*(6), 6860-6866. doi:10.1016/j.actbio.2013.02.028

Lewis, J.L., Krawczak, D.A., Oegema, T.R., Jr., & Westendorf, J.J. (2010). Effect of decorin and dermatan sulfate on the mechanical properties of a neocartilage. *Connect Tissue Res, 51*(2), 159-170. doi:10.3109/03008200903174342

Liao, J., & Vesely, I. (2007). Skewness angle of interfibrillar proteoglycans increases with applied load on mitral valve chordae tendineae. *J Biomech, 40*(2), 390-398. doi:10.1016/j.jbiomech.2005.12.011

Lichtwark, G.A., Cresswell, A.G., & Newsham-West, R.J. (2013). Effects of running on human Achilles tendon length-tension properties in the free and gastrocnemius components. *J Exp Biol, 216*(Pt 23), 4388-4394. doi:10.1242/jeb.094219

Longo, U.G., Franceschi, F., Ruzzini, L., Rabitti, C., et al. (2008). Histopathology of the supraspinatus tendon in rotator cuff tears. *Am J Sports Med, 36*(3), 533-538. doi:10.1177/0363546507308549

Losic, D., Short, K., Mitchell, J.G., Lal, R., et al. (2007). AFM nanoindentations of diatom biosilica surfaces. *Langmuir, 23*(9), 5014-5021. doi:10.1021/la062666y

Lujan, T.J., Underwood, C.J., Henninger, H.B., Thompson, B.M., et al. (2007). Effect of dermatan sulfate glycosaminoglycans on the quasi-static material properties of the human medial collateral ligament. *J Orthop Res, 25*(7), 894-903. doi:10.1002/jor.20351

Lujan, T.J., Underwood, C.J., Jacobs, N.T., & Weiss, J.A. (2009). Contribution of glycosaminoglycans to viscoelastic tensile behavior of human ligament. *J Appl Physiol (1985), 106*(2), 423-431. doi:10.1152/japplphysiol.90748.2008

Luna, L.G. (1968). Manual of histologic staining methods of the Armed Forces Institute of Pathology.

Lynch, H.A., Johannessen, W., Wu, J.P., Jawa, A., et al. (2003). Effect of fiber orientation and strain rate on the nonlinear uniaxial tensile material properties of tendon. *J Biomech Eng, 125*(5), 726-731.

Maffulli, N. (1999). Current Concepts Review-Rupture of the Achilles Tendon. *J Bone Joint Surg Am, 81*(7), 1019-1036.

Maffulli, N. (2011). Achilles tendon pathology, present and future. *J British Journal of Sports Medicine, 45*(2), e2-e2. doi:10.1136/bjsm.2010.081570.18 %

Maffulli, N., Barrass, V., & Ewen, S.W.B. (2000). Light Microscopic Histology of Achilles Tendon Ruptures: A Comparison with Unruptured Tendons. *The*

American journal of sports medicine, 28(6), 857-863. doi:10.1177/03635465000280061401

Maffulli, et al. (2008). Surgery for chronic Achilles tendinopathy produces worse results in women. Disabil Rehabil, 30(20-22), 1714-1720. https://doi.org/10.1080/09638280701786765

Maffulli, N., & Kader, D. (2002). Tendinopathy of tendo achillis. *J Bone Joint Surg Br, 84*(1), 1-8.

Maffulli, N., Via, A.G., & Oliva, F. (2017). Chronic Achilles Tendon Rupture. *Open Orthop J, 11*, 660-669. doi:10.2174/1874325001711010660

Magnusson, P., Hansen, P., & Kjaer, M. (2003). Tendon properties in relation to muscular activity and physical training. *Scand J Med Sci Sports, 13*(4), 211-223.

Magnusson, S.P., Hansen, P., Aagaard, P., Brond, J., et al. (2003). Differential strain patterns of the human gastrocnemius aponeurosis and free tendon, in vivo. *Acta Physiol Scand, 177*(2), 185-195. doi:10.1046/j.1365-201X.2003.01048.x

Magnusson, S.P., Langberg, H., & Kjaer, M. (2010). The pathogenesis of tendinopathy: balancing the response to loading. *Nat Rev Rheumatol, 6*(5), 262-268. doi:10.1038/nrrheum.2010.43

Magra, M., & Maffulli, N. (2008). Genetic aspects of tendinopathy. *J Sci Med Sport, 11*(3), 243-247. doi:10.1016/j.jsams.2007.04.007

Maquirriain, J. (2011). Achilles tendon rupture: avoiding tendon lengthening during surgical repair and rehabilitation. *The Yale journal of biology and medicine, 84*(3), 289-300.

Marchini, M., Morocutti, M., Ruggeri, A., Koch, M.H., et al. (1986). Differences in the fibril structure of corneal and tendon collagen. An electron microscopy and X-ray diffraction investigation. *Connect Tissue Res, 15*(4), 269-281.

Martufi, G., & Gasser, T.C. (2012). Turnover of fibrillar collagen in soft biological tissue with application to the expansion of abdominal aortic aneurysms. *Journal of the Royal Society Interface, 9*(77), 3366-3377. doi:10.1098/rsif.2012.0416

Masic, A., Bertinetti, L., Schuetz, R., Galvis, L., et al. (2011). Observations of Multiscale, Stress-Induced Changes of Collagen Orientation in Tendon by Polarized Raman Spectroscopy. *Biomacromolecules, 12*(11), 3989-3996. doi:10.1021/bm201008b

Matyas, J., Edwards, P., Miniaci, A., Shrive, N., et al. (1994). Ligament tension affects nuclear shape in situ: an in vitro study. *Connect Tissue Res, 31*(1), 45-53. doi:10.3109/03008209409005634

McGough, R.L., Debski, R.E., Taskiran, E., Fu, F.H., et al. (1996). Mechanical properties of the long head of the biceps tendon. *Knee Surg Sports Traumatol Arthrosc, 3*(4), 226-229. doi:10.1007/bf01466622

Mehdizadeh, A., Gardiner, B.S., Lavagnino, M., & Smith, D.W. (2017). Predicting tenocyte expression profiles and average molecular concentrations in Achilles tendon ECM from tissue strain and fiber damage. *Biomech Model Mechanobiol, 16*(4), 1329-1348. doi:10.1007/s10237-017-0890-x

Meijering, E. (2010). Neuron tracing in perspective. *Cytometry A, 77*(7), 693-704. doi:10.1002/cyto.a.20895

Meijering, E., Jacob, M., Sarria, J.C., Steiner, P., et al. (2004). Design and validation of a tool for neurite tracing and analysis in fluorescence microscopy images. *Cytometry A, 58*(2), 167-176. doi:10.1002/cyto.a.20022

Merrilees, M.J., & Flint, M.H. (1980). Ultrastructural study of tension and pressure zones in a rabbit flexor tendon. *Am J Anat, 157*(1), 87-106. doi:10.1002/aja.1001570109

Microscopy, N.A.F. Nanoscience. Atomic Force Microscopy http://www.nanoscience.com/products/afm/technology-overview/.

Miller, K.S., Connizzo, B.K., & Soslowsky, J. (2012). Collagen fiber re-alignment in a neonatal developmental mouse supraspinatus tendon model. *Ann Biomed Eng, 40*(5), 1102-1110. doi:10.1007/s10439-011-0490-3

Miller, K.S., Edelstein, L., Connizzo, B., & Soslowsky, J. (2012). Effect of preconditioning and stress relaxation on local collagen fiber re-alignment: inhomogeneous properties of rat supraspinatus tendon. *J Biomech Eng, 134*(3), 031007. doi:10.1115/1.4006340

Miller, K.S., Connizzo, B.K., Feeney, E., & Soslowsky, L.J. (2012). Characterizing local collagen fiber re-alignment and crimp behavior throughout mechanical testing in a mature mouse supraspinatus tendon model. *J Biomech, 45*(12), 2061-2065. doi:10.1016/j.jbiomech.2012.06.006

Minns, R.J., Soden, P.D., & Jackson, D.S. (1973). The role of the fibrous components and ground substance in the mechanical properties of biological tissues: A preliminary investigation. *J Biomech, 6*(2), 153-165. doi:https://doi.org/10.1016/0021-9290(73)90084-5

Misof, K., Landis, W.J., Klaushofer, K., & Fratzl, P. (1997). Collagen from the osteogenesis imperfecta mouse model (oim) shows reduced resistance against tensile stress. *J Clin Invest, 100*(1), 40-45. doi:10.1172/JCI119519

Misof, K., Rapp, G., & Fratzl, P. (1997). A new molecular model for collagen elasticity based on synchrotron X-ray scattering evidence. *Biophysical Journal, 72*(3), 1376-1381.

Mokaberi, B., & Requicha, A.A.G. (2006). Drift compensation for automatic nanomanipulation with scanning probe microscopes. *IEEE Transactions on Automation Science and Engineering, 3*(3), 199-207. doi:10.1109/TASE.2006.875534

Mosler, E., Folkhard, W., Knorzer, E., Nemetschek-Gansler, H., et al. (1985). Stress-induced molecular rearrangement in tendon collagen. *J Mol Biol, 182*(4), 589-596.

Movin, T. (1999). Aspects of aetiology, pathoanatomy and diagnostic methods in chronic mid-portion achillodynia.

Movin, T., Gad, A., Reinholt, F.P., & Rolf, C. (1997). Tendon pathology in long-standing achillodynia. Biopsy findings in 40 patients. *Acta Orthop Scand, 68*(2), 170-175.

Muramatsu, T., Muraoka, T., Takeshita, D., Kawakami, Y., et al. (2001). Mechanical properties of tendon and aponeurosis of human gastrocnemius muscle in vivo. *J Appl Physiol (1985), 90*(5), 1671-1678. doi:10.1152/jappl.2001.90.5.1671

Nakama, L.H., King, K.B., Abrahamsson, S., & Rempel, D.M. (2005). Evidence of tendon microtears due to cyclical loading in an in vivo tendinopathy model.

Journal of Orthopaedic Research, 23(5), 1199-1205. doi:http://dx.doi.org/10.1016/j.orthres.2005.03.006

Neviaser, A., Andarawis-Puri, N., & Flatow, E. (2012). Basic mechanisms of tendon fatigue damage. *J Shoulder Elbow Surg, 21*(2), 158-163. doi:10.1016/j.jse.2011.11.014

Nissi, M.J., Toyras, J., Laasanen, M.S., Rieppo, J., et al. (2004). Proteoglycan and collagen sensitive MRI evaluation of normal and degenerated articular cartilage. *J Orthop Res, 22*(3), 557-564. doi:10.1016/j.orthres.2003.09.008

O'Brien, M. (1992). Functional anatomy and physiology of tendons. *Clin Sports Med, 11*(3), 505-520.

Obst, S.J., Newsham-West, R., & Barrett, R.S. (2016). Changes in Achilles tendon mechanical properties following eccentric heel drop exercise are specific to the free tendon. *Scand J Med Sci Sports, 26*(4), 421-431. doi:10.1111/sms.12466

Odetti, P., Aragno, I., Rolandi, R., Garibaldi, S., et al. (2000). Scanning force microscopy reveals structural alterations in diabetic rat collagen fibrils: role of protein glycation. *Diabetes/Metabolism Research and Reviews, 16*(2), 74-81. doi:10.1002/(SICI)1520-7560(200003/04)16:2<74::AID-DMRR80>3.0.CO;2-1

Okabe, T., Takeda, N., Kamoshida, Y., Shimizu, M., et al. (2001). A 3D shear-lag model considering micro-damage and statistical strength prediction of unidirectional fiber-reinforced composites. *Composites Science and Technology, 61*(12), 1773-1787. doi:http://dx.doi.org/10.1016/S0266-3538(01)00079-3

Okuda, M., Takeguchi, M., Tagaya, M., Tonegawa, T., et al. (2009). Elemental distribution analysis of type I collagen fibrils in tilapia fish scale with energy-filtered transmission electron microscope. *Micron, 40*(5-6), 665-668. doi:10.1016/j.micron.2009.04.001

Onambele-Pearson, N.L., & Pearson, S.J. (2007). Time-of-day effect on patella tendon stiffness alters vastus lateralis fascicle length but not the quadriceps force-angle relationship. *J Biomech, 40*(5), 1031-1037. doi:10.1016/j.jbiomech.2006.04.001

Orchard, J.W., Cook, J.L., & Halpin, N. (2004). Stress-shielding as a cause of insertional tendinopathy: the operative technique of limited adductor tenotomy supports this theory. *Journal of Science and Medicine in Sport, 7*(4), 424-428. doi:https://doi.org/10.1016/S1440-2440(04)80259-7

Orgel, J.P., Miller, A., Irving, T.C., Fischetti, R.F., et al. (2001). The in situ supermolecular structure of type I collagen. *Structure, 9*(11), 1061-1069.

Orgel, J.P., San Antonio, J.D., & Antipova, O. (2011). Molecular and structural mapping of collagen fibril interactions. *Connect Tissue Res, 52*(1), 2-17. doi:10.3109/03008207.2010.511353

Orgel, J.P.R.O., Irving, T.C., Miller, A., & Wess, T.J. (2006). Microfibrillar structure of type I collagen in situ. *Proceedings of the National Academy of Sciences, 103*(24), 9001-9005. doi:10.1073/pnas.0502718103

Ottani, V., Raspanti, M., & Ruggeri, A. (2001). Collagen structure and functional implications. *Micron, 32*(3), 251-260.

Paavola, M., Kannus, P., Jarvinen, T.A., Khan, K., et al. (2002). Achilles tendinopathy. *J Bone Joint Surg Am, 84-a*(11), 2062-2076.

Paavola, M., Paakkala, T., Kannus, P., & Jarvinen, M. (1998). Ultrasonography in the differential diagnosis of Achilles tendon injuries and related disorders. A comparison between pre-operative ultrasonography and surgical findings. *Acta Radiol, 39*(6), 612-619.

Parent, G., Huppe, N., & Langelier, E. (2011). Low stress tendon fatigue is a relatively rapid process in the context of overuse injuries. *Ann Biomed Eng, 39*(5), 1535-1545. doi:10.1007/s10439-011-0254-0

Peltz, C.D., Sarver, J.J., Dourte, L.M., Wurgler-Hauri, C.C., et al. (2010). Exercise following a short immobilization period is detrimental to tendon properties and joint mechanics in a rat rotator cuff injury model. *J Orthop Res, 28*(7), 841-845. doi:10.1002/jor.21059

Piez, K.A., & Trus, B.L. (1981). A new model for packing of type-I collagen molecules in the native fibril. *Bioscience Reports, 1*(10), 801-810. doi:10.1007/bf01114803

Pike, A.V., Ker, R.F., & Alexander, R.M. (2000). The development of fatigue quality in high- and low-stressed tendons of sheep (Ovis aries). *J Exp Biol, 203*(Pt 14), 2187-2193.

Pingel, J., Lu, Y., Starborg, T., Fredberg, U., et al. (2014). 3-D ultrastructure and collagen composition of healthy and overloaded human tendon: evidence of tenocyte and matrix buckling. *J Anat, 224*(5), 548-555. doi:10.1111/joa.12164

Pollock, C.M., & Shadwick, R.E. (1994). Relationship between body mass and biomechanical properties of limb tendons in adult mammals. *American Journal of Physiology-Regulatory, Integrative and Comparative Physiology, 266*(3), R1016-R1021.

Prockop, D.J., & Hulmes, D.J.S. (1994). Assembly of Collagen Fibrils de Novo from Soluble Precursors: Polymerization and Copolymerization of Procollagen, pN-Collagen, and Mutated Collagens A2 - YURCHENCO, PETER D. In Birk & Mecham (Eds.), *Extracellular Matrix Assembly and Structure* (pp. 47-90). San Diego: Academic Press.

Provenzano, P.P., Alejandro-Osorio, A.L., Valhmu, W.B., Jensen, K.T., et al. (2005). Intrinsic fibroblast-mediated remodeling of damaged collagenous matrices in vivo. *Matrix Biol, 23*(8), 543-555. doi:10.1016/j.matbio.2004.09.008

Provenzano, P.P., & Vanderby, R., Jr. (2006). Collagen fibril morphology and organization: implications for force transmission in ligament and tendon. *Matrix Biol, 25*(2), 71-84. doi:10.1016/j.matbio.2005.09.005

Purohit, N.B., & King, L.J. (2015). Ultrasound of lower limb sports injuries. *Ultrasound, 23*(3), 149-157. doi:10.1177/1742271x15588809

Purslow, P.P., Wess, T.J., & Hukins, D.W. (1998). Collagen orientation and molecular spacing during creep and stress-relaxation in soft connective tissues. *J Exp Biol, 201*(Pt 1), 135-142.

Putman, C.A., van der Werf, K.O., de Grooth, B.G., van Hulst, N.F., et al. (1994). Viscoelasticity of living cells allows high resolution imaging by tapping

mode atomic force microscopy. *Biophys J, 67*(4), 1749-1753. doi:10.1016/s0006-3495(94)80649-6

Puxkandl, R., Zizak, I., Paris, O., Keckes, J., et al. (2002). Viscoelastic properties of collagen: synchrotron radiation investigations and structural model. *Philosophical Transactions of the Royal Society B: Biological Sciences, 357*(1418), 191-197. doi:10.1098/rstb.2001.1033

Quinn, et al. (2011). Preconditioning is correlated with altered collagen fiber alignment in ligament. J Biomech Eng, 133(6), 064506. https://doi.org/10.1115/1.4004205

Rahe, P., Bechstein, R., & Kühnle, A. (2010). Vertical and lateral drift corrections of scanning probe microscopy images. *Journal of Vacuum Science & Technology B - J VAC SCI TECHNOL B, 28*. doi:10.1116/1.3360909

Rainis, E.J. (2007). Characterizing the mechanical properties of the glenohumeral capsule: implications for finite element modeling. Master's Thesis, University of Pittsburgh

Raspanti, Manelli, A., Franchi, M., & Ruggeri, A. (2005). The 3D structure of crimps in the rat Achilles tendon. *Matrix Biology, 24*(7), 503-507. doi:http://dx.doi.org/10.1016/j.matbio.2005.07.006

Raspanti, M., Congiu, T., & Guizzardi, S. (2002). Structural aspects of the extracellular matrix of the tendon: an atomic force and scanning electron microscopy study. *Arch Histol Cytol, 65*(1), 37-43.

Raspanti, M., Viola, M., Forlino, A., Tenni, R., et al. (2008). Glycosaminoglycans show a specific periodic interaction with type I collagen fibrils. *J Struct Biol, 164*(1), 134-139. doi:10.1016/j.jsb.2008.07.001

Raspanti, M., Viola, M., Sonaggere, M., Tira, M.E., et al. (2007). Collagen fibril structure is affected by collagen concentration and decorin. *Biomacromolecules, 8*(7), 2087-2091. doi:10.1021/bm070091t

Redaelli, A., Vesentini, S., Soncini, M., Vena, P., et al. (2003). Possible role of decorin glycosaminoglycans in fibril to fibril force transfer in relative mature tendons--a computational study from molecular to microstructural level. *J Biomech, 36*(10), 1555-1569.

Reed, C.C., & Iozzo, R.V. (2002). The role of decorin in collagen fibrillogenesis and skin homeostasis. *Glycoconj J, 19*(4-5), 249-255. doi:10.1023/a:1025383913444

Rezakhaniha, R., Agianniotis, A., Schrauwen, J.T., Griffa, A., et al. (2012). Experimental investigation of collagen waviness and orientation in the arterial adventitia using confocal laser scanning microscopy. *Biomech Model Mechanobiol, 11*(3-4), 461-473. doi:10.1007/s10237-011-0325-z

Ricci, D., & Braga, P. (2004). Recognizing and avoiding artifacts in AFM imaging. *Methods in molecular biology (Clifton, N.J.), 242*, 25-37.

Richards, P.J., Win, T., & Jones, P.W. (2005). The distribution of microvascular response in Achilles tendonopathy assessed by colour and power Doppler. *Skeletal Radiol, 34*(6), 336-342. doi:10.1007/s00256-004-0834-2

Rigby, B.J. (1964). Effect of Cyclic Extension on the Physical Properties of Tendon Collagen and its Possible Relation to Biological Ageing of Collagen. *Nature, 202*, 1072-1074.

Rigby, B.J., Hirai, N., Spikes, J.D., & Eyring, H. (1959). The Mechanical Properties of Rat Tail Tendon. *J Gen Physiol, 43*(2), 265-283.
Riggin, C.N., Sarver, J.J., Freedman, B.R., Thomas, S.J., Soslowsky, L.J. Analysis of collagen organization in mouse achilles tendon using high-frequency ultrasound imaging. *J Biomech Eng.* 2014;136(2):021029. doi:10.1115/1.4026285
Rigozzi, S., Stemmer, A., Müller, R., & Snedeker, J. (2011). Mechanical response of individual collagen fibrils in loaded tendon as measured by atomic force microscopy. *Journal of Structural Biology, 176*(1), 9-15.
Rigozzi, S., Muller, R., & Snedeker, J.G. (2009). Local strain measurement reveals a varied regional dependence of tensile tendon mechanics on glycosaminoglycan content. *J Biomech, 42*(10), 1547-1552. doi:10.1016/j.jbiomech.2009.03.031
Rigozzi, S., Muller, R., & Snedeker, J.G. (2010). Collagen fibril morphology and mechanical properties of the Achilles tendon in two inbred mouse strains. *J Anat, 216*(6), 724-731. doi:10.1111/j.1469-7580.2010.01225.x
Rigozzi, S., Müller, R., Stemmer, A., & Snedeker, J.G. (2013). Tendon glycosaminoglycan proteoglycan sidechains promote collagen fibril sliding—AFM observations at the nanoscale. *J Biomech, 46*(4), 813-818. doi:http://dx.doi.org/10.1016/j.jbiomech.2012.11.017
Rigozzi, S., Stemmer, A., Muller, R., & Snedeker, J. (2011). Mechanical response of individual collagen fibrils in loaded tendon as measured by atomic force microscopy. *J Struct Biol, 176*(1), 9-15. doi:10.1016/j.jsb.2011.07.002
Riley, G. (2008). Tendinopathy--from basic science to treatment. *Nat Clin Pract Rheumatol, 4*(2), 82-89. doi:10.1038/ncprheum0700
Robinson, P., Lin, T., Jawad, A., Iozzo, R., et al. (2004). Investigating Tendon Fascicle Structure–Function Relationships in a Transgenic-Age Mouse Model Using Multiple Regression Models. *Ann Biomed Eng, 32*(7), 924-931. doi:10.1023/B:ABME.0000032455.78459.56
Robinson, P.S., Huang, T.F., Kazam, E., Iozzo, R.V., et al. (2005). Influence of decorin and biglycan on mechanical properties of multiple tendons in knockout mice. *J Biomech Eng, 127*(1), 181-185.
Robinson, P.S., Lin, T.W., Reynolds, P.R., Derwin, K.A., et al. (2004). Strain-rate sensitive mechanical properties of tendon fascicles from mice with genetically engineered alterations in collagen and decorin. *J Biomech Eng, 126*(2), 252-257.
Ros, S.J., Andarawis-Puri, N., & Flatow, E.L. (2013). Tendon extracellular matrix damage detection and quantification using automated edge detection analysis. *J Biomech, 46*(16), 2844-2847. doi:10.1016/j.jbiomech.2013.09.002
Ros, S.J., Muljadi, P.M., Flatow, E.L., & Andarawis-Puri, N. (2019). Multiscale mechanisms of tendon fatigue damage progression and severity are strain and cycle dependent. *J Biomech, 85*, 148-156. doi:10.1016/j.jbiomech.2019.01.026
Ruggeri, A., & Benazzo, F. (1984). Collagen-proteoglycan interaction. In Ruggeri & Motta (Eds.), *Ultrastructure of the Connective Tissue Matrix* (pp. 113-125). Boston, MA: Springer US.

Sacks, M.S. (2000). Biaxial Mechanical Evaluation of Planar Biological Materials. *Journal of elasticity and the physical science of solids, 61*(1), 199. doi:10.1023/a:1010917028671

Santos, S., Barcons, V., Christenson, H.K., Font, J., et al. (2011). The intrinsic resolution limit in the atomic force microscope: implications for heights of nano-scale features. *PLoS One, 6*(8), e23821. doi:10.1371/journal.pone.0023821

Sasaki, N., & Odajima, S. (1996). Elongation mechanism of collagen fibrils and force-strain relations of tendon at each level of structural hierarchy. *J Biomech, 29*(9), 1131-1136.

Sasaki, N., & Odajima, S. (1996). Stress-strain curve and Young's modulus of a collagen molecule as determined by the X-ray diffraction technique. *J Biomech, 29*(5), 655-658.

Sasaki, N., Shukunami, N., Matsushima, N., & Izumi, Y. (1999). Time-resolved X-ray diffraction from tendon collagen during creep using synchrotron radiation. *J Biomech, 32*(3), 285-292.

Sasaki, N., Tagami, A., Goto, T., Taniguchi, M., et al. (2002). Atomic force microscopic studies on the structure of bovine femoral cortical bone at the collagen fibril-mineral level. *Journal of Materials Science: Materials in Medicine, 13*(3), 333-337. doi:10.1023/A:1014079421895

Schechtman, H., & Bader, D.L. (1997). In vitro fatigue of human tendons. *J Biomech, 30*(8), 829-835.

Schmitt, F.O., Hall, C.E., & Jakus, M.A. (1942). Electron microscope investigations of the structure of collagen. *Journal of Cellular and Comparative Physiology, 20*(1), 11-33. doi:10.1002/jcp.1030200103

Schochlin, M., Weissinger, S.E., Brandes, A.R., Herrmann, M., et al. (2014). A nuclear circularity-based classifier for diagnostic distinction of desmoplastic from spindle cell melanoma in digitized histological images. *J Pathol Inform, 5*(1), 40. doi:10.4103/2153-3539.143335

Scott, A., Cook, J.L., Hart, D.A., Walker, D.C., et al. (2007). Tenocyte responses to mechanical loading in vivo: a role for local insulin-like growth factor 1 signaling in early tendinosis in rats. *Arthritis Rheum, 56*(3), 871-881. doi:10.1002/art.22426

Scott, J.E. (1980). Collagen--proteoglycan interactions. Localization of proteoglycans in tendon by electron microscopy. *Biochem J, 187*(3), 887-891.

Scott, J.E. (1988). Proteoglycan-fibrillar collagen interactions. *Biochemical Journal, 252*(2), 313-323.
for Experimental Biology, 6(9), 2639-2645.

Scott, J.E. (1992). Supramolecular organization of extracellular matrix glycosaminoglycans, in vitro and in the tissues. *Faseb j, 6*(9), 2639-2645.

Scott, J.E. (1995). Extracellular matrix, supramolecular organisation and shape. *J Anat, 187 (Pt 2)*, 259-269.

Scott, J.E. (2003). Elasticity in extracellular matrix ‘shape modules’ of tendon, cartilage, etc. A sliding proteoglycan-filament model. *The Journal of Physiology, 553*(Pt 2), 335-343. doi:10.1113/jphysiol.2003.050179

Scott, P.G., Nakano, T., & Dodd, C.M. (1997). Isolation and characterization of small proteoglycans from different zones of the porcine knee meniscus. *Biochim Biophys Acta, 1336*(2), 254-262.

Screen, H.R. (2008). Investigating load relaxation mechanics in tendon. *J Mech Behav Biomed Mater, 1*(1), 51-58. doi:10.1016/j.jmbbm.2007.03.002

Screen, H.R., Chhaya, V.H., Greenwald, S.E., Bader, D.L., et al. (2006). The influence of swelling and matrix degradation on the microstructural integrity of tendon. *Acta Biomater, 2*(5), 505-513. doi:10.1016/j.actbio.2006.05.008

Screen, H.R., Lee, D.A., Bader, D.L., & Shelton, J.C. (2003). Development of a technique to determine strains in tendons using the cell nuclei. *Biorheology, 40*(1-3), 361-368.

Screen, H.R., Lee, D.A., Bader, D.L., & Shelton, J.C. (2004). An investigation into the effects of the hierarchical structure of tendon fascicles on micromechanical properties. *Proc Inst Mech Eng H, 218*(2), 109-119. doi:10.1243/095441104322984004

Screen, H.R., Shelton, J.C., Chhaya, V.H., Kayser, M.V., et al. (2005). The influence of noncollagenous matrix components on the micromechanical environment of tendon fascicles. *Ann Biomed Eng, 33*(8), 1090-1099. doi:10.1007/s10439-005-5777-9

Screen, H.R., Shelton, J.C., Bader, D.L., & Lee, D.A. (2005). Cyclic tensile strain upregulates collagen synthesis in isolated tendon fascicles. *Biochemical and Biophysical Research Communications, 336*(2), 424-429. doi:https://doi.org/10.1016/j.bbrc.2005.08.102

Sereysky, J.B., Andarawis-Puri, N., Jepsen, K.J., & Flatow, E.L. (2012). Structural and mechanical effects of in vivo fatigue damage induction on murine tendon. *J Orthop Res, 30*(6), 965-972. doi:10.1002/jor.22012

Sereysky, et al. (2010). Automated image analysis method for quantifying damage accumulation in tendon. J Biomech, 43(13), 2641-2644. https://doi.org/10.1016/j.jbiomech.2010.04.043

Sharma, P., & Maffulli, N. (2005). Tendon injury and tendinopathy: healing and repair. *J Bone Joint Surg Am, 87*(1), 187-202. doi:10.2106/jbjs.d.01850

Sheehan, F.T., & Drace, J.E. (2000). Human patellar tendon strain. A noninvasive, in vivo study. *Clin Orthop Relat Res*(370), 201-207.

Shen, Z.L., Dodge, M.R., Kahn, H., Ballarini, R., et al. (2008). Stress-Strain Experiments on Individual Collagen Fibrils. *Biophysical Journal, 95*(8), 3956-3963. doi:10.1529/biophysj.107.124602

Shepherd, J., Legerlotz, K., Demirci, T., Riley, G., et al. (2013). *The fatigue behaviour of functionally distinct bovine tendons*.

Shepherd, J.H., Legerlotz, K., Demirci, T., Klemt, C., et al. (2014). Functionally distinct tendon fascicles exhibit different creep and stress relaxation behaviour. *Proc Inst Mech Eng H, 228*(1), 49-59. doi:10.1177/0954411913509977

Shepherd, J.H., Riley, G.P., & Screen, H.R. (2014). Early stage fatigue damage occurs in bovine tendon fascicles in the absence of changes in mechanics at either the gross or micro-structural level. *J Mech Behav Biomed Mater, 38*, 163-172. doi:10.1016/j.jmbbm.2014.06.005

Shepherd, J.H., & Screen, H.R. (2013). Fatigue loading of tendon. *Int J Exp Pathol, 94*(4), 260-270. doi:10.1111/iep.12037

Shi, F., Harman, J., Fujiwara, K., & Sottile, J. (2010). Collagen I matrix turnover is regulated by fibronectin polymerization. *Am J Physiol Cell Physiol, 298*(5), C1265-1275. doi:10.1152/ajpcell.00341.2009

Shoulders, M.D., & Raines, R.T. (2009). Collagen structure and stability. *Annual review of biochemistry*, 78, 929-958.

Silver, F.H., Ebrahimi, A., & Snowhill, P.B. (2002). Viscoelastic properties of self-assembled type I collagen fibers: molecular basis of elastic and viscous behaviors. *Connect Tissue Res, 43*(4), 569-580.

Silver, F.H., Freeman, J.W., & Seehra, G.P. (2003). Collagen self-assembly and the development of tendon mechanical properties. *J Biomech, 36*(10), 1529-1553.

Silver, F.H., Horvath, I., & Foran, D.J. (2002). Mechanical implications of the domain structure of fiber-forming collagens: comparison of the molecular and fibrillar flexibilities of the alpha1-chains found in types I-III collagen. *J Theor Biol, 216*(2), 243-254. doi:10.1006/jtbi.2002.2542

Simonin, M.A., Gegout-Pottie, P., Minn, A., Gillet, P., et al. (2000). Pefloxacin-induced achilles tendon toxicity in rodents: biochemical changes in proteoglycan synthesis and oxidative damage to collagen. *Antimicrob Agents Chemother, 44*(4), 867-872.

Sivaguru, M., Eichorst, J.P., Durgam, S., Fried, G.A., et al. (2014). Imaging horse tendons using multimodal 2-photon microscopy. *Methods, 66*(2), 256-267. doi:10.1016/j.ymeth.2013.07.016

Sivakumar, P., Czirok, A., Rongish, B.J., Divakara, V.P., et al. (2006). New insights into extracellular matrix assembly and reorganization from dynamic imaging of extracellular matrix proteins in living osteoblasts. *J Cell Sci, 119*(Pt 7), 1350-1360. doi:10.1242/jcs.02830

Slane, L.C., & Thelen, D.G. (2014). Non-uniform displacements within the Achilles tendon observed during passive and eccentric loading. *J Biomech, 47*(12), 2831-2835. doi:10.1016/j.jbiomech.2014.07.032

Smith, R.K., Birch, H.L., Goodman, S., Heinegard, D., et al. (2002). The influence of ageing and exercise on tendon growth and degeneration--hypotheses for the initiation and prevention of strain-induced tendinopathies. *Comp Biochem Physiol A Mol Integr Physiol, 133*(4), 1039-1050.

Smolinski, D., Jones, C.W., Wu, J.P., Miller, K., et al. (2008). Confocal arthroscopic assessment of osteoarthritis in situ. *Arthroscopy, 24*(4), 423-429. doi:10.1016/j.arthro.2007.10.003

Sonnabend, D.H., Yu, Y., Howlett, C.R., Harper, G.D., et al. (2001). Laminated tears of the human rotator cuff: a histologic and immunochemical study. *J Shoulder Elbow Surg, 10*(2), 109-115. doi:10.1067/mse.2001.112882

Soslowsky, L.J., Carpenter, J.E., DeBano, C.M., Banerji, I., et al. (1996). Development and use of an animal model for investigations on rotator cuff disease. *J Shoulder Elbow Surg, 5*(5), 383-392.

Soslowsky, L.J., Thomopoulos, S., Tun, S., Flanagan, C.L., et al. (2000). Neer Award 1999. Overuse activity injures the supraspinatus tendon in an animal

model: a histologic and biomechanical study. *J Shoulder Elbow Surg, 9*(2), 79-84.
Spiesz, E.M., Thorpe, C.T., Chaudhry, S., Riley, G.P., et al. (2015). Tendon extracellular matrix damage, degradation and inflammation in response to in vitro overload exercise. *Journal of Orthopaedic Research, 33*(6), 889-897.
Starborg, T., Kalson, N.S., Lu, Y., Mironov, A., et al. (2013). Using transmission electron microscopy and 3View to determine collagen fibril size and three-dimensional organization. *Nat. Protocols, 8*(7), 1433-1448. doi:10.1038/nprot.2013.086
Stinson, R.H., & Sweeny, P.R. (1980). Skin collagen has an unusual d-spacing. *Biochimica et Biophysica Acta (BBA) - Protein Structure, 621*(1), 158-161. doi:http://dx.doi.org/10.1016/0005-2795(80)90071-9
Stouffer, D.C., Butler, D.L., & Hosny, D. (1985). The relationship between crimp pattern and mechanical response of human patellar tendon-bone units. *J Biomech Eng, 107*(2), 158-165.
Stylianou, A. (2017). Atomic Force Microscopy for Collagen-Based Nano-biomaterials. *Journal of Nanomaterials*, 2017, 9234627. doi:10.1155/2017/9234627
Su, H.-N., Ran, L.-Y., Chen, Z.-H., Qin, Q.-L., et al. (2014). The ultrastructure of type I collagen at nanoscale: large or small D-spacing distribution? *Nanoscale, 6*(14), 8134-8139. doi:10.1039/C4NR01268B
Sullo, A., Maffulli, N., Capasso, G., & Testa, V. (2001). The effects of prolonged peritendinous administration of PGE1 to the rat Achilles tendon: a possible animal model of chronic Achilles tendinopathy. *J Orthop Sci, 6*(4), 349-357. doi:10.1007/s0077610060349
Sun, Y.-L., Luo, Z.-P., Fertala, A., & An, K.-N. (2002). Direct quantification of the flexibility of type I collagen monomer. *Biochemical and Biophysical Research Communications, 295*(2), 382-386. doi:http://dx.doi.org/10.1016/S0006-291X(02)00685-X
Svensson, M., Kartus, J., Christensen, L.R., Movin, T., et al. (2005). A long-term serial histological evaluation of the patellar tendon in humans after harvesting its central third. *Knee Surgery, Sports Traumatology, Arthroscopy, 13*(5), 398-404. doi:10.1007/s00167-004-0590-9
Svensson, R.B., Hassenkam, T., Hansen, P., Kjaer, M., et al. (2011). Tensile force transmission in human patellar tendon fascicles is not mediated by glycosaminoglycans. *Connect Tissue Res, 52*(5), 415-421. doi:10.3109/03008207.2010.551569
Svensson, R.B., Mulder, H., Kovanen, V., & Magnusson, S.P. (2013). Fracture mechanics of collagen fibrils: influence of natural cross-links. *Biophysical journal, 104*(11), 2476-2484.
Sylvain Ferrero, A.s.P., and Claude R. Henry. (2001). Atomic Scale Imaging by UHV-AFM of Nanosized Gold Particles on Mica. *Nano Letters, Vol. 1*,(5), 227-230.
Szczesny, S.E., Aeppli, C., David, A., & Mauck, R.L. (2018). Fatigue loading of tendon results in collagen kinking and denaturation but does not change local tissue mechanics. *J Biomech, 71*, 251-256. doi:10.1016/j.jbiomech.2018.02.014

Szczesny, S.E., Driscoll, T.P., Tseng, H.Y., Liu, P.C., et al. (2017). Crimped Nanofibrous Biomaterials Mimic Microstructure and Mechanics of Native Tissue and Alter Strain Transfer to Cells. *ACS Biomater Sci Eng, 3*(11), 2869-2876. doi:10.1021/acsbiomaterials.6b00646

Szczesny, S.E., & Elliott, D.M. (2014). Incorporating plasticity of the interfibrillar matrix in shear lag models is necessary to replicate the multiscale mechanics of tendon fascicles. *J Mech Behav Biomed Mater, 40*, 325-338. doi:10.1016/j.jmbbm.2014.09.005

Szczesny, S.E., & Elliott, D.M. (2014). Interfibrillar shear stress is the loading mechanism of collagen fibrils in tendon. *Acta Biomater, 10*(6), 2582-2590. doi:10.1016/j.actbio.2014.01.032

Tallon, C., Maffulli, N., & Ewen, S.W. (2001). Ruptured Achilles tendons are significantly more degenerated than tendinopathic tendons. *Medicine and Science in Sports and Exercise, 33*(12), 1983-1990.

Tang, Y., Ballarini, R., Buehler, M.J., & Eppell, S.J. (2010). Deformation micromechanisms of collagen fibrils under uniaxial tension. *J R Soc Interface, 7*(46), 839-850. doi:10.1098/rsif.2009.0390

Taylor, D.C., Dalton, J.D., Jr., Seaber, A.V., & Garrett, W.E., Jr. (1990). Viscoelastic properties of muscle-tendon units. The biomechanical effects of stretching. *Am J Sports Med, 18*(3), 300-309.

Thomas, S.J., Miller, K.S., & Soslowsky, L.J. (2012). The upper band of the subscapularis tendon in the rat has altered mechanical and histologic properties. *J Shoulder Elbow Surg, 21*(12), 1687-1693. doi:10.1016/j.jse.2011.11.038

Thompson, J.B., Kindt, J.H., Drake, B., Hansma, H.G., et al. (2001). Bone indentation recovery time correlates with bond reforming time. *Nature, 414*(6865), 773-776.

Thornton, G.M., Shrive, N.G., & Frank, C.B. (2002). Ligament creep recruits fibres at low stresses and can lead to modulus-reducing fibre damage at higher creep stresses: a study in rabbit medial collateral ligament model. *Journal of Orthopaedic Research, 20*(5), 967-974. doi:10.1016/S0736-0266(02)00028-1

Thornton, G.M., Shrive, N.G., & Frank, C.B. (2003). Healing ligaments have decreased cyclic modulus compared to normal ligaments and immobilization further compromises healing ligament response to cyclic loading. *Journal of Orthopaedic Research, 21*(4), 716-722. doi:http://dx.doi.org/10.1016/S0736-0266(03)00051-2

Thorpe, C., Udeze, C.P., Birch, H., Clegg, P.D., et al. (2013). Capacity for sliding between tendon fascicles decreases with ageing in injury prone equine tendons: a possible mechanism for age-related tendinopathy? *Eur Cell Mater, 25*, 48-60.

Thorpe, C.T., Chaudhry, S., Lei, II, Varone, A., et al. (2015). Tendon overload results in alterations in cell shape and increased markers of inflammation and matrix degradation. *Scand J Med Sci Sports, 25*(4), e381-391. doi:10.1111/sms.12333

Thorpe, C.T., Klemt, C., Riley, G.P., Birch, H.L., et al. (2013). Helical sub-structures in energy-storing tendons provide a possible mechanism for

efficient energy storage and return. *Acta Biomater, 9*(8), 7948-7956. doi:10.1016/j.actbio.2013.05.004

Thorpe, C.T., Riley, G.P., Birch, H.L., Clegg, P.D., et al. (2014). Effect of fatigue loading on structure and functional behaviour of fascicles from energy-storing tendons. *Acta Biomater, 10*(7), 3217-3224. doi:10.1016/j.actbio.2014.04.008

Thorpe, C.T., Udeze, C.P., Birch, H.L., Clegg, P.D., et al. (2012). Specialization of tendon mechanical properties results from interfascicular differences. *J R Soc Interface, 9*(76), 3108-3117. doi:10.1098/rsif.2012.0362

Tolksdorf, C., & Revenko, I. (2005). Choosing AFM probes for biological Applications. *Veeco Instruments Inc*.

Torriani, M., & Kattapuram, S.V. (2003). Musculoskeletal ultrasound: an alternative imaging modality for sports-related injuries. *Top Magn Reson Imaging, 14*(1), 103-111. doi:10.1097/00002142-200302000-00008

Trelstad, R.L., & Hayashi, K. (1979). Tendon collagen fibrillogenesis: Intracellular subassemblies and cell surface changes associated with fibril growth. *Developmental Biology, 71*(2), 228-242. doi:http://dx.doi.org/10.1016/0012-1606(79)90166-0

Usha, R., Subramanian, V., & Ramasami, T. (2001). Role of Secondary Structure on the Stress Relaxation Processes in Rat Tail Tendon (RTT) Collagen Fibre. *Macromolecular Bioscience, 1*(3), 100-107. doi:10.1002/1616-5195(20010301)1:3<100::AID-MABI100>3.0.CO;2-6

Vahabi, S., Nazemi Salman, B., & Javanmard, A. (2013). Atomic force microscopy application in biological research: a review study. *Iran J Med Sci, 38*(2), 76-83.

van der Rijt, J.A., van der Werf, K.O., Bennink, M.L., Dijkstra, P.J., et al. (2006). Micromechanical testing of individual collagen fibrils. *Macromol Biosci, 6*(9), 697-702. doi:10.1002/mabi.200600063

Vashishth, D., Gibson, G.J., Khoury, J.I., Schaffler, M.B., et al. (2001). Influence of nonenzymatic glycation on biomechanical properties of cortical bone. *Bone, 28*(2), 195-201.

Veres, S.P., Harrison, J.M., & Lee, J.M. (2013). Repeated subrupture overload causes progression of nanoscaled discrete plasticity damage in tendon collagen fibrils. *J Orthop Res, 31*(5), 731-737. doi:10.1002/jor.22292

Veres, S.P., Harrison, J.M., & Lee, J.M. (2014). Mechanically overloading collagen fibrils uncoils collagen molecules, placing them in a stable, denatured state. *Matrix Biology, 33*, 54-59. doi:https://doi.org/10.1016/j.matbio.2013.07.003

Veres, S.P., & Lee, J M. (2012). Designed to Fail: A Novel Mode of Collagen Fibril Disruption and Its Relevance to Tissue Toughness. *Biophysical Journal, 102*(12), 2876-2884. doi:10.1016/j.bpj.2012.05.022

Vesentini, S., Redaelli, A., & Gautieri, A. (2013). Nanomechanics of collagen microfibrils. *Muscles Ligaments Tendons J, 3*(1), 23-34. doi:10.11138/mltj/2013.3.1.023

Vesentini, S., Redaelli, A., & Montevecchi, F.M. (2005). Estimation of the binding force of the collagen molecule-decorin core protein complex in collagen fibril. *J Biomech, 38*(3), 433-443. doi:10.1016/j.jbiomech.2004.04.032

Vidal, B.C., & Mello, M.L. (1984). Proteoglycan arrangement in tendon collagen bundles. *Cell Mol Biol, 30*(3), 195-204.
Viidik, A. (1969). Tensile strength properties of Achilles tendon systems in trained and untrained rabbits. *Acta Orthop Scand, 40*(2), 261-272.
Vogel, K.G., & Koob, T.J. (1989). Structural specialization in tendons under compression. *International review of cytology, 115*, 267-293.
Vogel, K.G., Paulsson, M., & Heinegard, D. (1984). Specific inhibition of type I and type II collagen fibrillogenesis by the small proteoglycan of tendon. *Biochem J, 223*(3), 587-597.
Vogel, K.G., & Trotter, J.A. (1987). The effect of proteoglycans on the morphology of collagen fibrils formed in vitro. *Coll Relat Res, 7*(2), 105-114.
Voleti, P.B., Buckley, M.R., & Soslowsky, L.J. (2012). Tendon healing: repair and regeneration. *Annu Rev Biomed Eng, 14*, 47-71. doi:10.1146/annurev-bioeng-071811-150122
Wallace, J.M. (2012). Applications of atomic force microscopy for the assessment of nanoscale morphological and mechanical properties of bone. *Bone, 50*(1), 420-427. doi:http://dx.doi.org/10.1016/j.bone.2011.11.008
Wallace, J.M., Chen, Q., Fang, M., Erickson, B., et al. (2010). Type I Collagen Exists as a Distribution of Nanoscale Morphologies in Teeth, Bones, and Tendons. *Langmuir, 26*(10), 7349-7354. doi:10.1021/la100006a
Wallace, J.M., Orr, B.G., Marini, J.C., & Holl, M.M.B. (2011). Nanoscale morphology of Type I collagen is altered in the Brtl mouse model of Osteogenesis Imperfecta. *J Struct Biol, 173*(1), 146-152. doi:http://dx.doi.org/10.1016/j.jsb.2010.08.003
Wallace., Erickson, B., Les, M., Orr, G., et al. (2010). Distribution of Type I Collagen Morphologies in Bone: Relation to Estrogen Depletion. *Bone, 46*(5), 1349-1354. doi:10.1016/j.bone.2009.11.020
Wang, J.H. (2006). Mechanobiology of tendon. *J Biomech, 39*(9), 1563-1582. doi:10.1016/j.jbiomech.2005.05.011
Wang, T., Chen, P., Zheng, M., Wang, A., et al. (2018). In vitro loading models for tendon mechanobiology. *J Orthop Res, 36*(2), 566-575. doi:10.1002/jor.23752
Wang, T., Lin, Z., Day, R.E., Gardiner, B., et al. (2013). Programmable mechanical stimulation influences tendon homeostasis in a bioreactor system. *Biotechnology and bioengineering, 110*(5), 1495-1507.
Wang, X.-d., & Wolfbeis, O.S. (2014). Optical methods for sensing and imaging oxygen: materials, spectroscopies and applications. *Chemical Society Reviews, 43*(10), 3666-3761.
Wang, X.T., & Ker, R.F. (1995). Creep rupture of wallaby tail tendons. *J Exp Biol, 198*(Pt 3), 831-845.
Waterston, S.W., Maffulli, N., & Ewen, S.W. (1997). Subcutaneous rupture of the Achilles tendon: basic science and some aspects of clinical practice. *Br J Sports Med, 31*(4), 285-298.
Wearing, S.C., Hooper, S.L., Grigg, N.L., Nolan, G., et al. (2013). Overweight and obesity alters the cumulative transverse strain in the Achilles tendon immediately following exercise. *J Bodyw Mov Ther, 17*(3), 316-321. doi:10.1016/j.jbmt.2012.11.004

Weber, I.T., Harrison, R.W., & Iozzo, R.V. (1996). Model structure of decorin and implications for collagen fibrillogenesis. *J Biol Chem, 271*(50), 31767-31770.
Weiner, S., & Wagner, H.D. (1998). The material bone: structure-mechanical function relations. *Annual Review of Materials Science, 28*(1), 271-298.
Weiss, J.A., & Gardiner, J.C. (2001). Computational Modeling of Ligament Mechanics. *29*(3), 303-371. doi:10.1615/CritRevBiomedEng.v29.i3.20
Wenger, M.P.E., Bozec, L., Horton, M.A., & Mesquida, P. (2007). Mechanical Properties of Collagen Fibrils. *Biophysical Journal, 93*(4), 1255-1263. doi:http://dx.doi.org/10.1529/biophysj.106.103192
Wenstrup, R.J., Florer, J.B., Brunskill, E.W., Bell, S.M., et al. (2004). Type V collagen controls the initiation of collagen fibril assembly. *J Biol Chem, 279*(51), 53331-53337. doi:10.1074/jbc.M409622200
Wenstrup, R.J., Smith, S.M., Florer, J.B., Zhang, G., et al. (2011). Regulation of collagen fibril nucleation and initial fibril assembly involves coordinate interactions with collagens V and XI in developing tendon. *J Biol Chem, 286*(23), 20455-20465. doi:10.1074/jbc.M111.223693
Whitley, C., Ridnour, M., Draper, K., Dutton, C., et al. (1989). Diagnostic test for mucopolysaccharidosis. I. Direct method for quantifying excessive urinary glycosaminoglycan excretion. *Clinical chemistry, 35*(3), 374-379.
Williams, L.N., Elder, S.H., Bouvard, J., & Horstemeyer, M. (2008). The anisotropic compressive mechanical properties of the rabbit patellar tendon. *Biorheology, 45*(5), 577-586.
Woo, S., Lee, T., Abramowitch, S., & Gilbert, T. (2005). Structure and function of ligaments and tendons. *Basic orthopaedic Biomechanics & Mechanobiology, Ed. Mow VC, Hayes WC. 3rd ed. Philadelphia: Lippincott, Williams & Wilkins*, 301-342.
Woo, S.L. (2000). Anatomy, biology, and biomechanics of tendon and ligament. *Orthopaedic basic science : biology and blamechanics of the musculoskeletal system*, 582-616.
Woo, S.L., Debski, R.E., Zeminski, J., Abramowitch, S.D., et al. (2000). Injury and repair of ligaments and tendons. *Annu Rev Biomed Eng, 2*, 83-118. doi:10.1146/annurev.bioeng.2.1.83
Woo, S.L., Johnson, G.A., & Smith, B.A. (1993). Mathematical modeling of ligaments and tendons. *J Biomech Eng, 115*(4b), 468-473.
Wren, T.A., Lindsey, D.P., Beaupré, G.S., & Carter, D.R. (2003). Effects of creep and cyclic loading on the mechanical properties and failure of human Achilles tendons. *Ann Biomed Eng, 31*(6), 710-717.
Wren, T.A., Yerby, S.A., Beaupre, G.S., & Carter, D.R. (2001). Mechanical properties of the human achilles tendon. *Clin Biomech (Bristol, Avon), 16*(3), 245-251.
Wright, S.J., Centonze, V.E., Stricker, S.A., DeVries, P.J., et al. (1993). Introduction to confocal microscopy and three-dimensional reconstruction. *Methods Cell Biol, 38*, 1-45.
Wu, J.J. (2006). Quantitative constitutive behaviour and viscoelastic properties of fresh flexor tendons. *Int J Artif Organs, 29*(9), 852-857.

Wu, J.P., Walton, M., Wang, A., Anderson, P., et al. (2015). The development of confocal arthroscopy as optical histology for rotator cuff tendinopathy. *J Microsc, 259*(3), 269-275. doi:10.1111/jmi.12260

Wu, J.Z., Cutlip, R.G., Welcome, D., & Dong, R.G. (2006). Estimation of the viscous properties of skin and subcutaneous tissue in uniaxial stress relaxation tests. *Biomed Mater Eng, 16*(1), 53-66.

Yahia, L.-H., & Drouin, G. (1988). Collagen structure in human anterior cruciate ligament and patellar tendon. *Journal of materials science, 23*(10), 3750-3755.

Yamamoto, E., Hayashi, K., & Yamamoto, N. (1999). Mechanical properties of collagen fascicles from the rabbit patellar tendon. *J Biomech Eng, 121*(1), 124-131.

Yoon, J.H., & Halper, J. (2005). Tendon proteoglycans: biochemistry and function. *J Musculoskelet Neuronal Interact, 5*(1), 22-34.

You, H.X., & Yu, L. (1999). Atomic force microscopy imaging of living cells: progress, problems and prospects. *Methods Cell Sci, 21*(1), 1-17.

Young, S.R., Gardiner, B., Mehdizadeh, A., Rubenson, J., et al. (2016). Adaptive Remodeling of Achilles Tendon: A Multi-scale Computational Model. *PLOS Computational Biology, 12*(9), e1005106. doi:10.1371/journal.pcbi.1005106

Zanetti, M., Metzdorf, A., Kundert, H.P., Zollinger, H., et al. (2003). Achilles tendons: clinical relevance of neovascularization diagnosed with power Doppler US. *Radiology, 227*(2), 556-560. doi:10.1148/radiol.2272012069

Zhang, G., Ezura, Y., Chervoneva, I., Robinson, P.S., et al. (2006). Decorin regulates assembly of collagen fibrils and acquisition of biomechanical properties during tendon development. *J Cell Biochem, 98*(6), 1436-1449. doi:10.1002/jcb.20776

Zipfel, W.R., Williams, R.M., & Webb, W.W. (2003). Nonlinear magic: multiphoton microscopy in the biosciences. *Nat Biotechnol, 21*(11), 1369-1377. doi:10.1038/nbt899

The following statement has been included at the end of the Bibliography/Reference List in the thesis; “Every reasonable effort has been made to acknowledge the owners of copyright material. I would be pleased to hear from any copyright owner who has been omitted or incorrectly acknowledged.”